Doctor of Engineering Thesis

Gas-Liquid Two-Phase Flow Distributions in Multi-pass Channels

多分岐構造をもつ流路内の気液二相分配

Zuradzman Bin Mohamad Razlan

Division of Systems Engineering
Graduate School of Engineering
Mie University
Japan

March 2012

Supervisor:
Professor Dr. Masafumi Hirota

博士学位論文

多分岐構造をもつ流路内の気液二相分配

三重大学大学院　工学研究科
博士後期課程　システム工学専攻

ズラズマン　ビン　モハマド　ラズラン

2012 年 **3** 月

PREFACE

This thesis is submitted for the Degree of Doctor Engineering at Mie University, Japan. The thesis is based on studies carried out at the Energy System Design laboratory of Mechanical Engineering Faculty. This research is a joint research with Micro thermal fluid laboratory, Mechanical engineering department of Nagoya University at the beginning stage. Subsequently, advancing the research on two phase flow which focusing to direct observation of real refrigerant flow inside a simulated compact evaporator with Fuji Electric Retail Systems Company.

The close relationship with these two organizations personnel makes the research flow in my three years of tenure at Mie University, smooth and according to the original milestone. Not to mentioned the great assist and supports from my supervisor, Professor Dr. Masafumi Hirota that ensure me from not to fall behind on the development of this research.

Shukur Alhamdulillah, thank you God for giving me strength and willingness upon achieving my goal.

Many people have contributed and helped me during the three years of study, and I would like to take this opportunity to thank you:

- Professor Dr. Masafumi Hirota, for being my main supervisor and for initiating the project with Nagoya University and Fuji Retail Co. Ltd.
- Associate Professor Dr. Naoki Maruyama, for being my co-supervisor and for believing and accepting me to joint this laboratory.
- Assistant Professor Dr. Akira Nishimura, for being my second co-supervisor and the chairman of our laboratory internal colloquium session.
- Professor Dr. Koichi Tsujimoto and Professor Dr. Takao Maeda of Mechanical engineering department, Mie University, for being patience to review and commenting this thesis. Also for being the co-examiners for pre and final

examination of my PhD course.

- Mr. Hiroaki Goshima, Mr. Yamato Nakagawa and Mr. Wu Cheng Hao, for being my co-researcher and a great assistance through the years doing the testing together. Also for not giving up providing precise testing data for the best outcome of our research.
- Mr. Kohji Takiguchi, Mr. Toshiaki Tsuchiya and Mr. Yujiro Kitade of Fuji Electric Retail Systems, for the funding, great technical support and creative ideas on the development of this research.
- Mr. Ryota Isobe of Chubu Electric Power Company, a great assist and guidance on the testing apparatus assembly, setup and method when transferring the testing equipment from Nagoya University to here.
- Mr. Mohamad Hisham Hamdan of Lean Applied Pte. Ltd., Subang Jaya, Malaysia, for the tremendous support on the six sigma consultancy focusing on the design of experiment method through Minitab 15 statistical software.
- Y. Bhg. Brig. Jen. Prof. Dato' Dr. Kamarudin Hussin the vice chancellor, Professor Dr. Ali Yeon Md. Shakaff the deputy vice chancellor and Mrs. Sharifah Husna Syed Idrus the assistant registrar of University Malaysia Perlis, upon your kind approval on sponsorship and great support through the years.
- Dr. Zunaidi Ibrahim, Deputy rector of Tati University College, Malaysia, Associate Professor Dr. Hazry Desa and Dr. Shahriman Abu Bakar of University Malaysia Perlis, for believing in me. Also, for your great recommendation to Mie University for my PhD placement and to University Malaysia Perlis for funding my total of 42 months of study here in Japan.
- Mr. Norio Takahashi, Mr. Takashi Sugai and Mr. Kazuo Odate of Hitachi Limited, for guiding me to be an excellent R&D engineer and your time spending to answer a lot of question about air conditioning and refrigerant cycle problem.

Last but not least I want to express my appreciation to my wife, Nurhazlina Ramli, and to my wonderful daughters Aishah, Maisarah, Nasha and Nisa, for their great patience and tolerance. I apologize to you, my family in Malaysia and friends for any neglect while I single-mindedly pursued my goal.

Zuradzman Bin Mohamad Razlan
Mie University, Japan
February, 2012

Summary

In order to improve the performance of a heat pump system, this research has focused on the improvement of the thermal performance of an evaporator. In particular, the gas-liquid flow distributions in multi-pass channels that simulate a compact evaporator which is currently used for an automobile air-conditioning system and soon will be introduced to other heat pump appliances has been examined experimentally. In this research, the study was divided into two parts.

1. Study on two-phase flow distribution behavior of air-water flow in a multi-pass channel

In this study, the influences of several parameters on the two-phase flow distributions in the multi-pass channel have been investigated in an isothermal air-water flow system. The test channel has a horizontal header with a square cross section of 20mm × 20mm and a length of 255mm, and ten upward branches with a length of 200mm were connected to it. The superficial air velocity j_G and superficial water velocity j_W at the entrance of the header are determine based on the quality and mass flow rate of the refrigerant encountered in a real evaporator. In this study, j_G and j_W are set equal to the superficial velocities of vapor and liquid of the refrigerant flow (R-134a) in a real evaporator of a automobile air-conditioner, and they are 1.0 - 5.0 m/s and 0.015 - 0.045 m/s, respectively. These velocity conditions correspond to the range of quality x = 0.2 - 0.7 and mass flow rate M = 40 - 160 kg/h in R-134a refrigerant flow in a real evaporator.

Special attention was directed to influences of (i) flow-inlet condition at the header

entrance (stratified-flow inlet and mist-flow inlet), (ii) pressure condition at the branch outlets (uniform backpressure and non-uniform backpressure), (iii) pressure-loss characteristics of branches (flat tubes and multi-port tubes) on the gas-liquid distribution characteristics. Based on the results of the experiments, he most influenced parameter to the flow distribution uniformity is determined by using the design of experiment method. In addition to the gas-liquid distributions to branches, the pressure distributions in the headers are measured to make clear the pressure condition in a real evaporator.

It has been found that the outlet pressure condition of branches exerts great influence on the gas-liquid distributions to branches in the channel with flat tube branches, but it has only minor influence in the channel with multi-port tube branches. The flow-inlet condition at the header entrance has significant influence on the gas-liquid distribution, and the uniformity of the liquid distribution to branches is improved under the mist-flow inlet condition. The pressure in the headers shows uniform distributions in the stream-wise direction, suggesting that the uniform backpressure condition at the branch outlets is appropriate for reproducing the flow in a real compact evaporator with multi-pass channels. The flow distribution uniformity of gas phase is influenced mostly by superficial air velocity, and the flow distribution uniformity of liquid phase is mostly influence by 2-way interaction of parameters which are the flow-inlet condition at the header entrance and the superficial air velocity.

2. Study on similarity of two-phase flow distribution behaviors of real refrigerant (R-134a) flow and air-water flow in a multi-pass channel

As a next stage of the study, an experimental study was conducted on the gas-liquid two-phase flow distributions in the multi-pass channel that simulated a compact evaporator in a heat pump system. Attention was directed to the similarity between the refrigerant (R-134a) flow and the air-water flow in upward and continue with downward channel. This to confirm the result on similarity of real refrigerant with air-water flow distribution behavior in upward multi-pass channel is significance in other orientation of multi-pass channel, i.e., in this study shall be the downward multi-pass channel. The body of the test channel was made of transparent PVC to allow the optical access, and the multiport aluminum tubes were used as branches. The horizontal dividing and combining headers with cross sections of 20mm x 20mm were connected by 22 branches with cross sections of 20mm x 2mm, lengths of 120 mm and pitches of 12mm.

At first, concentrate on multi-pass upward channel, the refrigerant two-phase flow was visualized to clarify the flow characteristics in the headers. Then, using exactly the same test channel, the air-water flow in the headers was observed under following four air and water velocity conditions at the dividing header entrance to seek the similarity with the flow pattern of the refrigerant flow: (ⅰ) superficial gas and liquid velocities equal to those of the refrigerant flow, (ⅱ) equal kinetic energies, (ⅲ) equal quality and mass flow rate, (ⅳ) equal Baker's flow pattern map parameters. From a comparison of the flow patterns in the dividing header, it was found that the air-water flow under the inlet conditions of the equal kinetic energies and equal Baker's flow pattern map parameters could simulate the refrigerant flow quite closely. Then, based on this result, the air and water distribution ratios in the branches were measured under these two conditions to examine the influence of the flow inlet conditions on the flow distribution characteristics. A close comparison of the air-water distributions and refrigerant flow in the combining header revealed that the inlet condition of equal Baker's flow pattern map parameters gave better results than the equal kinetic energy condition.

Secondly, using the same research flow and same testing apparatus and method, the multi-pass downward channel was examined. From a comparison of the flow patterns in the dividing header, it was found that the air-water flow under the inlet conditions of the equal kinetic energies and equal superficial velocities of gas and liquid phase of real refrigerant could simulate the refrigerant flow quite closely. Then, based on this result, the air and water distribution ratios in the branches were measured under all four conditions to examine the influence of the flow inlet conditions on the flow distribution characteristics. A close comparison of the air-water distributions and refrigerant flow in the combining header revealed that the inlet condition of superficial velocities of gas and liquid phase of real refrigerant gave better results than the equal kinetic energy condition.

Thirdly, to confirm the result in downward test channel, the inlet pipe has been swaged at the end of it to be a smaller inner diameter, i.e., 1.5mm, as a new parameter for further study on this flow distribution behavior similarities between real refrigerant and air-water flow. Also as a counter measure to improve the flow distribution uniformity. From the result of comparing the qualitative result of real refrigerant visual observation and air-water flow distribution ratio measurement, it was found that the inlet condition of air-water flow that equal to superficial velocities of those in real refrigerant are the one that could simulated the real refrigerant flow distribution

behavior in multi-pass downward channel.

However, to fit both upward and downward oriented multi-pass channel flow distribution of liquid phase flow simultaneously, it is better and safer to use the inlet condition that equal to kinetic energies of real refrigerant. Thus, these studies and new conclusions are able to make the development of new compact evaporators with higher thermal performance, more efficient and faster.

Contents

List of Figures and Tables

Figures

Tables

Nomenclature

Latin letters

A	Annular flow	
B	Bubble flow	
CH	Churn flow	
COP	Coefficient of performance	[-]
Case A	Non-uniform backpressure condition	
Case B	Uniform backpressure condition	
D	Pipe diameter	[m]
DB	Dispersed bubble	
DF	Degree of freedom	
DOE	Design of experiment	

D_h	Hydraulic diameter	[mm]
EER	Energy efficiency ratio	
F	F test, equality of variance between factor levels	
G	Fluid mass flux	[kg/m^{2}s]
G	Mass flow rate same as *M*	[kg/hr]
G_g	Gas mass velocity	[kg/m^2.h]
G_l/G_g	Ratio of liquid and gas mass flow rates	[-]
H	Horizontal	
HCFC	Hydro-chlorofluorocarbon	
I	Intermittent	
ID	Inner diameter	[mm]
L	Length	[m]
LME	London metal exchange	
M	Mass	[kg]
M	Mass flow rate	[kg/h], [kg/s], [g/min]
MS	Means of squares	
MS	Multi-tank and super slim	
N	Compressor motor revolution	[rpm]
P	Absolute pressure	[MPa]
P	Pressure	[kPa]
P-value	P-values range from 0 to 1	
PVC	Polyvinyl chloride	
Q	Refrigerating capacity	[kJ/hr]
Q	Total heat input	[W]

RS	Revolutionary super-slim	
Re	Reynolds number	[-]
S	Stratified	
SL	Slug flow	
SS	Stratified smooth	
SS	Sums of squares	
SW	Stratified wavy	
T	Time	[s]
T_1	Condensing temperature in the condenser	[˚K]
T_2	Evaporation temperature in the evaporator	[˚K]
V	Compressor displacement volume	[m^3/rev]
VD	Vertical Downwards	
V_{TH}	Theoretical exhaust volume of compressor	[m^3/hr]
VU	Vertical Upwards	
W	Mass flow rate	[kg/s]
W_{TH}	Theoretical compressor power consumption	[W]
g	Acceleration of gravity	[$m.s^{-2}$]
h	Intrusion height or protrusion depth	[mm]
i	Enthalpy	[kJ/kg]
j	Dimensionless and independent quantities (n-k)	
j	Superficial velocity	[m/s]
k	Primary variable	
$k_{T,M}$	Two-phase momentum flux	[$N.s/m^2.s$]
n	Variable	

p	Pressure	[mPa]
ppm	Parts per million	
q''	Heat flux	[kW/m^2]
s	Entropy	[kJ/kg.˚K]
t	Temperature at indexed point in Mollier diagram	[˚C]
v	Specific volume	[m^3/kg]
v_s	Specific volume of refrigerant at compressor suction	[m^3/kg]
x	Quality (Gas phase dryness in weight fraction)	[kg/kg]

Greek letters

β	Pipe inclination angle	[-]
γ	Solid liquid gas contact wetting angle	[-]
ε	Pipe roughness	[m]
η_{St}	Standardized correction value	[-]
η_{ad}	Adiabatic efficiency	[-]
η_m	Compressor motor efficiency	[-]
η_v	Volumetric efficiency of the compressor	[-]
λ	Dimensionless correction factors	[-]
μ	Viscosity	[μPa·s]
ρ	Density	[kg/m^3]
σ	Liquid phase surface tension	[mN/m], [kg.s^{-2}]
σ	Standard deviation of flow distribution ratios	[-]
ψ	Dimensionless correction factors	[-]

Subscripts

A	air
G	gas phase of R-134a
L	liquid phase of R-134a
R	R-134a refrigerant
W	water
f	Liquid
g	Gas phase
i	Index number of branch
in	Inlet (header entrance)
l	Liquid phase

Chapter 1

Introduction

1.1 Background

The aim of this research is to improve the COP of a heat pump system of appliances that used a huge amount of electric energy, technically by study the two phase flow distribution behavior of a multi-flow type compact evaporator. This improvement is important to the development of human kind through the entire world.

Mainly to improve the global warming problem and energy depletion by reducing the usage of electric energy and indirectly reduced the releasing amount of carbon dioxide from the fossil fuel power plant and also from automobiles. Global warming, which is a continuing temperature increment of earth's atmosphere and oceans. Atmospheric carbon dioxide increased from 280 to 300 parts per million in 1880 to 335 to 340 ppm in 1980, mainly, cause by increased concentrations of greenhouse gases in the atmosphere, resulting from human activities such as deforestation and burning of fossil fuels as reported by Hansen J. et al. (1981). Also mentioned, the global temperature rose by 0.2 ˚C between middle 1960's and 1980, yielding a warming of 0.4 ˚C in past century. This temperature increase is consistent with the calculated greenhouse effect due to measured increases of atmospheric carbon dioxide. The updated report on global warming by Hansen J. et al. (2010), mentioned that the rate of warming has not declined. Global temperature is rising as fast in the past decade as in the prior 2 decades, despite

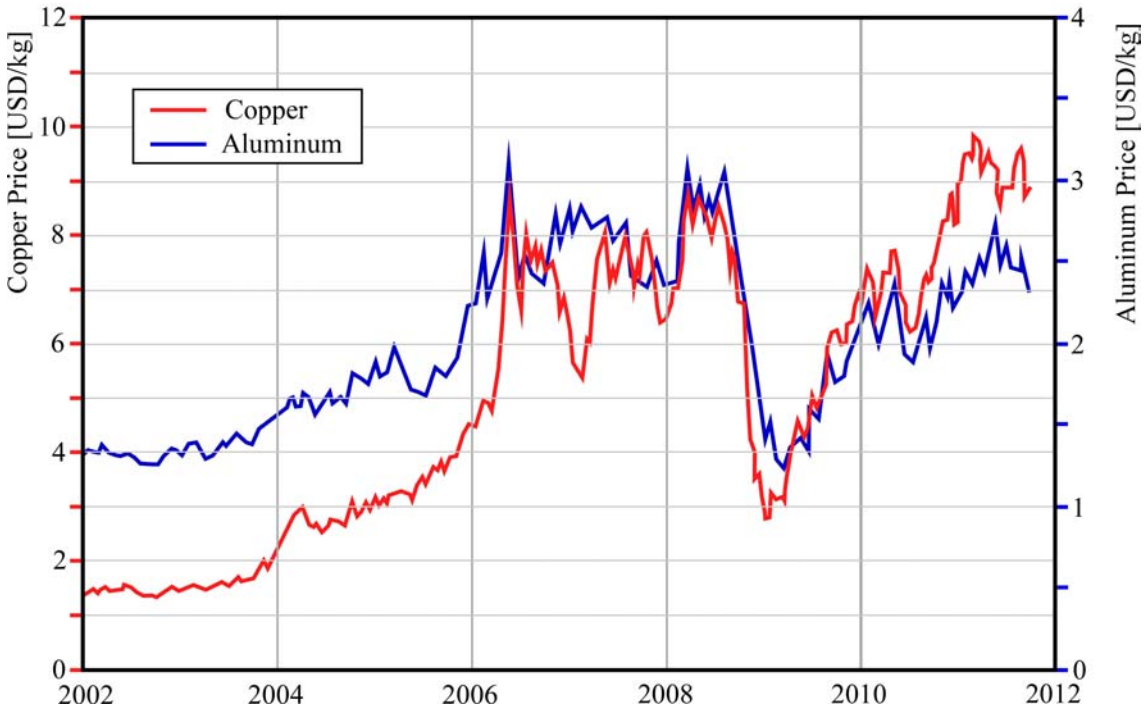

Fig. 1.1 Copper and Aluminum raw material market price trend from January 2002 until September 2011; recent report from London Metal Exchange (LME)

year-to-year fluctuations associated with the El Nino-La Nina cycle of tropical ocean temperature. The greenhouse effect is the process by which absorption and emission of infrared radiation by gases in the atmosphere warm a planet's lower atmosphere and surface. These unforgiving phenomena that created by human kind themselves have to be improved in any kind of way. Thus ours shall be as written onward.

This research also important to the heat pump appliances manufacturer as their main raw material for manufacturing the appliances is copper, while this compact evaporator is made from aluminum. It has been a nightmare for company that manufactured this heat pump system such as room air conditioner since early 2004 due to the drastic increasing of copper price. Copper, one of the main raw materials for producing a heat pump machine which occupied almost 30% of an ordinary room air conditioner, due to its thermodynamic properties that has a good heat transfer and electric conductance compare to other material as with its considerable price. Thus as in Fig. 1.1 this raw material price as recently reported by London Metal Exchange (LME) incline drastically in early 2004 and become unstable since then. This events makes the finding of other optional raw material to replace copper becomes important. Other than compressor, fan motor rotor coil and piping, the heat exchangers are the one that made

by huge amount of copper. To change the usage of heat exchanger that made from copper hairpin and aluminum fin to a aluminum cooling coil as in automobiles air conditioner system are not an easy task. An accurate confirmation on the performances and a study of a new compact evaporator with high efficiency has to be ensured due to a huge cost upon changing the production of the heat exchanger. The fix asset cost for new machinery on casting the aluminum coil has to be covered by the efficiency improvement of new evaporator concept.

Even, recent devastating disaster that cause a holocaust in east Japan, implore for a drastic improvement of electric energy economically usage. Thus, one of electrical appliances that used a huge amount of energy is the one which using a heat pump or cooling system, e.g., refrigerator, car and room air conditioner. Therefore, improvement on energy efficiency of a heat pump system becomes a serious issue.

1.2 Objectives

This research shall focus on the improvement of the heat exchanger, i.e., the compact evaporator, one of the main devices in the heat pump system. However a perfect multiple flow type evaporator, i.e., a compact evaporator with a set of dividing and combining headers with multiple parallel branches attached, that has a perfect balance of gas-liquid phase flow distribution is yet to be completely discovered and understood. This kind of evaporator, mainly the liquid phase flow mal-distribution at dividing header to the multiple branches occurred and creates an uneven temperature distribution on this evaporator surface. Thus makes the efficiency of evaporator dropped. Therefore, literature study in engineering field on behavior of gas liquid two phase flow focusing on flow distribution in multi-pass channel is become important. A great number of studies have been done due to this reason. Thus, the mechanism of two phase flow distribution in multi-pass channel is much complicated. Also, the flow distribution behavior reacts with many parameters in a complicated manner, makes the uniform distribution universal modus operandi difficult to accomplish, understand and simplify.

In this study, there are a few development stages divided.

① The first stage is the study on behavior of air-water flow distribution in upward multi-pass channel, concentrate on the following influences.
   1) Inlet flow pattern
   2) Superficial velocity of air and water
   3) Backpressure condition

4) Pressure loss

② The second stage shall be the analysis of the uniformity of air and water flow distribution measurement result in the test channel. By calculate the standard deviation value of each testing data, a standard deviation value at each test condition can be plotted and reviewed. Also, the analysis shall continue further by using the DOE method, i.e., design of experiment, or the analysis of variance as in mathematic statistical study, the most influenced parameters and its combination to the flow distribution uniformity of each phase can be known.

③ The third stage is the measurement on pressure distribution along dividing and combining header of the test channel, i.e., the 10 branches upward multi- flow test channel that simulated from a compact evaporator. This experimental study is important upon confirming the backpressure condition of the test channel. Due to the result of flow distribution ratio of gas and liquid are much depending on this backpressure condition when the pressure loss is in a small value.

④ The forth stage is the visual observation of real refrigerant inside the test channel with 22 branches simulated from a multi-flow type evaporator. In this stage a different transparent test channel with 22 branches made from PVC has been used. A few arrangements on the orientation of the test channel for a few kind of refrigerant flow has been made and visualized, i.e. upward, downward, horizontal and lying leveled flow. With a few header inlet condition of quality x and mass flow M that simulate from a real usage of a heat pump appliances, a visual test has been done and studied. The test channel orientation with the flow in upward condition has been chosen as the first one to get further investigation.

⑤ The fifth stage is the visual observation of air-water two phase flow distribution using the same test channel as in stage 4. By set a few inlet condition of superficial velocity of air and water that has been chosen to be similar in a thinkable manner of behavior to the real refrigerant flow. Then, a comparison with the visual observation data, i.e., the motion picture, of real refrigerant flow distribution. The most identical test condition data shall be selected for further investigation. Noted, only qualitative judgments are required at this stage as an initial result for visual confirmation.

⑥ The sixth stage, a flow distribution ratio of real refrigerant quantitatively needed to be confirmed. To measure the flow distribution of real refrigerant directly is basically difficult. So, in this research we measure the flow distribution to each

branch by using the air-water flow to simulate the real refrigerant. Same as in stage 5, with a few similarities condition consideration, 4 inlet condition of air and water superficial velocity has been decided to simulate the flow inlet condition of real refrigerant. Upon doing this study, a few findings has been acknowledge and reported.

⑦ This research continues, focusing on flow distribution behavior study on flow distribution in downward flow in the same test channel. At this stage also, a various inlet pipe that the end of it were swaged to a smaller diameter were used to study the flow distribution behavior at high superficial velocity at header entrance. As previous stage, a synchronization of flow distribution in a simulated test channel with air and water were done to get the qualitative and quantitative data of flow distribution ratio of gas and liquid phase of real refrigerant. At the same time, a study on which inlet condition of superficial velocity of air and water that suitable for synchronization with real refrigerant flow inside the test channel can be indentify.

1.3 Synopsis of the thesis

Started with the introduction stretching the importance of the research, continue with chapter 2, the literature review. Firstly, a literature reviews on heat pump system and the coefficient of performance of the system. After that, review on previous studies improving the heat pump system efficiency performance through the years. Then continue with the compact evaporator development by a company but unfortunately have a mal-distribution problem that cannot be understand clearly by engineering point of view. Then, a literature reviews on flow pattern transition in two-phase gas liquid flows. Continue with a study from some journals that focusing on mal-distribution of two phase flow in multi-pass channel. Then a review of some other researcher that study and contribute much to this study on two phase flow distribution in a multi-pass evaporators, directly with the real refrigerant and simulation with air and water.

Chapter 3 shall cover the experimental method, apparatus details and setup. Explanation on the test channel detail dimensions, testing method on air-water flow distribution ratio measurement in two backpressure conditions. Also, the visual testing apparatus of real refrigerant in test channel that simulate from multi flow type evaporator. Continue with the air-water flow visual test apparatus details.

Chapter 4 shall explain on experimental results and findings, which divided into 2 segments, the experimental result of the study on parameters that influence the flow distribution, which using the test channel with 10 branches. The explanation shall begin with the test condition, i.e. the superficial velocity of air and water, or the quality x and mass flow rate M of the real refrigerant at the header entrance. Continue with the second segment, study on the similarity of real refrigerant and air-water two phase flow distribution behavior which discussing the visual observations and flow distributions ratio measurement results and some initial conclusions.

Chapter 5 shall conclude the research overall result and findings of this thesis. In this chapter, some breakthrough upon analyzing the experimental result that has been written and published earlier shall be explain. The first one shall be the pressure distribution along the dividing and combining headers. Then, the analysis of variances or parameters by design of experiment method to find the most significant parameters that contributes to the uniformity of flow distribution ratio of air and water. Also, pressure loss between headers influences to the flow distributions behavior. Then, the conclusion on the most significant inlet condition of air and water that can simulate the behavior of real refrigerant flow distribution inside a multi flow type evaporator. The synchronization of real refrigerant R-134a with air-water shall be confirmed upon knowing the test channel headers and branches orientation that determine the flow route of the substance inside the test channel.

Chapter 2

Literature Review

2.1 Chapter overview

This chapter reviews some of the previous work on improving the efficiency of the performance of a heat pump system, which concentrates on improving the efficiency of its main devices, e.g., compressor, evaporator's heat transfer area and a development of compact evaporators with multiple branches.

An explanation on occurrence of mal-distribution of gas and liquid phase flow inside evaporators shall be address, continue with the study on flow pattern transition in two-phase gas liquid flows. Then, a review on other researchers reports on the study of two phase flow distribution behavior in a multi-pass channel.

2.2 Heat pump system coefficiency of performance

2.2.1 Heat pump system

Heat is the energy of the molecular movement and every substance without reference to gas, liquid and solid consists of the moving molecules. Substance phase or state usually has 3 stages. Each state change known as: (1) Evaporation, the state change from liquid to vapor, e.g., alcohol evaporation. The opposite of it shall be the condensation. (2) Fusion, the state change from solid to liquid, e.g., ice fusion. The opposite of it shall be

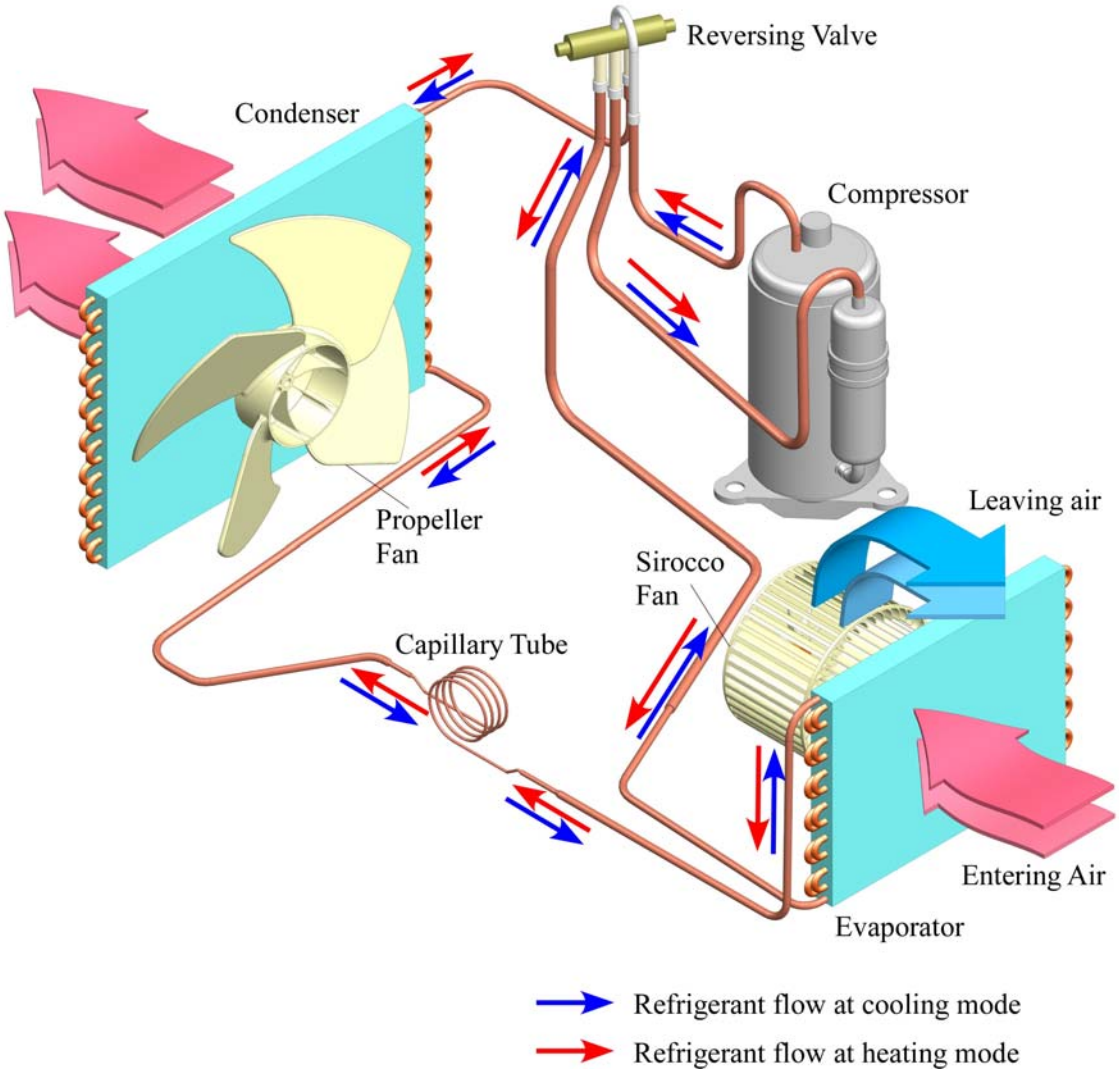

Fig. 2.1 Sample of an ordinary heat pump system refrigerant cycle of a room air conditioner

the solidification. (3) Sublimation, the state change from solid to vapor, e.g., carbon dioxide solid to gas. Heat can be classified as two categories, which are sensible and latent heat. Sensible heat is the heat used for changing the substance temperature and latent heat is the heat used for changing the substance state.

Heat pump is a system commonly use for appliances with two main objective, to generate cooling and heating. Generally define as a machine that control the temperature, humidity, air circulation and purity of one closed space, e.g., car and room air conditioner, also temperature control in can drinks vending machine compartment.

This heat pump system consists of the compressor, condenser, expansion device i.e.,

capillary tubes or expansion valve, evaporator and reversing valve as its main devices. A fixed amount of refrigerant is charged inside the system and the refrigerant shall flows circulate the system while changing the phase from gas to liquid and vice versa repeatedly, releasing and gaining heat energy from surroundings. Fig. 2.1 is a typical example of an ordinary of a heat pump system for ordinary room air conditioner.

Compressor: the compressor sucks in the refrigerant gas which has been evaporated by the evaporator. This refrigerant is then compressed to the high pressure and high temperature gas phase refrigerant in which it can be easily liquefied by the use of coolant water or air circulation at low temperature at condenser.

Condenser (changes the refrigerant from liquid to gas): the gaseous refrigerant which comes out of the compressor at high temperature and high pressure now enters the condenser where it is heat exchanged by coolant water or air circulation at low temperature. The heat removed from the refrigerant here is called “Condensed latent heat”.

Expansion device, i.e., capillary tube or Expansion valve, (places the liquid refrigerant in an easily vaporizable state in a low temperature): this device is important for decreasing the pressure and temperature of the liquid refrigerant, makes it to be in a state of easy evaporation before it enters the evaporator. Also, at the same time it also controls the amount of liquid phase refrigerant flow of the system.

Evaporator (changes the refrigerant state from liquid to gas by absorption of heat energy from air circulation): the liquid refrigerant in the evaporator removes the heat required by evaporation (Evaporation latent heat) from the air circulation at the evaporator and turns into a gas phase. The air that had the heat removed from it is cooled and has it water dehumidified. A fan circulates the air throughout the room to maintain the room air at the thermostat optimum temperature.

Reversing Valve (controlling the heat pump system running the cooling or heating mode): mainly controlled by electromagnetic switch, manage the refrigerant flow from compressor to be directed to evaporator for heating or to the condenser for cooling mode. Simultaneously, maintaining the refrigerant flow in and out of the compressor at the same route at all time.

When the compressor operates in an actual heat pump refrigerating cycle, the refrigerant flow constantly through the above first four actions in the heat pump unit and remove the heat from one closed space to the other side of it or generally to the

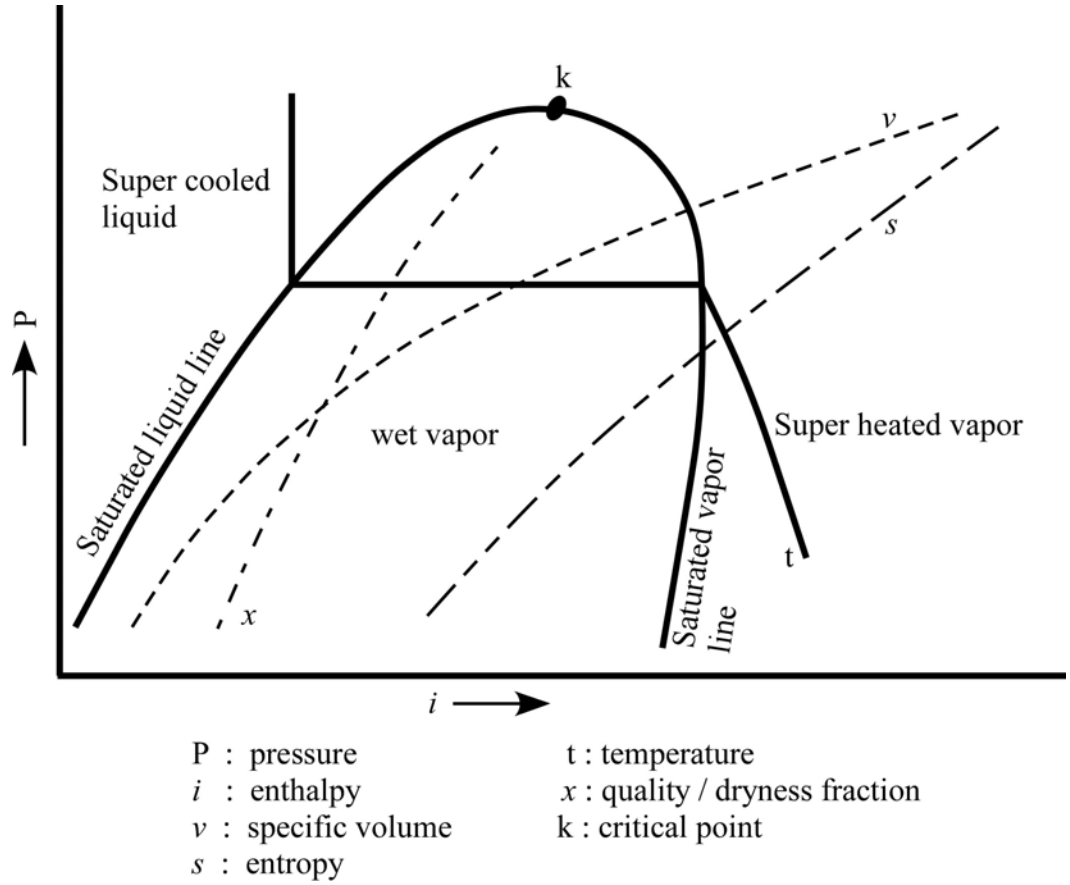

Fig. 2.2 Mollier diagram

outdoor side. Meanwhile, the reversing valve shall control the system to generate a cooling or heating mode to the closed space or to the room.

2.2.2 Coefficient of performance (COP)

The heat pump system basically works with the concept of Mollier diagram. Each four main devices of the system can be shown as four main line in the diagram. This Mollier diagram consists of the abscissa that shows the enthalpy *i* differential and the ordinate that shows the absolute pressure P of the refrigerant. Generally, it is used for investigation of refrigerant state or phase change in the heat pump system and for calculation to determine the specifications of the system reliability such as the cooling or heating capacity and also the system COP.

As in Fig. 2.2, the Mollier diagram also shows all the necessary thermodynamic properties of the refrigerant at a range of pressure and temperature of the refrigerant in

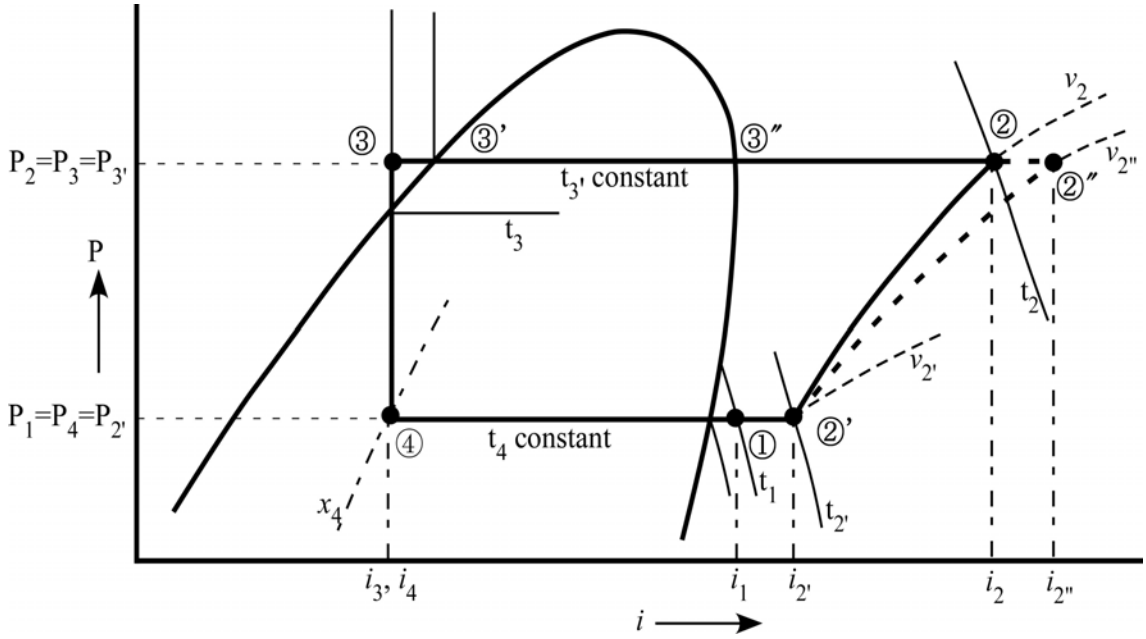

Fig. 2.3 Refrigerant cycle of a typical cooling mode illustrate in a Mollier diagram

the heat pump system. The thermodynamic properties are enthalpy, entropy, specific volume and quality *x*, i.e., gas phase dryness in weight fraction. Noted, those values are constant at along each property line as in the Fig. 2.2.

In a heat pump system study, the refrigerant thermodynamic property at each main point of the refrigerant flow inside the system can be known by plotting the pressure and temperature value of each main point of the system. As in Fig. 2.3, a refrigerant flow of a heat pump system with cooling mode is shown by four line connected to each other from the main point showing a circulation inside the system.

Each point numbered in a circle in Fig. 2.3 has it own explanation of it thermodynamic properties and its state or phase of the fluid.

① : Refrigerant at exit of an evaporator, theoretically in gas phase. Evaporation temperature is t_4 °C and temperature at exit of the evaporator is t_1 °C so the vapor is super heated by $(t_1–t_4)$ °C.

②': Refrigerant at entrance of compressor. Refrigerant is heated along piping from exit of the evaporator to the compressor and again heated by high temperature in the compressor. Shown by ①-②', even if the temperature of the refrigerant at exit of the evaporator is as low as t_1 °C, its temperature rises to $t_{2'}$ °C at the suction valve of the compressor.

② : Refrigerant at delivery valve of the compressor, i.e. the compressor exit, after it is compressed by the compressor. If there is no heat exchange between ②' and ②, the temperature changes from $t_{2'}$ °C to t_2 °C along a constant entropy line, i.e., isentropic. The compression rate shall be $P_2/P_{2'}$.

③': The refrigerant enter the condenser at ② and its heat radiates (releases) to the surroundings mainly condenser. So its temperature drops from t_2 °C to $t_{3'}$ °C (③"). The heat radiates further and the refrigerant phase changes from vapor to the two phase flow of vapor and liquid. It becomes saturated liquid, i.e., quality $x = 0$, at ③'.

③ : Heat of the vapor which is liquefied entirely at ③' radiates (release) further and the liquid changes from the liquid of $t_{3'}$ °C to the super cooled liquid of t_3 °C. Then it enters the capillary tube. The refrigerant super cooled by $(t_{3'}-t_3)$ °C.

④ : The refrigerant state at exit of the capillary tube. Its temperature is t_4 °C and the quality x is x_4. The refrigerant returns to ① again, when the refrigerant is heated, i.e., gained heat energy from surrounding of the evaporator and its enthalpy increases.

Further study on the Mollier diagram in Fig. 2.3, a lot more information can be acknowledge about a designed heat pump system. Thus the cooling or refrigerating capacity of the system can be calculate as in formula below.

$$Q = (i_1 - i_4)G \tag{2.1}$$

Q : Refrigerating capacity (kJ/hr)
G : Mass flow rate (kg/hr) or M

Where

$$G = \eta_v \frac{V_{TH}}{v_s} \tag{2.2}$$

η_v : Volumetric efficiency of the compressor (m^3/hr)
V_{TH} : Theoretical exhaust volume of compressor (m^3/hr)
v_s : Specific volume of refrigerant at compressor inlet or suction, i.e., point ②' in Fig. 2.3

$$V_{TH} = V \times N \times \eta_m \tag{2.3}$$

V : Compressor displacement volume (m^3/rev)

N : Compressor motor revolution (rpm)

η_m : Compressor motor efficiency

The coefficient of performance (COP) of the heat pump system of Fig. 2.3 shall be as follows.

$$COP = \frac{T_2}{T_2 - T_1} \quad \text{or} \quad \frac{Q}{W} \tag{2.4}$$

Where

T_1 : Condensing temperature of refrigerant in the condenser (°K), i.e., t_3, °K in Fig. 2.3

T_2 : Evaporation temperature in the evaporator (°K), i.e. t_4 °K in Fig. 2.3

$$W = \frac{W_{TH}}{\eta_{ad}} \tag{2.5}$$

W_{TH} : Theoretical compressor power consumption

η_{ad} : Adiabatic efficiency

From Fig. 2.3, $\eta_{ad} = \frac{(i_2 - i_{2'})}{(i_{2''} - i_{2'})}$ (2.6)

Therefore, from all the formula,

$$COP = \frac{Q}{W} = \frac{\eta_v \cdot \eta_{ad} \cdot \eta_m \cdot G \frac{(i_1 - i_4)}{v_s}}{W_{TH}} = \frac{(i_1 - i_4)}{(i_{2''} - i_{2'})} \tag{2.7}$$

Understanding the magnitude of each point of thermodynamic properties in Mollier diagram and the formula of COP from it, shows that the main item that contribute most to the COP of the system are the adiabatic, motor and volumetric efficiency or the compressor. Makes the improvement on COP of a heat pump system should be focus on the compressor, thus through the years a lot of improvement has been done and further improvement shall be also focus on other devices efficiency such as the heat exchanger.

2.3 Review on heat pump system appliances high efficiency improvements

In this section, a review on the pass improvement of the heat pump system efficiency is presented. The big step on improvement of compressor was the inverter driven technology. Besides the compressor, other important step of improvement of other devices through the years also shall be reviewed onward.

Ito M. et al. (1977) reported on the development of high efficiency heat exchanger for ordinary room air conditioner with concentration on (1) Slit fins with high heat transfer coefficient, (2) Surface-treated fins with a small pressure drop of air in a wet condition, and (3) an internal-spirally-grooved tube with a high heat transfer performance. The slit fin comparing with the either plain or wavy fins shows approximately 35% higher heat transfer coefficient. While the surface treatment of fin made it hydrophilic and washed off the dew that formed on it. The desired hydrophilic property was achieved in rough surface fins provided with fine bumps of about 20μ on surface. Reported also the pressure drop of air flow in wet condition is approximately 30% smaller compare with the ordinary smooth and rough surface fins. Also a development of spirally grooved hairpin pipe that increase the boiling heat transfer coefficient 1.5 to 2 times higher than ordinary smooth inner surface of hairpin pipe tube without increasing the pressure drop value of the refrigerant cycle of the heat pump system.

Arai A. et al. (1981) reported a development of high efficiency reciprocating compressor and heat exchangers for small room air conditioner, i.e., with compressor capacities of 2.2 kW, 3.0 kW and 3.75 kW. This series of room air conditioner features high EER (energy efficiency ratio) with smaller depth of indoor units. Cooling EER values of the air conditioners increased from 2.55 to 2.72 for cooling type and from 2.53 to 2.70 for the heat pump type. The electric power consumptions have been reduced by about 20% as compared with conventional units. The compressor was developed by concentration on the improvement of volumetric and motor efficiency factors. While the heat exchanger improvement was divided into two section. Improvement of the air side heat transfer and the improvement of the refrigerant side heat transfer. The air side heat transfer was improved by concentrated on the development of new aluminum fin called super slit fin, and the improvement of the refrigerant side heat transfer was focusing on the inner grove of copper hairpin pipe development.

Tatsumi A. et al. (1982) reported on details of application of copper pipe tubes with inner groove which the trade name in Japan is “Thermo-fin Tube” and a special aluminum fin which very high in performance to air conditioner. This developed thermo-fin tube improved the heat transfer coefficient for boiling and condensation of a refrigerant inside the tube 1.6 to 2 times higher than the plain hairpin tube, while keeping the refrigerant pressure loss at the same level. The special aluminum fin has many small, upwardly convex louver strips which project against the air flow, and the surface heat transfer coefficient is approximately 70% higher than the conventional wavy fin, while the pressure loss of air flow is only 40% higher. When these hairpin and fins combinations are used in a air conditioner as heat exchangers, the heat transfer performance becomes approximately 70% higher in the condenser and 60% higher in the evaporator compared with the conventional heat exchanger made from plain copper tube and wavy fin. This combination of heat exchanger is still in use until today.

Kashiwazaki S. et al. (1989) continue the improvement and report on inverter technology in heat pump system, which not only increase the efficiency of the system, but have other features which is the compressor rotational speed is controlled to run according to the cooling or heating load. Thus operates at high capacity from the start until the room temperature reaches the thermostat setting in short time. After the desired temperature is reached, the air conditioner responds to the cooling or heating need by controlling the rotational speed of the compressor. By this, the air conditioner can operate with high EER, i.e. energy efficiency ratio. Since the air conditioner operates according to cooling or heating load, the compressor will continuously running with various speeds and a comfortable temperature is stably maintained.

Nakamura H. et al. (1995) reported on the development of an inverter driven heat pump room air conditioner which dehumidifies while reducing power consumption. This kind of dehumidification method uses an indoor heat exchanger which is divided into two heat exchangers. Indoor side air is cooled and dehumidified through one of the two indoor heat exchangers which operates as an evaporator, and is then reheated through the other one which operates as part of the condensers. A dehumidification control valve is installed in between the two heat exchangers as a restrictor in the dehumidification mode. The dehumidification capacity and reheating capacity are controlled by changing the rotational speed of both the compressor and the outdoor fan. By this, the temperature of the air flow can be controlled with low electric power consumption.

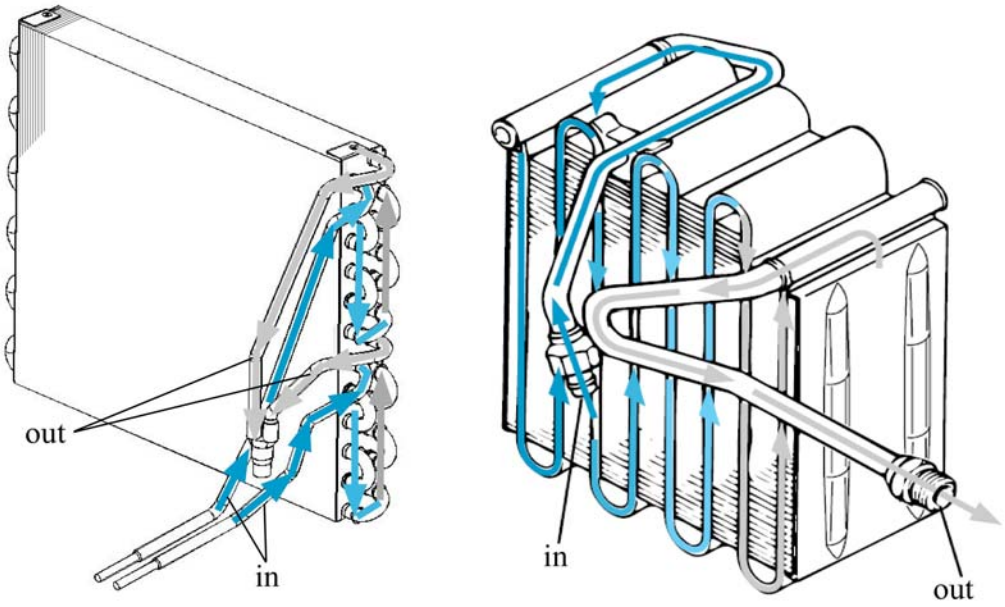

(a) Room air conditioner (b) Car air conditioner

Fig. 2.4 Sample of ordinary evaporators

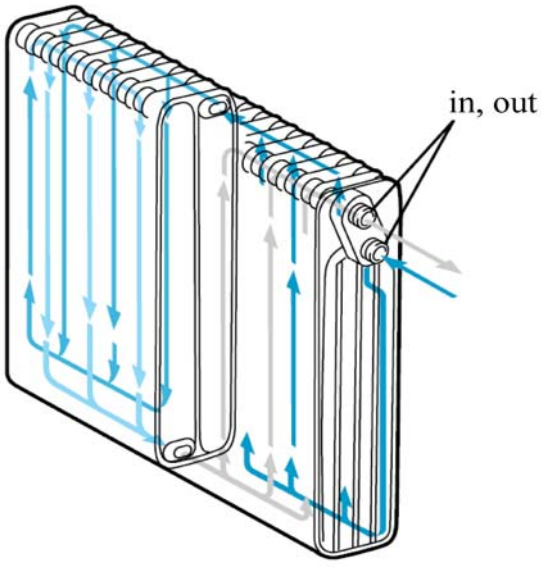

Fig. 2.5 Multi pass compact evaporator

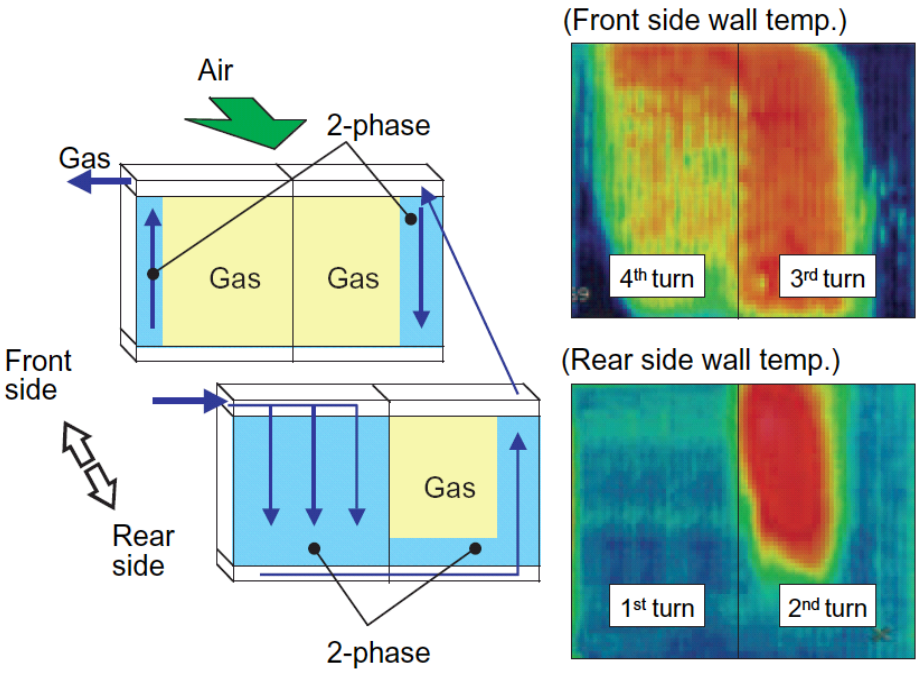

Fig. 2.6 Uneven surface temperature of evaporator as reported by T. Nakamura et al. (2003)

Nakamura T. et al. (2003) reported on the development of an ultra-thin and light-weight RS evaporator, i.e., revolutionary super-slim evaporator with only 38mm of thickness. About 35% of size reduction compared with the previous model which is the MS evaporator, i.e., multi-tank and super slim structure evaporator with 58mm of thickness. Though manage maintaining equivalent cooling performance of the system. In this development they have encounter some difficulty to maximize the performance of this compact evaporator. One of it is the mal-distribution of surface temperature of the evaporator. This occurs due to the uneven flow distribution of gas and liquid phase of refrigerant that flow from the evaporator dividing header to the multiple branches. As in Fig. 2.6, the developed compact evaporator consists of 4 sections, which the refrigerant flow was distributed to a multiple branches, combined and redistribution again 4 times before flow back to the compressor. This phenomenon makes the range of quality x of the refrigerant inside the evaporator wider. Thus makes the mal-distribution easy to occur and become worse. In this report however the technical counter measure of the problem has been found and applied for mass production. The counter measure was by additional segment or a throttle along dividing header for controlling the velocity of the refrigerant when entering the branches. By these the mal-distribution of the refrigerant flow problem of the developed evaporator was solved. However the

complete understanding of the phenomena still a mystery and to figure it out has become the main objective of our research. This is due to enhancement of new multi-pass evaporator with more compact and more branches to be developed in shorter period are become important.

2.4 Mal-distribution of two phase flow in a multi-pass channel

The Mal-distribution of gas and liquid in two phase flow is because the value of Void fraction and quality x at one cross section area in one conduit at one time is always different. Vist S. (2003), two phase flow mal-distribution is mainly because of the different physical properties (density, viscosity and surface tension) affects the inertial, gravitational, shear and capillary forces of the vapor and liquid phases. Bernoux P. et al. (2003) mentioned that flow mal-distribution in heat exchangers is a cause of deterioration of both thermal and hydraulic performances. Reviewing the Mueller (1987) and Mueller and Chiou (1988), mal-distribution could be caused by geometric factors (manifold cross-sectional design, branch couplings, location and orientation of the tubes) or operating factors (mass flow rate, flow regime and vapor fraction at the inlet of the manifold and heat load on the tubes).

2.5 Flow Pattern Transition in Two-Phase Gas-Liquid Flows

Barnea D. and Taitel Y. (1986) reported an extensive review about the two phase flow of gas and liquid characteristic in one conduit. Basically focus on the flow pattern identification, classification of the various characteristic to several groups of flow pattern. Explain on methods that have been developed and conducted by researchers on detection of the flow pattern of two-phase gas-liquid flow in a conduit. Also on prediction of flow pattern by using dimensional and dimensionless coordinates maps.

2.5.1 Flow pattern classification

Mainly, to classify the flow patterns is to group together flow configurations that have common character according to some defined definitions, i.e. same character, pertaining to the distribution of the interfaces and the mechanisms dominating pressure drop and heat and mass transfer.

The designation of flow patterns has not yet been accurately standardized, and the author proposed the following definitions, which are fairly close to the recent trend.

2.5.1.1 Horizontal pipes

Stratified (S), liquid flows at the bottom of the pipe with gas at the top. This includes the stratified smooth (SS) and stratified wavy (SW).

Intermittent (I), the liquid inventory in the pipe is non-uniformly distributed axially. This includes the slug and bubble flow patterns.

Annular (A), the liquid flows as a film around the pipe wall. This includes annular, annular-mist and wavy annular flow.

Dispersed bubble (DB), the gas phase is distributed as discrete bubbles within a continuous liquid phase.

Fig. 2.7 shows the flow pattern configuration in horizontal pipe flow.

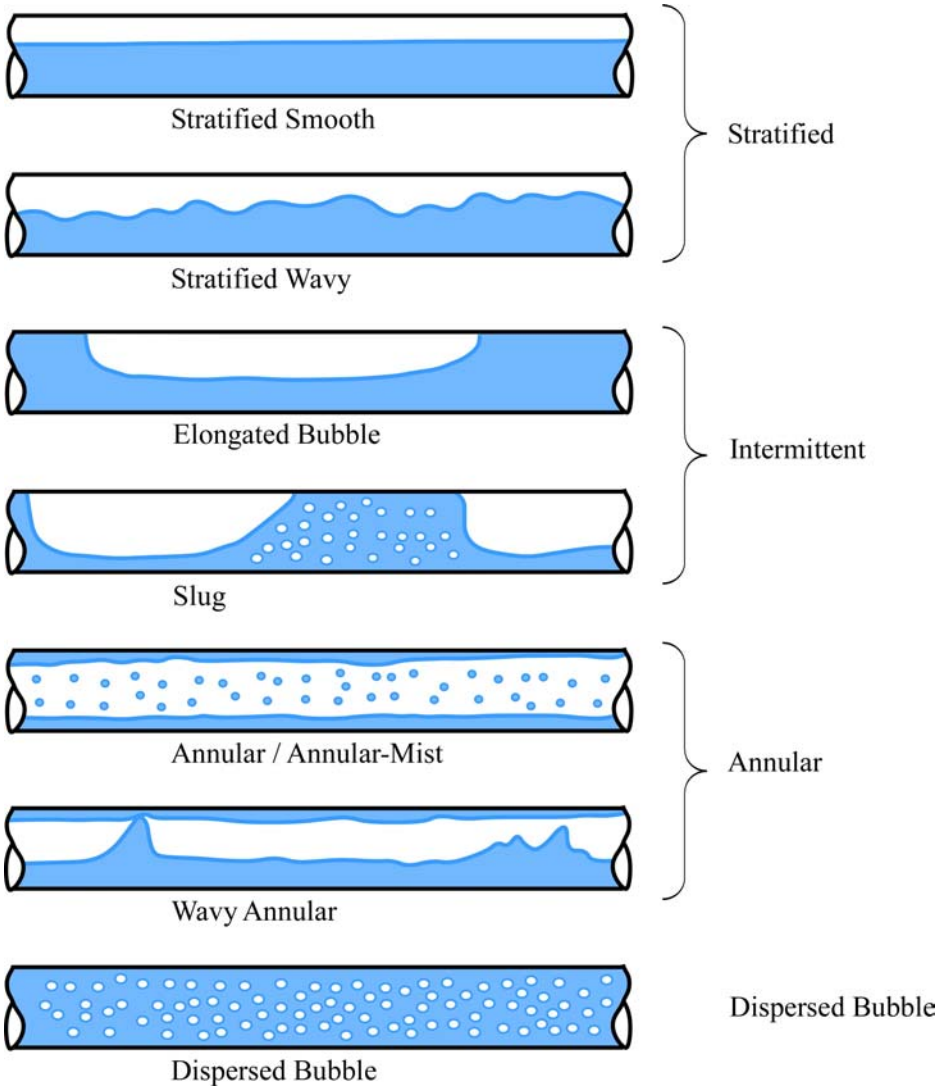

Fig. 2.7 Flow pattern in horizontal pipe flow

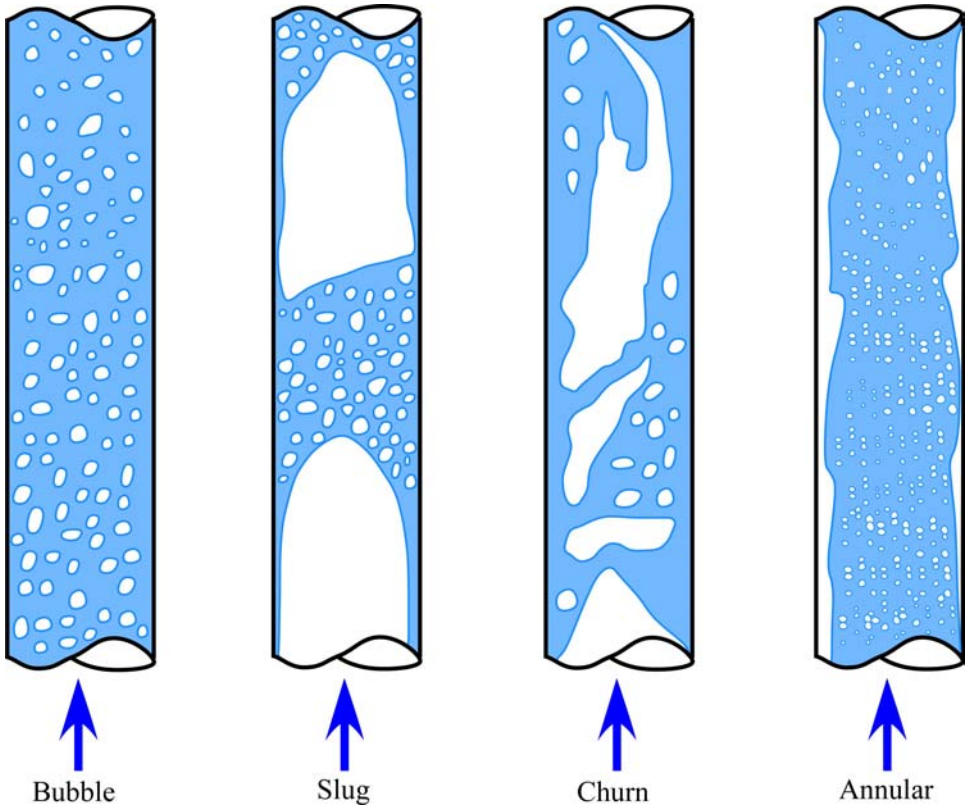

Fig. 2.8 Flow pattern in vertical pipe flow

2.5.1.2 Vertical pipes

Bubble flow (B), the gas phase is approximately uniformly distributed in the form of small discrete bubbles in a continuous liquid phase.

Slug flow (SL), most of the gas is located in large bullet-shaped bubbles that have a diameter almost equal to the pipe diameter and move upward.

Churn flow (CH), this is similar to slug flow, but is much more chaotic, frothy and disordered.

Annular flow (A), this flow is characterized by the continuity of the gas phase along the pipe in the core.

Fig. 2.8 shows the flow pattern configuration in vertical pipe flow.

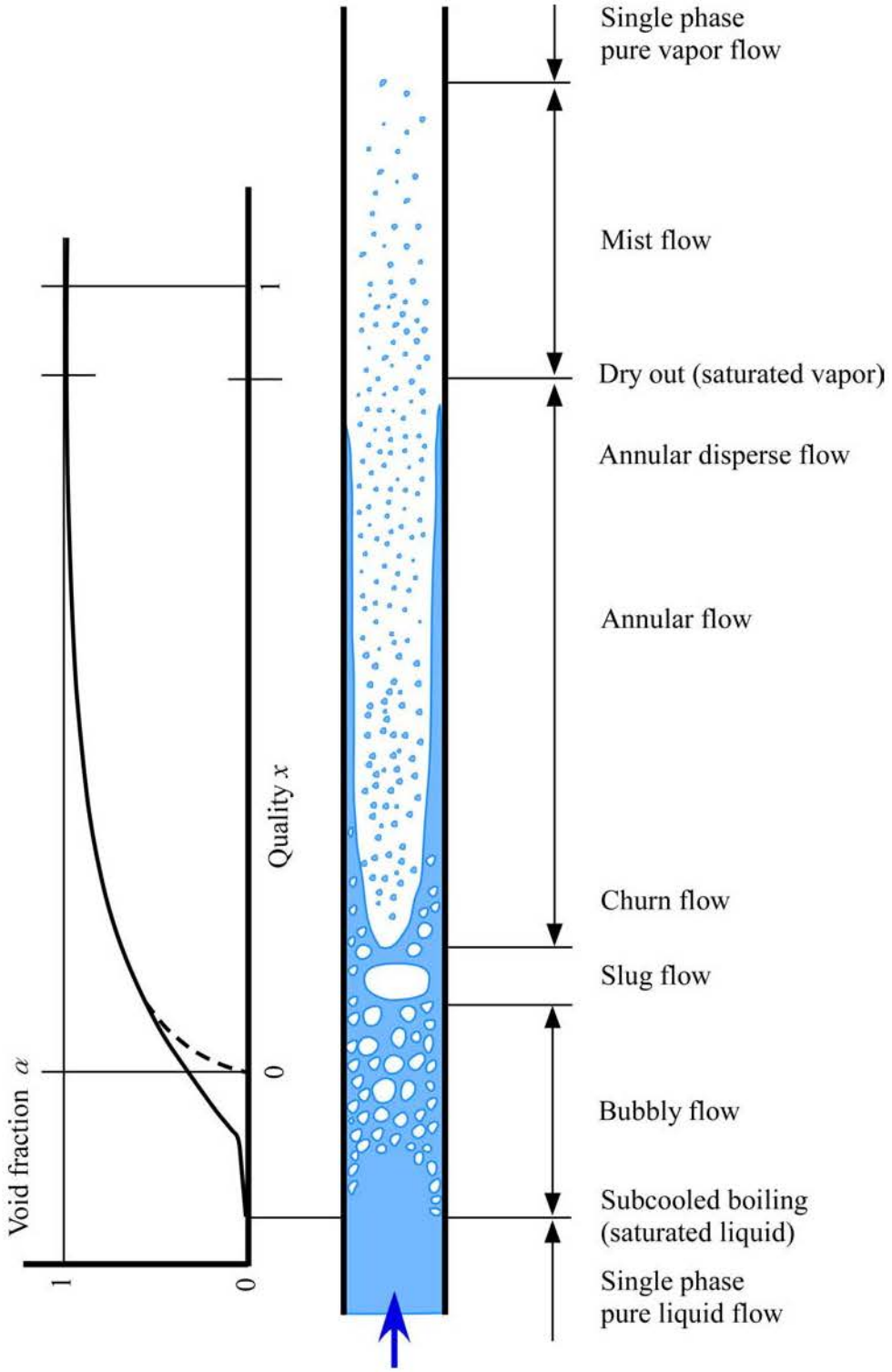

Fig. 2.9 Sequence of flow regimes observed during upward flow boiling in a vertical tube

2.5.2 Flow pattern detection

Flow pattern detection is important in two phase flow study. In most engineering problem regarding fluid dynamic, e.g., air conditioning refrigerant cycle, we have to detect and confirm the flow pattern first before take any counter measures of one problem. Although the two phase flow knowledge has small amount of efficiency contribution to be improved in one refrigerant cycle compare with the thermodynamic and air flow system, it is important due to air conditioning manufacturer competition on COP improvement.

There are two basic concepts to detect the flow pattern in one conduit, which are as follows.

2.5.2.1 Void fraction

There are a few techniques in detection by using this concept. The easiest and most substantiate is by visualization test, e.g., using a transparent pipe and high speed camera to capture the flow photograph and motion picture. However, the result is very subjective. To be more objective, we can use the "Conductance Probe" or "Hot Wire Probe" or "Photon Attenuation" technique.

Void fraction shows the relative of quantity of vapor (volume, area) to the total quantity of vapor and liquid in one define time in one conduit. It is difference with the quality of vapor x, as in a thermodynamic such in a refrigerant Mollier diagram. Quality x shows the ratio of weight of vapor to total weight of vapor and liquid in one defined conduit (or cut face area of one conduit).

Example, imagine a bottle have half of its volume with water, and another half with air. The void friction inside the bottle is 1/2, and if the weight of water is 5 times heavier than air; the quality x is 1/6.

2.5.2.2 Pressure Fluctuation

Base on experimental observation, the pressure fluctuations along a pipe seem to depend on the flow pattern. The analysis of pressure fluctuations to identify flow pattern was used by Hubbard and Dukler who measured the pressure fluctuations in horizontal air-water flows and developed a method to determine the flow pattern from the spectral

distribution of the wall pressure fluctuations. However, they could not discriminate between stratified and annular flows or between the dispersed liquid and dispersed gas flows by using this method.

The Void detection method seems to be superior to the pressure detection method because void detection is more closely related to the fluids distribution.

2.5.3 Flow pattern prediction

The author explained on how to make a map with an experimental data to predict other various kind of gas-liquid two phase flow pattern. However, due to various amount of parameter, make it difficult and complicated to show it in a single map. Basically, experimental data on flow patterns and the transition boundaries is map on two dimensional or dimensionless coordinates plot.

2.5.3.1 Dimensional coordinate's maps

Two basic types of coordinates are use for this mapping. Such as superficial velocities, mass superficial velocities and momentum flux. However, they are inherently limited to the range of data and flow conditions under which the experiments were conducted.

2.5.3.2 Dimensionless coordinate's maps

Some kind of dimensionless groups are used as coordinates. Dimensionless analysis is the straightforward approach to select the proper dimensionless coordinates. It is applied by "guessing" the physical variables that affect the flow patterns. Under isothermal incompressible condition these are all the dimensional parameters.

(1, 2) Gas, liquid superficial velocity (j_g, j_l) [$m.s^{-1}$]
(3, 4) Gas, liquid density (ρ_g, ρ_l) [$kg.m^{-3}$]
(5, 6) Gas, liquid viscosity (μ_g, μ_l) [$kg.m^{-1}.s^{-1}$]
(7) Pipe diameter (D) [m]
(8) Pipe roughness (ε) [m]
(9) Pipe inclination angle (β) [none]
(10) Acceleration of gravity (g) [$m.s^{-2}$]
(11) Liquid surface tension (σ) [$kg.s^{-2}$]
(12) Solid liquid gas contact wetting angle (γ) [none]

The flow pattern transition boundaries should be a function of all these variables or parameters. Note that this is already a reduced set of variables as it is assumed that the

entrance geometry has no influence on the steady state flow pattern. Using Buckingham Π method, i.e., as below,

$\Phi(\Pi_1, \Pi_2 \ldots \Pi_{n-k}) = 0$ or equivalently $\Pi_1 = \Phi(\Pi_2 \ldots \Pi_{n-k})$

k is the number of fundamental dimensions required to describe the n variables, which in this case is only three ,i.e., mass (M), length (L) and time (T). There will be k primary variables and the remaining j=(n-k) variables can be expressed as (n-k) dimensionless and independent quantities or 'Pi groups', $\Pi_1, \Pi_2 \ldots \Pi_{n-k}$. So, the quantity of dimensionless variables in this case shall be (12-3) = 9.

By using this method the matrix for the each dimensional parameter and fundamental dimension is as below.

	j_g	j_l	ρ_g	ρ_l	μ_g	μ_l	D	ε	β	g	σ	γ
M	0	0	1	1	1	1	0	0	0	0	1	0
L	1	1	-3	-3	-1	-1	1	1	0	1	0	0
T	-1	-1	0	0	-1	-1	0	0	0	-2	-2	0

(2.8)

$$\Pi_1 = j_l \rho_l^b \mu_l^c D^d \tag{2.9}$$

$$M : b + c = 0, \tag{2.10}$$

$$L : 1 - 3b - c + d = 0, \tag{2.11}$$

$$T : -1 - c = 0, \tag{2.12}$$

From above equation, b = 1, c = -1, d = 1

$$\therefore \pi_1 = \frac{j_l \rho_l D}{\mu_l} \tag{2.13}$$

Also the other 8 dimensionless parameters ($\Pi_2 \ldots \Pi_{n-k}$) are as below.

$$\frac{j_g \rho_l D}{\mu_l}, \ \frac{g \rho_l^2 D^3}{\mu_l^2}, \ \frac{\rho_g}{\rho_l}, \ \frac{\mu_g}{\mu_l}, \ \frac{\sigma \rho_l D}{\mu_l^2}, \ \beta, \ \frac{\varepsilon}{D}, \ \gamma \tag{2.14}$$

This list of dimensionless parameter is not unique. An infinite number of sets of dimensionless parameters exist. The normal way is to fine an explicit functional relation among one set of variables base on experimental data. However, it is impractical to find the relation among nine parameters base only upon experimental data. Thus, the practical implementation of using dimensionless analysis to correlate the experimental

data that makes this “straightforward” approach unrealistic and impossible.

A different logical method of solving problems as complex as flow pattern transition is by understanding and identifying the important physical mechanisms in each transition. And a mathematical model that describes each transition can be formulated.

The well known Baker map used a mixed coordinate system. G_g/λ vs. $G_l\lambda\psi/G_g$, where G_g is the gas mass velocity (a dimensional coordinate) and G_l/G_g is a ratio of liquid and gas mass flow rates. The fluid properties enter as the dimensionless correction factors defined as

$$\lambda = \left[\left(\frac{\rho_g}{\rho_A}\right)\left(\frac{\rho_l}{\rho_W}\right)\right]^{1/2}$$
$$\psi = \frac{\sigma_W}{\sigma}\left[\frac{\mu_l}{\mu_W}\left(\frac{\rho_W}{\rho_l}\right)^2\right]^{1/3} \qquad (2.15)$$

Where, ρ_g, ρ_l, ρ_A and ρ_W are the gas, liquid, air and water densities respectively. μ_l and μ_W are the liquid and water viscosities. σ and σ_W are the liquid and water surface tensions. Note that all water and air properties are the values at atmospheric pressure and temperature of 20ºC.

2.6 Review on study of two phase flow distribution in multi-pass channel

2.6.1 Study on two phase flow distribution behavior of real refrigerant

Watanabe et al. (1995) reported on the two phase flow distribution study on refrigerant R11 in a test channel with a horizontal rounded shaped header (ID 20 mm) with four upward branches (rounded shape with ID 6 mm), simulating an automobile air-conditioning evaporator. Several geometrical parameters that effect the two phase flow distribution in the test channel were identified. They are the cross-sectional area ratio of branch and header, also the location and orientation of branches. In addition, other parameters such as operational factors which are the mass flow rate M or mass flux G and quality x in the header entrance and the heat load on the branches, are important for the two-phase flow distribution in the multi-flow type channel. Moreover, it has been found that the gas phase was preferentially distributed to the first branch and that the liquid phase level in the header was rising further downstream due to the gas

phase take-off. The last branch of test channel was always the one with the lowest gas phase flow distribution ratio. Reducing the number of the branches changed only the quantitative results. Qualitatively, the two-phase flow distribution results were almost the same. The author also pointed out, adding heat load to the branches reduced the mal-distribution of the two-phase flow in the test channel.

Watanabe et al. (1996) in their first report studied experimentally the characteristic of two-phase refrigerant HCFC-123 flow distribution. The test channel consists of a rounded shape vertical upward header with five horizontal rounded shape branches. Both header and branches inner diameter are 6 mm. A number of tests were made under a constant mixture mass flux at the inlet of header, G = 430 kg/m^{2}s, where header inlet quality x and total heat input Q are varied from 0.07 to 0.3, from 0 to 900 W, respectively. Experimental data indicates that there were some differences in data trend between low and high quality x region. At high quality x condition, i.e., $x > 0.1$, gas phase flow tends to be unevenly distributed to each pass with the peak at branch no. 3, and the variation of Q merely affects the flow distribution profiles. On the other hand, at low quality x region, gas phase flow distribution is dominated by global conditions of whole system, where liquid flow is affected by local flow state in the vicinity of each junction.

In Watanabe et al. (1996) second report, the effect of unequal heating load, i.e., step heating load, applied to each pass two-phase flow distribution in multi-pass evaporator was experimentally studied. Four step heating patterns were determined to take into account the flow rate and the flow direction of the air flow outside of the evaporator tube in the actual heat exchanger. Three total heat input conditions were taken as Q = 300, 450, 600 W. For each heating condition, header inlet quality was varied from 0.07 to 0.3. From the experimental result of flow distribution, it was found that step heating load obviously affect the flow distribution. Step heating load causes the difference among the pressure at the inlet of each pass, which affect the liquid division ratio at the junction. But this effect does not clearly appear when the momentum flux of fluid in the header just before the branch is large. It is concluded that liquid phase flow is directed by the kinetic condition in the vicinity of each junction of the branch. Together with the results obtained at the authors' first report, the empirical correlation for estimating the liquid division ratio at each junction of the branch which was successfully applied to any condition of heating load was derived. Additionally, from the result of pressure drop measurement, it was found that the gas phase flow distribution had strong relation to the profile of the pressure drop along each pass.

Watanabe et al. (1998), as an extension of their earlier work, also have studied the distribution of an annular flow to the multiple parallel branches from a header, which this time also all made of 6mm inner diameter tubes using HCFC-123. They have reported that, for the second branch, the values of η referred as "correction value", defined as the ratio of the measured values of W_{f3}/W_{f1} to the predicted ones based on the model by Hwang et al. (1988) were smaller than the unity, and the discrepancy increased with larger volumetric flux of gas in the main (at the immediate upstream of the second branch). Small value of η at the second branch is attributed to the deficiency of the annular liquid film due to the upstream branch, and this effect is accumulated at the downstream junctions of the header. That is, the value of η at the third junction is the square value of that at the second junction. Likewise, the value of η at the fourth junction is the third power value of that at the second junction, etc. Therefore, in general, Watanabe et al. (1998) proposed a simple empirical relation for the standardized correction value as follows:

$$\eta_{St} = 1 - 0.0087 k_{T,M}{}^{0.435} \qquad (2.16)$$

Here $k_{T,M}$ stands for the two-phase momentum flux in the main (header) at immediate upstream of each channel. However, this equation does not take account of the distance effect between the branches. Also, the relation is not applicable near the end plate due to flow reversal (or flow recirculation) similar to the case already noted.

Bernoux P. et al. (2001) presents experimental results on two-phase flow distribution of real refrigerant R-113 in the inlet port of a compact heat exchanger. A testing apparatus consist with a horizontal header and eight downward rectangular branches have been instrumented. The distribution of gas and liquid phases is obtained by measurement of the total mass flow rate and the calculation of the quality x. The presence of transparent windows allows the observation of two-phase flow pattern for different operating conditions. Comparison between quantitative and qualitative results gives a general understanding of the process of phase distribution and is the starting point of other studies with more complex geometries.

Vist S. et al. (2004) presented an experimental study to investigate two-phase flow distribution of refrigerant R-134a in compact heat exchanger manifolds, i.e., a header with a multiple branches connected to it. An experimental test rig to measure the flow distribution in realistic manifold geometries and under relevant operating conditions was built. To elucidate the effect on the flow distribution, the following factors are

investigated: vapor fraction at the header entrance, heating load on the heat exchanger branches, i.e., heat exchanger tubes, diameter of the header and header entrance inlet tube length. The experimental system simulated an evaporator for an automobile air conditioner with a design cooling capacity of 5 kW. From the horizontal header, the two-phase refrigerant flow was distributed in ten parallel heat exchanger tubes. The orientation of the test rig could be varied to measure both upward and downward flow out of the manifold. To ensure similarity to an actual heat exchanger, counter-flowing water was used as heat source in the evaporator section. The experimental setup made it possible to measure the heat added to the evaporating refrigerant in each tube by using separate water flow circuits.

Koyama S. et al. (2006) carried out experiments on refrigerant flow distribution inside an evaporator header. A test section consists of a 9 mm inner diameter header and six vertically downward mini channel-branching conduits. Since the CO_2 system operates at around the supercritical conditions, it is impossible to observe the flow regime for CO_2 and so R134a is used as the working fluid in this study. The modified Baker flow pattern map is applied to define the equivalent experimental conditions for both R134a and CO_2. The experiments are conducted at saturation temperature of about 21° C, refrigerant mass flow rate of about 30 kg/h, and average vapor quality x in the header inlet of about 0.1, 0.2, 0.3 and 0.4. As the conclusion of the study, the liquid distributes most easily at the first branch and the vapor flows down directly the downstream of the header, probably due to that the inertia effect in the downstream direction is more obvious than the gravity effect. The inertia and gravity act in different directions for downward flow. The vapor quality x in the header inlet influences the vapor phase and liquid phase distributions. Increasing the vapor quality in the header inlet gives better distribution of the vapor phase. However, the liquid phase is generally better distributed for the low inlet vapor quality flows. The phase separation increases with increase of mal-distribution. No phase separation means that all vapor qualities from the header inlet to the downstream of the header is constant.

Ahmad M. et al. (2009), an experimental loop representing a compact plate heat exchanger was built up to study the two-phase distribution in the different header channels. The test section consists of a cylindrical horizontal header and eight rectangular channels in which the liquid and vapor flow rates are evaluated and the flow inside the header can be visualized. Several geometrical and functional parameters to study the two-phase distribution were tested using “HFE 7100” at a temperature close to 57°C and a pressure close to 100kPa. The flow rate in each channel was measured and

the vapor fraction was calculated by an enthalpy balance based on measurements of flow rates at the two sides of the exchanger and that of temperature and pressure. For the case of vertically downward channels, measurement showed better a distribution for both phases as mass quality x increases. The influence of the inlet mass flux on the distribution was more visible at high pace. Reducing the header diameter deteriorated the two-phase distribution. Experiment with horizontal distribution channels showed enhanced vapor and liquid distribution even at low inlet mass quality. For the case of vertically upward channels, flow distribution was highly heterogeneous even for high inlet mass quality. The presence of expansion devices has a great influence on the flow structure inside the header. The use of an expansion orifice produces a liquid jet configuration inside the header. High jet velocities rendered the distribution more homogeneous. The presence of a splashing grid at the inlet produces multidirectional droplets that that highly improves the two-phase distribution. The two-phase flow distribution in a compact heat exchanger is strictly related to the flow configuration at the header inlet and the two-phase momentum together with the header geometry. The presence of high-momentum phases and especially that of liquid favors the occurrence of impacts, fragmentation of liquid phase, the presence of a homogenized multidirectional two-phase structure and this renders the distribution more homogeneous. This study treats certain specific geometries but the comparison between quantitative and qualitative obtained results allows the understanding of the physical phenomena of the two-phase flow inside the header and the improvement of the flow distribution by adjusting the convenient functional and geometrical parameters.

Table 2.1 Recent up to date works on the flow distribution in a test channel contain a header with multiple parallel branches using real refrigerant as testing fluid

Authors	Header/ Branches Orient-ation	Header size (mm)	Branch quantity / size (mm)	Testing condition (Flow pattern) at header entrance etc.	Fluid	Remark
Watanabe M. et al. (1995)	H / VU	Ø20	4 / Ø 6	Non-heating mode : $x_{in} < 0.4$ G_{in}= 40-120 kg/m^{2}s Heating mode: q''= 6.25 - 25.4 kW/m^2 G_{in}= 80 kg/m^{2}s (stratified)	R-11	-Flow distribution depends strongly on the mass flux and header inlet quality
Watanabe M. et al. (1996) 1st report	VU / H	Ø 6	5 / Ø 6	G_{in}= 430 kg/m^{2}s x_{in} = 0.07 - 0.3 Q_{in} = 0 – 900 W Equal heat load on each branch. (slug, Annular)	HCFC -123	-Gas phase flow distribution uniformity comparatively better at quality x < 0.1
Watanabe M. et al. (1996) 2nd report	VU / H	Ø 6	5 / Ø 6	G_{in}= 430 kg/m^{2}s x_{in} = 0.07 - 0.3 Q_{in} =300, 450, 600 W Unequal heat load on each branch. (slug, Annular)	HCFC -123	-Un equal heat load affect the liquid flow distribution -Liquid phase flow is directed by the kinetic condition in the vicinity of each branch junction
Watanabe M. et al. (1998)	VU / H	Ø 6	5 / Ø 6	G_{in} ~ 430 kg/m^{2}s $x_{in} < 0.3$ (slug, Annular)	HCFC -123	-Effect of heat load on the channels is minor
Bernoux P. et al. (2001)	H / VD	Ø 50	8 / 2x50	G_{in} = 35-100 kg/m^{2}s x_{in} = 0.1 – 0.8 p = 0.07 – 0.15 mPa (slug, Annular)	R- 113	-Effect of the inlet flow pattern is large
Vist S. et al. (2004)	H / VU H / VD	Ø 16, Ø 8	10 / Ø 4	M_{in} = 90-162 kg/hr x_{in} = 0.11 – 0.5 p_{in} = 690-710 kPa (Churn, Annular)	R-134a	-Effect of diameter of the header cross section in minor
Koyama S. et al. (2006)	H / VD	Ø9	6 /Ø0.85	M_{in} = 30 kg/h x_{in} = 0.1, 0.2, 0.3, 0.4 Intrusion height h = 4.5 mm (Slug, Stratified)	R-134a	-The inertia and gravity influenced the flow distribution in different directions for downward flow -Quality x influences both phase distributions -Phase separation increases by increase of mal-distribution
Ahmad M. et al. (2009)	H / VD H / VU	Ø50, Ø30, Ø17.3	8 / 2x50	G_{in} = 70-400 kg/m^{2}s x_{in} = 0.05 – 0.45 presence of expansion devices (Stratified, Annular)	HFE 7100	-The influence of mass flux is more visible at high pace -The two-phase flow distribution is strictly related to the flow configuration at the header inlet and the two-phase momentum also with the header geometry

H: Horizontal; VU: Vertical Upwards; VD: Vertical Downwards

2.6.2 Study on two phase flow distribution behavior of air-water

Osakabe M. et al. (1999) studied single-phase (air) and two-phase (air-water) distribution in a horizontal manifold (40 x 40 mm in cross-section) with four vertical branch tubes (ID 10 mm) in upward configuration. Air and water flow rates in each branch tube were recorded. When introducing a small amount of bubbles in the manifold, the water distribution rate to the first branch tube increased as in an airlift pump, while the flow rates to the other branch tubes decreased. Increasing the inlet air flow rate, the water flow rate to the first branch tube reached a maximum and tended to decrease. At even larger inlet air flow rates, the flow pattern at the manifold inlet became stratified and the first two branch tubes were starved with water. In a further study by Horiki and Osakabe (1999), the branch tubes protruded into the manifold, and the effect of protrusion length on the water distribution was studied. By increasing the protrusion length, mal-distribution of the water was reduced because the gas-phase was distributed more evenly. The best result was obtained when the four branch tubes were protruded into the center of the manifold.

Lee J. K. et al. (2004) examine the distribution of two-phase annular flow at header−channel junctions simulating the corresponding parts of compact heat exchangers. The parameters considered were mass quality at the inlet of the vertical header and intrusion depth of the horizontal channels into the header wall. The cross-section of the header and the channels were fixed to 24 x 24 mm and 22 x 1.8 mm, respectively. Three different intrusion depths (0, 6 and 12 mm beyond the inner wall of the header) were tested for the mass flux and the mass quality x ranges of 54−134 kg/m^{2}s and 0.2−0.5, respectively. Air and water were used as the test fluids. With zero intrusion-depth, less amount of liquid was separated out through the channels at the rear part. However, with the deeper intrusion (6 and 12 mm), the trend was reversed. The deeper intrusion hindered the liquid to flow into the channels installed at the fore part of the header. Finally, a uniform liquid-flow distribution through the parallel channels could be achieved simply by adjusting the intrusion depth.

Webb R. et al. (2005) addresses two-phase flow distribution phenomena in multiple header–tube junctions used in heat exchangers. Because of phase separation, it is very difficult to obtain uniform two-phase flow distribution to the branch tubes. The flow distribution is strongly influenced by the header orientation (horizontal or vertical) and the number of branch tubes. Other factors that influence the flow distribution are the

flow direction in the header (up-flow or down-flow), the header shape and tube end projection into the header, and the location and orientation of the inlet and exit connections. The source of mal-distribution is the flow in the dividing headers. This investigation shows that solutions, which provide uniform flow distribution, are very design-specific. Change of the geometry or operating parameters will require modification of the design.

Katsuta M. et al. (2008) reported on improvement two-phase flow mal-distribution in multi-pass tube and to establish its prediction method. The experimental study uses air-water two-phase flow and multi-pass channel that consist of horizontal header or pipe and three downward branches. The study focusing on the effects of branch pitch length and insertion or intrusion height. As a result, the longer branch pitch makes the phase separation identical to that of single T-junction. Also, the insertion depresses the liquid diversion into the branch. Thus, controlling insertion depth of each branch can be effective for realize equal distribution.

Marchitto A. et al. (2008), measurements of the two-phase air−water distributions occurring in a cylindrical horizontal header supplying 16 vertical branches are reported for upward flow. The effects of the operating conditions, of the header-channel (branch) distribution area ratios and of the inlet port orifice plates (located between header and branches inlet) were investigated. The flow rates of each phase flowing in the different branches were measured. Time varying, void fraction data were also analyzed to characterize the two-phase flow patterns. Video records were taken in order to infer different flow patterns (from intermittent to annular) inside the header channel system. Experimental results showed that the operating conditions exerted a strong influence on the structure of the two-phase flow pattern inside the header and therefore on the flow distribution to the branches. Thus, confirm the complexity of two-phase flow distribution phenomena and the difficulty of designing a header−multiple channel system able to achieve even distributions for a given range of operating conditions. Indeed, the whole experimental activity indicated that the flow pattern at the header entrance and flow rate distribution inside each vertical channel depend on the interaction of several coexisting factors: gas and liquid superficial velocity, area restriction ratio, presence and geometry of an inlet nozzle, and other geometrical parameters (inlet port length and diameter, orifice diameter).

The air and water flow distribution are experimentally studied by Kim N-H. et al. (2008), for a heat exchanger composed of round headers and 10 flat tubes. The effects of tube protrusion depth as well as header mass flux, and quality are investigated, and

the results are compared with previous 30 channel data. The flow at the header inlet is annular. For the downward flow configuration, water flow distribution is significantly affected by tube protrusion depth. For flush-mounted geometry, significant portion of water flows through frontal part of the header. As the protrusion depth increases, more water is forced to rear part of the header. The effect of header mass flux or quality is qualitatively the same as that of the protrusion depth. For the upward flow configuration, however, significant portion of water flows through rear part of the header. The effect of protrusion depth is the same as that of the downward flow. However, the effect of header mass flux or quality is opposite to the downward flow case. The general flow distribution trend of the 10 channel is approximately the same that of the 30 channel, although the effects of tube protrusion depth, header mass flux and quality on flow distribution are much stronger. Comparison of the difference between the maximum and the minimum water flow, and the comparison of the standard deviation of the water flow ratio reveal that the flow distribution is more uniform for the 10 channel as compared with the 30 channel.

Lee J. K. (2009) again examine the flow distribution of two-phase mixture to parallel channels and to investigate the flow behavior at header-channel junctions simulating the corresponding parts of compact heat exchangers. This time the cross-section of the header and the channels were fixed to 14 x 14mm and 12 x 1.6mm, respectively. The mass flux and the mass quality ranges were 70-165 kg/m^2s and 0.3-0.7, respectively. Air and water were used as the test fluids. The two-phase mixture flows upwards through a square vertical header connected to 15 parallel, horizontal rectangular channels. The experiments were carried out for the annular flow regime at the header inlet. This is because the annular flow pattern is mostly probable to occur once the mass quality becomes large (larger than 0.1). At the same time, in many practical cases, the channels are in a flat rectangular shape with sub-channels divided by membranes (thin wall) to enhance heat transfer performance. The distribution shape of the flow through the channels was determined by the flow recirculation occurred at the rear part of the header. The header flow consists of three zones, named region A, B and C, regardless inlet flow rates of liquid. At the fore part of the header (region A), the amount of the liquid separation out through the channels was decreased as the two-phase mixture proceeds to the down stream direction. At the immediate upstream of the end plate (region C), the amount of the liquid separation also decreased but the differences of the liquid flow rates between the channels are not large due to the flow recirculation. In between those region (i.e., in region B), the liquid separation rate increased along the header flow because of the interaction between the reverse flow (by the flow recirculation in region

C) and the forward flow (in region A). For the gas flow distribution, the trend appeared opposite to liquid case throughout the header section, but the variation is relatively small. Moreover, the effect of the membranes in channels was investigated, but that was minor.

Katsuta M. et al. (2009) reported again on mal-distribution of two-phase flow in multi-pass tube improvement and to establish its prediction method, using the same apparatus and same fluid but this time focus on the effects of branch's local geometry. As a result, the vapor phase flow has been basically understood to be the uniform distribution. On the other hand, the liquid phase flow distribution is changed by the effect of branch's local geometry such as branch diameter and insertion and end-effect.

Table 2.2 Recent up to date works on the flow distribution in a test channel contain a header with multiple parallel branches using air-water as testing fluid

Authors	Header/ Branches Orient-ation	Header size (mm)	Branch quantity / size (mm)	Testing condition (Flow pattern) at header entrance etc.	Fluid	Remark
Osakabe M. et al. (1999)	H / VU	40 x 40	4 / Ø10	Re_{in} = 2000-4000 (Bubbly, Stratified)	Air - Water	-Prediction of the flow distribution using the Single T-junction model
Lee J. K. et al. (2004)	VU / H	24 x 24	6 / 22 x 1.8	G_{in} = 50-134 kg/m^{2}s x_{in} = 0.2 – 0.5 Intrusion depth h = 0, 6, 12 mm (Annular)	Air - Water	-The uniform distribution through the parallel channels could be achieved by adjusting the intrusion depth
Webb R. et al. (2005)	H / VD H / VU	D-shape, D_h=32	D_h=1.3	M_{in} = 36.01-189.19 kg/hr,	Air - Water	-Change of the geometry or operating parameters require modification of the designed
Katsuta M. et al. (2008)	H / VD	Ø10	3 / Ø10	M_{in} = 30 - 120 kg/hr, x_{in} = 0.2-0.5;(R-134a) Intrusion h = 0-6 mm (Slug, Annular)	Air - Water	-controlling intrusion depth of each branch can be effective for realize uniform distribution
Marchitto A. et al. (2008)	H / VU	Ø26	16 /15x18	j_A = 1.50-16.50 m/s j_W = 0.20-1.20 m/s orifice dia. = 2-6 mm (Intermittent, Annular)	Air - Water	-The flow pattern at the header entrance and flow distribution rate depend on the interaction of: fluid superficial velocities, area restriction ratio; inlet nozzle; geometrical parameters
Kim N-H et al. (2008)	H / VD H / VU	Ø17	10 / Al- port tube D_h=1.32 (8 holes)	G_{in} = 70-130 kg/m^{2}s x_{in} = 0.2 – 0.6 protrusion depth h = non-dimensional, 0, 4.25, 8.5 mm (Annular)	Air - Water	-Downward flow, the effect of header mass flux or quality is qualitatively the same as that of the protrusion depth -Upward flow, the protrusion depth effects the distribution. However, the effect of header mass flux or quality is minor
Lee J. K. et al. (2009)	VU / H	14 x 14	15 / 12 x 1.6 (with/ without Al-port)	G_{in} = 70-165 kg/m^{2}s x_{in} = 0.3 – 0.7 (Annular)	Air - Water	-The flow distribution through branches is determined by the flow recirculation occurred at the rear part of the header. The header flow consists of three zones, regardless inlet flow rates of liquid -The effect of the or Al-port in channels was minor
Katsuta M. et al. (2009)	H / VD	Ø10	3 / Ø10	M_{in} = 30 - 120 kg/hr, x_{in} = 0.2-0.5;(R-134a) (Slug, Annular)	Air - Water	-the liquid phase flow distribution changed by the effect of branch local geometry

H: Horizontal; VU: Vertical Upwards; VD: Vertical Downwards; D_h: Hydraulic Diameter

2.6.3 Parameters that reported to be significant to the flow distribution behavior

Reported by Lee J. K (2006), the significant parameters that involved directly and indirectly to the uniformity of flow distribution inside channel that simulate the multi-pass flow evaporator has been reviewed and summarized as in Table 2.3 below.

Table 2.3 Relative significance of parameters tested (Summary)

Parameters	Relative significance
Header inlet direction and flow pattern, Header orientation (vertical, horizontal), Channel orientation, Channel intrusion depth	Major effect
Header size and cross-sectional shape, Number of junctions to channels, Channel spacing, Header inlet flow rate, Channel membranes, Channel heat load, Channel length	Minor effect
Fluid properties, Fouling, Manufacturing tolerances	Insufficient information to judge

Chapter 3

Experimental Apparatus

3.1 Chapter overview

This chapter explains about the testing apparatus of the testing that has been done on this research through all the years. It shall include all the explanation on the testing methods, setup, instrument specifications and tolerances. Also, the details of the test channel dimensions and assemblies shall be discussed.

In this research the study of two phase flow distribution behavior in a compact evaporator has been divided into 2 segments. The first segment is the study on parameters that influence the flow distribution uniformity. Using air and water as the testing fluid, this segment mainly concentrate on the parameters that influence the uniformity of liquid phase flow, due to our study is focus on the increment of efficiency performance of a heat pump system. The parameters that have been studied in this research are: flow pattern at the header entrance, superficial velocities of each phase flow of fluid at the header entrance, backpressure distribution along the combining header and pressure loss create from the specification of branch profiles. The testing shall include the flow distribution measurement of air and water in a selected test conditions, also a measurement of pressure distribution at along the dividing and combining headers.

The second segment of this research is the study on the similarities of real

refrigerant and air-water two phase flow distribution behavior. The testing involved in this segment shall include the visual observation on the test channel of a real refrigerant (R-134a) and air-water flow. A motion picture and photos has been taken for qualitative judgment on which inlet condition (that has been setup a few) to matched or being similar to the real refrigerant flow. Also, a flow distribution of air-water flow has been measured quantitatively and compared qualitatively to the flow distribution of real refrigerant.

3.2 First segment: Study on parameters that influence the flow distribution

3.2.1 Test channel

Figure 3.1 is a schematic diagram of the experimental apparatus. The experiments were conducted with an isothermal air-water flow system. Air and water was controlled at 20 °C in the constant temperature bath and it was supplied to the test channel after flowing through the mass flow controller (air) or mass flow meter (water). In this segment a test channel consist of 10 branches has been used and to simulate the actual operating condition of the evaporator equipped in the compartment of an automobile, the dividing header is set horizontally.

Fig. 3.2 shows details of the test channel. The body of test channel is made of transparent acrylic resin plates. The dividing header has a square cross section of 20 mm × 20 mm and a length of 255 mm. 10 upward branches are connected to this header. We tested two kinds of branch profiles with different pressure loss characteristics. One is a flat tube with a cross section of 20 mm × 2 mm and a length of 200 mm. The other is a multi-port tube with a cross section of 17 mm × 1.8 mm and length of 200 mm as in Fig. 3.3. These tubes are connected to the header at intervals of 20 mm. The multi-port tube is an aluminum tube that is used in a real compact evaporator of an automobile air-conditioning system. It contains twelve rectangular shaped holes and two triangle shaped holes at both ends. The average hydraulic diameter of the holes is 0.86 mm. The dividing header has straight sections of 55 mm before the first branch and of 20 mm after the tenth (last) branch. These dimensions of the header and the branches were determined based on the real compact evaporator of a car air conditioner.

Fig. 3.4 shows a relation of gas phase flow rate and pressure differential between headers, i.e. pressure loss, for branch profile with flat smooth tube and with aluminum

multi-port tube. It shows that the pressure loss of branch with aluminum multi-port increases as the gas phase flow rate is increase. As in Fig. 3.4, the pressure loss of this multi-port tube for a single phase flow was about 25 times larger than that of the flat tube were used in this study under an equal flow rate range.

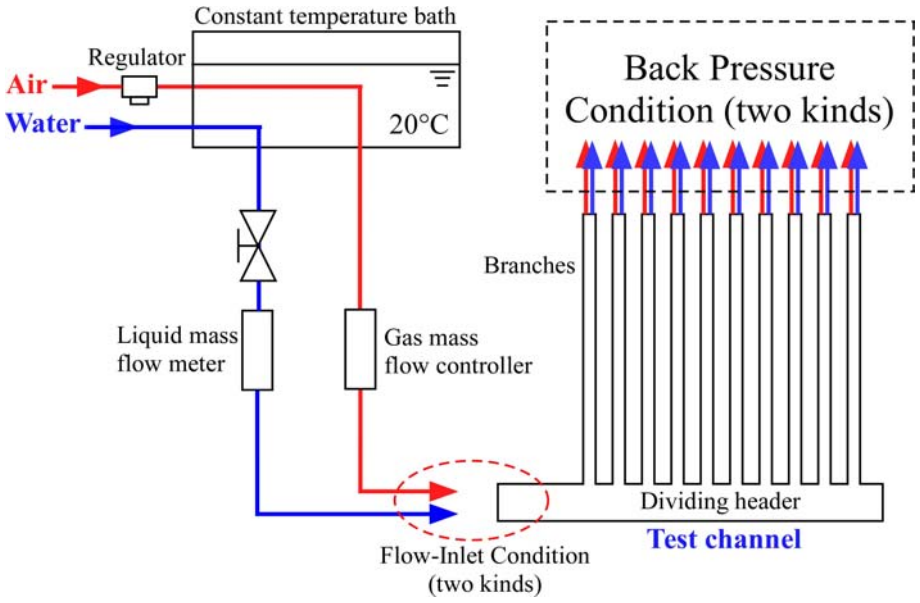

Fig. 3.1 Schematic diagram of the experimental apparatus for air and water flow distribution measurement

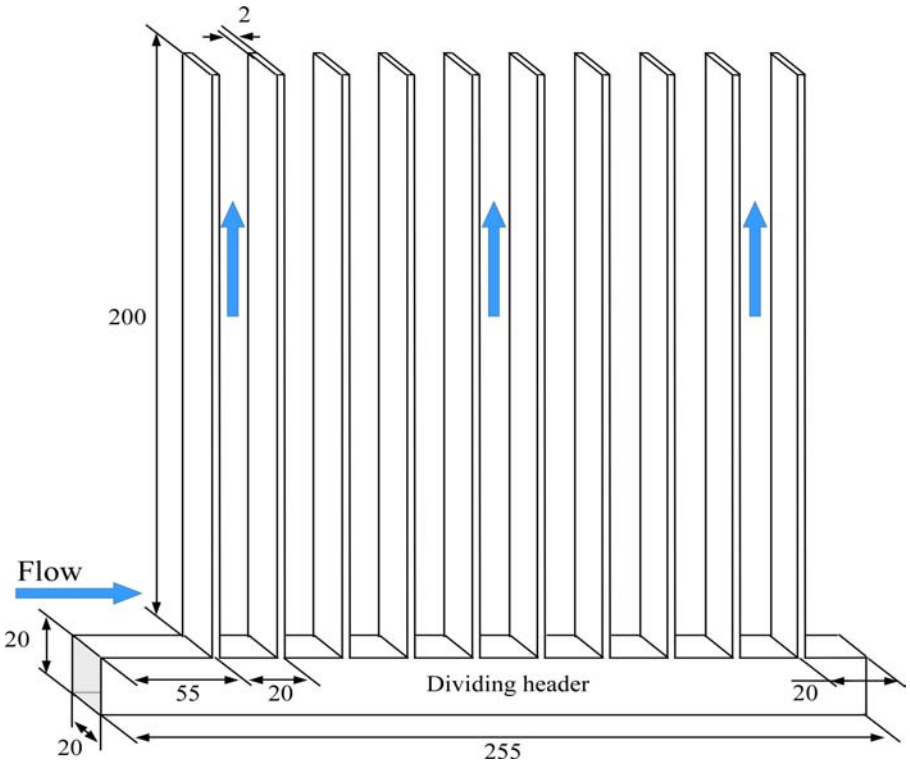

Fig. 3.2 Detail dimension of 10 branches test channel

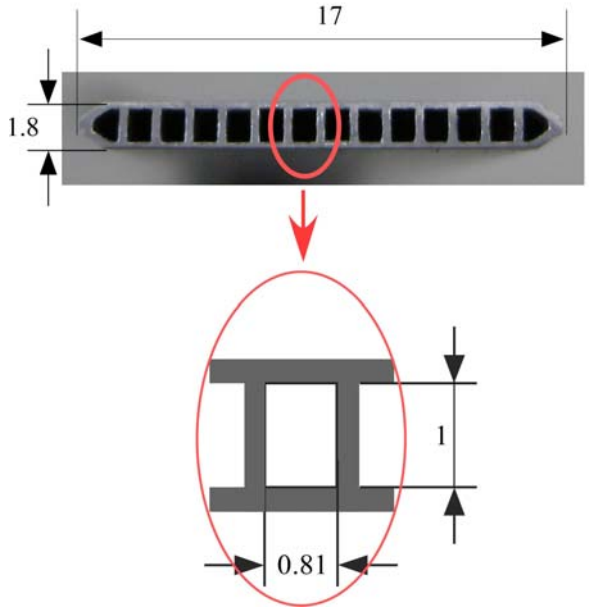

Fig. 3.3 Detail dimensions of multi-port aluminum tube

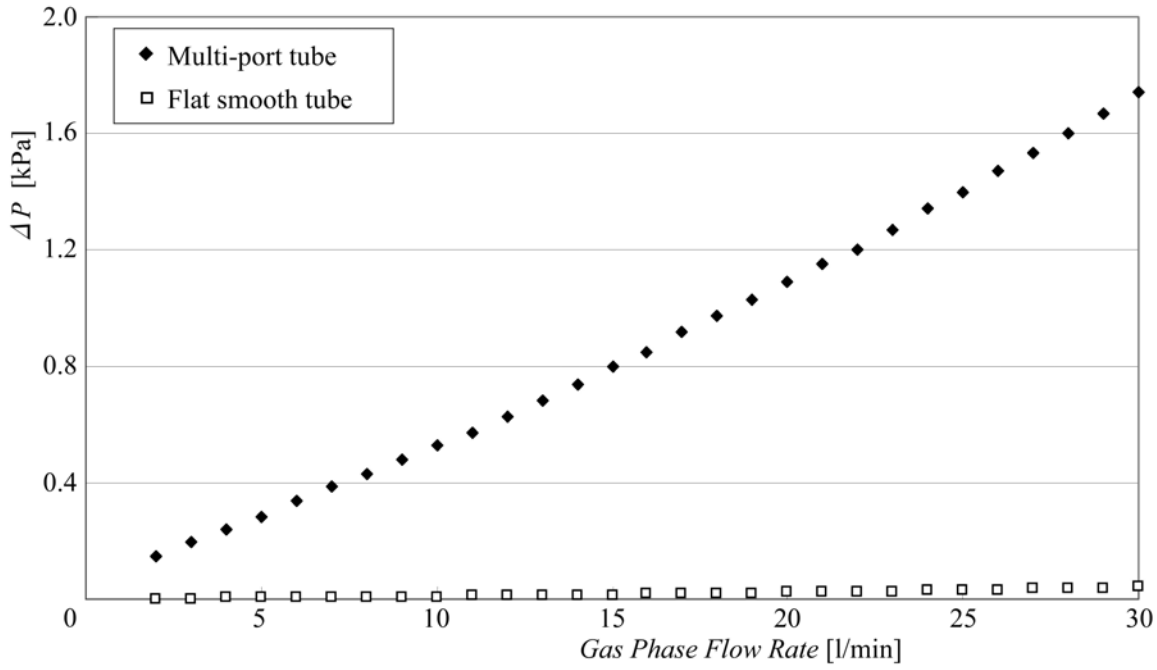

Fig. 3.4 Pressure differential between headers (Single phase flow – air)

3.2.2 Flow-inlet conditions at the header entrance

It is thought that the gas-liquid distributions to the branches are greatly influenced by the flow pattern in the dividing header. Hence, in this study, two contrastive flow-inlet conditions of the header entrance are adopted. One is the stratified-flow inlet. In this case, an air filter with a porous structure (rectifier material) is stuffed in the developing region attached upstream the dividing header, and air and water is supplied separately at the upstream end of this developing region as in Fig. 3.5. The developing region has the same cross section as the header and a length of 290 mm which is connected to the dividing header inlet, i.e., 55mm from the first branch. The stratified flow is formed at the entrance of the header. Fig. 3.7 (a) shows a snapshot of the flow near the entrance of the dividing header. It is observed that air and water is flowing separately and the stratified-flow inlet condition is realized at the header entrance. Under most conditions of the air and water superficial velocities tested in this study, the wavy-stratified flow was observed at the header entrance and the void fraction estimated from the visualized images was about 0.5 - 0.6.

The other flow-inlet condition is the mist-flow inlet. A two-fluid nozzle is attached at the entrance of the header to generate a mist flow as in Fig. 3.6. The snapshot of the flow near the header entrance is shown in Fig. 3.7 (b). Air and water enters the header forming a mist flow, but water droplets are soon deposited on the header walls. Therefore, the walls of the dividing header are covered by water films and the annular mist flow is formed just before the first branch. The two-fluid nozzle used in this study can generate water droplets with diameters of 10 μm - 70 μm.

The superficial air velocity j_g and superficial water velocity j_l at the entrance of the header are determined based on the quality and mass flow rate of the refrigerant encountered in a real evaporator. In this study, j_g and j_l are set equal to the superficial velocities of vapor and liquid of the refrigerant flow (R-134a) in a real evaporator, and they are 1.0 - 5.0 m/s and 0.015 - 0.045 m/s, respectively. These velocity conditions correspond to the range of quality x = 0.2 - 0.7 and mass flow rate M = 40 - 160 kg/h in R-134a refrigerant flow in a real evaporator.

Real refrigerant (R-134a) and air-water flow as in Table 3.1 has a differences with their physical properties, and the gas phase density is one of the biggest among them. As explain earlier, in this study j_g and j_l are set equal to the superficial velocities of vapor and liquid of the refrigerant flow (R-134a) in a real evaporator, thus make a differential

with the quality x of air-water in the test channel as shown in Table 3.2.

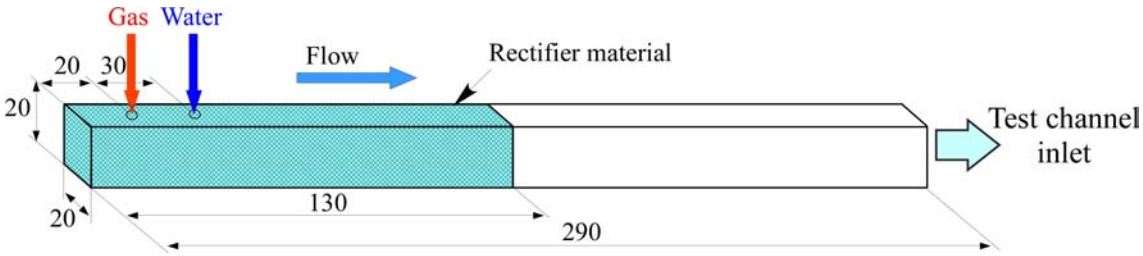

Fig. 3.5 Generating stratified flow

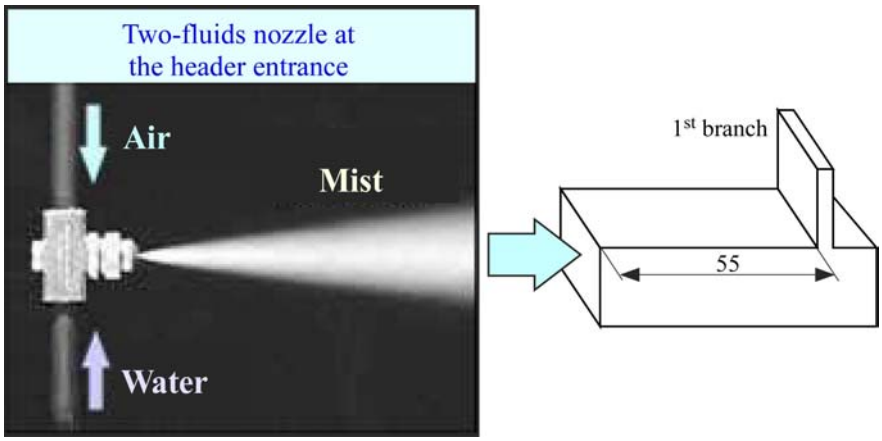

Fig. 3.6 Generating Mist flow

Table 3.1 Physical properties difference between refrigerant and air-water

	HFC-134a (0.3MPa)	Air-water (20°C)
Gas phase density [kg/m^3]	14.7	1.2
Liquid phase density [kg/m^3]	1291	998
Surface tension [mN/m]	8.7	73

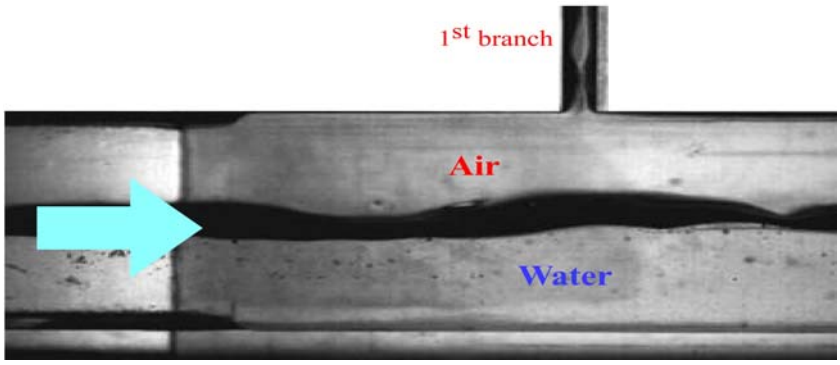

(a) Stratified flow inlet

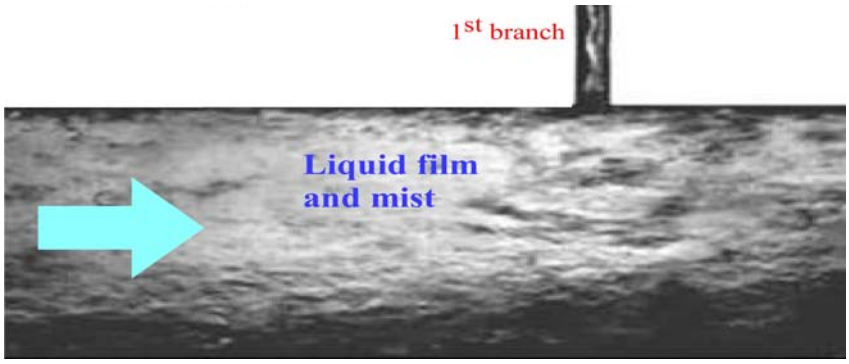

(b) Mist flow inlet

Fig. 3.7 Snapshots of inlet flows near the entrance of the dividing header

Table 3.2 Superficial velocity range in actual compact evaporator

HFC-134a
(Air-Water)

Mass flow rate M [kg/h] \ Quality x	0.9 (0.49)	0.8 (0.30)	0.7 (0.20)	0.6 (0.14)	0.5 (0.10)	0.4 (0.07)	0.3 (0.04)	0.2 (0.03)
150	6.36 0.81×10^{-2}	5.66 1.61×10^{-2}	4.95 2.42×10^{-2}	4.24 3.23×10^{-2}	3.54 4.03×10^{-2}	2.83 4.84×10^{-2}	2.12 5.65×10^{-2}	1.41 6.45×10^{-2}
100	4.24 0.54×10^{-2}	3.77 1.08×10^{-2}	3.30 1.61×10^{-2}	2.83 2.15×10^{-2}	2.36 2.69×10^{-2}	1.89 3.23×10^{-2}	1.41 3.76×10^{-2}	0.94 4.3×10^{-2}
50	2.12 0.27×10^{-2}	1.89 0.54×10^{-2}	1.65 0.81×10^{-2}	1.41 1.08×10^{-2}	1.18 1.34×10^{-2}	0.94 1.61×10^{-2}	0.71 1.88×10^{-2}	0.47 2.15×10^{-2}
30	1.27 0.16×10^{-2}	1.13 0.32×10^{-2}	0.99 0.48×10^{-2}	0.85 0.65×10^{-2}	0.71 0.81×10^{-2}	0.57 0.97×10^{-2}	0.42 1.13×10^{-2}	0.28 1.29×10^{-2}

Red : Superficial velocity of gas [m/s]
Blue : Superficial velocity of liquid [m/s]

3.2.3 Pressure conditions at the outlets of branches

At the downstream end of the branches, the outlet ports of gas and liquid flows are equipped. In order to examine the influence of the outlet pressure condition of branches on the flow distributions, we have tested two kinds of outlet conditions as shown in Fig. 3.8. In Case A shown in Fig. 3.8 (a), the gas-liquid separators and the air-flow meters are connected to the outlet ports of all the branches. The two-phase flows that exit the branches are lead to the gas-liquid separators, and the air flow rates in all the branches are measured simultaneously by the air-flow meters equipped at the exit of the separators. The water flow rates in the branches are measured by weighing waters that are accumulated in the separator tanks. The errors included in the air flow rates and water flow rates in the branches are estimated to be about 4 % and 1 %, respectively. The sum of air flow rates in the branches comply with the air flow rate at the header entrance within difference of 4 %. As for the water flow rate, the error was less than 1 %. The pressure in each separator, i.e., backpressure of each branch, is also measured by a pressure gauge. In this measuring condition, the pressure at the outlets of the branches can vary depending on the flow rates in the separators due to the flow resistance of the air-flow meters. Therefore, as shown later, a non-uniform backpressure condition is imposed on the branches in Case A.

On the other hand, in Case B shown in Fig. 3.8 (b), one branch to measure the flow rate is connected to the gas-liquid separator and other branches are connected to a combining tank which has a large volume. The valves at the exits of the separator and the combining tank are adjusted so that the pressure difference between them becomes zero. We confirmed that the pressure in the combining tank was uniform. Therefore, in Case B, one can measure the flow distributions under the constant backpressure condition for all the branches.

In many studies conducted to date, the flow distributions to the branches have been measured with the method equivalent to Case A. Therefore, those data are regarded as the results obtained under the non-uniform backpressure condition at the branch outlets.

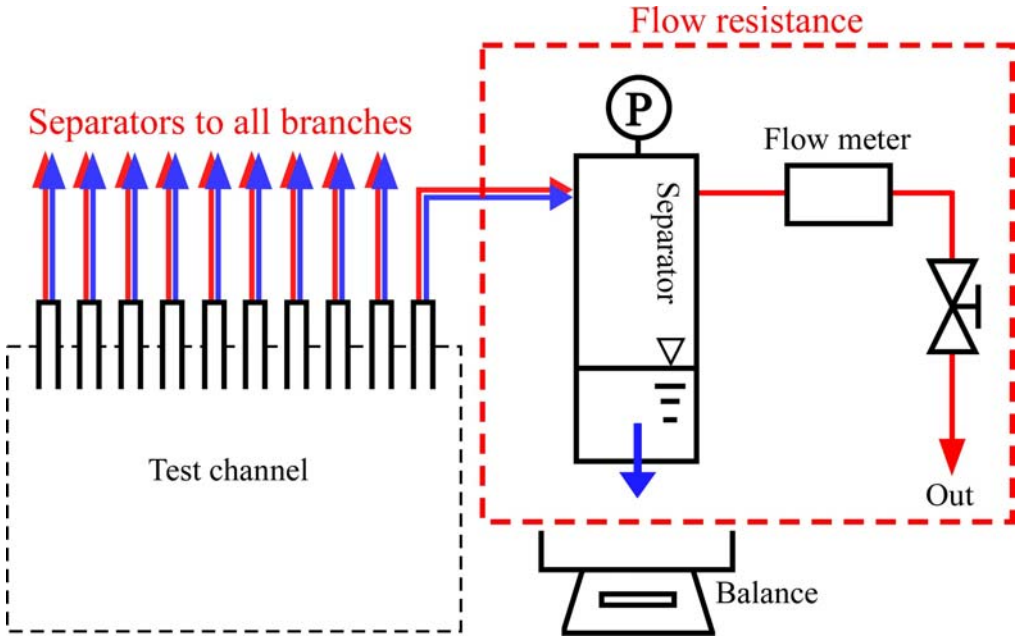

(a) Non-uniform backpressure condition (Case A)

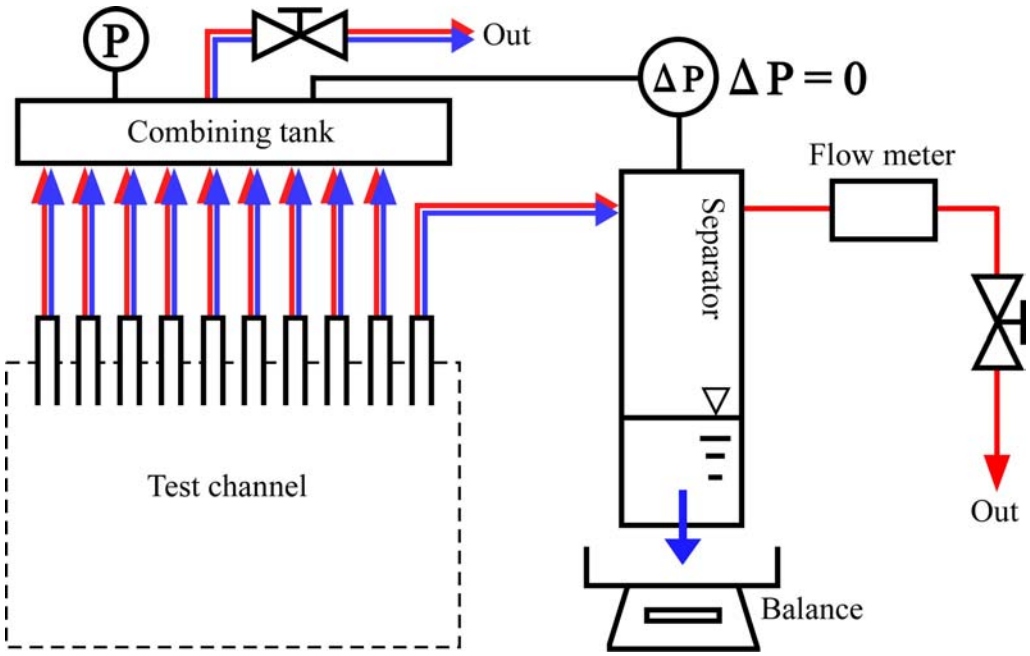

(b) Uniform backpressure condition (Case B)

Fig. 3.8 Pressure conditions at outlets of branches

3.2.4 Measurements of pressure distributions in the headers

In a real compact evaporator, the downstream ends of the branches are connected to a combining header. In this study, we have measured the pressure distributions in the dividing and combining headers to make clear the pressure conditions at the branch outlets in a real evaporator. Fig. 3.9 shows an experimental apparatus for the measurements of the pressure distributions inside the headers. The dimensions of the test channel are essentially the same as those shown in Fig. 3.2, except that a horizontal combining header with a square cross section of 20 mm×20 mm is attached to the outlets of the branches. As shown in Fig. 3.9, the pressure distributions are measured at nine locations of each header. The pressure transducers are allocated at the middle of the side walls of the headers above and beneath the branches except for the first branch as in Fig. 3.10 which also showing the detail of pressure transducer probe sensor attachment to the headers wall in detail. They were calibrated with errors of less than 0.15 kPa. The sampling frequency of the pressure is 10 Hz and the measuring time is 60 seconds. In the combining header there are outlets at its right and left hand ends, and we have tested two flow conditions. One is the parallel flow, in which the gas and liquid enter the dividing header, go up through the branches to the combining header and exit from its right outlet. The other is the reverse flow, in which the flow exits from the left outlet of the combining header. The flow-inlet conditions at the entrance of the dividing header are the same as those for the flow-distribution measurements. The experimental conditions of this study are summarized in Table 3.3.

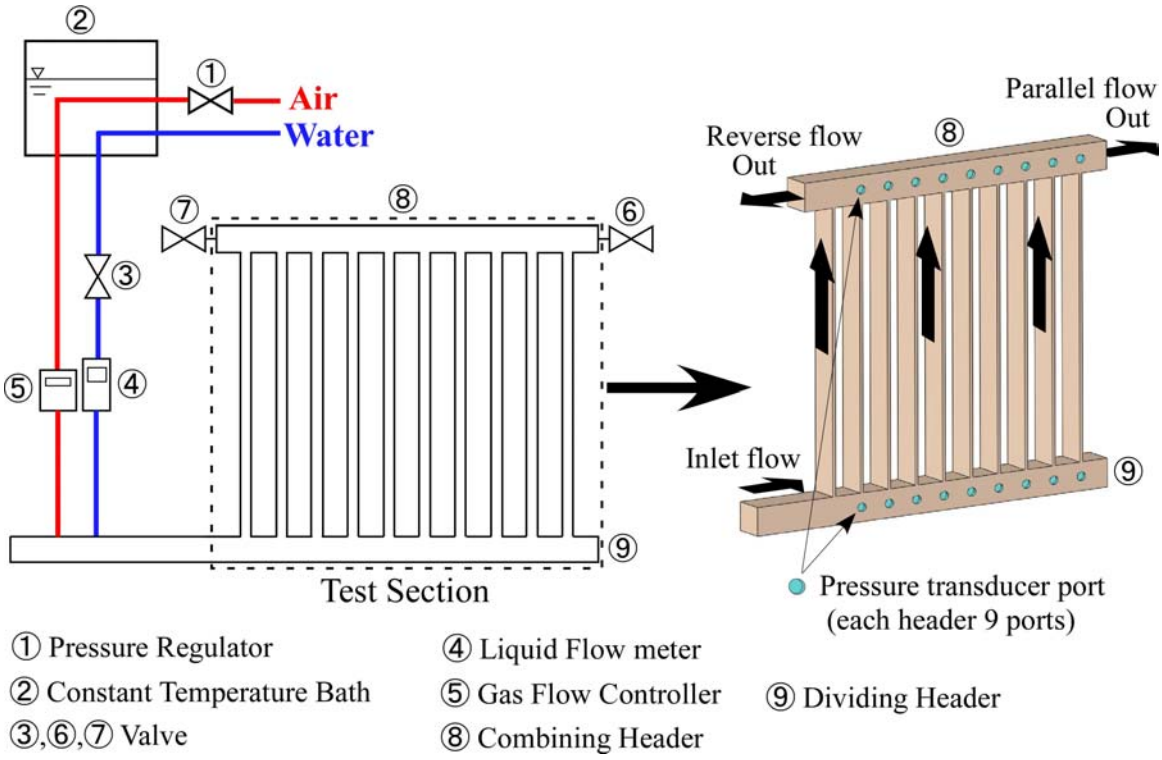

Fig. 3.9 Test channel for the pressure distribution measurements in the headers

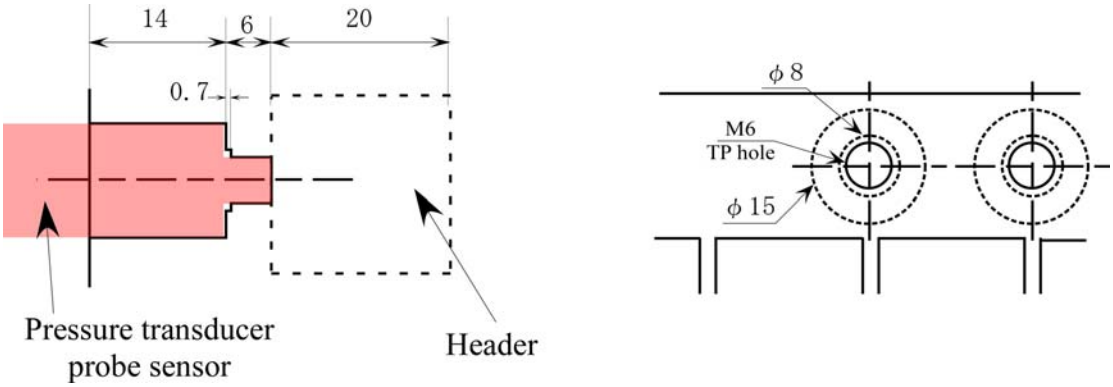

Fig. 3.10 Details of pressure transducer probe sensor attachment at the test channel

Table 3.3 Summary of the experimental conditions

Fluids	Isothermal air and water
Superficial air velocity at the header entrance j_g	1.0 m/s, 3.0 m/s, 5.0 m/s
Superficial water velocity at the header entrance j_l	0.015 m/s, 0.03 m/s, 0.045 m/s
Pressure condition at the branch outlets	Non-uniform backpressure (Case A) Uniform backpressure (Case B)
Flow-inlet condition at the header entrance	Stratified-flow inlet Mist-flow inlet
Header attitude	Horizontal
Branch attitude	Vertical upward
Branch profile	Flat tubes Multi-port tubes

3.3 Second segment: Study on the similarity of real refrigerant and air-water two phase flow distribution behavior

In this segment, the testing apparatus for visual observation are mainly to be discussed. Visual observation test apparatus are divided into two sections. One is for real refrigerant i.e. R-134a and another one is for air-water visual test apparatus.

3.3.1 Refrigerant visual test apparatus

Figure 3.11 is the schematic diagram of the R-134a visual test apparatus. It shows a complete refrigerant cycle of a heat pump system with a simulated multi-pass upward test channel made from a clear polycarbonate material for the visual test, fixed between the expansion valve and evaporators. The test channel is allocated at the nearest position to expansion valve, which is just after the pressure gauge and thermocouple as in Fig. 3.11. This research is mainly focusing on visual observation of flow patterns at the entrance of dividing header, i.e., from inlet copper pipe at header entrance to the upward aluminum tube branches. Due to this, the evaporation process of R-134a in the test channel has been avoided by using a proper material for the test channel. For that

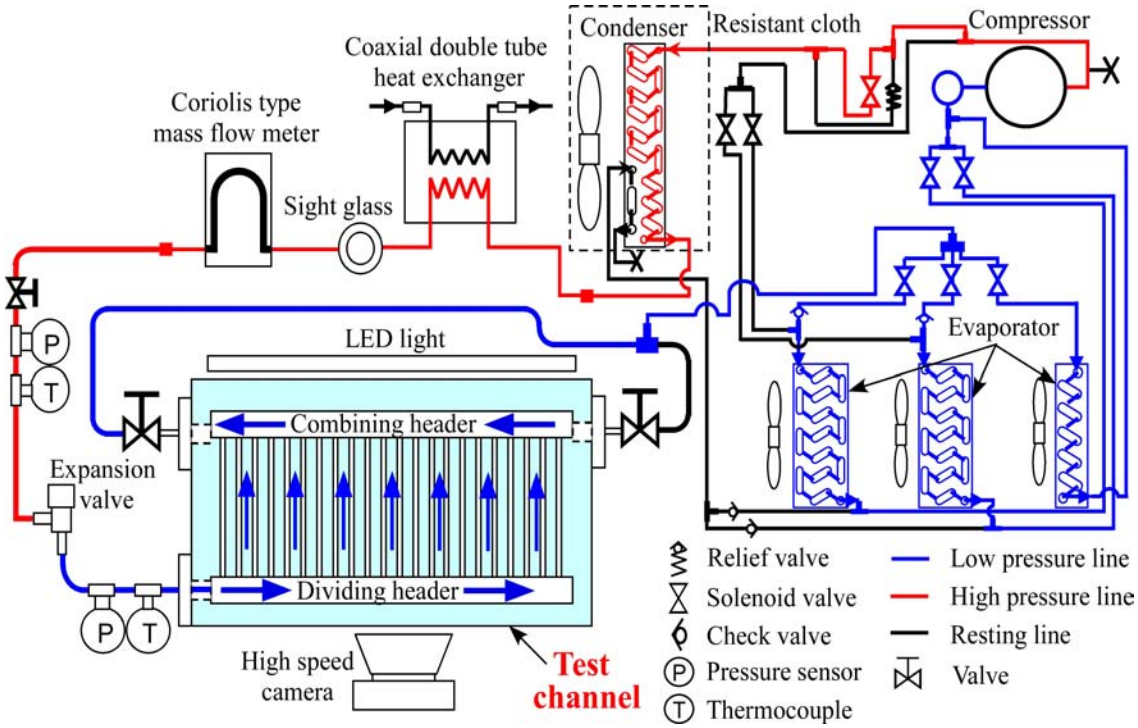

Fig. 3.11 Refrigerant flow visual observation apparatus

reason, there shall be no evaporation processes occur in this test channel.

In this experiment, the test conditions are the thermodynamic property of quality x and mass flow rate M of the refrigerant at the header entrance, which is at point no. ④ of R-134a refrigerant cycle in Mollier diagram as in Fig. 3.12. These two values shall be controlled to be as in Table 1, by adjusting properly the (1) Compressor revolution, (2) Expansion valve opening, (3) Condenser side heat energy capacity, which are water flow rate at coaxial double tube heat exchanger , fan revolution of the condenser and resistant cloth amount for environment temperature control of condenser. Also, a proper reference from Mollier diagram of R-134a is needed for achieving the desired test condition. For this test, the low pressure line was control at 200 kPa absolute with upper and lower limit of 50 kPa to maintain the same condition of actual heat pump system which the mean temperature of the evaporator is about -10ºC. A Coriolis type mass flow meter is attached at high pressure line between outdoor heat exchanger (i.e., condenser and coaxial double tube heat exchanger) and expansion valve to measure the refrigerant mass flow amount of the tested cycle. Noted, for Coriolis type mass flows meter to work efficiently, the condition of refrigerant that flow inside the meter should be in a single phase flow, therefore, the condition of refrigerant at no. ③ in Mollier diagram in Fig. 3.12 should be beyond the saturated liquid line, i.e., in sub cool condition. A thermocouple and pressure gauge sensor are allocated at entrance and exit of the

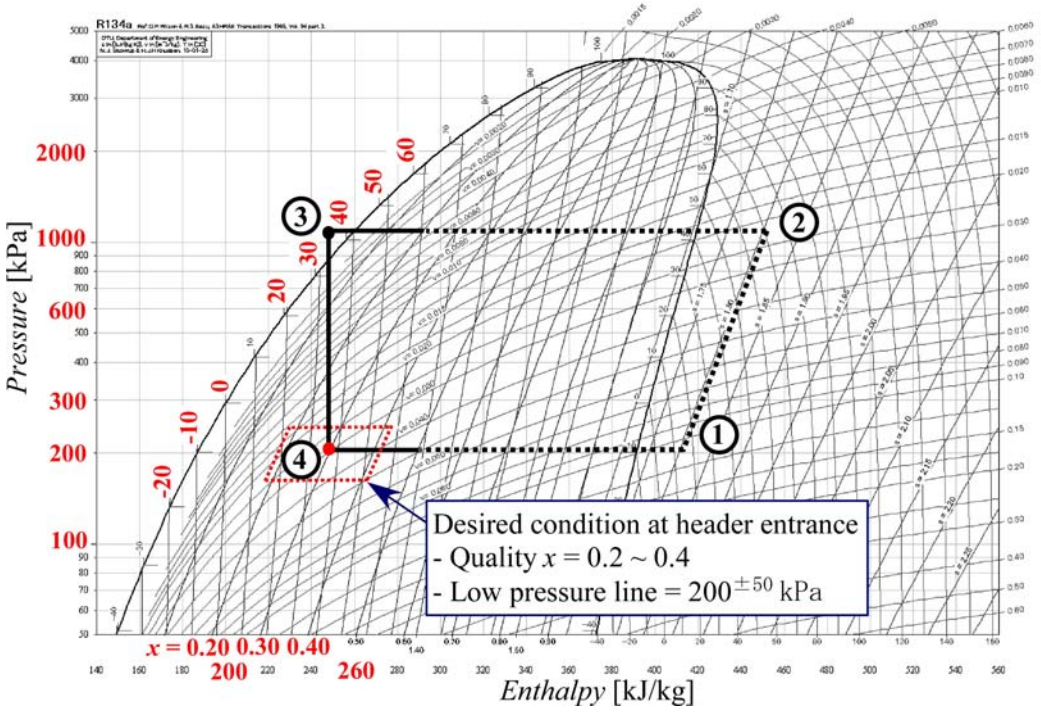

Fig. 3.12 Mollier diagram of R-134a cooling cycle of desired test condition

Table 3.4 Mass flow rate and quality of R-134a at header entrance

Quality x	Mass flow rate M [kg/h]			
0.2	4.15	5.2	6.4	8.5
0.3	4.15	5.2	6.4	8.5
0.4	4.15	5.2	6.4	8.5

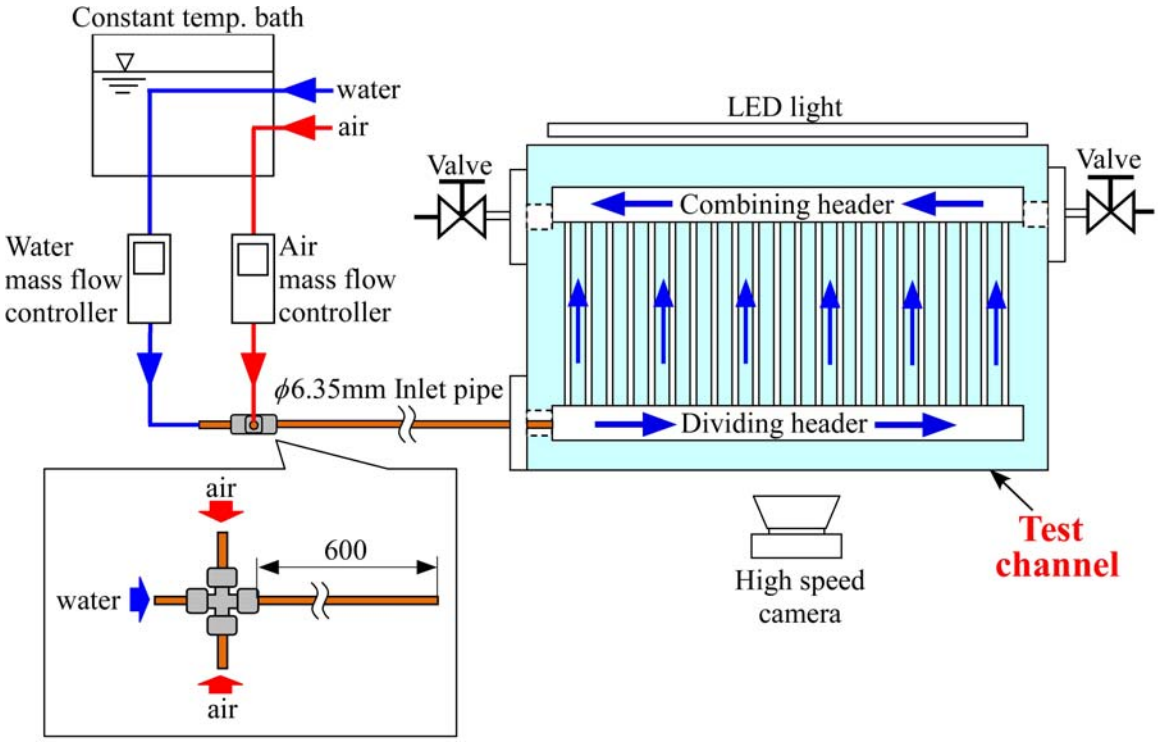

Fig. 3.13 Air-water flow visual observation apparatus

expansion valve, for measuring the temperature and pressure of refrigerant inside the copper pipe. This data is for quality x calculation at test channel header entrance position for that to be identical with the desired condition in table 3.4.

3.3.2 Air-water visual test apparatus

Figure 3.13 is the schematic diagram of an experimental apparatus for air-water two phase flow visual observation. The dimensions and specifications of the test channel that simulate the compact evaporator is identical with the one that being used in real refrigerant visual observation. The experiment was conducted in an isothermal air-water flow system. The air and water temperature were controlled at 25ºC in a constant

temperature bath before flowing to each flow controller. The mass flow rate of the air and water shall be control by each flow controller. To generate the flow pattern at the header entrance, Ø4.75mm inner diameter (Ø6.35mm outer diameter) copper pipe with 600mm of length was used. As in Fig. 3.13, air and water was mixed at the beginning of this copper pipe where a cross pipe connected to it, which another same size of copper pipe from water mass flow controller was connected to the opposite end of it. Also, another 2 pipes were connected at left and right side of the cross pipe from the air mass flow controller. All these pipes were connected to these cross pipe horizontally as shown in Fig. 3.13. Therefore, with the appropriate mass flow rate of water and air as a test condition that shall be explain in detail afterward, the two phase flow behavior, especially at the header entrance shall be observe. A LED light and a digital video camera were used for recording the visual observation at the test channel and same goes with the R-134a refrigerant visual test. Noted here that the water and air mass flow controller that used in this segment were different with the one that been used in first segment testing, this due to the desired superficial velocities range of both phase for this test condition were enormously different.

3.3.3 Test channel specification, orientation and other parameters

Figure 3.14 shows the detail dimensions of the test channel. The channel contain a dividing and combining header lying horizontally, parallel and 120mm separated to each other with 22 branches connected to them. Both headers cross section area is 20mm x

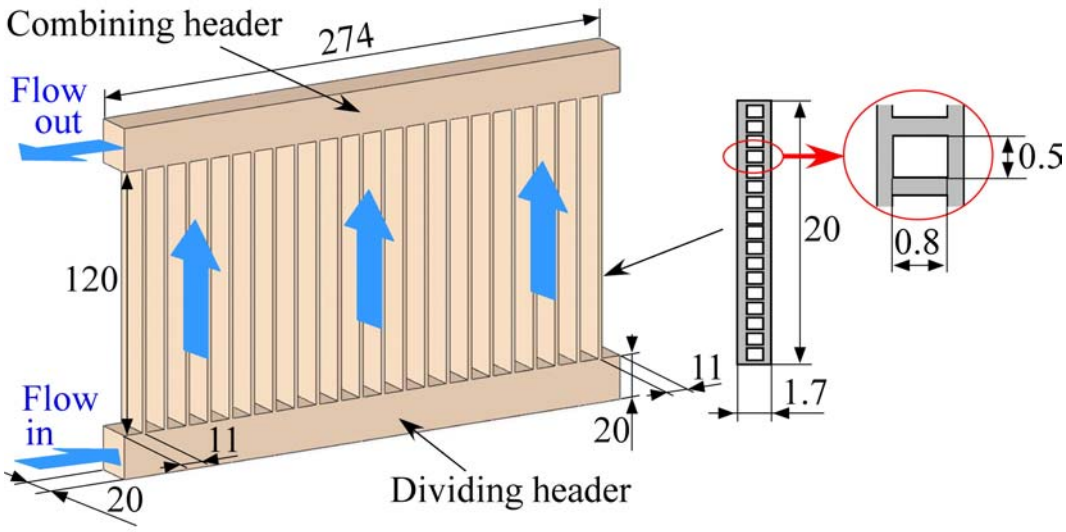

Fig. 3.14 Details of simulated test channel

20mm with a length of 274mm. The branch cross section area is 2mm x 20mm with 120mm of length, with 12mm of pitch, inserted into it with a multi-port aluminum tube that has a cross section area of 1.7mm x 20mm. The multi-port aluminum tube contains 17 small rectangular holes with a cross section area of 0.5mm x 0.8mm. In this study at first stage the test was conducted at condition of test channels headers in horizontal position with upward branches perpendicular to it. Also, the flow shall be from dividing header at the bottom of the channel goes upward to combining header and in a reverse flow motion goes out to the opposite direction of the inlet flow. At the header entrance, an outer diameter of 1/4 inches copper pipe, i.e. a copper pipe with a dimension of inner diameter Ø4.75mm (outer diameter Ø6.35mm with a thickness of 0.8mm), is connected. Table 3.4 show the test condition of quality x at the inlet position of the test channel and mass flow rate M of the refrigerant cycle. These values were selected upon studying the heat pump system of the actual appliance. From table 3.4, the real refrigerant R-134a at the header entrance, superficial velocity of vapor j_G should be at range of 0.06 ~ 0.22 m/s, while the superficial velocity of liquid j_L should be at 1.3 ~ 3.6 mm/s. Fig. 3.15 shows the Baker map (1954), a map of a flow pattern in one horizontal conduit. A prediction of a stratified flow at the header entrance of test channel as the calculated values from table 3.4 being plot in Baker map in Fig. 3.15.

Also, by using the same test channel, a few other testing were done by different orientation of branch and header to observe initially which orientation of test channel are best for the uniformity of flow distribution. The orientation of branch and header were as Table 3.5, and only visual test of real refrigerant are been done first. Thus, the selected orientation condition shall be preceded to the next stage of testing, i.e., the visual observation of air-water phase flow and the flow distribution rate measurement test.

Later on, the inlet pipe end were swaged to several inner diameter and the intrusion of aluminum multi-port tube branches height h from the dividing header surface also being change to become a parameter for questing the correct geometric combination of the test channel to perform a uniform liquid phase flow distribution. In the end, the branch quantity was reduced to half to be the final test condition of this research.

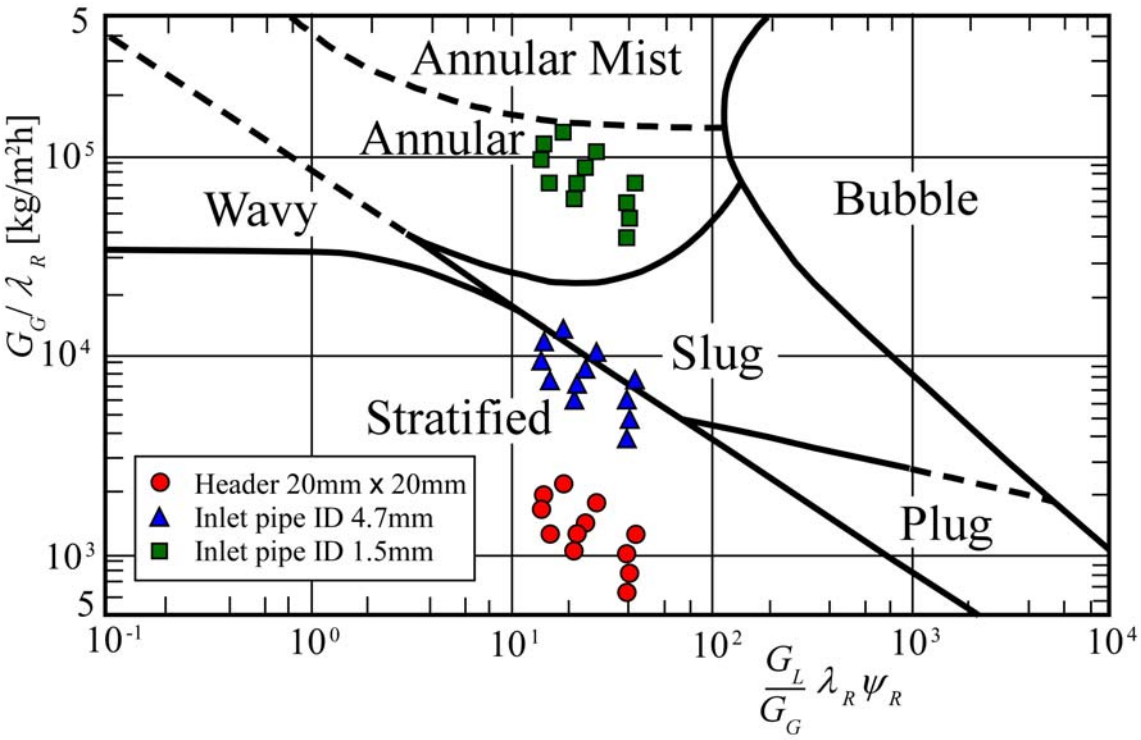

Fig. 3.15 Baker's flow pattern map of the refrigerant flow at the dividing header entrance and inlet pipe

Table 3.5 Same test channels with different orientation (branch and header), inlet position and flow direction

	Vertical Upward	**Vertical Downward**	**Horizontal downward**	**Lying Leveled**
Header orientation	Horizontal	Horizontal	Vertical	Horizontal
Branch orientation	Vertical	Vertical	Horizontal	Horizontal
Inlet position	Bottom	Top	Top	Horizontal
Flow direction	Reverse	Reverse	Parallel	Reverse
Configuration	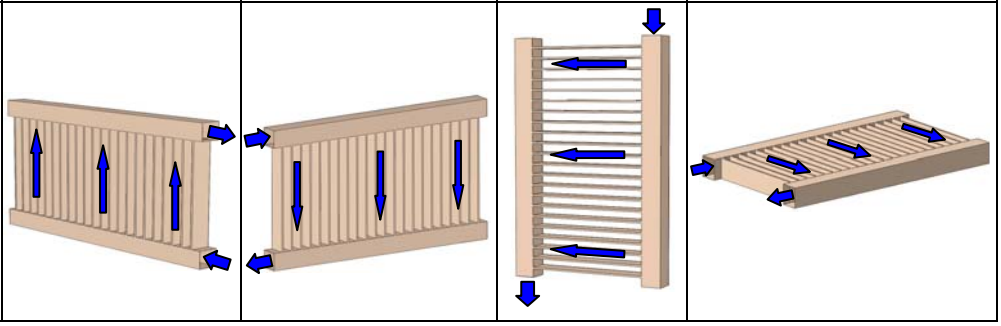			

3.3.4 Air-water flow distribution test apparatus

Figure 3.16 is the schematic diagram of air-water flow distribution measurement apparatus. These apparatus has been introduced, used and reported in our previous segment of this research. The pressure distribution at along the dividing and combining headers are most likely uniform. Due to this, a uniform backpressure condition of flow distribution measurement apparatus has been selected. By using another test channel, i.e., as in Fig. 3.17, that has a same specification as the visual test channel, except for this one, the combining header was not connected. At the end of the branches they were fixed to a plastic hose and connected to the measurement apparatus as in Fig. 3.16. One branch to measure the flow rate was connected to the separator and other branches were connected to a combining tank that had a large volume. The valves at the exits of the separator and the combining tank were adjusted so that the pressure difference between them becomes zero. Since the combining tank was quite large, also the pressure distribution inside the combining tank were measured and confirmed that the pressure in it was practically constant. By repeating this method with all the 22 branches, the flow distribution under the constant backpressure condition for all the branches can be measured. The inlet condition of air-water flow pattern at the header entrance shall be generated by the same method as in Fig. 3.13.

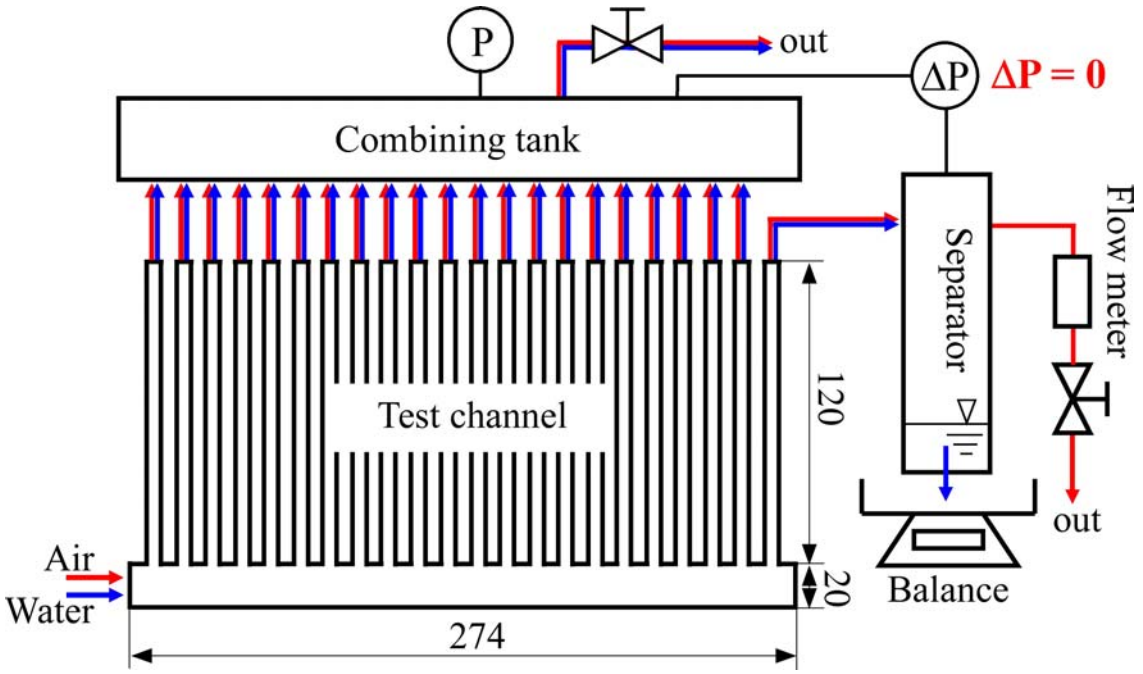

Fig. 3.16 Air-water flow distribution measurement apparatus

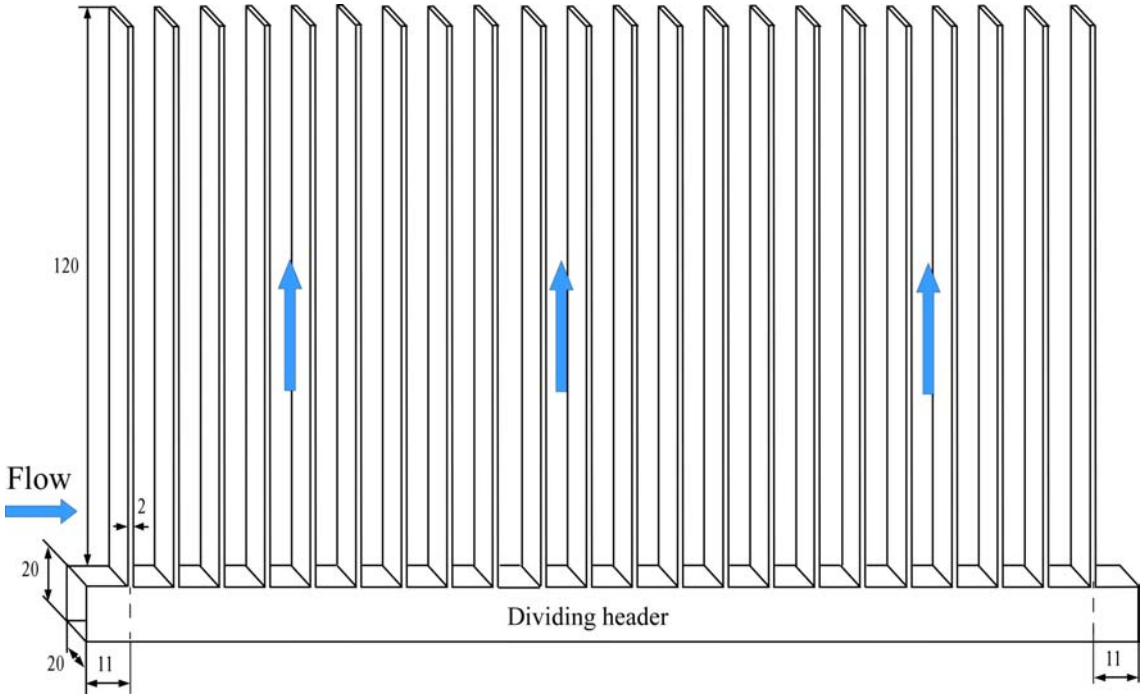

Fig. 3.17 Detail dimension of simulated test channel with 22 branches for air-water flow distribution measurement

3.4 Specification and detail of measuring devices and testing apparatus

3.4.1 Air and water phase inlet flow control

In the first segment, for testing apparatus as in Fig. 3.1, the instruments (name, specification and detail) that been used for generating, measuring and controlling the accurate inlet flow condition are as below.

- Constant temperature bath
  Product of Thomas Kagaku Co. Ltd., Desktop low temperature model constant temperature bath, Model name: T-22L

- Mass flow controller for air phase
  Product of Yamatake Co. Ltd., Digital mass flow controller, CMQ-V series
  ① MQV0020 (0 ~ 20.0 L/min)
  ② MQV0200 (0 ~ 200 L/min)

- Water phase mass flow meter
  Product of Mitsuba Co. Ltd., Two gear type flow sensor, Model name: XFS-1204
  (0 ~ 72 L/h), (0 ~ 120 L/h)

In the second segment, for testing apparatus as in Fig. 3.13 and 3.16, the instruments that been used for generating, measuring and controlling the accurate inlet flow condition are basically the same as the one that been used in the first segment except below instrument due to the differences of air and water phase superficial velocities ranges.

- Mass flow controller for air phase
  Kofloc brand (Kojima instrument Inc.), Thermal mass flow controller 8500 series, Model8550, Standard flow range up to 10 L/min

- Mass flow controller for water phase
  Horibastec brand (product of Horiba limited), Digital liquid mass flow controller LV-F series, Model name: LV-F60PO, Standard flow range up to 50 g/min.

- Mass flow meter for water phase
  Coriolis Digital Flow Sensor FD-S Series
  Product of Keyence Corporation, Model name: FD-SF1, measuring range from 0 to 1000 mL/min.

3.4.2 Air and water phase flow distribution measurement

Continuing from above, after the inlet flow being generated to be the desired flow pattern at the entrance and distributed to the branches, as in Fig. 3.8 for first segment, also as in Fig. 3.16 for the second segment of this research, the air and water phase flow shall be measured separately. The instruments that used for measuring the air and water flow are as below.

- Air phase flow rate measurement
  Product of Yamatake Co. Ltd., Mass flow meter for gas phase,
  Model name: CMS0005 (0 ~ 5 L/min)
  CMS0050 (0 ~ 50 L/min)

- Water phase mass measurement
  Product of Shimadzu Corporation, Electronics scales,
  Model name: UX4200H (0～4200g)

3.4.3 Equipments for visual observation

In the first and second segment of this research, the visual observation on the flow pattern at the header entrance and also the observation of flow behavior along dividing header were done mostly by recording the visual data using below equipment.

- Hi speed camera
  Product of Photron Limited, Model name: FASTCAM-ultima1024 R2

Table 3.6 Recording condition

Frame Rate	500 fps
Resolution	1024×512 pixels
Shutter Speed	1/4000 sec
Sensitivity	×4

- Digital camera
  Casio digital camera, Model name: EX-FH25.
  - Snapshot image size used was 10 and 9 Megapixels.
  - Movies image quality for Hi definition mode is (1280 x 720) pixels, approximate data rate is 30 Megabits/sec (30 fps); for Standard mode is (640 x 480) pixels, approximate data rate is 10 Megabits/sec (30 fps); for Hi speed mode at 30 – 240 fps is (448 x336) pixels, approximate data rate is 6.25 Megabits/sec at 30 fps and 50 megabits/sec at 240 fps.

  Noted that, this equipment was started being used for photo and movie shooting from the second segment of this research.

3.4.4 Pressure measurement

- Pressure gauge used to measure the pressure in side separator for flow distribution measurement test as in Fig. 3.8.
  Product of Nagano Keiki Co. Ltd., Digital differential pressure gauge,
  Model name: GC62 (-2 ~ 2 kPa)

- Pressure measurement equipment used for measuring pressure at along header surface as in Fig. 3.9.
  Product of JTEKT Corporation, Semiconductor pressure transducer (Diffusion type / Silicon diaphragm type),
  Model name: PD104SW (Measurement pressure range -30 ~ 30 kPa)

This diffusion type semiconductor pressure transducer, a formation of strain gauge located at the silicon diaphragm surface is the section that received the pressure signal. The pressure detection system basically works by the changes of resistance according to Piezo resistance effect. The pressure value is obtained when a strain is present at the diaphragm which proportion to the value of the output current signal that was supplied from a DC amplifier. DC Amplifier made by the same manufacturer with model name AA6010 and AA6210 was used due to the output current signal range is small. More over, a required and well balance of electric circuit with applied power supply included in the system makes this DC amplifier perfect to be used with the transducer. Also, at the sensor position of this transducer, silicon oil is added to avoid air from entering inside.

- Pressure measurement device for measuring pressure of refrigerant cycle at point no. ③ and ④ in Mollier diagram as in Fig. 3.12.
  These devices were located each near the expansion valve at leaving and entering position as in Fig. 3.11 measuring the low and high pressure side of the system.
  - High pressure side (point no. ③), the pressure gauge was from product of Yokogawa.
    Model name: FP101-E32-L20A*B, with output signal range from 1 to 5V DC. Cover the pressure measurement range from 0 to 5 MPaG.
  - Low pressure side (point no. ④), the pressure gauge was from product of Yokogawa.
    Model name: FP101-C32-L20A*B, with output signal range from 1 to 5V DC. Cover the pressure measurement range from 0 to 1 MPaG.

3.4.5 Temperature measurement

As the pressure gauge for heat pump cycle, these devices were located near the expansion valve as in Fig. 3.11.

- Thermocouple
  Product of Hakko Co. Ltd., Model name or references are H8XC and ST-2-A-1.0-U.

3.4.6 Refrigerant mass flow measurement

In the second segment, the mass flows that circulate inside the heat pump cycle were measured using below mass flow meter.

- Coriolis Digital Flow Sensor FD-S Series
  Product of Keyence Corporation, Model name: FD-SS2, measuring range from 0 to 2000 mL/min.

3.4.7 A/D converter (Analog to digital converter)

For first segment testing, gas phase flow measurement and pressure along the header data were transfer by a voltage signal via A/D converter to PC for data compiling process and graph plotting for straightforward understanding of the behavior of the two phase flow distribution inside the test channel.

- Multi-input data acquisition system (Wave logger)
  Product of Keyence Co. Ltd., Model name: NR-600 was used.

Also, noted that, in the second segment, this same apparatus has been used to transfer the data of temperature, pressure and mass flow rate of the refrigerant cycle to PC for calculation of quality x at point no. ④ in the Mollier diagram of the tested condition for accurate labeling of visual data for further study. For monitoring and data collection of air and water flow distribution rate in the second segment, the new purchased data logger has been used and the details are as below.

- Data logger
  Product of Graphtec, Midi logger GL800, Model name: GL800-UM-801.

Chapter 4

Experimental Results, Analysis and Discussion

4.1 Chapter overview

In this chapter, the results of the experiment are reported, analyzed and discussed. As in previous chapter, this chapter also has the same two segments. However after the second segment there are other explanations on flow distribution behavior of two phase flow with other perceptive approach of different parameters and test conditions.

The first segment is the result on the study of parameters that influence the flow distribution uniformity, which in this study the experiments on the gas-liquid flow distribution characteristics in multi-pass channels with ten upward branches has been made. Attention has been directed the influences of (i) the flow pattern in the dividing header, i.e., flow-inlet condition at the header entrance, (ii) the pressure distribution in the combining header, i.e., pressure condition at the branch outlets, and (iii) pressure-loss characteristics of refrigerant tubes, i.e., branch profiles, on the flow distributions. The pressure distributions in the combining and dividing headers as well to make clear the backpressure condition of the branches in a real evaporator also has been measured. The experiments have been conducted with the isothermal air-water system that is suitable for grasping the fundamental flow characteristics in the channel.

Also an analysis of finding the most influenced parameter to the flow distribution uniformity in multi-pass channel has been done by using DOE, i.e., the design of experiment method which is one of the six sigma tools or “anova”, i.e., an analysis of variance in statistical mathematics term. It is expected that the data of the gas-liquid distributions obtained under these specified inlet and outlet conditions are helpful not only to understand the two-phase flow distribution characteristics in the multi-pass channels but also as a database to examine the reliability of numerical simulations.

The second segment of this chapter is the result and discussion on the study of the similarities of real refrigerant and air-water two phase flow distribution behavior. The testing result involved in this segment shall include the visual observation result on the test channel of a real refrigerant (R-134a) and air-water. A comparison of both substances flow distribution characteristic shall be discussed with the qualitative and quantitative data that has been taken.

4.2 First segment: Study on parameters that influence the flow distribution

4.2.1 Flow distributions under the stratified-flow inlet

In this section, the air and water flow distribution characteristics measured under the stratified-flow inlet condition (Fig. 3.7(a)) are addressed. Fig. 4.1 shows an example of snapshots of the flow in the dividing header under the stratified-flow inlet condition. It was found that water was distributed to the branches unsteadily by large waves but the downstream region of the dividing header was blocked by stagnant water.

At first, the influence of the backpressure condition at the branch outlets on the flow distributions is examined in detail. As a baseline, the results of air and water distributions obtained in the channel with flat tube branches are shown in Fig. 4.2. The abscissa shows the branch number and the branch located nearest the header entrance is

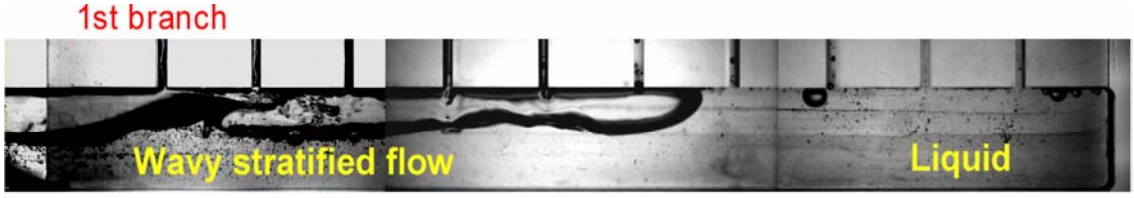

Fig. 4.1 Snapshot of the flow in the dividing header under the stratified-flow inlet condition

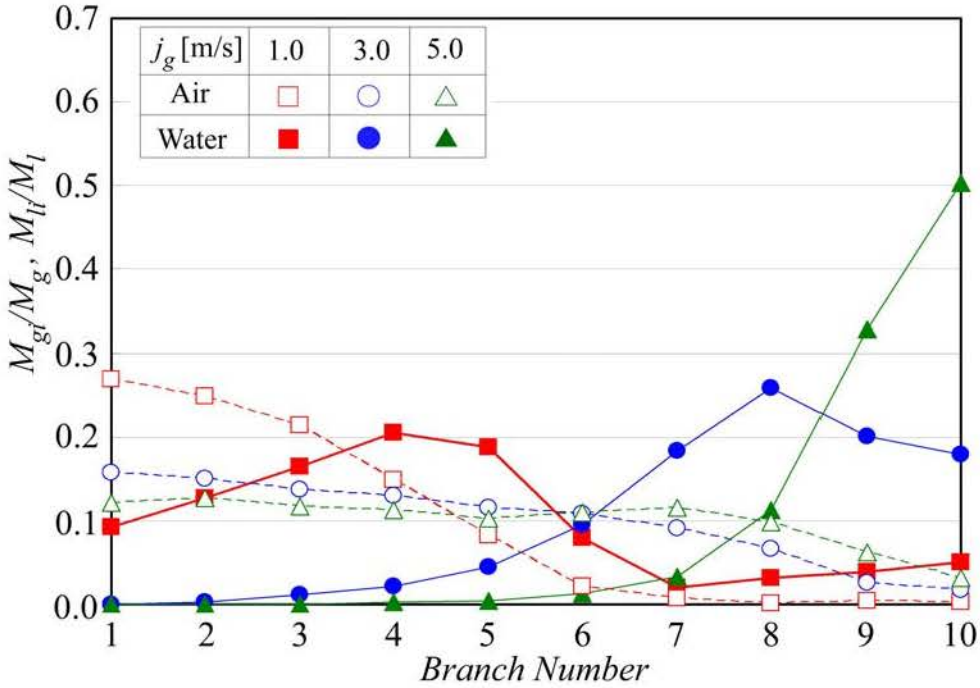

(a) Case A (Non-uniform backpressure condition)

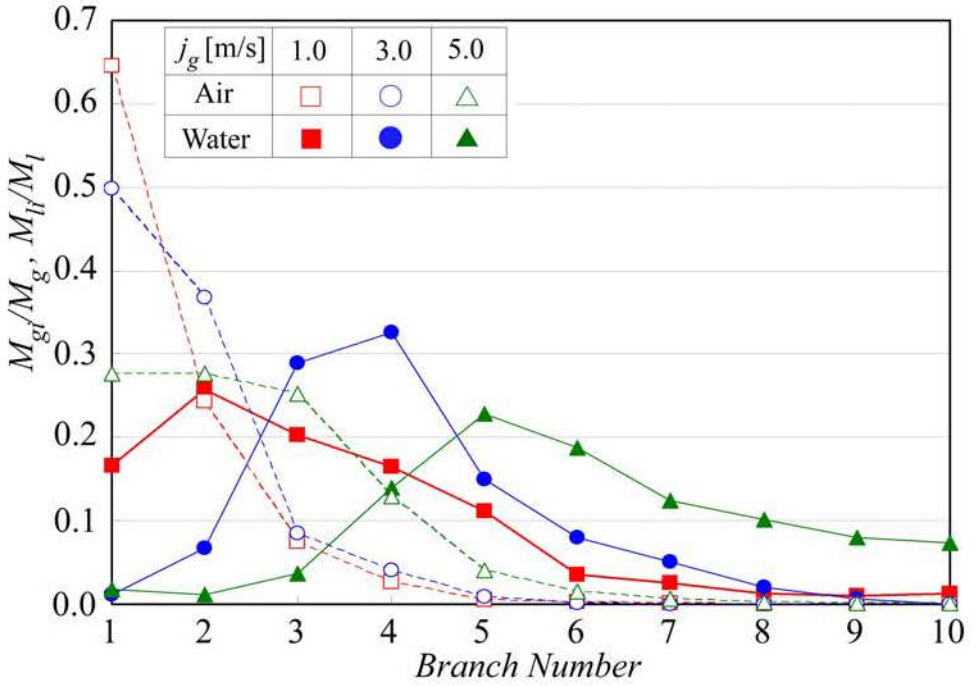

(b) Case B (Uniform backpressure condition)

Fig. 4.2 Flow distributions under the stratified-flow inlet condition
(Flat tubes, j_l = 0.03 m/s)

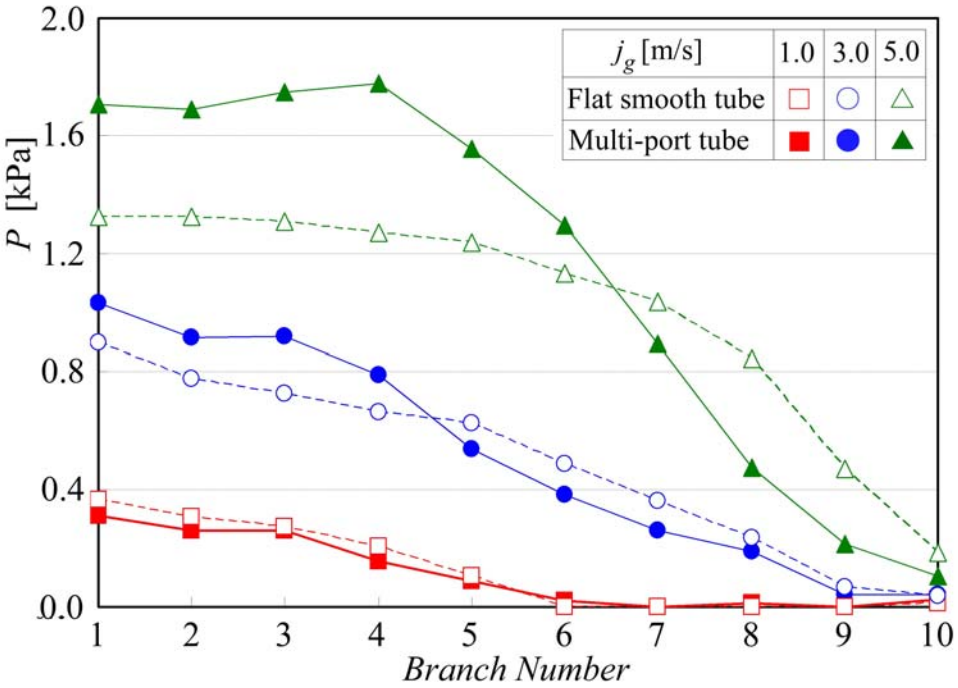

Fig. 4.3 Pressure distributions at the branch outlets in Case A (Flat tubes, j_l = 0.03 m/s)

denoted as "1". The ordinate shows the air distribution ratio M_{gi}/M_g (broken lines) and the water distribution ratio M_{li}/M_l (solid lines) measured in the i th branch (i = 1 ~ 10). The superficial water velocity at the header entrance j_l is fixed at 0.030 m/s, and the superficial air velocity j_g is varied as 1.0 m/s, 3.0 m/s and 5.0 m/s. The pressure distributions at the branch outlets measured in Case A are shown in Fig. 4.3. The backpressure is highest in the first branch, and it decreases gradually in the branches located further downstream. From this result one can confirm that the non-uniform backpressure condition is imposed on the branches in Case A.

Fig. 4.2(a) shows the results obtained under the non-uniform backpressure condition (Case A in Fig. 3.8(a)). At the lowest air velocity of j_g = 1.0 m/s, larger amount of air is distributed to branches located nearer the header entrance and M_{gi}/M_g is almost zero after the 6th branch. The water distribution ratio M_{li}/M_l also shows relatively large values in upstream branches but it attains the maximum in the 4th branch. This branch corresponds to the location at which the crests of the large waves generated in the header reach the top wall of the dividing header. As observed in Fig. 4.1, water is distributed to the branches unsteadily by large waves generated in the dividing header and it was found that the location where they occurred moved downstream as j_g was increased. At low j_g, the downstream region of the header is blocked by stagnant water as observed in Fig. 4.1 and very little amount of air and water is distributed to the

branches there.

As j_g is increased, air tends to be distributed to more downstream branches and air is distributed almost uniformly to all the branches at j_g = 5 m/s. A close correlation is observed between the air distribution ratios and the pressure distribution at the outlets of the branches shown in Fig. 4.3. This is because the pressure loss in the gas-flow meter settled at the exit of the separator increases in proportion to the air flow rate. On the other hand, the water tends to be distributed preferentially to the downstream branches as j_g is increased, and the mal-distribution of water is further enhanced at higher j_g. These results mean that a uniform distribution of liquid that is desirable to evaporators cannot be obtained even if gas is distributed uniformly to all the branches.

Fig. 4.2(b) shows the results obtained under the condition of Case B in Fig. 3.8(b), the uniform backpressure condition at the branch outlets. Similar to the results of Case A described above, both air and water tends to be distributed to more downstream branches as j_g is increased. The mal-distribution of air to upstream branches is, however, more serious than that in Case A, and M_{gi}/M_g is almost zero after the 7th branch even in the highest air velocity condition of j_g = 5 m/s. On the other hand, the preferential distribution of water to downstream branches observed at higher j_g in Case A is remarkably relieved in Case B. For example, at j_g = 5 m/s, the location of the maximum M_{li}/M_l moves from the 10 th branch in Case A to the 5 th branch in Case B. The reason for such a difference of flow distributions in Case A and Case B is explained as follows. In Case A, the backpressure of a branch becomes higher as the air flow rate in it increases. Therefore, the air distribution is suppressed automatically if excessive amount of air is distributed to a branch. On the other hand, in Case B, the backpressure of the branch does not change depending on the air distribution. As a result, the air distribution is not suppressed even if larger amount of air is distributed to a branch; this causes larger values of M_{gi}/M_g in branches located near the header entrance.

The results obtained in the channel with multi-port tube branches are shown in Fig. 4.4, in which j_l is fixed at 0.030 m/s and j_g is varied from 1.0 m/s to 5.0 m/s. Fig. 4.4(a) presents the air and water distribution ratios obtained under the non-uniform backpressure condition (Case A). At the lowest j_g = 1.0 m/s, a larger amount of air is distributed to branches located nearer the header entrance and M_{gi}/M_g is almost zero after the 6th branch. The water distribution ratio M_{li}/M_l, however, shows quite a uniform distribution. As j_g is increased, air tends to be distributed to further downstream branches and at j_g = 5 m/s air is distributed almost uniformly to the branches except last two branches. On the other hand, water tends to be distributed preferentially to

downstream branches as j_g is increased, thus the mal-distribution of water is enhanced at higher j_g. These results of air and water distributions in the multi-port tube channel for Case A are qualitatively similar to those observed in the flat tube channel for Case A shown in Fig. 4.2(a). The mal-distribution of water to downstream branches at high j_g is, however, relieved with the multi-port tubes.

Fig. 4.4(b) shows the results for the uniform outlet pressure condition (Case B). The flow distribution characteristics observed under this backpressure condition agree well with those of Case A described above. This means that, in case of the multi-port tubes, the backpressure conditions at the branch outlets exert only minor influences on the flow distributions. Because the pressure losses of the multi-port tubes are much larger than those of the flat tubes, the influence of the pressure variations at the branch outlets on the flow distributions becomes relatively small.

Next, the influences of the superficial water velocity j_l on the flow distributions are discussed. Figs. 4.5(a) and 4.5(b) show the results obtained with the flat tubes under the backpressure conditions of Case A and Case B, respectively. The super air velocity j_g is fixed at 5.0 m/s, and j_l is changed from 0.015 m/s to 0.045 m/s. In Case A, the air and water distribution ratios do not change depending on j_l, and it follows that the flow distribution characteristics are determined solely by j_g. In Case B, both M_{gi}/M_g and M_{li}/M_l in the upstream branches become larger as j_l is increased. From a comparison of Fig. 4.2(b) and Fig. 4.5(b), however, it is found that j_g exerts greater influences on the gas and liquid distributions than j_l in Case B as well as in Case A.

The results obtained in the multi-port tube channel are shown in Fig. 4.6. The influences of the backpressure conditions and of j_l are not observed at all in M_{gi}/M_g and M_{li}/M_l, and the flow distribution characteristics are qualitatively similar to those observed in Case A with the flat tube channel.

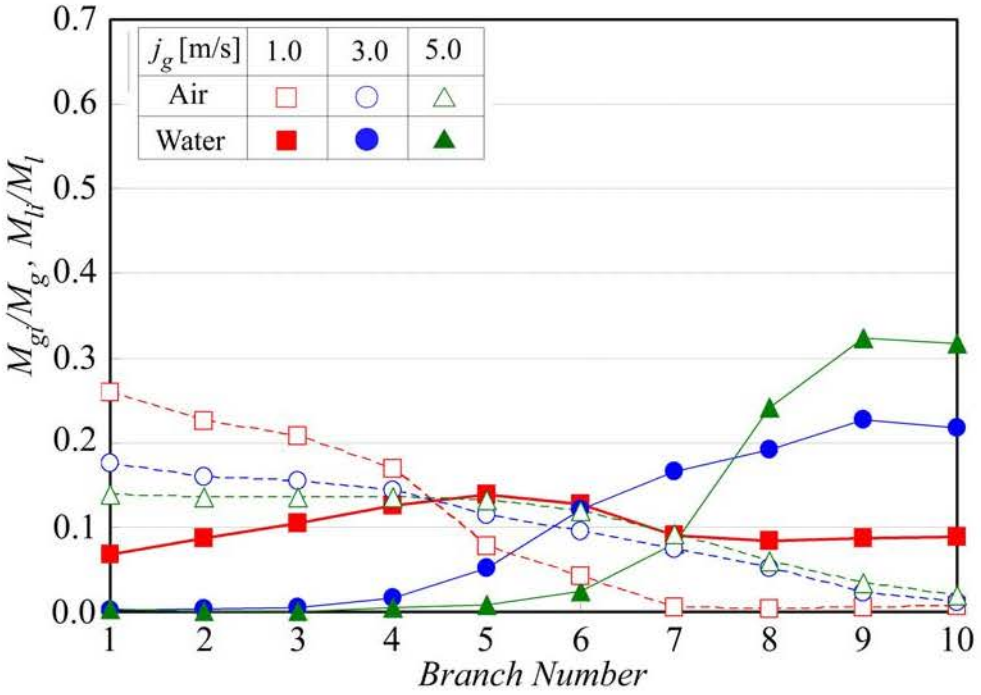

(a) Case A (Non-uniform backpressure condition)

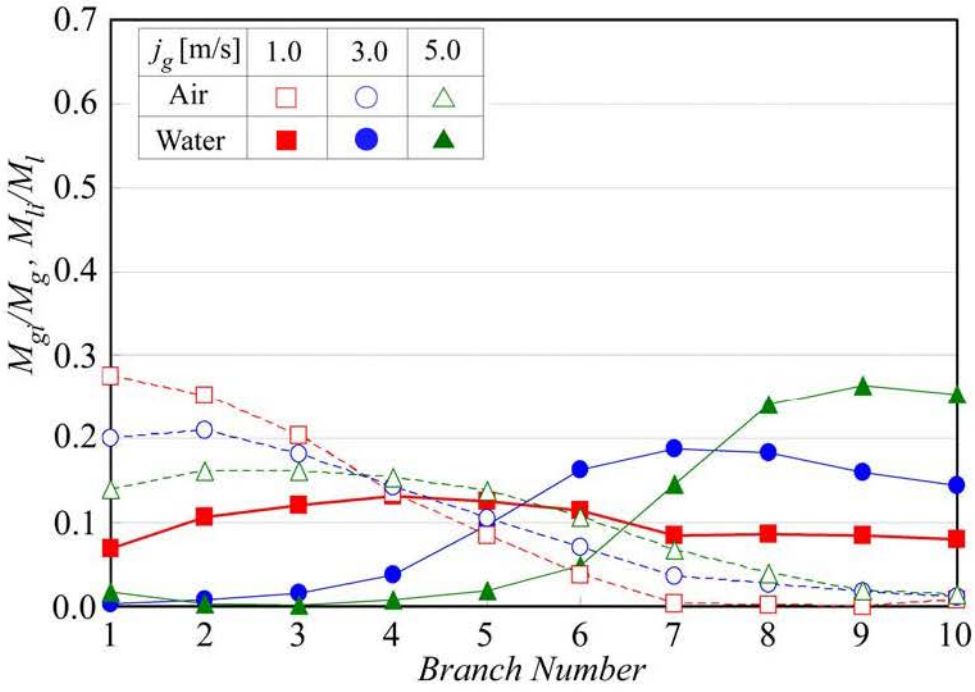

(b) Case B (Uniform backpressure condition)

Fig. 4.4 Flow distributions under the stratified-flow inlet condition
(Multi-port tubes, j_l = 0.03 m/s)

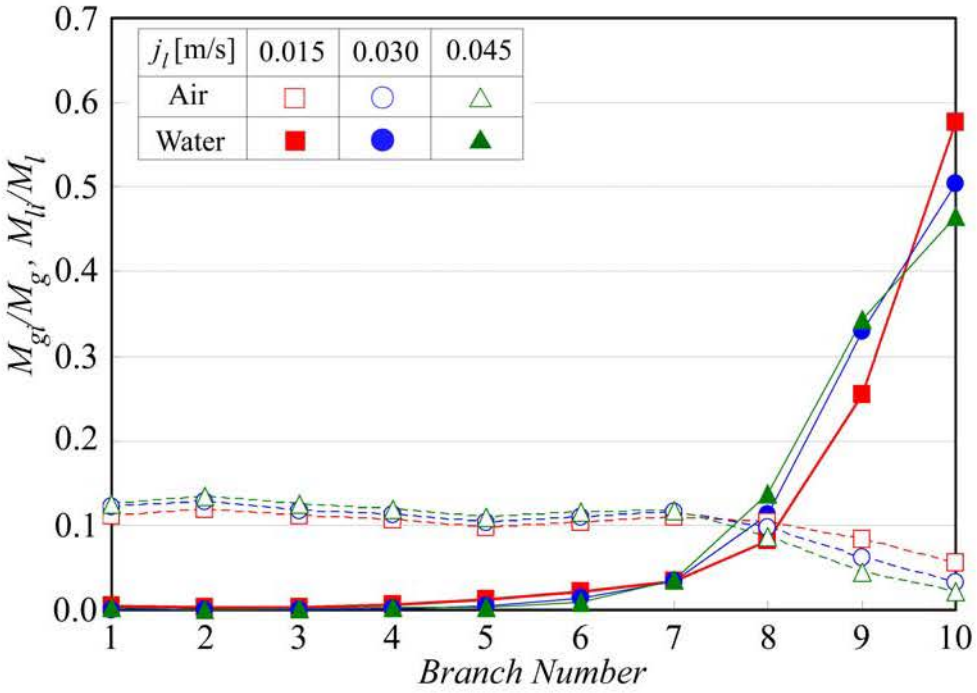

(a) Case A (Non-uniform backpressure condition)

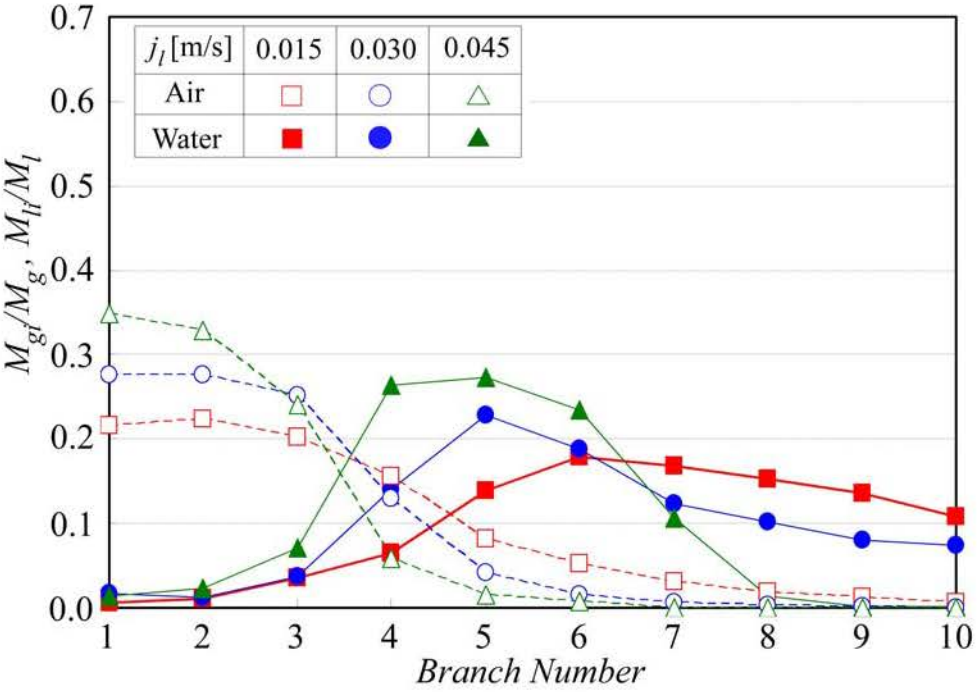

(b) Case B (Uniform backpressure condition)

Fig. 4.5 Flow distributions under the stratified-flow inlet condition
(Flat tubes, j_g = 5 m/s)

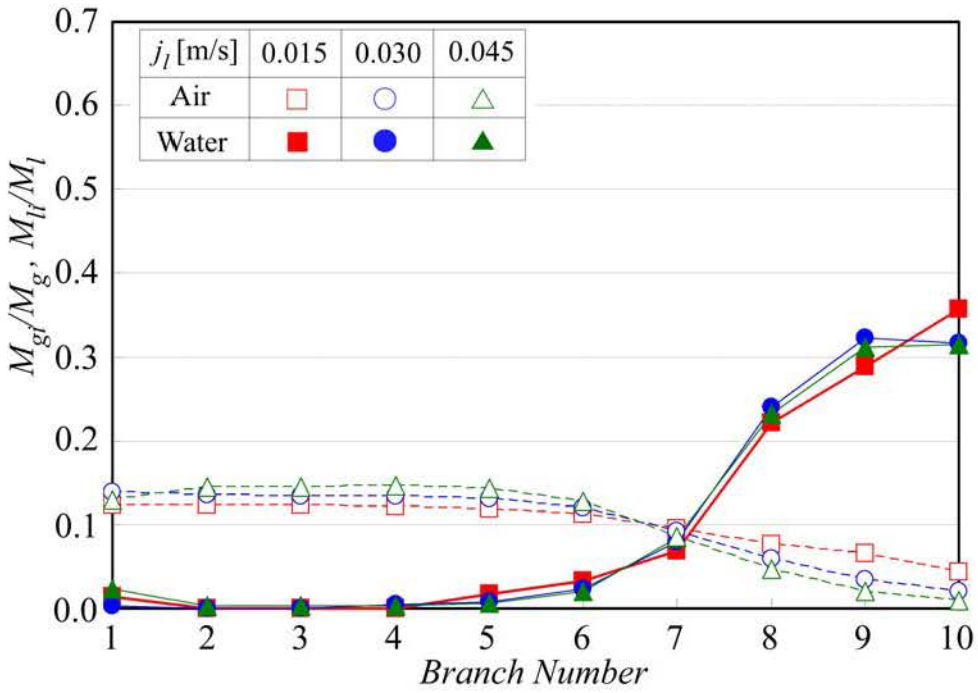

(a) Case A (Non-uniform backpressure condition)

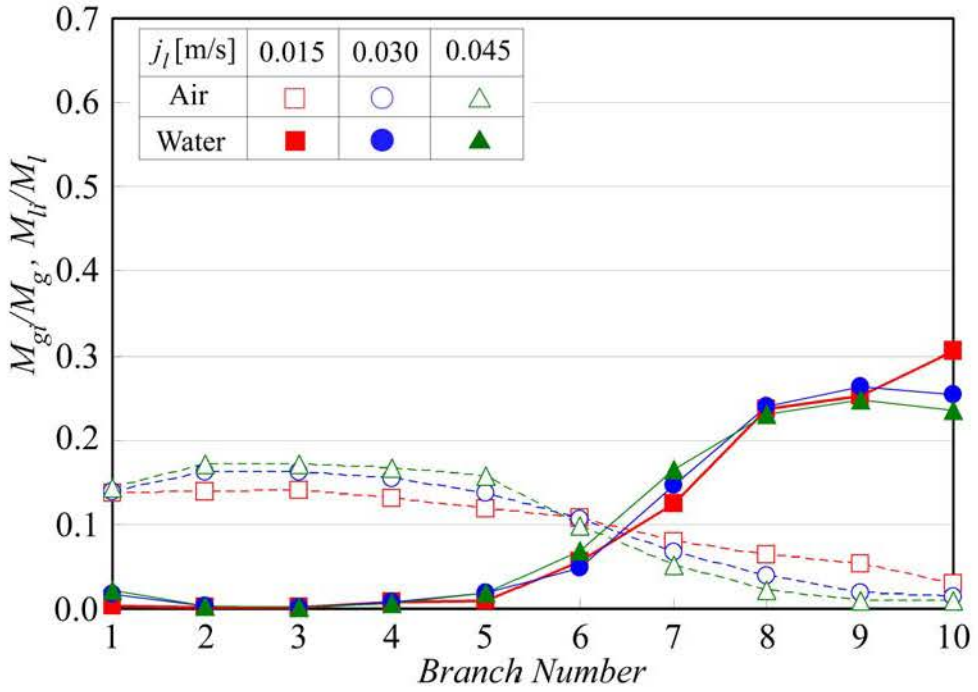

(b) Case B (Uniform backpressure condition)

Fig. 4.6 Flow distributions under the stratified-flow inlet condition
(Multi-port tubes, j_g = 5 m/s)

4.2.2 Flow distributions under the mist-flow inlet

The results shown so far were obtained under the stratified-flow inlet condition. As a contrastive case, we measured the flow distributions under the mist-flow inlet condition and the results are discussed in this section. A snapshot of the flow in the dividing header is shown in Fig. 4.7. It is observed that the annular mist flow is formed near the header entrance, but air and water tends to be separated in a downstream region of the header. The large waves such as observed in the stratified-flow inlet are not generated in this flow-inlet condition. At low j_g, water stagnates in the downstream region of the dividing header as is the case with the stratified-flow inlet.

At first, the results obtained in the channel with flat tubes are addressed. Figures 4.8(a) and 4.8(b) show the air and water distributions measured under the non-uniform backpressure condition (Case A) and the uniform backpressure condition (Case B), respectively, at constant j_l = 0.03 m/s. The superficial air velocities at the header entrance j_g are the same as those of Fig. 4.2.

In Case A, the air distribution ratios M_{gi}/M_g show qualitatively similar characteristics to those in the stratified-flow inlet shown in Fig. 4.2(a), but the uniformity of the water distribution is improved especially at high j_g. At the lowest j_g of 1 m/s, however, M_{li}/M_l is very low in the 4th - 7th branches. This is explained as follows. In this middle region of the dividing header, water flows in the lower part of the header cross section at low j_g and is not distributed to the branches because the water film initially formed over the top wall of the header is distributed into the upstream branches. At larger air velocity, water droplets are distributed to the branches located in the middle region and relatively uniform distribution of water is achieved.

In Case B shown in Fig. 4.8(b), similar to the results obtained in the stratified-flow inlet under the uniform backpressure condition, most of air is distributed to the first and second branches at low j_g of 1.0 m/s. As j_g is increased, M_{gi}/M_g in these branches

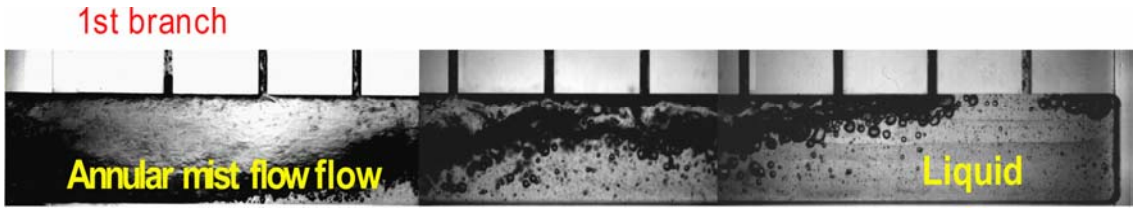

Fig. 4.7 Snapshot of the flow in the dividing header under the mist-flow inlet condition

decreases and air tends to be distributed to the branches in the downstream region as well. As a result, the uniformity of the air distribution is improved in comparison with that for the stratified-flow inlet. The mal-distribution of air to the upstream branches is, however, enhanced in comparison with Case A of the mist-flow inlet. The water distribution shows qualitatively similar characteristics to that of Case A. From a comparison of Fig. 4.2 and Fig. 4.8, it follows that under the mist-flow inlet condition with flat tubes the pressure condition at the branch outlets exerts minor influence on the water distributions in comparison with the stratified-flow inlet. In the mist-flow inlet, water droplets and liquid film formed over the header walls have a direct influence on the water distributions to the branches. Since they are generated at the header entrance, it is though that the influences of the backpressure condition of branches and local air velocity in the dividing header on the water distribution are lessened in comparison with the stratified-flow inlet.

The flow distributions measured in the channel with multi-port tubes are presented in Fig. 4.9(a) (Case A) and Fig. 4.9(b) (Case B). In this channel, the influence of the pressure condition at the branch outlets on the flow distributions is very small, and this tendency is similar to that observed in the stratified-flow inlet. The air distribution ratios M_{gi}/M_g shows qualitatively similar characteristics to those measured in the flat tube channel under the non-uniform backpressure condition (Fig. 4.8(a)). The water distribution ratios M_{li}/M_l increase remarkably in the 9th and 10th branches at higher air velocities, but the uniformity of the water distribution is improved in comparison with the stratified-flow inlet shown in Fig. 4.4.

Next, the influences of the superficial water velocity j_l on the flow distributions are examined. Fig. 4.10 shows the results of the flat tube channel, in which j_g is fixed at 5 m/s. Under both backpressure conditions, M_{gi}/M_g and M_{li}/M_l are almost zero in the first branch at relatively low j_l. Since j_g is quite high in Fig. 4.10, the inertia of air is large near the header entrance. Thus, air and water droplets entrained by air tend to go straight in the header passing over the entrance to this branch at the dividing T-junction. This causes the low air and water distribution ratios in the first branch. The influences of j_l on the flow distributions appear more clearly in Case B than in Case A. In Case A, air is distributed almost uniformly irrespective of j_l while water is distributed preferentially to upstream branches at low j_l and to downstream branches at high j_l. In Case B, as j_l is increased, the air distribution ratio M_{gi}/M_g in the upstream branches becomes higher while that in the downstream branches decreases. This tendency is similar to that observed in the stratified-flow inlet with Case B (Fig. 4.5(b)), but the

influence of j_l on the air distribution is more significant in the mist-flow inlet. The water distribution ratio M_{li}/M_l shows relatively uniform distribution at large j_l.

The results in the multi-port tube channel are shown in Fig. 4.11. As is the case with the stratified-flow inlet shown in Fig. 4.6, the pressure condition at the branch outlets exerts only minor influences on the flow distribution. The dependences of M_{gi}/M_g and M_{li}/M_l on j_l are similar to those observed in the flat tube channel under the non-uniform backpressure condition (Fig. 4.10(a)).

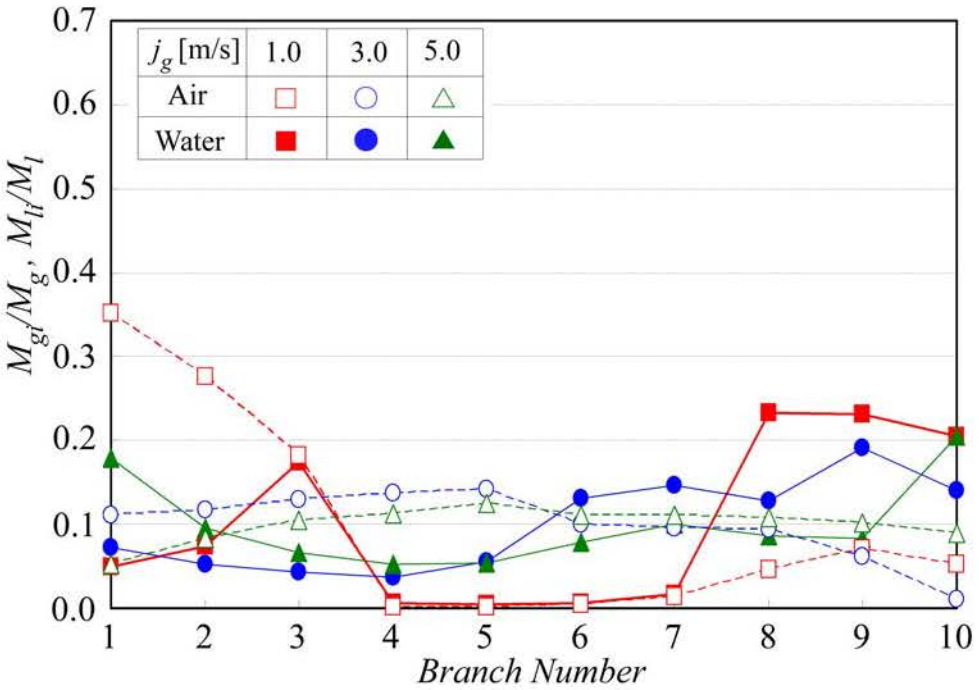

(a) Case A (Non-uniform backpressure condition)

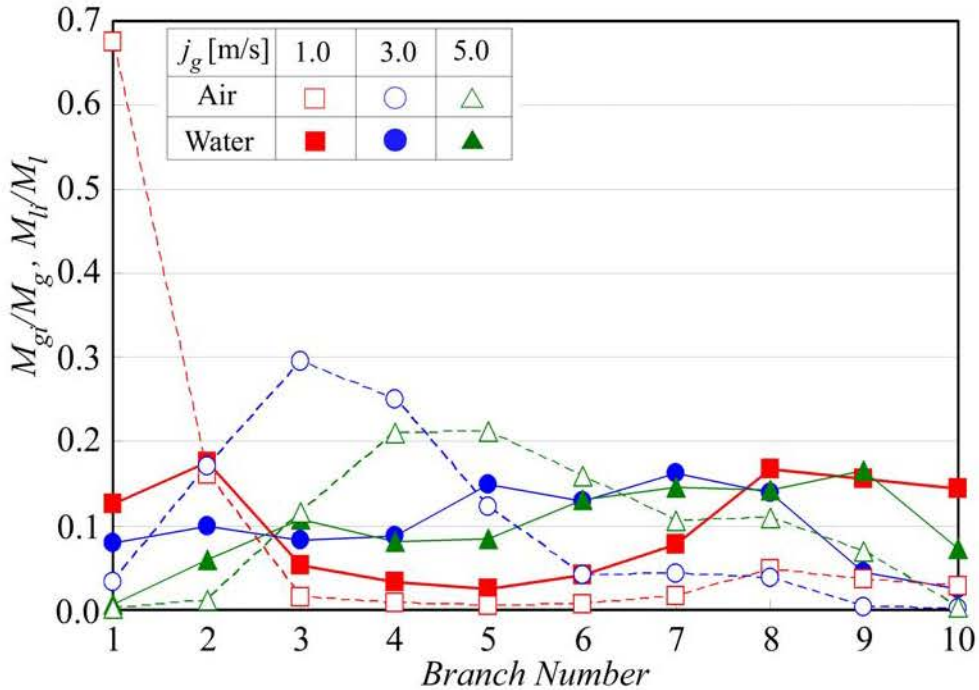

(b) Case B (Uniform backpressure condition)

Fig. 4.8 Flow distributions under the mist-flow inlet condition (Flat tubes, j_l = 0.03 m/s)

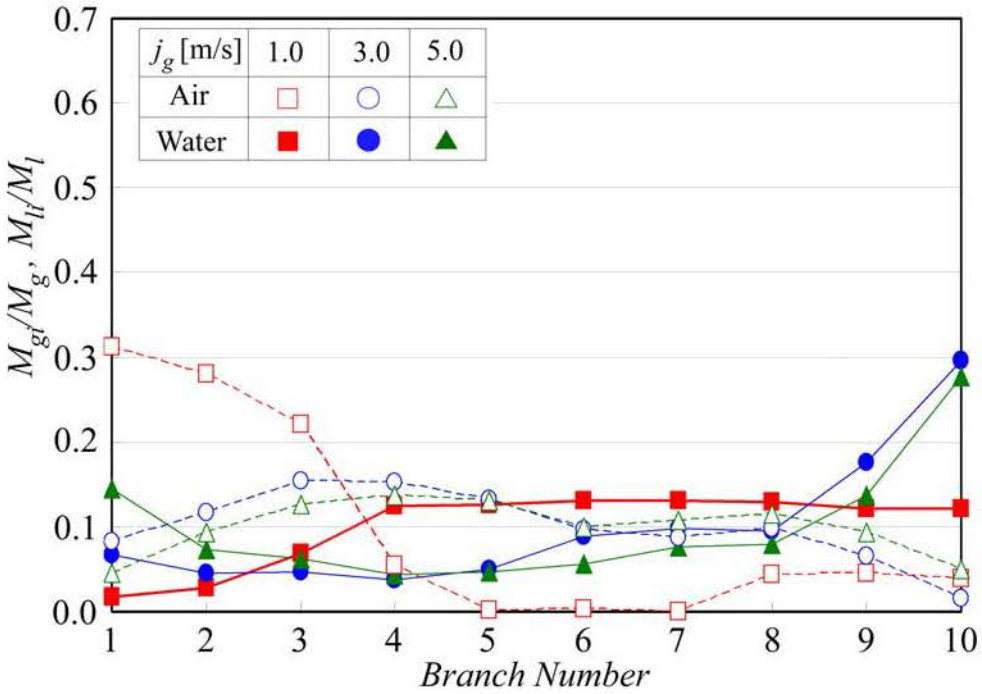

(a) Case A (Non-uniform backpressure condition)

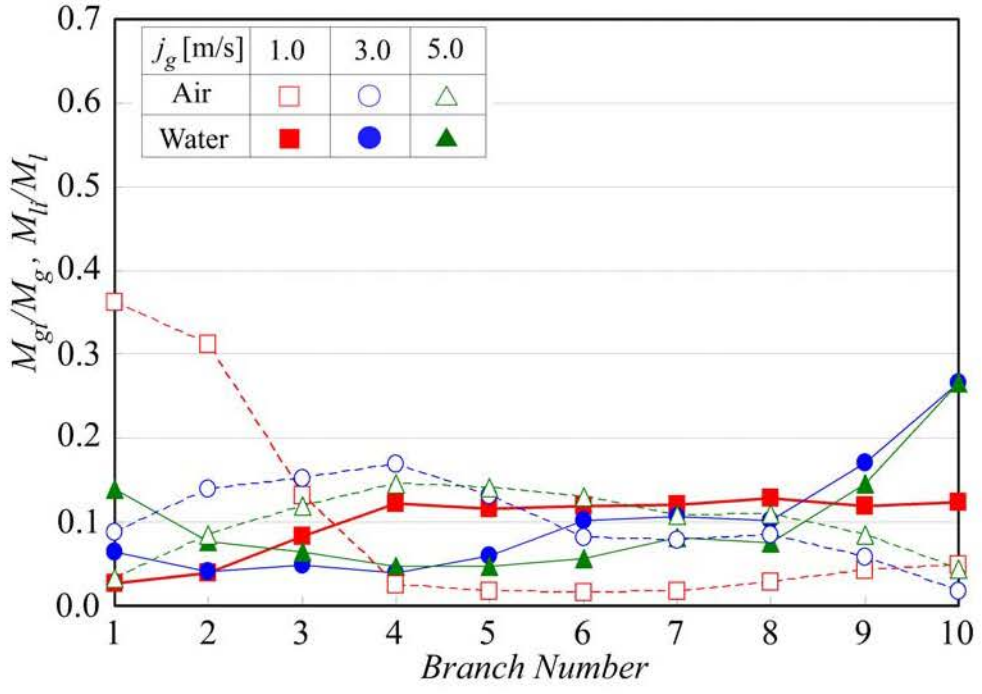

(b) Case B (Uniform backpressure condition)

Fig. 4.9 Flow distributions under the mist-flow inlet condition
(Multi-port tubes, j_l = 0.03 m/s)

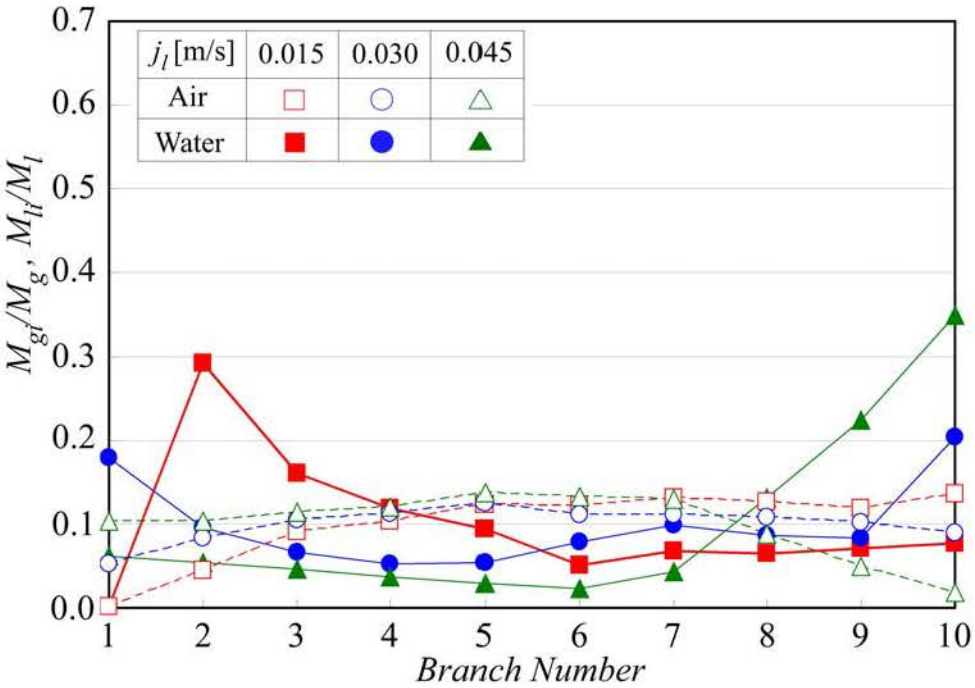

(a) Case A (Non-uniform backpressure condition)

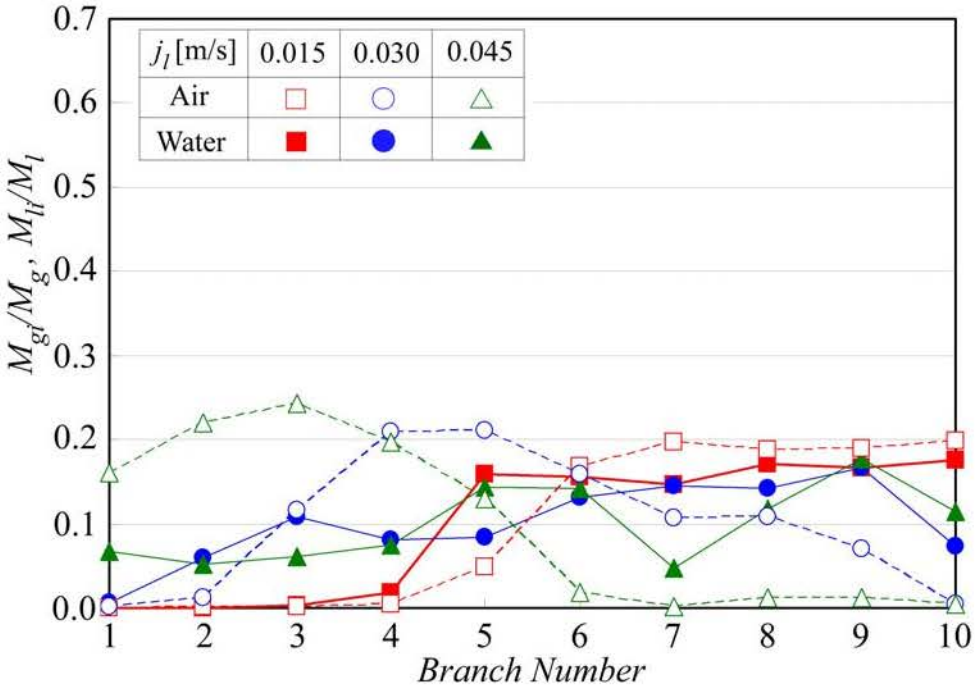

(b) Case B (Uniform backpressure condition)

Fig. 4.10 Flow distributions under the mist-flow inlet condition (Flat tubes, j_g = 5 m/s)

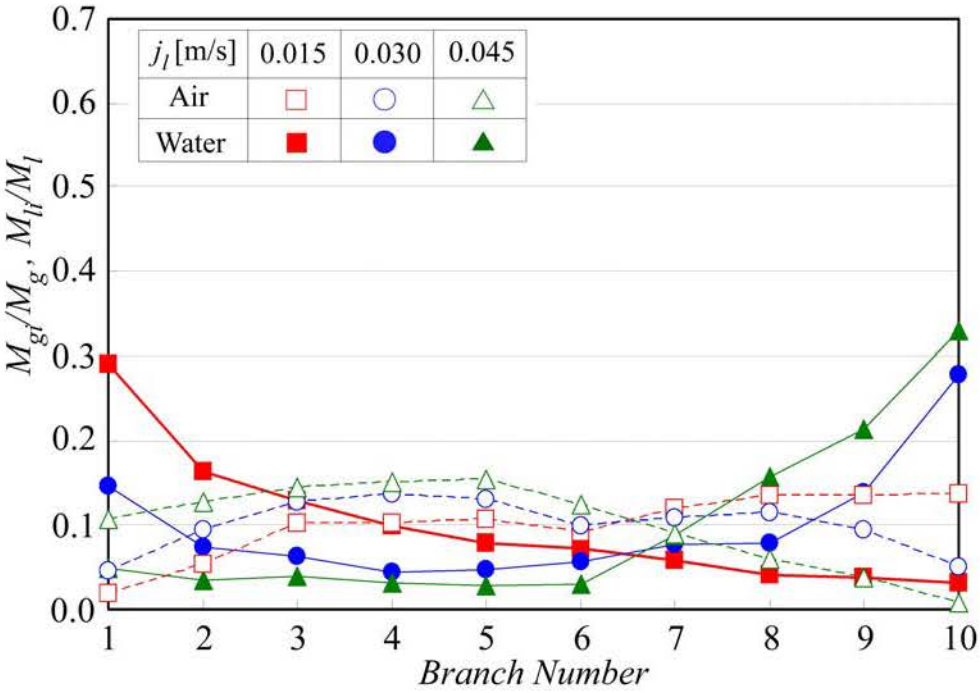

(a) Case A (Non-uniform backpressure condition)

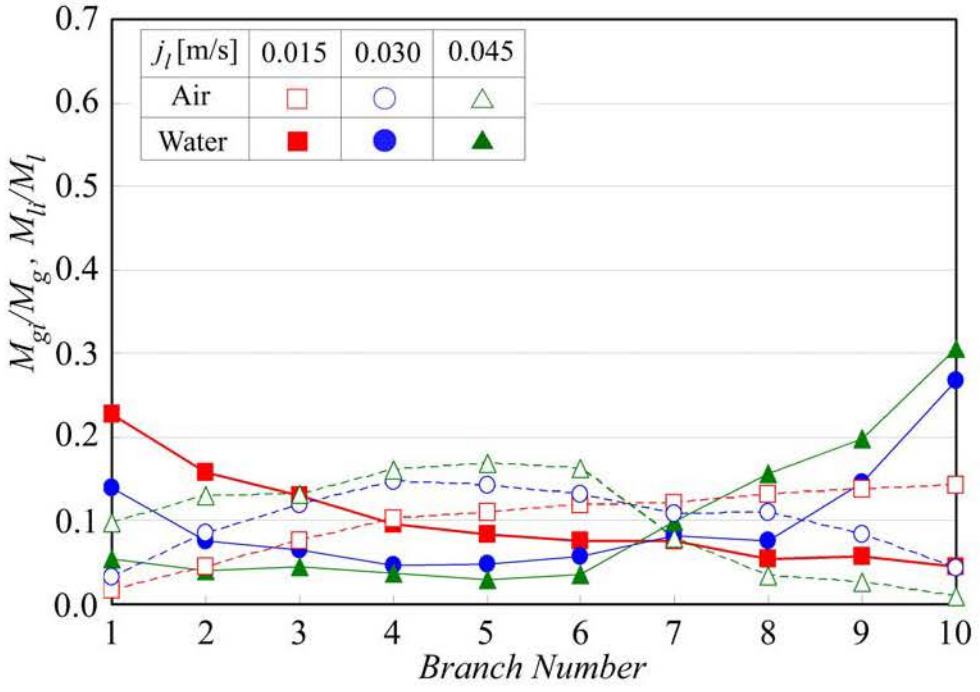

(b) Case B (Uniform backpressure condition)

Fig. 4.11 Flow distributions under the mist-flow inlet condition
(Multi-port tubes, j_g = 5 m/s)

4.2.3 Evaluation of uniformity of flow distributions

As described so far, the air-water distribution characteristics in the multi-pass channels change in a complex manner depending on the flow inlet condition at the header entrance, pressure condition at the branch outlet, and the branch profile. In the application of these channels to compact heat exchangers, a uniform flow distribution to all the branches is ideal for high thermal performance. In this study, in order to evaluate the uniformity of the air and water distributions to the branches, the standard deviations of M_{gi}/M_g and M_{li}/M_l, denoted as σ_g and σ_l respectively, have been calculated by the following equations. The smaller values of σ_g and σ_l statistically correspond to the higher uniformity of the air and water distributions as reported by Marchitto A. et al. (2008).

$$\sigma_g = \sqrt{\sum_{i=1}^{N}\left(\frac{M_{gi}}{M_g}-\frac{1}{N}\right)^2 / N} \qquad (N=10) \qquad (4.1)$$

$$\sigma_l = \sqrt{\sum_{i=1}^{N}\left(\frac{M_{li}}{M_l}-\frac{1}{N}\right)^2 / N} \qquad (N=10) \qquad (4.2)$$

Figs. 4.12 and 4.13 show the results of σ_g and σ_l, respectively, obtained with the stratified flow inlet. Figs. (a) and (b) correspond to the backpressure conditions of Case A and Case B, respectively. The abscissa shows the superficial air velocity j_g, and the results in the flat tube channel and the multi-port tube channel are compared in each figure. In both branch profiles and backpressure conditions, σ_g decreases as j_g is increased. The influence of the branch profile on σ_g appears clearly in Case B (uniform backpressure condition). On the other hand, σ_l increases almost linearly with j_g. As a whole, the standard deviation of the water distribution ratios shows smaller values in the multi-port tube channel. This means that the uniformity of the liquid distributions to the branches is improved with the multi-port tubes in the stratified-flow inlet condition.

Next, the results of σ_g and σ_l for the mist-flow inlet are shown in Fig. 4.14 and Fig.

4.15. The distributions of σ_g are qualitatively similar to those obtained with the stratified-flow inlet, but the difference between the flat tubes and the multi-port tubes in Case B is somewhat smaller than that found in Fig. 4.12(b). In σ_l, no distinct difference is observed between these tube profiles. As a general trend, σ_l for the mist-flow inlet shows smaller values than that for the stratified-flow inlet irrespective of the backpressure condition and the branch profile. This suggests that the flow pattern in the dividing header is the decisive factor for the uniformity of the liquid distribution to the branches.

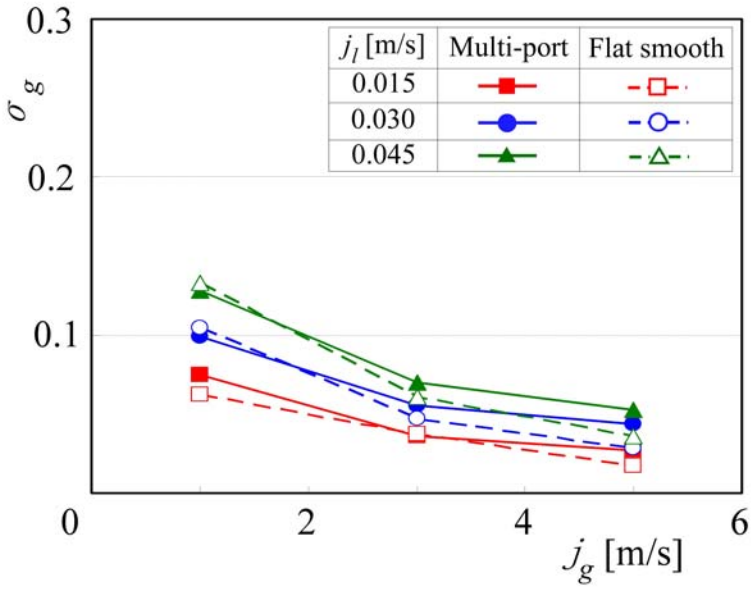

(a) Case A (Non-uniform backpressure condition)

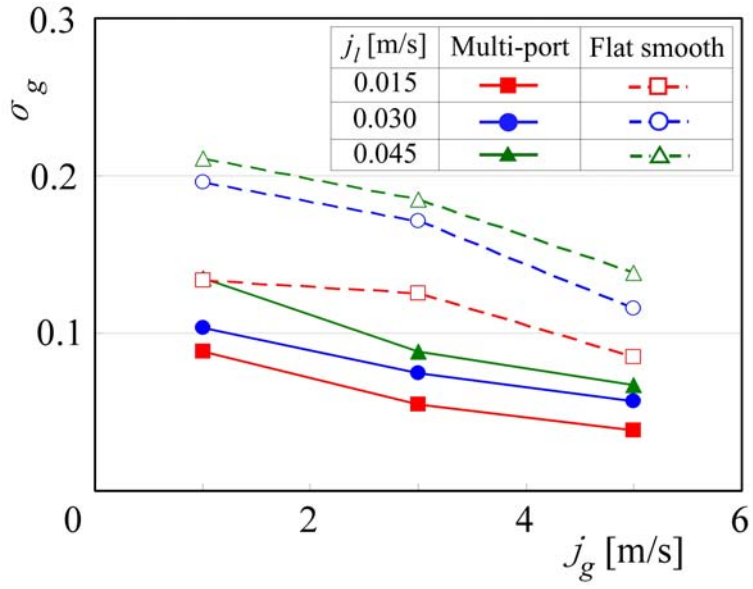

(b) Case B (Uniform backpressure condition)

Fig. 4.12 Standard deviations of the air distribution ratios σ_g under the stratified-flow inlet condition

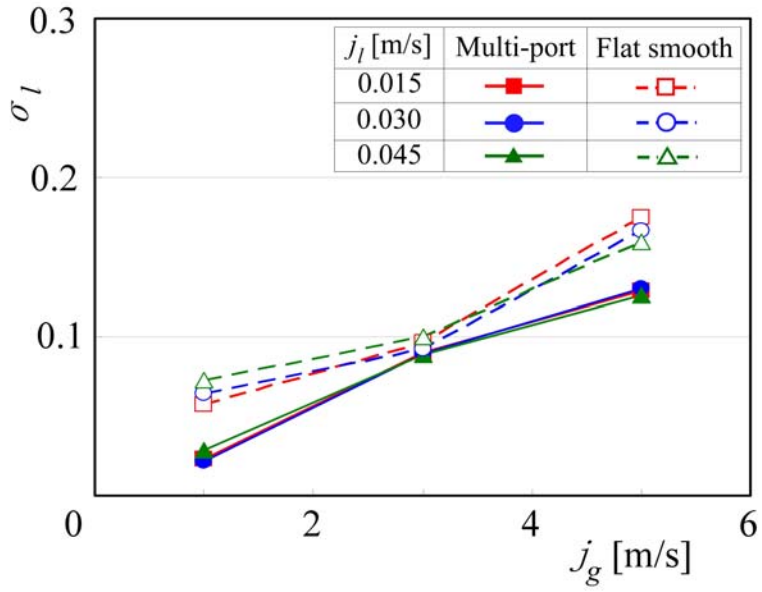

(a) Case A (Non-uniform backpressure condition)

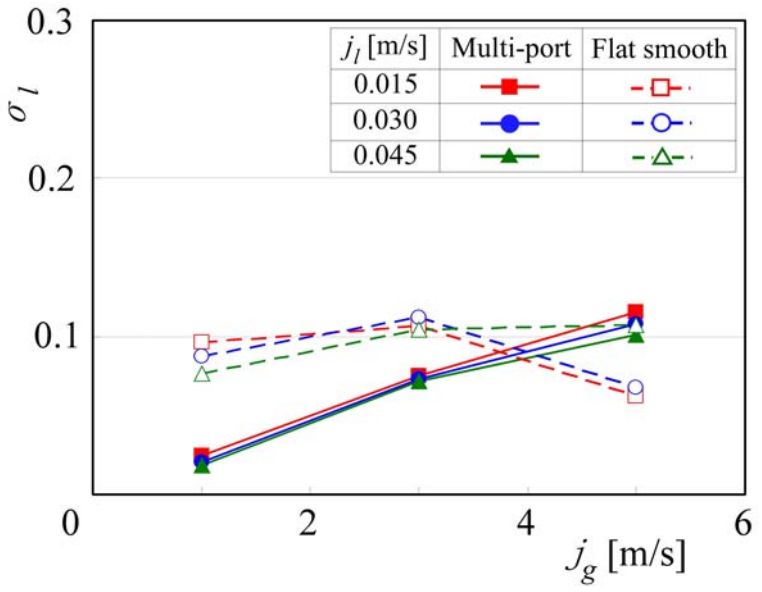

(b) Case B (Uniform backpressure condition)

Fig. 4.13 Standard deviations of the water distribution ratios σ_l under the stratified-flow inlet condition

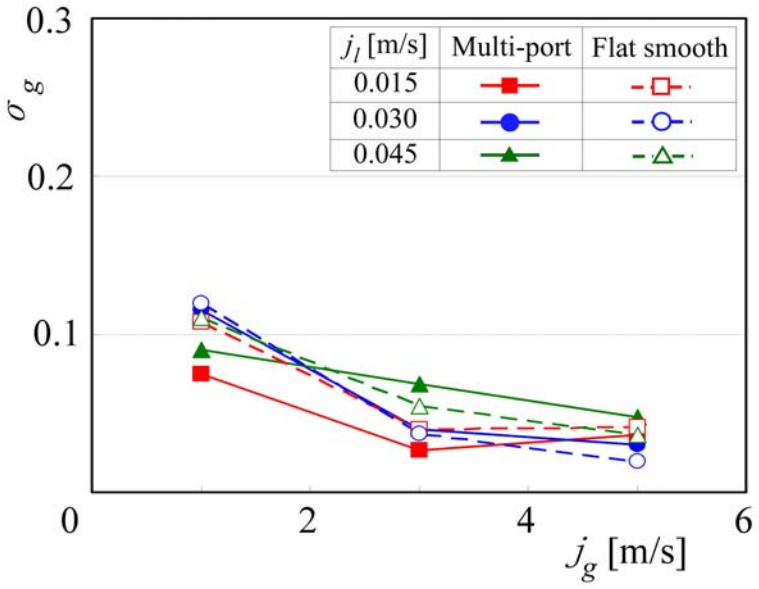

(a) Case A (Non-uniform backpressure condition)

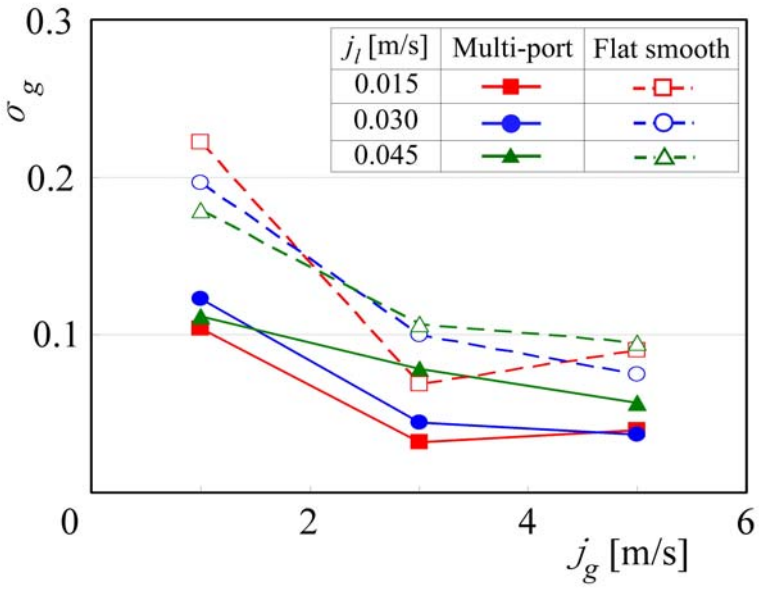

(b) Case B (Uniform backpressure condition)

Fig. 4.14 Standard deviations of the air distribution ratios σ_g under the mist-flow inlet condition

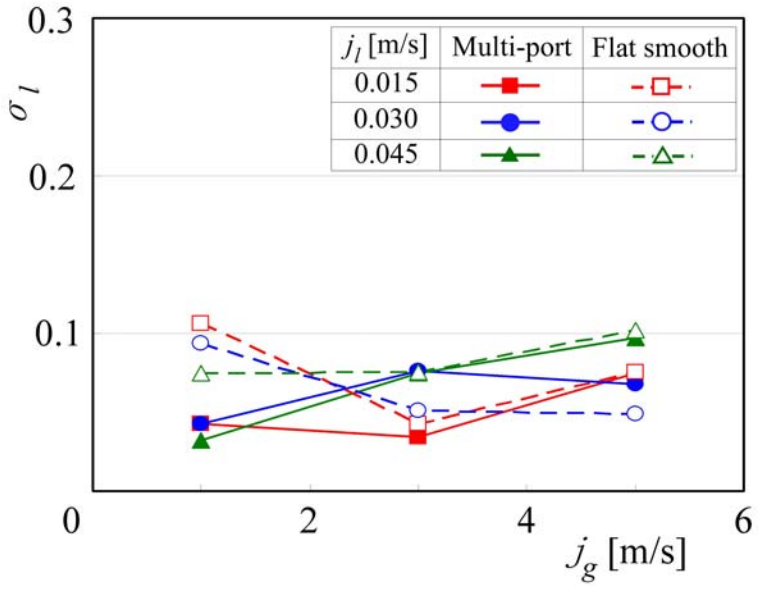

(a) Case A (Non-uniform backpressure condition)

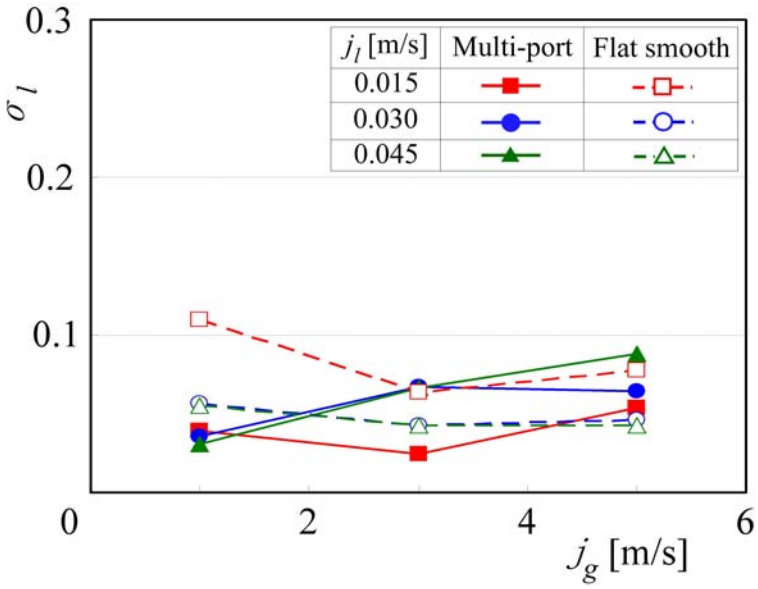

(b) Case B (Uniform backpressure condition)

Fig. 4.15 Standard deviations of the water distribution ratios σ_l under the mist-flow inlet condition

4.2.4 Pressure distributions inside headers

As described earlier, we tested two kinds of pressure conditions at the branch outlets and found that the backpressure conditions exerted a great influence on the flow distribution to the branches especially in the stratified-flow inlet. In a real compact evaporator, the downstream ends of the branches are connected to a combining header, and it is not clear which backpressure condition is appropriate to reproduce a flow condition in it. Hence, in this study, we measured the pressure distributions in the dividing and combining headers to make clear the pressure conditions at the branch outlets in a real evaporator and to find out an appropriate backpressure condition in the measurement of the flow distributions.

Since the flow-inlet condition and the direction of the flow in the combining header (parallel flow or reverse flow in Fig. 3.9) did not exert significant influences on the pressure distributions in the headers, the results measured under the stratified-flow and mist-flow inlet with the parallel flow condition are shown here. Figs. 4.16 and 4.17 under stratified-flow, while Fig. 4.18 and 4.19 under mist-flow inlet, present the typical pressure distributions along the dividing and combining headers measured in the flat tube channel and the multi-port tube channel, respectively. The abscissa shows the positions of the pressure sensors along each header, starting from the second branch. The pressure distributions in the dividing and combining headers are shown by the solid and broken lines, respectively. j_l is set at 0.030 m/s with the variation of j_g from 1.0 m/s to 5.0 m/s. In these figures, the pressures in both headers show almost constant values in the longitudinal direction irrespective of the values of j_g and branch profiles. This suggests that, in real evaporators, the outlets of all the branches are kept at the same pressure. Therefore, in the measurements of the flow distribution characteristics, the gas-liquid distribution ratios close to a real evaporator are expected to appear by imposing the uniform backpressure condition, Case B in Fig. 3.8(b), on the branches. As described in this paper, the backpressure condition of the branches exerts direct influences on the flow distributions in the flat tube channel. Thus, considerable care should be given to the pressure condition at the branch outlets in the interpretation of experimental data published in literature.

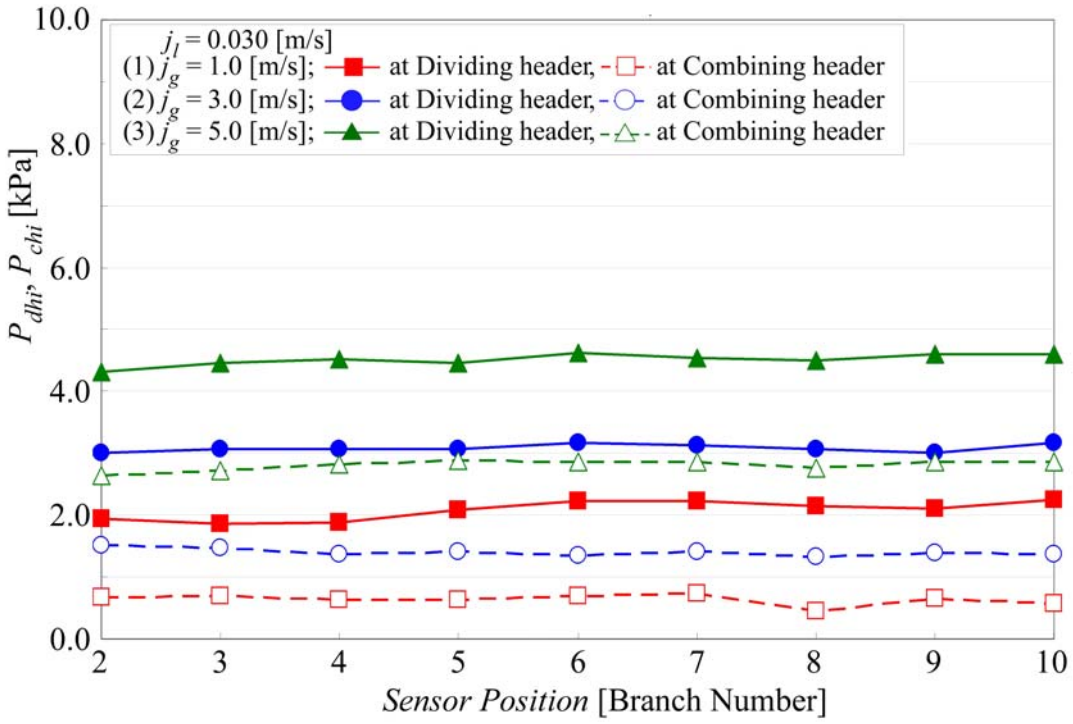

Fig. 4.16 Pressure distributions in the dividing and combining headers under the stratified-flow inlet (Flat tubes, j_l = 0.03 m/s)

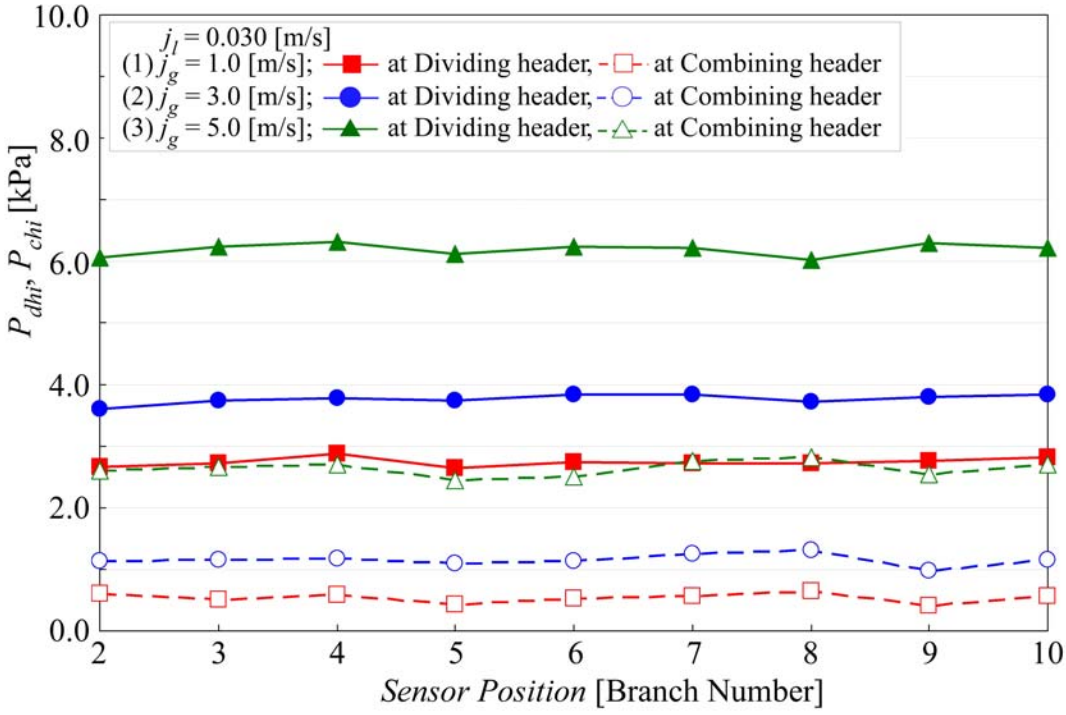

Fig. 4.17 Pressure distributions in the dividing and combining headers under the stratified-flow inlet (Multi-port tubes, j_l = 0.03 m/s)

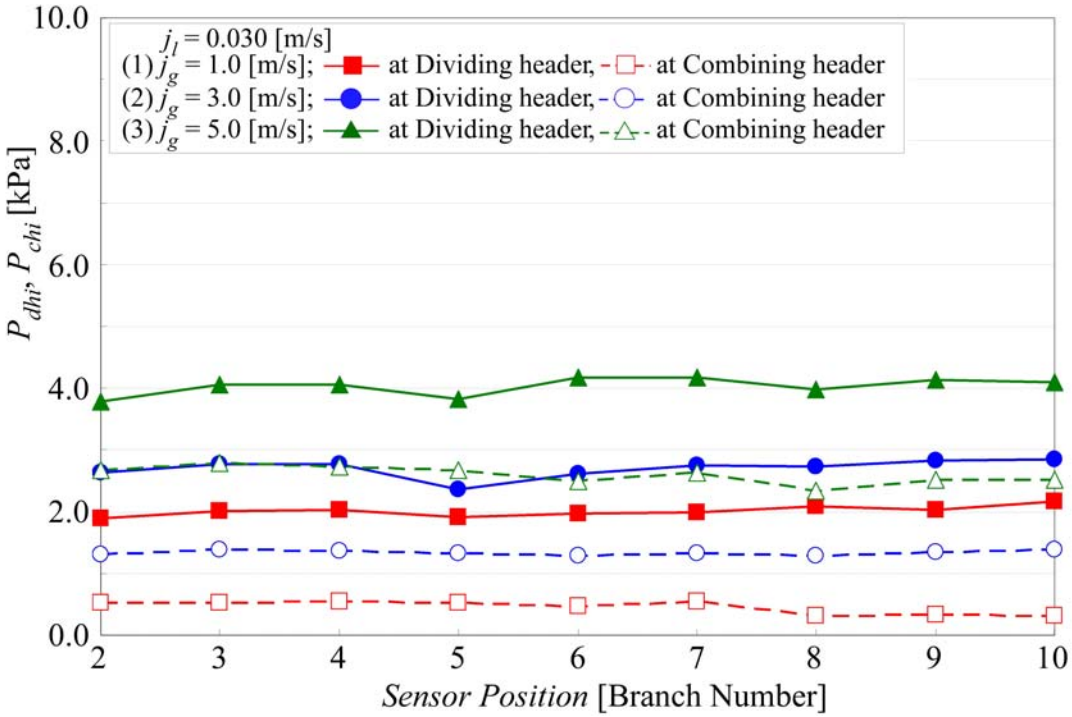

Fig. 4.18 Pressure distributions in the dividing and combining headers under the mist-flow inlet (Flat tubes, j_l = 0.03 m/s)

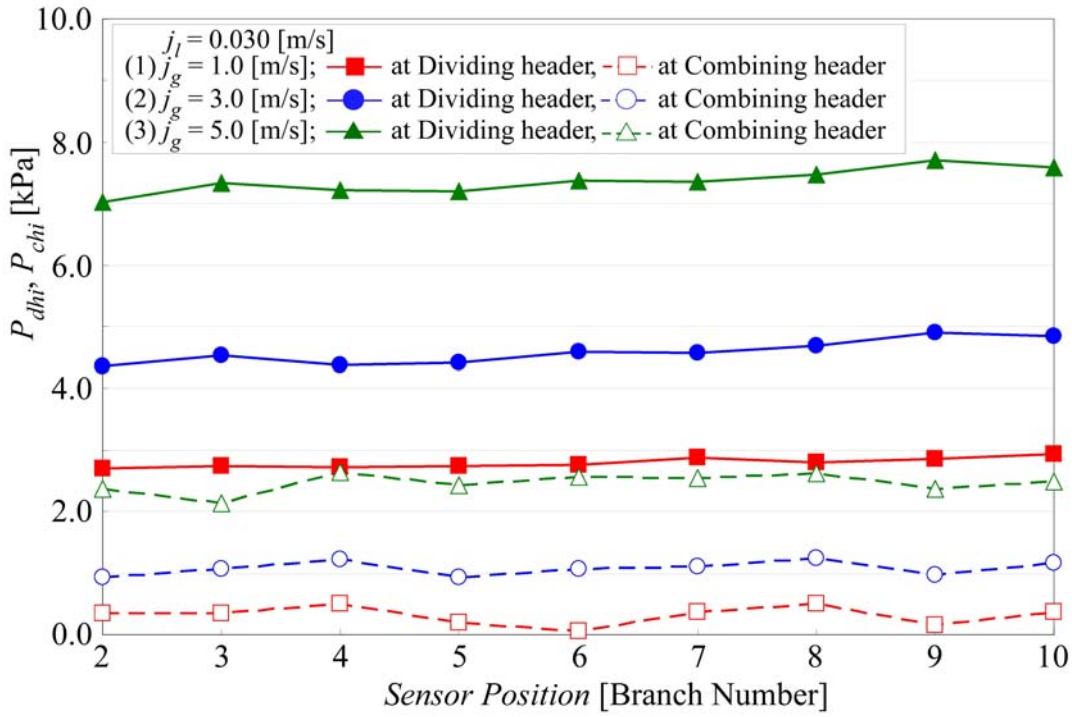

Fig. 4.19 Pressure distributions in the dividing and combining headers under the mist-flow inlet (Multi-port tubes, j_l = 0.03 m/s)

4.2.5 Analysis of most influenced parameter to uniformity of flow distributions

In this session, an analysis of parameters or factors that influenced the uniformity of flow distribution is discussed. Seems the liquid superficial velocity has been observed clearly that has a small influence to the uniformity of flow distributions, it has been decided to focus the analysis with these sources; (1) Flow pattern, (2) Backpressure, (3) Superficial air velocity (4) 2-way and 3-way interactions between parameters. This analysis is important for discovery the most valuable parameter that contributed to the uniformity of the flow distribution and the best setting of the parameters level to archive the lowest σ_g and σ_l.

As in the previous session, total of 72 combinations of test configuration with 5 parameters has been done and σ_g and σ_l has been calculated and being plot as in Fig. 4.12, 4.13, 4.14 and 4.15. A branch profile with bare smooth tube has been chose for this analysis; superficial water velocity j_l has a minor influence to the uniformity of flow distribution and by considering only 3 parameters as in table 4.1. The σ_g and σ_l that to be analyzed is reduces to 8 combinations. By, repeating the combination 3 times which the first, second and third 8 is the test data at j_l = 0.015 m/s, 0.030 m/s and 0.045 m/s respectively. Total data to be analyzed are 24 combinations. By using the "Design of Experiment" method, or in mathematics and statistics study in area of "Analysis of Variance (ANOVA)", Brookes C. J. et al. (1979), the analysis has been done by using a program called Minitab 15 statistical software.

First, the result of gas phase flow distribution uniformity analysis is addressed. An ANOVA table as in Table 4.2 has been made by using General Linear Model in Minitab 15 software from the 24 combination results of σ_g. From the table, clearly shows only

Table 4.1 Summary of the selected analyzed parameters and its level

Parameter	Level
Flow pattern at header entrance	Stratified-flow, Mist-flow
Backpressure	Non-uniform, Uniform
j_g (m/s)	1.0 m/s, 5.0 m/s

Table 4.2 Summary of the ANOVA table for σ_g

Source	*DF*	*SS*	*MS*	*F*	*P-value*
flow pattern	1	0.000043	0.000043	0.08	0.7860
backpressure	1	0.035378	0.035378	63.30	0.0000
j_g	1	0.04134	0.04134	73.97	0.0000
flow pattern *backpressure	1	0.000241	0.000241	0.43	0.5210
flow pattern * j_g	1	0.001049	0.001049	1.88	0.1900
backpressure * j_g	1	0.000276	0.000276	0.49	0.4920
flow pattern * backpressure * j_g	1	0.000552	0.000552	0.99	0.3350
Error	16	0.008942	0.000559		
Total	23	0.08782			

backpressure and j_g are the main parameters contribute to the uniformity of gas phase flow distribution as the *P-value* in the table are less than 0.05. *P-value*, calculated from *F* raging from 0 to 1. It is a hypothesis test to check whether the parameter is significant to the contribution of the uniformity of the flow distribution or not. (*P-value* < 0.05≡ significant, *P-value* > 0.05≡not significant)

For further understanding on how large the contribution of these parameters, by calculate the percentage of *SS* value to the *SS* total from table 4.2, a simplified Pareto chart can be plot to show clearer contribution of each parameter and its interaction among each others to the uniformity of gas phase flow distribution as in Fig. 4.20. The abscissa shows the sources which are the parameters and its interaction combinations. The ordinate shows the percentage of contribution to the uniformity of the gas phase flow distribution. From the chart, the total of contribution by all the parameters to the uniformity of flow distribution of gas phase is 89.82%. The other 10.18% is the experimental error or considered unknown. From this 89.82% of contribution, the j_g with 47.07% continuing with backpressure with 40.28% contribute the most for the uniformity of gas phase. The other parameters and all the interaction shall be classified as not significant to the contribution of uniformity of flow distribution.

The next analysis is to find the best combinations of parameters and its level to create the best setting for the best uniformity of flow distribution. By using Minitab 15 software again with design of experiment cube plot tool, the result yield as in Fig. 4.21.

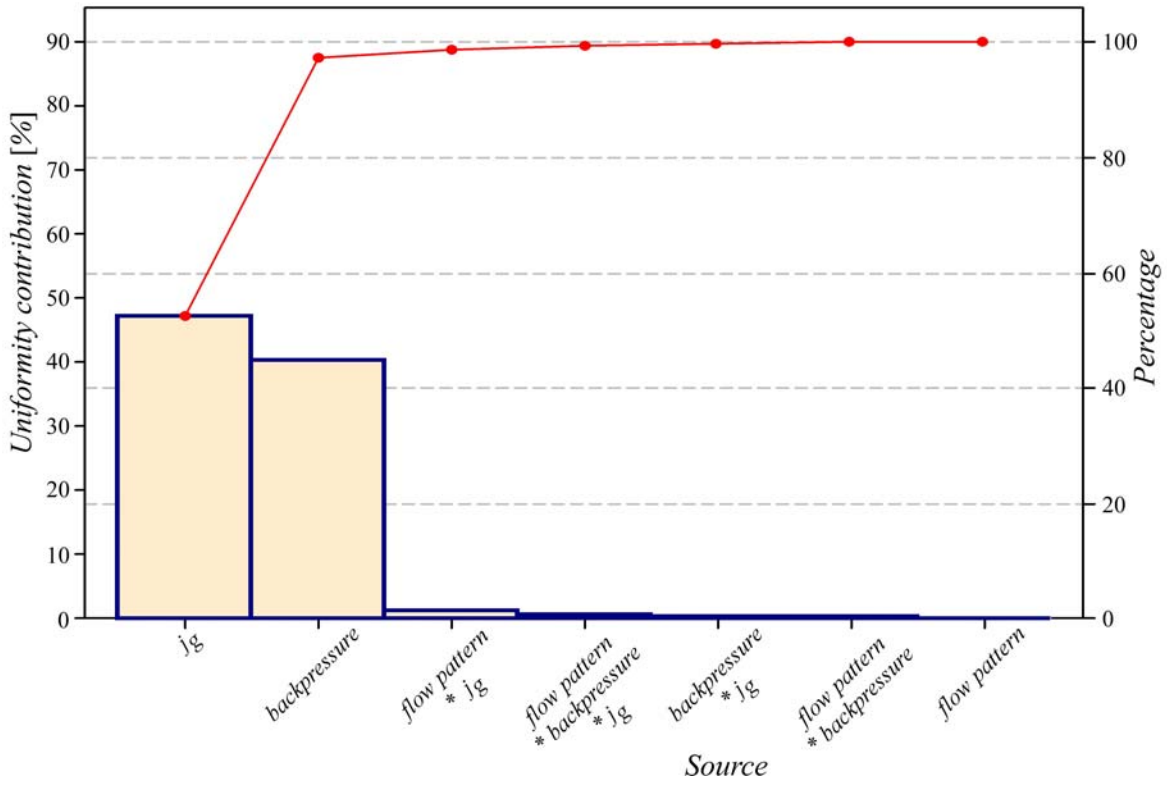

Fig. 4.20 Pareto chart of sources (parameters) contribute to the uniformity of gas phase flow distribution

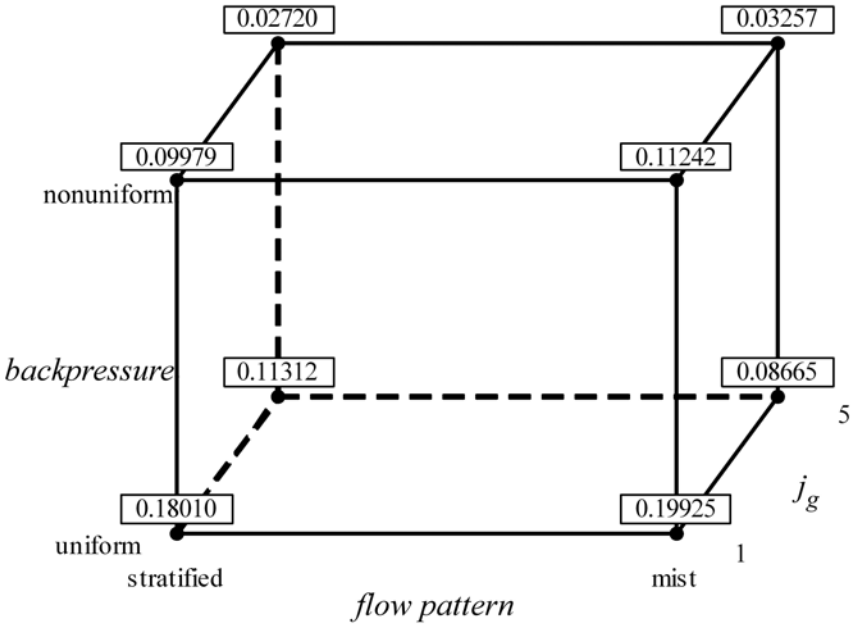

Fig. 4.21 Cube plot with means value of σ_g at each combination of setting level for each parameter

Table 4.3 Summary of the ANOVA table for σ_l

Source	*DF*	*SS*	*MS*	*F*	*P-value*
flow pattern	1	0.0038346	0.0038346	9.80	0.0060
backpressure	1	0.0039629	0.0039629	10.13	0.0060
j_g	1	0.0013102	0.0013102	3.35	0.0860
flow pattern * backpressure	1	0.0002948	0.0002948	0.75	0.3980
flow pattern * j_g	1	0.0062611	0.0062611	16.00	0.0010
backpressure * j_g	1	0.0047	0.0047	12.01	0.0030
flow pattern * backpressure * j_g	1	0.0043281	0.0043281	11.06	0.0040
Error	16	0.006261	0.0003913		
Total	23	0.0309525			

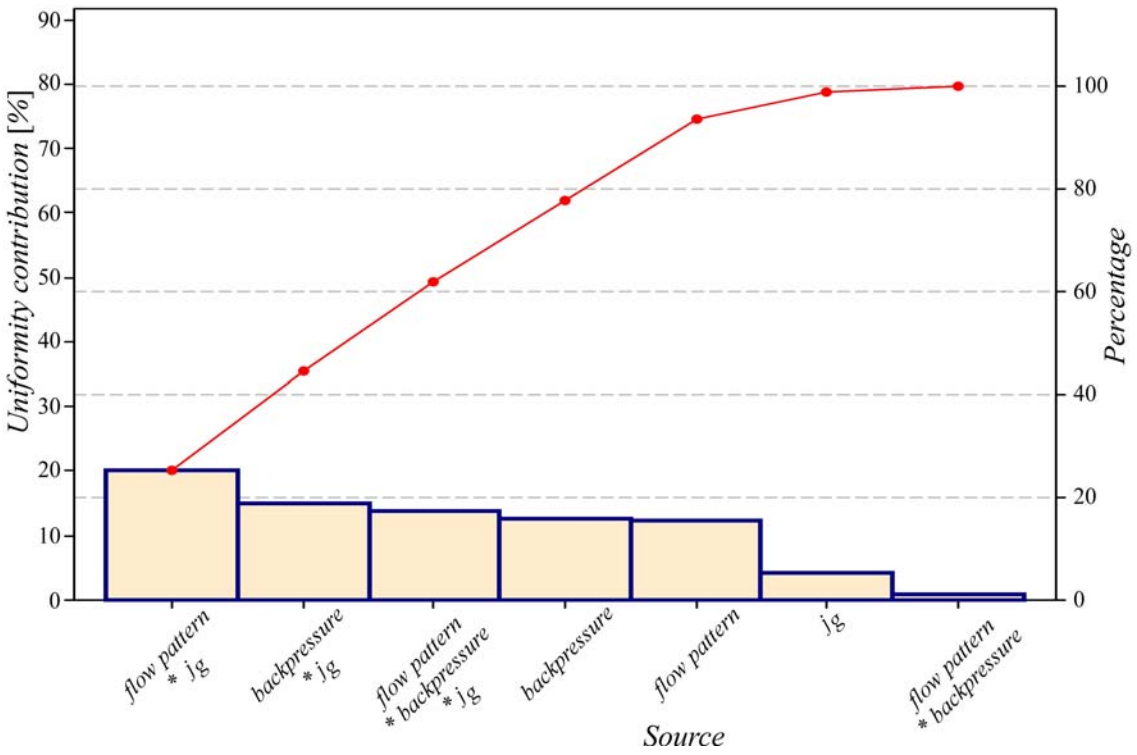

Fig. 4.22 Pareto chart of sources (parameters) contribute to the uniformity of liquid phase flow distribution

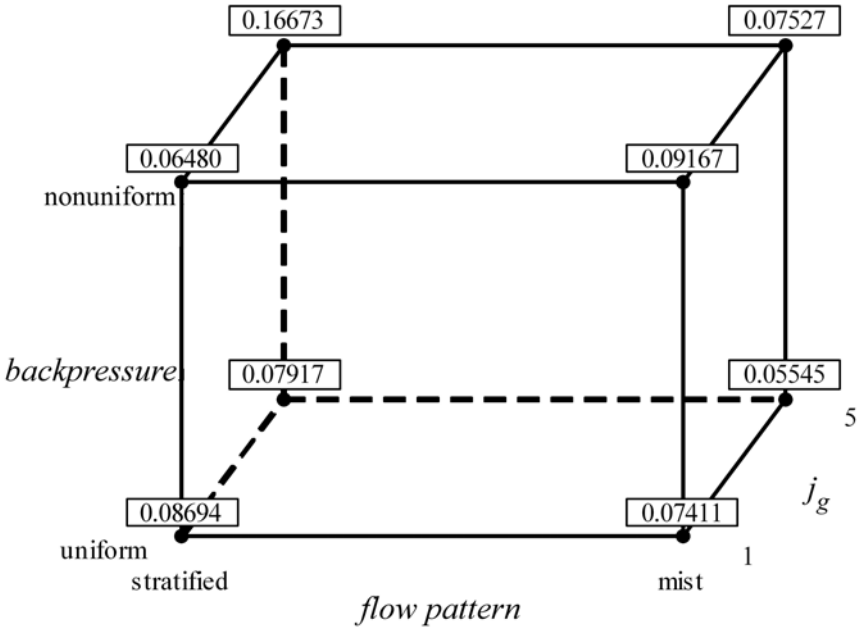

Fig. 4.23 Cube plot with means value of σ_g at each combination of setting level for each parameter

This cube plot shows the mean value of σ_g at each combination of the 3 parameters and its level as in Table 4.1. From the cube plot, the smallest mean value of σ_g is 0.02720 which is located at left, back and upper side of the plot. Thus to ensure the σ_g at minimum level, the setting of each parameter should be as follow. Backpressure should be at non-uniform condition, j_g should be set at 5.0 m/s and flow pattern should be set with stratified flow. Noted, the flow pattern is considered a not significant parameter as explain in table 4.2 and Fig. 4.20, thus make the differential of σ_g value between mist-flow and stratified-flow in Fig. 4.21 is relatively small.

Parameters that contribute the most to the uniformity of liquid phase flow distribution shall be discussed next. As previously explained, an ANOVA table from the 24 combination of parameters experiment σ_l result is been made as in Table 4.3. Different from gas phase ANOVA table, this table, the P-value for 3-ways interaction shows lower value than 0.05, meaning that it is significant to the contribution to the uniformity of liquid phase flow distribution. Only one of the 2-ways interaction combinations is not significant to the uniformity of flow distribution, i.e. flow pattern and backpressure. Nevertheless, j_g P-value is higher than 0.05, however due to its interactions among other parameters significant to the flow distribution, makes j_g significant as a main factor as others.

Fig. 4.22 shows a Pareto chart of contribution percentage to the uniformity of liquid phase flow distribution by its main parameters solely and also by its parameters interaction among each others. From the chart, the total of contribution by all the parameters and its interactions to the uniformity of flow distribution of liquid phase is 79.77%. The other 20.23% is the experimental error. The chart shows that the 2-ways interaction of flow pattern and j_g is the most influenced to the uniformity of liquid phase flow distribution that contributes 20.23% continue with combination of backpressure and j_g with 15.18%. From this observation of Fig. 4.22, it shows that the interaction among parameters are more important than the parameter itself to the contribution of the uniformity of liquid phase flow distribution.

Since interaction contributed more than the parameter itself, from the experiment to find the best setting for each factor that can sustain minimizing the standard deviation of liquid by a design of experiment cube plot tool as explain earlier. Fig. 4.23 is the result of cube plot for mean value of σ_l. From the figure, to archive the smallest value of σ_l the parameters should be set as follows. Flow pattern should be mist flow, the backpressure should be uniform condition and j_g should be set at 5.0 m/s.

4.3 Second segment: Study on the similarity of real refrigerant and air-water two phase flow distribution behavior

A lot of study on gas-liquid two phase flow distribution in multi-pass channel that has been reported examined the air-water two phase flow distribution to simulate the real refrigerant two phase flow as reported by Lee S. Y. (2006). For this kind of approach, it has been proposed to synchronize the phase separation between gas and liquid inside the header due to the differential of properties of the substance, by focusing on the flow pattern generation at the header entrance, also by deciding the mass flow rate *M* of the simulated substance by matching it with the Baker map (1954) parameter method as reported by Katsuta M. et al. (2009). However, experiment data on direct observation and comparison of flow pattern condition between air-water and real refrigerant inside the same specification of multi-pass channel is apparently very few, such as the one that reported by Kim N-H. et al. (2008), furthermore, present researchers find some argumentative of indistinct point when referred to previous work done by former researchers when advancing their research and development by this simulation method.

This research is mainly an experimental study of two phase flow distribution behavior in upward and downward multi-pass channel focusing on refrigerant R-134a and air-water substance similarity. By using an identical specification of multi-pass upward test channel simulated from a multi flow type compact evaporator, a direct visual test has been done to observe the flow distribution characteristic of each substance in multi-pass channel. A comparison of gas-liquid phase flow distribution behavior in multi-pass channel is also studied and discussed; however, the concentration shall be on liquid phase flow distribution behavior due to its priority on improvement of evaporator's COP. These mainly to clarify all the indistinct point when synchronize the R-134a refrigerant two phase flow to the air-water two phase flow at all desired test condition in multi-pass upward and downward channel. Thus, to find the accurate mass flow rate of air and water to generate a two phase flow pattern at header entrance to be visually identical with R-134a also to have an identical flow distribution behavior at combining header. Furthermore, for confirmation on visual observation result, an air-water flow distribution test was conducted. From this flow distribution measurement result, the value of flow distribution ratio of gas and liquid phase of R-134a that flow from the dividing header to all the branches can now be better understood and confirming inlet condition for air-water flow synchronization with R-134a gas and liquid two phase flow in upward and downward multi-pass channel.

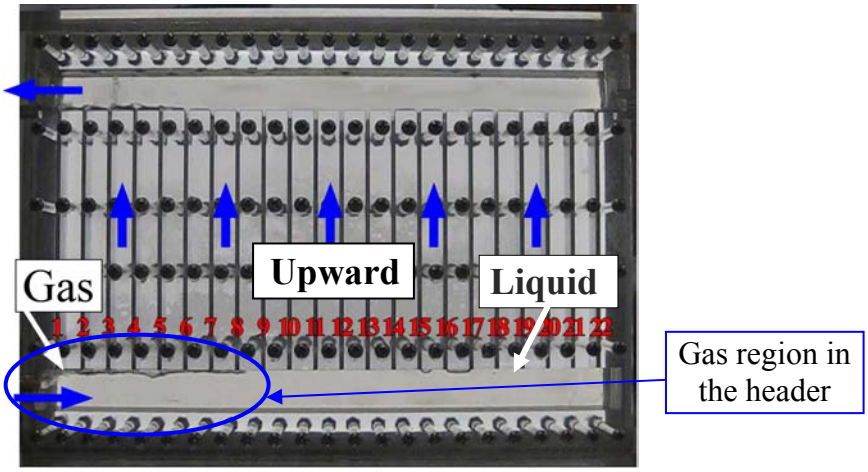

(a) M = 5.2 kg/h, x = 0.3

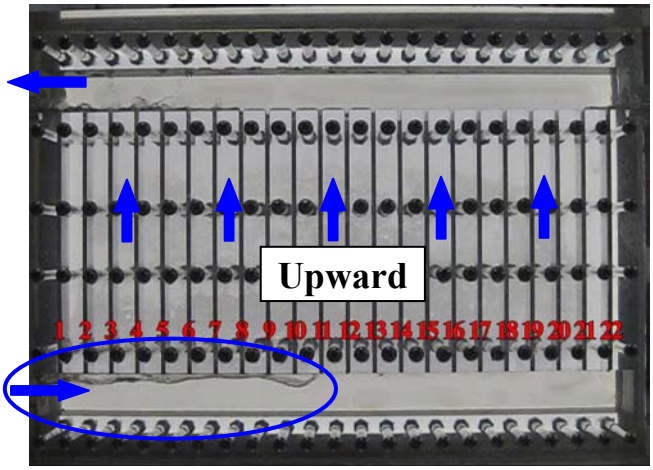

(b) M = 5.2 kg/h, x = 0.4

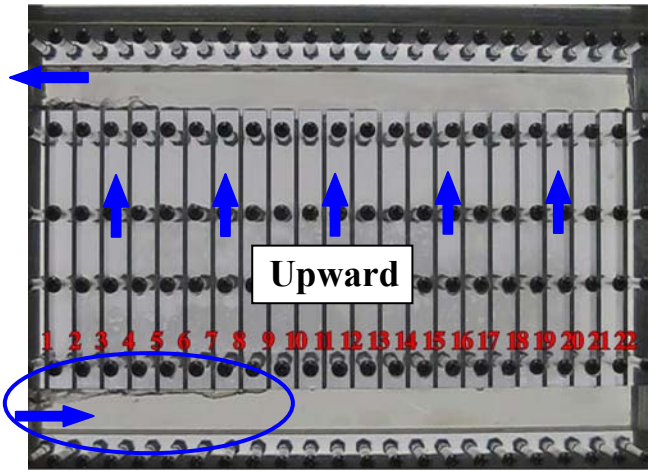

(c) M = 8.5 kg/h, x = 0.3

Fig. 4.24 Typical visual data of refrigerant flow

Also, from this basis, a study on improvement of mainly liquid phase flow distribution uniformity in multi-pass channel can be conduct in more accurate result and less difficulty.

4.3.1 R-134a two phase flow visual observation result in the upward orientation test channel

Snapshots in Fig. 4.24 show a typical result from the visual observation of flow pattern at the header entrance of the test channel. The data mostly being recorded and investigated by a motion picture data. Thus, the air-water two phase flow visual observation data also are in motion picture, and the comparison of both was base on this data. Noted, a general behavior of flow distribution at the combining header was also being observed, however it can only be as a reference data for confirmation on flow distribution behavior of air-water flow distribution measurement.

As an overall result for all the tested condition in table 3.4, the visual data shows that only at the upstream of the test channel, the gas phase occupied a small region at the top portion of the dividing header, while liquid phase fully occupied all the space of the header up to downstream. Thus, the gas phase region become larger as the quality x or mass flow rate M is increase. However, due to the test condition range, even at the highest j_G which the quality x = 0.4 and mass flow rate M = 8.5 kg/h, the gas phase of these R-134a could only occupied a small depth at the top portion, until approximately the half length of the header. Else, upon observing closely the test channel at the downstream region of the dividing header, it seems that the liquid is in a stagnant state. Also, at the combining header, only an aggressive movement of flow distribution has been observed at the upstream region. Thus at the downstream only a small quantity of liquid phase flow distribution can be observed and it becomes nil as it reached to the end of the header.

From the observation, visual test with this test channel specification as in Fig. 3.14, also with application of test condition as in table 3.4; as an initial conclusion, only a small quantity of branches at the upstream shall have a flow distribution of R-134a gas and liquid phase.

4.3.2 Air-water two phase flow visual observation result in the upward orientation test channel

4.3.2.1 Inlet flow condition at the header entrance

The main objective of this research is to find similarities between the refrigerant (R-134a) flow and the air-water flow, which is to synchronize the R-134a two phase flow pattern with air-water two phase flows in a simulated multi-flow type evaporator at several test condition, i.e., quality x and mass flow rate M at header entrance of evaporator as in Table 3.4. In this research a prediction of air-water flow pattern that can be generate by deciding the local velocity of air and water at the header entrance by compute it from the next 4 condition. Then, all these 4 condition shall be visually recorded and compared with the R-134a flow pattern.

(i) Equal superficial velocities

Superficial velocities of air (j_A) and water (j_W) are set equal to those of R-134a vapor (j_G) and liquid (j_L), respectively, at the entrance of the dividing header.

Namely,

$$j_A = j_G \quad , \quad j_W = j_L \tag{4.3}$$

(ii) Equal to kinetic energies

$$\rho_A j_A^{\,2} = \rho_G j_G^{\,2} \quad , \quad \rho_W j_W^{\,2} = \rho_L j_L^{\,2} \tag{4.4}$$

Under this condition, the difference of densities of vapor and air is the main reflections to the value of j_A.

(iii) Equal to quality x and mass flow M

Quality x :
$$\frac{\rho_A j_A}{\rho_A j_A + \rho_W j_W} = \frac{\rho_G j_G}{\rho_G j_G + \rho_L j_L} \tag{4.5}$$

Mass flow M:
$$\rho_A j_A + \rho_W j_W = \rho_G j_G + \rho_L j_L \tag{4.6}$$

Also, at this condition the differential of gas phase density determine the value of j_A, even stronger than the above-mentioned condition of (ii).

(ⅳ) Equal to Baker map (1954) parameters

$$G_A = \frac{G_G}{\lambda_R} \quad , \quad \lambda_R = \left[\left(\frac{\rho_G}{\rho_A} \right) \left(\frac{\rho_L}{\rho_W} \right) \right]^{\frac{1}{2}} \tag{4.7}$$

$$\frac{G_W}{G_A} = \frac{G_L}{G_G} \lambda_R \psi_R \quad , \quad \psi_R = \frac{\sigma_W}{\sigma_L} \left[\frac{\mu_L}{\mu_W} \left(\frac{\rho_W}{\rho_L} \right)^2 \right]^{\frac{1}{3}} \tag{4.8}$$

The liquid phase surface tension differentials determine the value of j_L. Unlike others, this condition usually being implemented as a model for simulation of real refrigerant to air-water flow distribution test by past researchers, e.g., Koyama S. et al. (2006) and Katsuta M. et al. (2009).

Figure 4.25 shows the comparison of j_A and j_W value upon calculated by formula produced from the above 4 test condition. All the calculations producing these results are base on the fluids physical properties as in table 4.4. From the graph, the j_A value of test condition that equal to quality x and mass flow rate M was several times larger than j_G. Seem different at test condition that equal to Baker's map parameters when the value of j_W was several times larger than j_L.

Noted also, in this study both channel orientation of upward and downward flow shall use this 4 inlet condition of air-water velocity to compare with real refrigerant two phase flow distribution behavior.

Table 4.4 Physical properties of R-134a and air-water

	R-134a (at -10ºC in saturated condition)		(at 25ºC and 1 atm)	
	Gas	Liquid	Air	Water
Surface tension σ [mN/m]		8.1		71.9
Density ρ [kg/m^3]	10.61	1326.5	1.21	997.0
Viscosity μ [μPa·s]	11.82	307.5	18.48	890.1

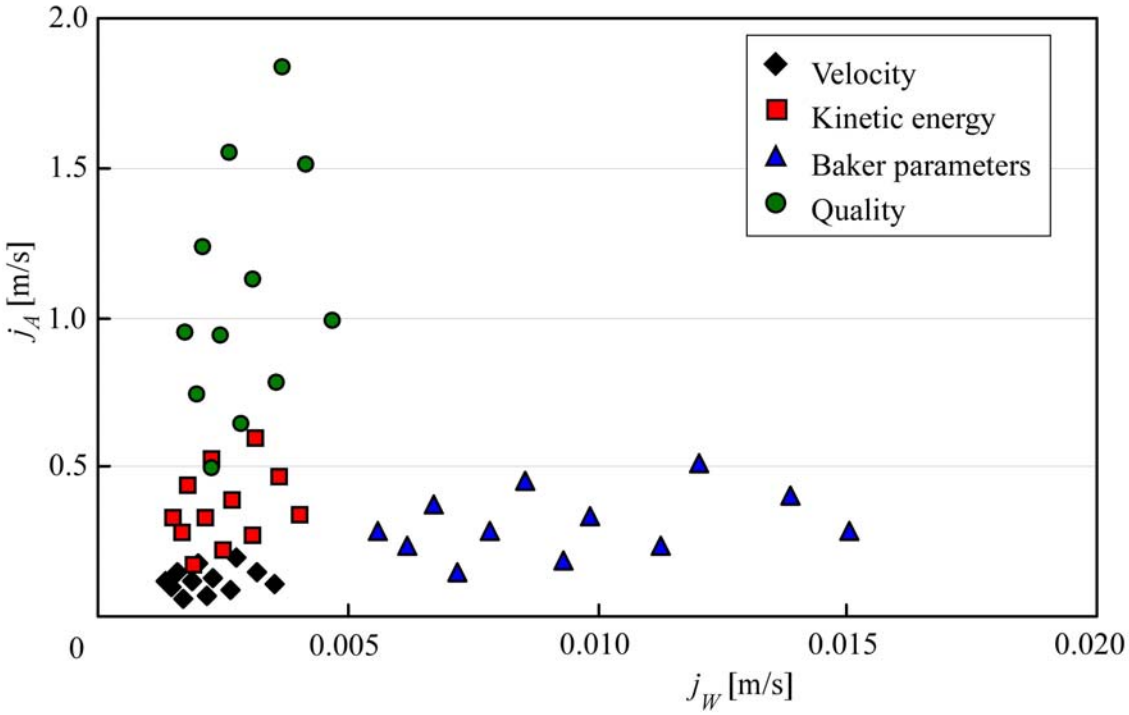

Fig. 4.25 Superficial velocities of air and water for (ⅰ) – (ⅳ)

4.3.2.2 Visual observation result

All visual data were recorded by a digital camera and a high speed video camera with 240 frames/sec. Fig. 4.26 shows the typical snapshots of air-water two-phase flows obtained under 4 conditions explained above, all of which simulate M = 5.2 kg/h and x = 0.3 of the refrigerant flow. With all these motion pictures, by focusing on the flow pattern at the dividing header entrance (blue circles in Fig. 4.26), a comparison was made with the R-134a motion picture to find the air-water inlet condition that gives the most identical two-phase flow pattern among 4 conditions. In particular, a gas phase maximum gained length in the dividing header and its temporal variations were compared. Fig. 4.27 shows the flow pattern in the dividing header, the gained length of gas phase is coordinated by blue arrows. The results of comparisons of the refrigerant flow and the air-water flow are summarized as follows.

(i) Equal superficial velocities: Dispersed air bubbles slowly flow in the upper part of the dividing header near its entrance as shown in Fig. 4.27(b). Compared with the gas phase region length of R-134a shown in Fig. 4.27(a), the air region length is shorter and disturbances of gas-liquid interface are quite small. This happens because the setting of j_A is too low.

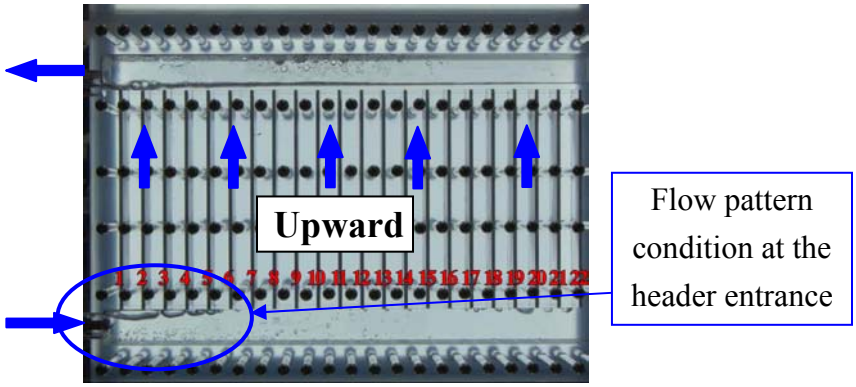

(a) Equal to superficial velocity

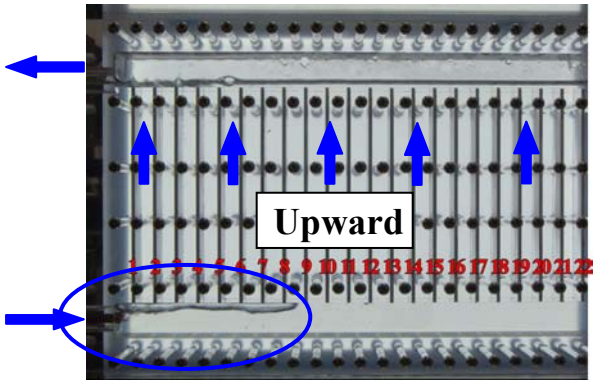

(b) Equal kinetic energies

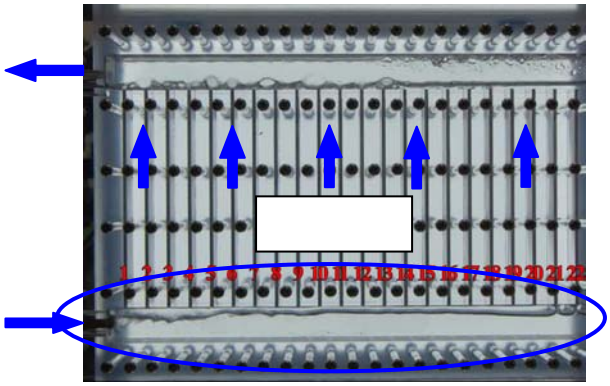

(c) Equal quality and mass flow rate

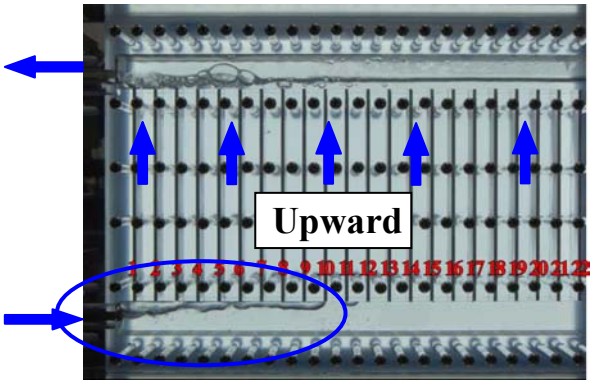

(d) Equal Baker's map parameters

Fig. 4.26 Typical results of air-water flow visualization when M = 5.2 kg/h and x = 0.3

(ii) Equal kinetic energies: The air region length and the air-water interface disturbance are visually quite similar to those observed in R-134a flow as found by the comparison of Fig. 4.27(a) and Fig. 4.27(c).

(iii) Equal quality and mass flow rate: As shown in Fig. 4.27(d), the air-water flow in the dividing header is in a wavy stratified flow and the air region exists to the end of the header. This flow pattern happens because the setting value of j_A is too high. This air-water flow behavior is considerably different from that of R-134a flow.

(iv) Equal Baker map parameters: It seems that under this condition the pattern of air-water flow in the dividing header is almost identical to that of the R-134a two-phase flow, meaning that the length of gas region gained in the upstream region of the dividing header in Fig. 4.27(e) is nearly the same as that observed in the refrigerant flow in Fig. 4.27(a). However, at relatively high mass flow rate, the disturbance of air-water interface was more intense compared to the gas-liquid interface of refrigerant flow.

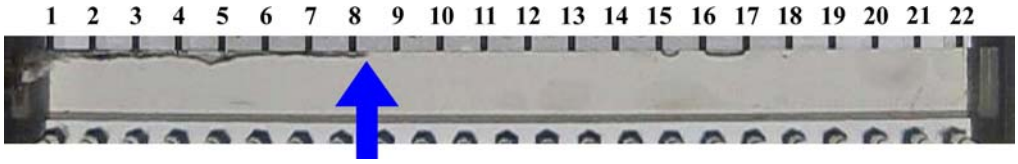

(a) Refrigerant flow

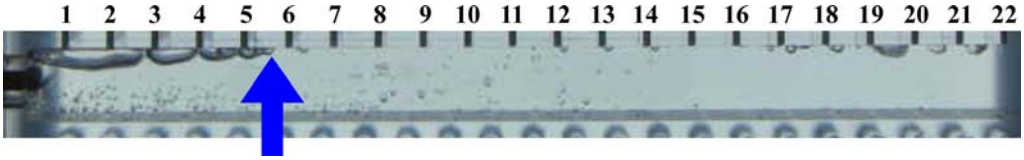

(b) Air-water flow under equal superficial velocities

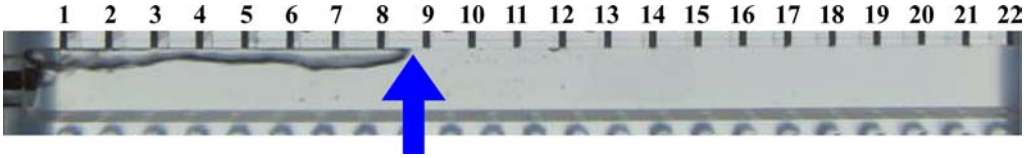

(c) Air-water flow under equal kinetic energies

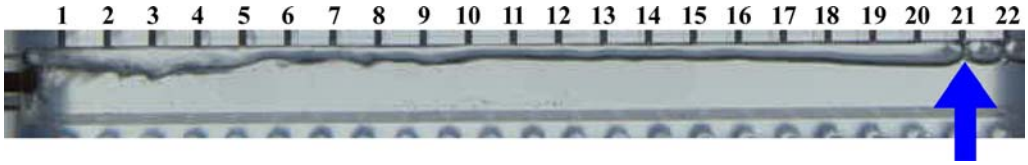

(d) Air-water flow under equal quality and mass flow rate

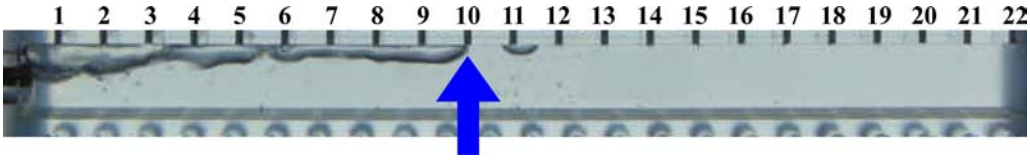

(e) Air-water flow under equal Baker's map parameters

Fig. 4.27 Flow pattern in the dividing header

4.3.3 Air-water flow distribution measurement result in upward orientation test channel

Base on the visual observation results of air-water two phase flow behavior in simulated test channel, an air-water flow distribution measurement test has been conducted. From the 4 tested condition, the visual observation result shows that especially at the header entrance flow pattern was the condition of air-water two phase flow that equal to kinetic energy of R-134a two phase flow result was the best fitted to the flow pattern of R-134a at the header entrance. By that reason this condition has been selected to go to the next stage of this study which is to measure the air-water flow distribution to each branch. These steps are required to confirm that the simulated test condition flow distribution behavior are the same as in the real R-134a as visually can be identify by observing liquid phase movement came out from the branches at along the combining header of the test channel. In this study, the test condition which the air-water two phase flow is equal to the R-134a Baker map (1954) parameters is also has been selected for measuring the flow distribution. Due to this type of condition has been long adopted by researchers. Thus, these two tested condition result of air-water flow distribution measurement shall be compared and discussed.

Figure 4.28 and 4.29 are the typical result of flow distribution ratio of air and water from the 22 branches of the test channel, the condition of quality x and mass flow rate M were the same as in Fig. 4.24. Fig. 4.28 is the result at test condition when the kinetic energy of the air-water two phase flows was equal to R-134a, while Fig. 4.29 at test condition when the Baker map (1954) parameters of the air-water two phase flow is the same with R-134a. Both test condition measurement result has been studied and compared with the visual data of R-134a two phase flows in Fig. 4.24. As an initial conclusion, both has the same characteristic of flow distribution trends which the gas and liquid phase flow distribution was focusing at the upstream region branches of the test channel. In general, the flow distribution was masses up to 10^{th} branch, and lesser to nil subsequently. Other similarity to the R-134a two phase flow visual observation result was the occurrence when the first branch was the maximum distribution of air, then suddenly drop however increase again and branch no. 4 was the second peak before decreasing as it goes to down stream region.

On the other hand, water flow distribution rate trend seems to be rather exists following the air flow distribution progress. Thus, the two test conditions of air-water two phase flow distribution measurement results shows similarities with R-134a even of

these precise characteristic. However, qualitative differential between these two test condition flow rate of air and water were existed, e.g. the second peak of air flow rate value and maximum water flow rate value. More over, an existing of impulsive water flow distribution from a small quantity of branches at downstream region of Fig. 4.28 can be spotted, though does not appear in Fig. 4.29.

From observing the visual data of R-134a at along combining header, the result shows insignificant behavior with flow distribution of air-water result as in Fig. 4.28, which concerning the specific details such as no. 2 peak of air flow distribution rate and occurrence of impulsive water flow distribution at down stream region branches. Therefore, even the inlet flow pattern of test condition Fig. 4.28 (equal kinetic energy) is similar to R-134a flow, the air-water two phase flow with test condition that equal to Baker map (1954) parameter which corresponds to Fig. 4.29 is favorable to used in simulating the gas-liquid flow distributions of refrigerant flow in multi-pass upward channel with the air-water flow. This is concluded as all the tested data in Fig. 4.28 and 4.29 show similarity behavior at all conditions (Table 3.4).

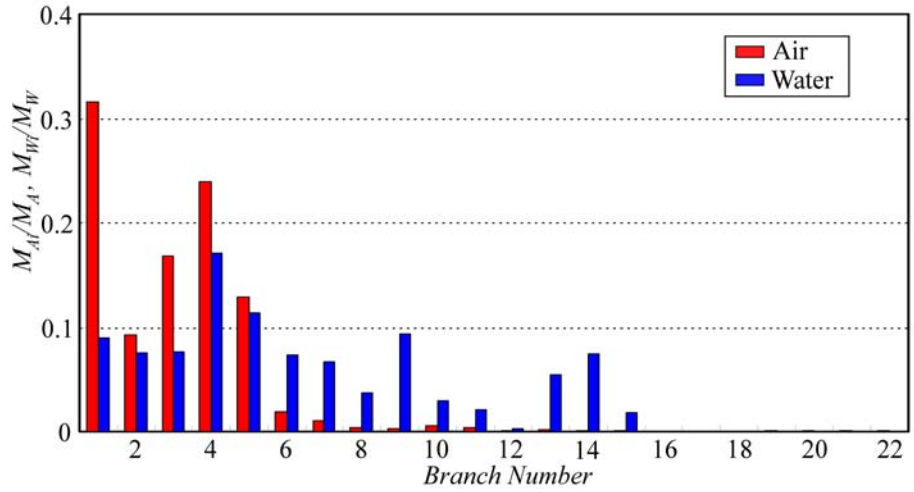

(a) M = 5.2 kg/h, x = 0.3

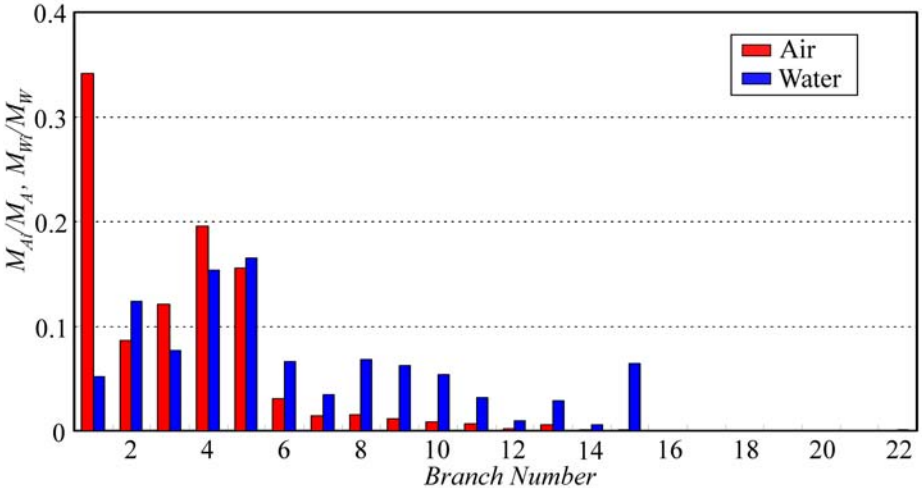

(b) M = 5.2 kg/h, x = 0.4

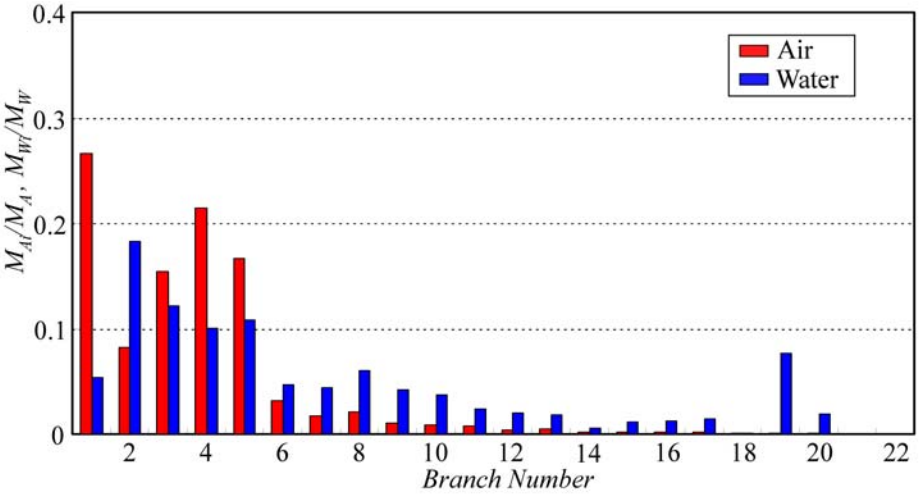

(c) M = 8.5 kg/h, x = 0.3

Fig. 4.28 Results of air-water flow distribution ratios at test condition equal to kinetic energy

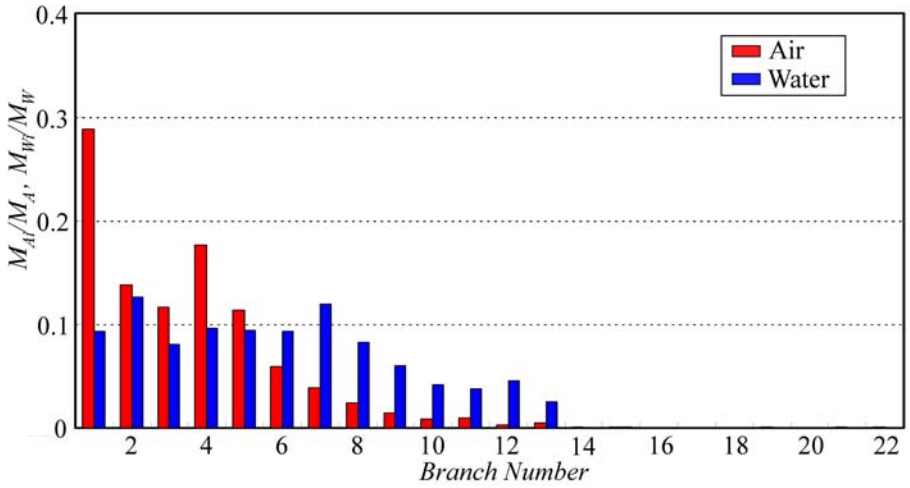

(a) M = 5.2 kg/h, x = 0.3

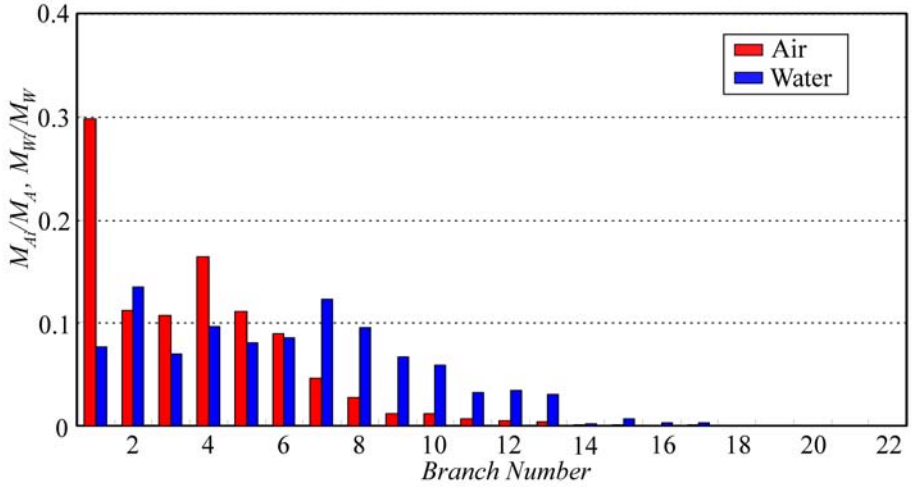

(b) M = 5.2 kg/h, x = 0.4

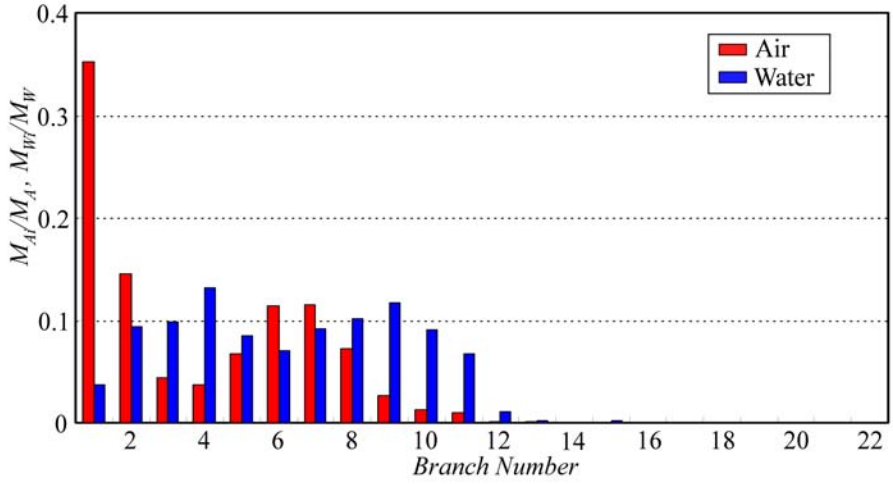

(c) M = 8.5 kg/h, x = 0.3

Fig. 4.29 Results of air-water flow distribution ratios at test condition equal to Baker's map parameters

4.3.4 Study on similarities of flow distribution behavior of real refrigerant and air-water flow in simulated downward multi-pass channel

Continue from first study on upward orientation of test channel, this further study on downward orientation flow is to verify that the selected inlet condition of air-water velocities in upward test channel good to use in other orientation of test channel. By using the same test channel as in upward test channel, the only different with the test channel in Fig. 3.14 are the inlet and outlet position, i.e., vice versa, also the arrow showing the downward flow movement of substance inside the test channel branches is in the opposite direction.

By using the same testing apparatus and method as in the upward test channel session, a visual observation test of R-134a refrigerant and air-water flow has been done. Also, the air-water flow distribution measurement was done to confirm the results from visual observation comparison between real refrigerant flow and air-water flow in this downward test channel.

4.3.4.1 R-134a flow observation result

Figure 4.30 shows a snapshot of a typical result of R-134a visual observation result focusing at the entrance of the test channel. This is due to the desired range of the mass flow rate M was to small that the maximum flow distribution of liquid phase to the dividing header just far as a few branches from the inlet pipe. The flow distribution behavior of liquid phase is being studied mainly by observing the motion picture that has been recorded focusing on the movement of liquid phase entering the dividing headers.

From observing this liquid phase activity on top of the surface of the dividing header, a qualitative judgment on the flow distribution behavior of liquid phase is done. As in Table 4.5, several tested results are shown. This is a qualitative judgment result on flow distribution of liquid phase to the branches in this downward test channel. The first 2 column shows the quality x and mass flow rate M of each inlet condition row, and the 3rd and the rest of the row shows the branch no. from the 1st to 22nd. The symbol in the table shows the flow distribution behavior of liquid phase flow to the numbered branch. The circle mark shows that there is a good amount of liquid phase that can be observed agitating on the floor of the dividing header that neighboring the branch, and suggesting that there is a liquid phase flow being distribute to the branch. The triangle mark shows

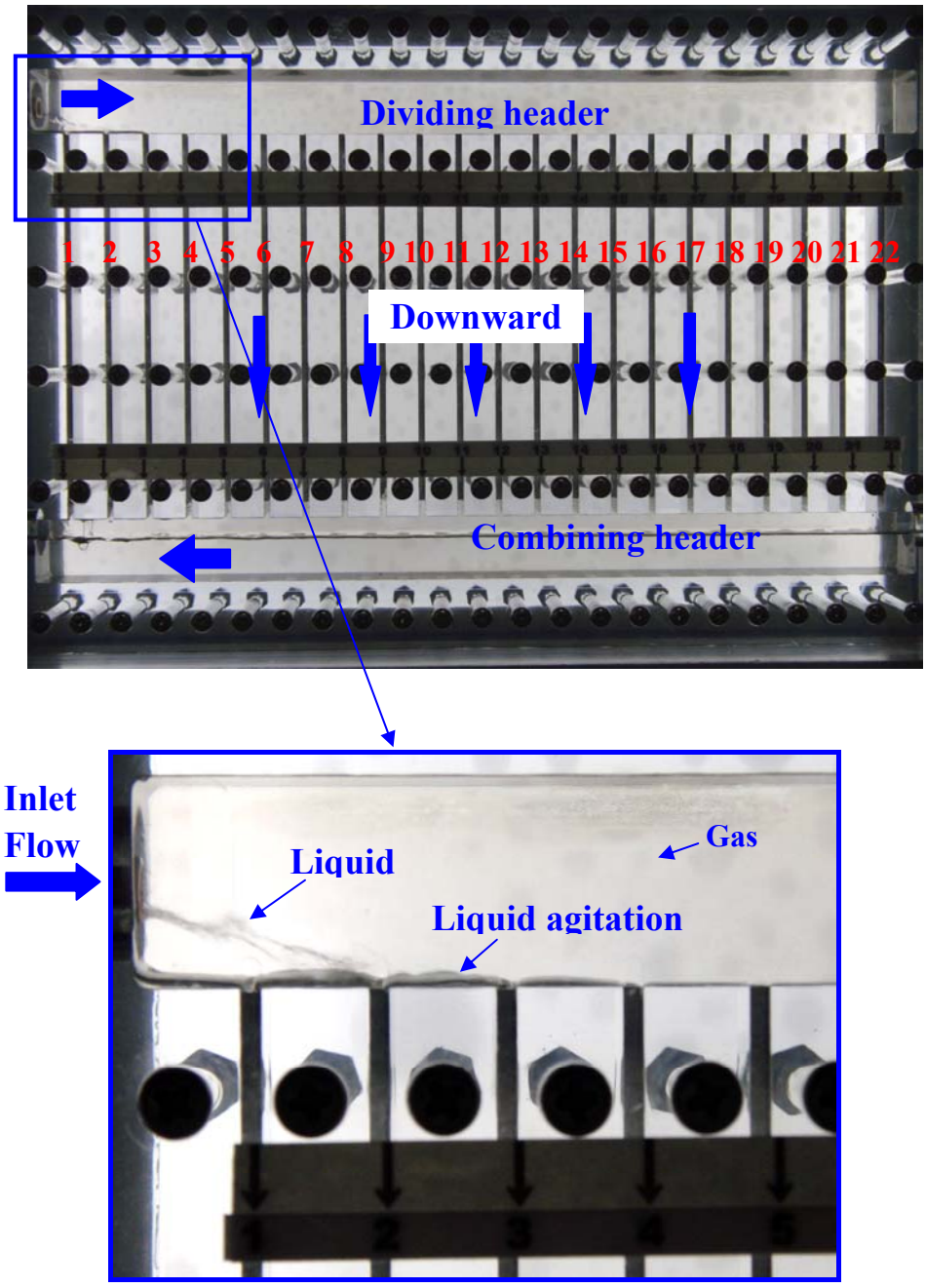

Fig. 4.30 Typical visual data of R-134a flow in downward test channel (M = 8.5 kg/h, x = 0.3 at header entrance)

Table 4.5 Liquid distribution observed in refrigerant flow

x	M	1st	2nd	3rd	4th	5th	6th - 22nd
0.3	4.15	○	○	△	×	×	×
0.3	5.2	○	○	△	×	×	×
0.3	6.4	○	○	○	△	×	×
0.3	8.5	○	○	○	○	△	×

that there is a small quantity of liquid phase that can be observed on the floor of the dividing header near to the branch. The X mark shows that there is no flow distribution of liquid phase that can be observed entering into the branches.

This typical visual data in Fig. 4.30 was at quality x at 0.3 and mass flow rate M at 8.5 kg/hr. From the visual data, unlike the upward channel, most of the dividing header space dominated by the gas phase of the real refrigerant flow. Only a small quantity of liquid slowly flows from the inlet pipe to the header entrance can be observed. Thus, different with the upward channel, this downward channel visual data is easier to comprehend the flow distribution of liquid to the branches due to the liquid phase is clearly visible agitating on the header's floor. Also, in Table 4.5 the typical result showing the flow distribution behavior of liquid phase as the mass flow rate M is increase; however, the result was about the same whereby the flow distribution only concentrates at the header entrance area, essentially not more than 5 branches of length.

4.3.4.2 Air-water flow observation result

Figure 4.31 shows a snapshot of visual data of air-water flow in downward test channel for each inlet condition. In this observation also, the flow pattern of air-water flow being blown to the dividing header and the agitation of water on the header's floor has been studied and qualitatively judged.

From the data, qualitatively the one that equal to superficial velocities and equal to kinetic energies has a similarity if compare with the R-134a flow visual data. However the one that equal to quality x and mass flow rate M; and even the one that equal to

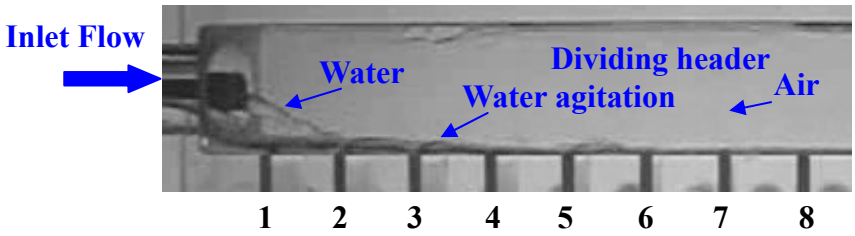

(a)Equal superficial velocities

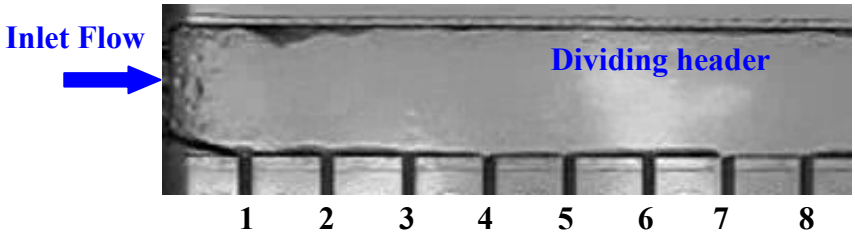

(b)Equal quality x and mass flow rate M

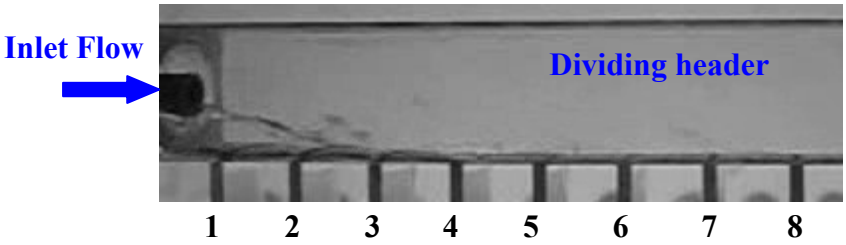

(c)Equal kinetic energies

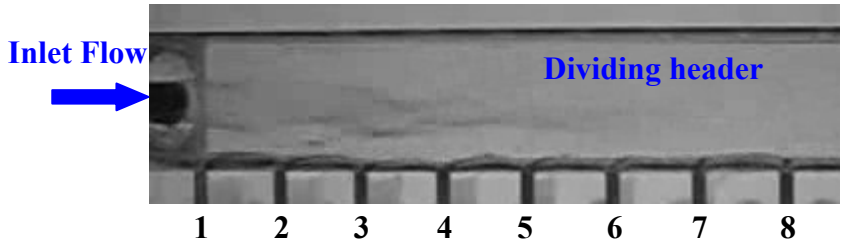

(d)Equal Baker's flow pattern map parameters

Fig. 4.31 Typical snapshot of air-water flow visualization in downward channel (M = 8.5 kg/h and x = 0.3)

Baker's map parameters are far off from similar with the flow distribution behavior of R-134a refrigerant.

Next, to confirm the results on which inlet condition of air-water flow that could simulate the flow distribution behavior of R-134a which concentrate on liquid phase, a flow distribution ratio measurement of air-water need to be done.

4.3.4.3 Air-water flow distribution measurement result

The flow distribution measurement for downward channel is the same as in upward test channel except the inlet position. Due to the surface tension between surface of header and water is different with R-134a refrigerant; it is difficult to visualize clearly which inlet condition that can simulate the flow distribution behavior of R-134a refrigerant. Thus, in this session, all 4 inlet condition shall be measured and studied.

Fig. 4.32 shows a typical result of air-water flow distribution ratio measurement in downward test channel for each inlet conditions. From all 4 typical data of each inlet condition, compare with the qualitative result from visual observation of R-134a liquid phase in Table 4.5, it is found that the result of air-water flow distribution measurement with inlet condition that equal to superficial velocities is favorable for simulating the flow distribution behavior of R-134a refrigerant in multi-flow type evaporator.

However, the result of the one that equal to Baker's map parameters is far off from similar to R-134a liquid phase flow behavior in this downward test channel even it was a favorite condition in the upward test channel.

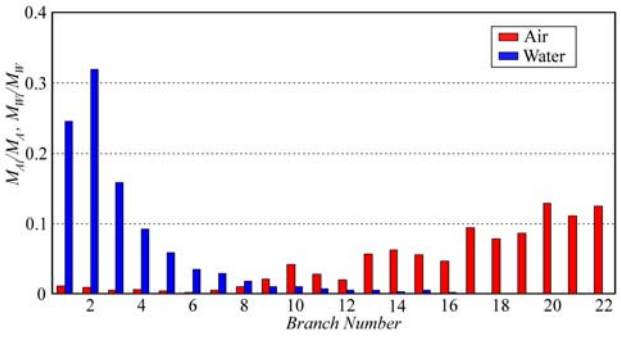

(a) Equal superficial velocities

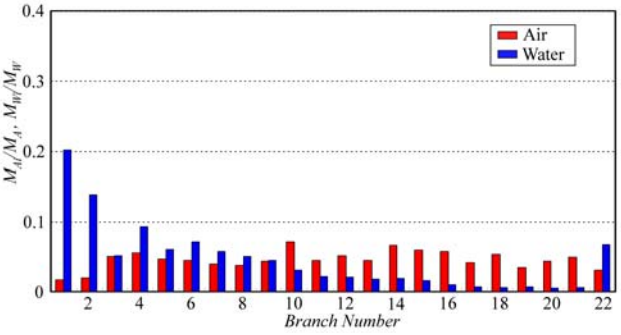

(b) Equal quality x and mass flow rate M

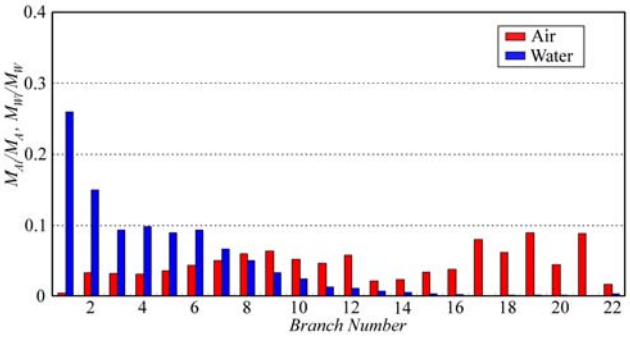

(c) Equal kinetic energies

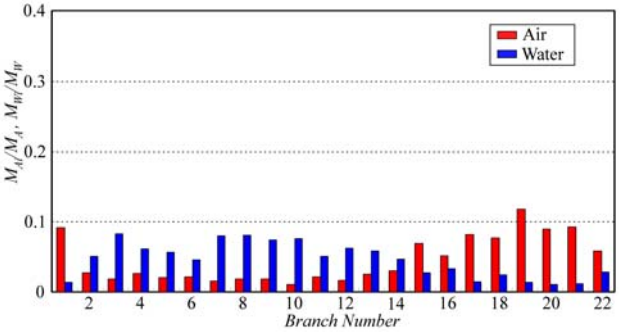

(d) Equal Baker's flow pattern map parameters

Fig. 4.32 Typical results of air-water flow distribution ratios in downward channel (M = 8.5 kg/h and x = 0.3)

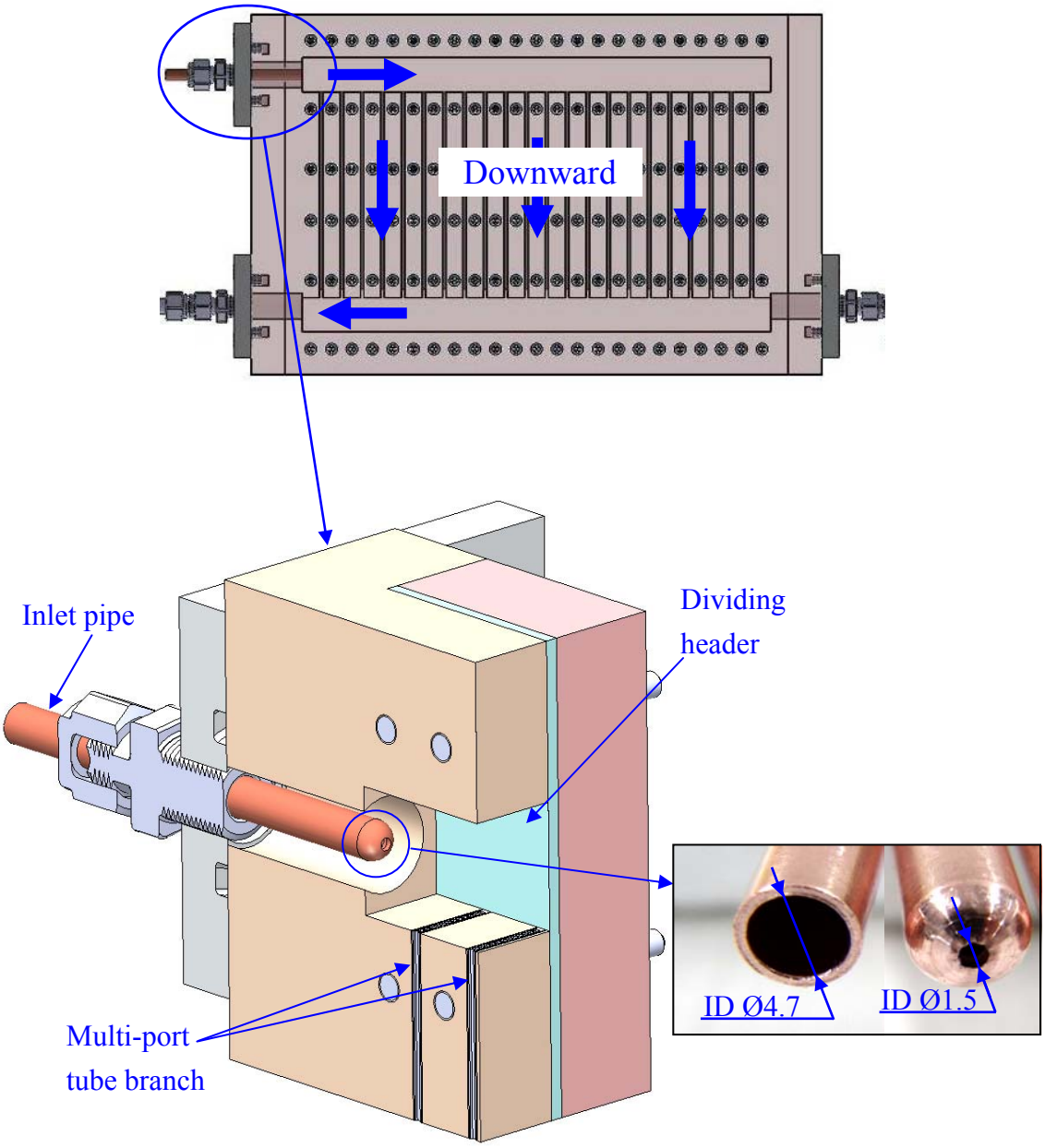

Fig. 4.33 Inlet pipe with swaging treatment details

4.3.5 Further investigate on similarities of R-134a and air-water flow in downward channel with inlet pipe swaged to smaller diameter

This further investigation is to confirm the inlet condition of air-water velocities that equal to superficial velocities of gas and liquid phase of real refrigerant is the one for simulate the real refrigerant flow in multi-pass downward channel. Also to improve the flow distribution uniformity of liquid phase in this downward test channel without increasing the mass flow rate range of the refrigerant cycle.

In this study, the inlet pipe, i.e., quarter inch copper pipe with ID 4.7mm, being added a swaging treatment at the end of it to be a smaller inner diameter, i.e., 1.5mm, as in Fig. 4.33. Using the same range of inlet condition of quality x and mass flow rate M at the header entrance as in Table 3.4, a visual test of R-134a two phase flows in downward test channel was conducted. Continue with the air-water visual test and air-water flow distribution measurement. The results has been investigate and compared with the data of inlet pipe with inner diameter of 4.7mm.

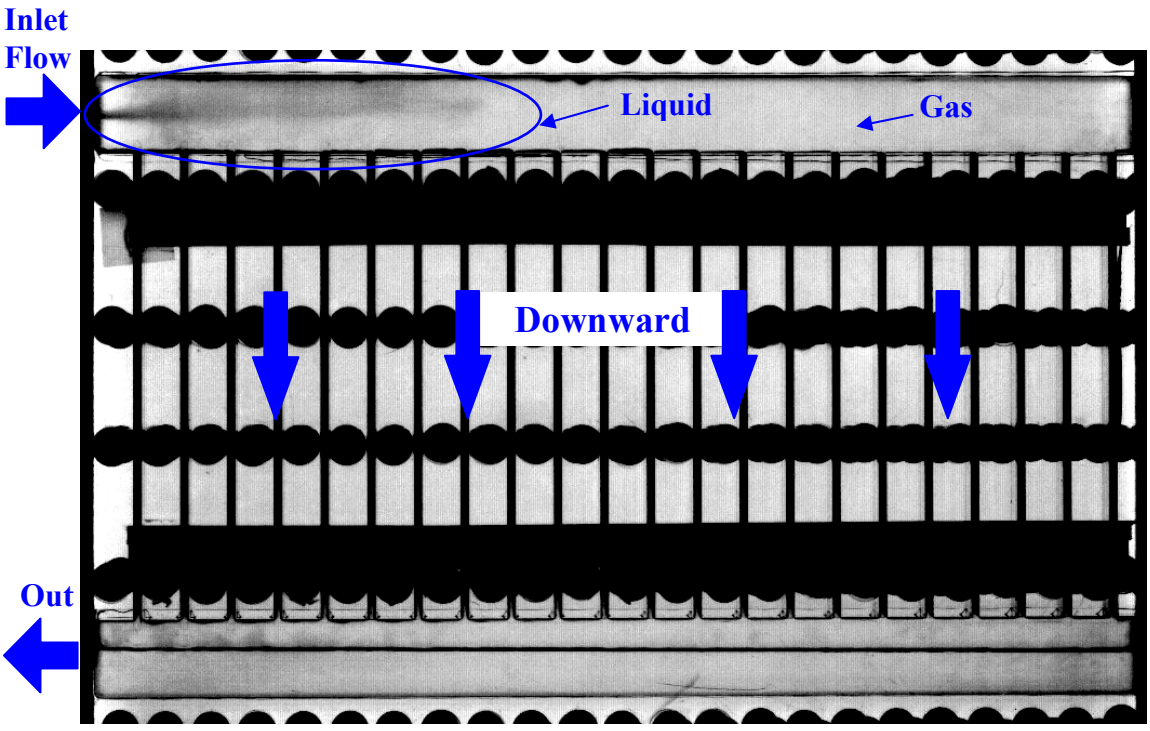

Fig. 4.34 Snapshot of typical visualization of R-134a in downward test channel with inlet pipe swaged to 1.5mm (M = 8.5 kg/h and x = 0.3)

Fig. 4.34 is a snapshot showing a typical visual data using a hi-speed camera at 500 fps. In this study, the flow pattern of R-134a flow from the inlet pipe that swaged to inner diameter 1.5mm can be observed clearly. Thus the flow of liquid phase being observe to be blown far to the downstream region of the dividing header, makes the flow distribution uniformity qualitatively becomes better.

A closer observation also has been done by observing carefully the agitated liquid phase of R-134a on the floor of the combining header using a high definition video camera focusing along the dividing header as in Fig. 4.35. A snapshot of this visual data has been taken and been shown in Fig. 4.36. Then qualitative judgment has been done upon observing the agitation liquid phase on the floor of the header at each branch along the header. A several result has been listed as in Table 4.6, clearly showing that as the inlet pipe being swaged to smaller inner diameter, the flow distribution uniformity of liquid phase is become better as comparing this result with the previous result of inlet pipe with inner diameter of 4.7mm as in Table 4.5. Also, upon comparing the flow pattern at the inlet pipe on Baker's flow pattern map in Fig. 3.15, confirm that the flow pattern transition from stratified to annular as the inlet pipe being swaged to inner diameter 1.5mm.

Thus, for confirming the result in the visual observation, the air-water flow distribution measurement has been done. This time, the inlet condition of the air-water velocities was set to be equal to superficial velocities of gas and liquid phase of R-134a as to confirm the finding in previous study using inlet pipe with inner diameter of 4.7mm in downward test channel. The result is as in Fig. 4.37. From the graph, the flow distribution ratio of water behavior in each inlet condition of quality x and mass flow

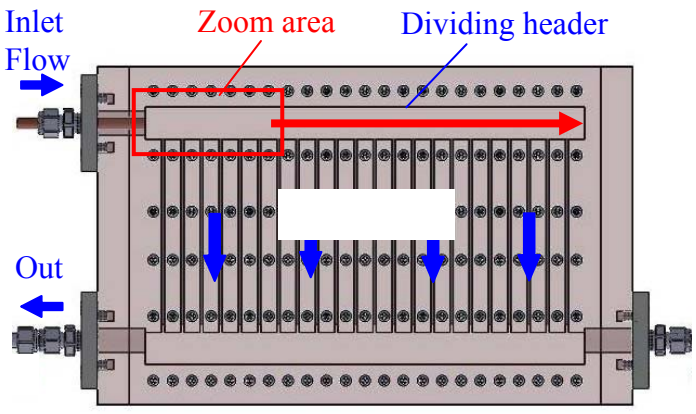

Fig. 4.35 Detail of zoom area for visual observation

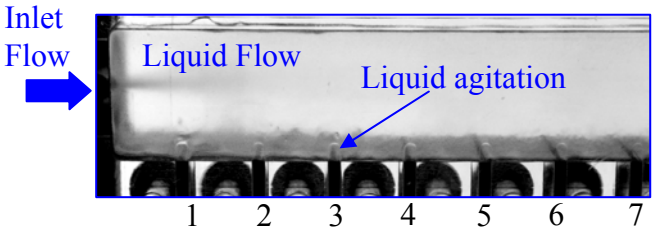

(a)From branch no. 1 to no. 7

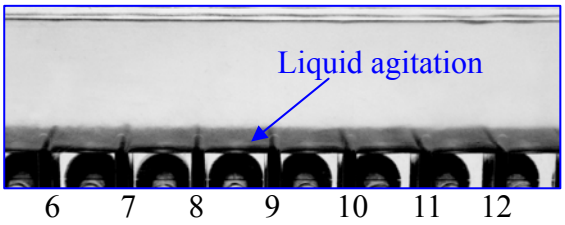

(b)From branch no. 6 to no. 12

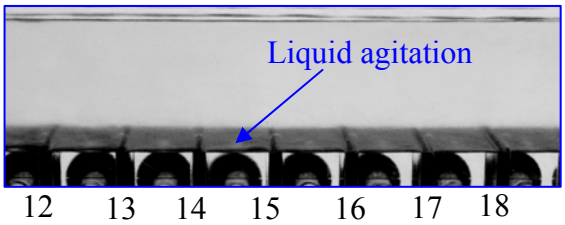

(c)From branch no. 12 to no. 18

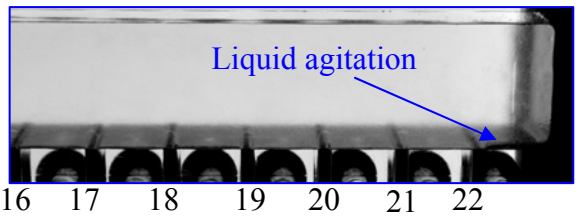

(d)From branch no. 16 to no. 22

Fig. 4.36 Zoom in snapshots along dividing header for R-134a liquid phase flow distribution qualitative judgment
(Inlet pipe swaged to 1.5mm, M = 8.5 kg/h and x = 0.3)

rate *M* at the header entrance seems to be similar with the flow distribution of liquid phase qualitative judgment as in Table 4.6. Also, the flow distribution uniformity of liquid phase become better compare with the one that using inlet pipe with inner diameter of 4.7mm as in Fig. 4.32(a); and from the result in Fig. 4.37 also shows that the flow uniformity of liquid phase become better as the mass flow rate *M* is become higher.

Table 4.6 Qualitative judgment of liquid distribution observed in refrigerant flow

x	*M*	1^{st} - 17^{th}	18^{th}	19^{th}	20^{th}	21^{st}	22^{nd}
0.3	4.15	○	○	△	△	×	○
0.3	5.2	○	○	○	△	△	○
0.3	6.4	○	○	○	△	○	○
0.3	8.5	○	○	○	○	○	○

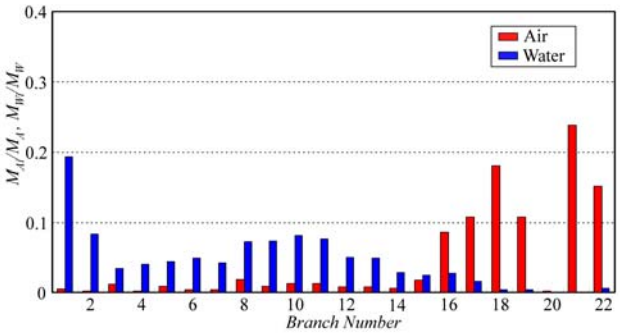

(a) M = 4.15 kg/h, x = 0.3

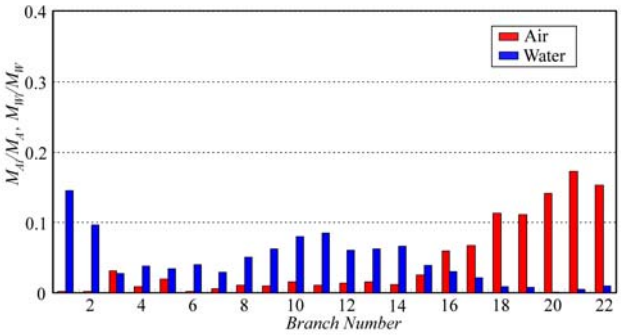

(b) M = 5.2 kg/h, x = 0.3

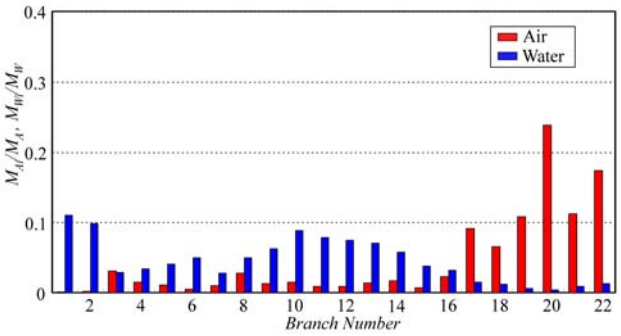

(c) M = 6.4 kg/h, x = 0.3

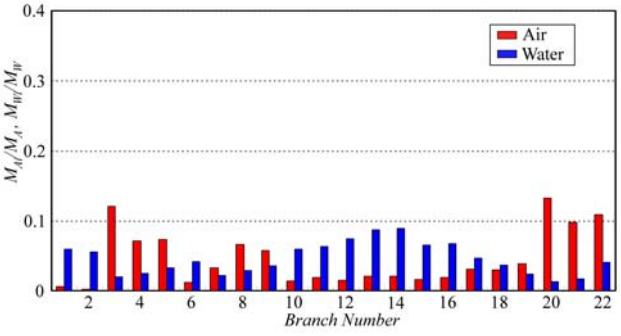

(d) M = 8.5 kg/h, x = 0.3

Fig. 4.37 Results of air-water flow distribution ratios at test condition equal to superficial velocities

4.3.6 Discussion on flow distribution behavior of R-134a and air-water flow in multi-pass channel

As been investigated and reported earlier in this paper, there are differences when simulate the R-134a flow with air-water flow in upward and downward multi-pass channel. In this session the differences and the root cause of it shall be discuss.

As in Fig. 4.24(a), due to the branches in upward direction, makes the dividing header become as a temporary liquid pool before the substance being forced entering the combining header through the branches. As a result, the liquid phase dominating the space in dividing header and only a small region of gas phase that can be observed near the header entrance. The movement of gas phase region at the header entrance, i.e., gas-liquid flow pattern, similar to the one in a horizontal conduit study. This kind of two phase flow pattern mainly has strong influences from not only the superficial velocity and density of each phase, but also from the viscosity and surface tension of liquid phase of the substance, which is similar to Baker's flow pattern parameters. Thus, the behavior of two phase flow pattern at the header entrance as being previously studied in first segment has huge influences to the flow distribution of gas and liquid phase in upward multi-pass channel.

For the downward multi-pass channel, from the visual data and air flow distribution measurement, also from confirmation test by difference superficial velocities, i.e., using inlet pipe being swaged to smaller inner diameter of 1.5mm, at the header entrance shows that the inlet condition of air-water velocities that could simulate the real refrigerant flow distribution behavior in downward multi-pass channel was the one that equal to superficial velocities of the real refrigerant gas and liquid phase. In other word, the flow distribution behavior of real refrigerant in downward multi-pass channel could not be simulating air-water flow using the inlet condition that equal to Baker's map parameters. As in Fig. 4.30, due to the range of mass flow rate M of this study is as low as in Table 3.4, to compare with the hydraulic diameter of multi-port branch hole and its quantity of branches in downward flow, makes the flow of liquid phase at the header entrance as been observed in the snapshot. Thus making the dividing header mostly filled by gas phase and the liquid phase can be observed entering the dividing header similar to the ordinary liquid entering an empty space. Theoretically the inlet condition of air-water flow that equal to kinetic energies supposed to be the favorite inlet condition, however due to the differences of R-134a gas phase and air density about 8.7

times as in Table 4.4, makes the one that equal to superficial velocities of gas and liquid phase of real refrigerant to be the best inlet condition to be fitted on synchronizing the flow distribution behavior of real refrigerant in multi-pass downward channel.

In order to simulate a flow distribution behavior of real refrigerant in multi-pass channel neither upward nor downward, or when a situation that has both upward and downward flow of multi-pass channel in one evaporator that need to be simulate simultaneously, which most of the compact evaporator do have, one universal inlet condition have to be selected. From the study, it has been confirmed that the inlet condition that equal to Baker's flow pattern map parameter and equal to superficial velocities of real refrigerant, both represent the upward and downward separately, and could not be vice versa. On the other hand, the inlet condition that equal to kinetic energies, even it was not the favorite inlet condition to be used in either upward or downward multi-pass channels; nevertheless in this case, it is wise and safe to use it as the inlet condition for the simulation with the real refrigerant flow.

Chapter 5

Conclusion

5.1 Chapter overview

In this chapter, the conclusions from discussion of results and data analysis of the experiment are reported. The conclusion has been divided into two segments.

5.2 First segment: Study on parameters that influence the flow distribution

An experimental study has been conducted on the gas-liquid flow distributions in the multi-pass channels with vertical upward branches that simulate the compact evaporators. The influences of the flow-inlet condition at the header entrance, pressure condition at the branch outlets and pressure loss characteristics of branches on the gas-liquid distribution have been examined with the isothermal air-water two-phase flow system. Moreover, the pressure distributions inside the dividing and combining headers have been measured. Main results are summarized as follows.

(1) Under the stratified-flow inlet condition, the flow distribution in the flat tube channel is seriously influenced by the backpressure condition of the branches. More water is distributed to downstream branches under the non-uniform backpressure condition, while the water distribution ratios in upstream branches

increase under the uniform backpressure condition.

(2) On the other hand, in the multi-port tube channel, the backpressure condition of the branches exerts only minor influences on the flow distributions. As is the case with the flat tube channel, the water distribution ratio increases in the downstream branches at high air velocity. The mal-distribution of water to downstream branches is, however, relieved in comparison with the flat tube channel.

(3) Under the mist-flow inlet condition, the influences of the backpressure condition of the branches on the flow distributions are significantly lessened in comparison with the stratified-flow inlet. The uniformity of the water distribution is much improved especially under high air velocity condition.

(4) In both flow-inlet conditions, the flow distribution characteristics in the multi-port tube channel are qualitatively similar to those of the flat tube channel obtained under the non-uniform backpressure condition.

(5) The pressures in the headers show constant values in the longitudinal direction irrespective of the flow-inlet conditions, branch profiles, superficial air and water velocities. This suggests that, in the measurements of the flow distribution ratios, the uniform backpressure condition is appropriate for reproducing the flow in a real compact evaporator with a multi-pass channel.

(6) The uniformity of the flow distributions was evaluated based on the standard deviations of the air or water distribution ratios (σ_g and σ_l, respectively). The backpressure condition has a decisive influence on σ_g, and non-uniform backpressure condition is favorable to the uniform distribution of air. σ_l is influenced by the flow inlet condition, and the mist-flow inlet is advantageous to improve the uniformity of the water distribution to the branches

(7) 24 selected standard deviation's data has been analyzed by using design of experiment method through Minitab 15 statistical software. For uniformity of gas phase flow distribution, the main parameter that contributed the most is j_g. For uniformity of liquid phase flow distribution, it was the 2-way interaction between flow pattern and j_g that contribute the most.

(8) The best setting of level of each parameter for getting the best uniformity of gas phase flow distribution are:
   (a) j_g shall be at 5.0 m/s.
   (b) Backpressure condition shall be set at non-uniform.

(c) Flow pattern at header entrance however shall be either stratified or mist-flow.

(9) Also, the best setting of level of each parameter for getting the best uniformity of liquid phase flow distribution are:

(a) Flow pattern at header entrance shall be Mist-flow.

(b) Backpressure condition shall be set at uniform.

(c) j_g shall be at 5.0 m/s.

5.3 Second segment: Study on the similarity of real refrigerant and air-water two phase flow distribution behavior

An experimental study on two phase flow distribution behavior in multi-pass upward and downward channel that simulate a multi flow type compact evaporator has been done, focusing on synchronizing the R-134a flow pattern at the header entrance to air-water flow pattern. A visual test, observing the R-134a and air-water flow pattern at the header entrance and at the combining header have been done. Also, an air-water flow distribution measurement has been done. Thus, upon confirmation on the result in downward channel, another parameter has been added to observed the flow distribution behavior of real refrigerant at higher superficial velocity at header entrance, also as a counter measure for improvement of liquid phase flow distribution uniformity. From the result, the conclusions are as below.

Upward channel

(1) From observing the R-134a visual data, the flows at the header entrance for all the test condition are most likely stratified flows. As the mass flow rate M and quality x are increased, the length gained by the gas phase increases. Quality x comparatively has more influence than the mass flow rate M.

(2) As for air-water two phase flow visual observation result, from all 4 tested inlet conditions, it has been found that the conditions of equal kinetic energies and Baker map parameters have similar flow patterns of R-134a at the dividing header entrance of the channel.

(3) The result of air-water flow distribution test confirmed that the test condition of equal Baker map parameters has the most identical two phase flow distribution behavior in the simulated test channel, even though it has lesser similarity of two phase flow pattern at the header entrance comparatively to the test condition of

equal kinetic energies.

Downward channel

(1) From the R-134a visual data, it was found that a clear visual of liquid phase flow being distribute only at near the header entrance when using the original inlet pipe, i.e., ID 4.7mm, and even the mass flow rate or quality *x* is increase (Table 3.4); the improvement of flow distribution behavior was not as expected.

(2) As for air-water two phase flow visual observation result, from all 4 tested inlet conditions, it has been found that the conditions of equal kinetic energies and superficial velocities of R-134a have similar flow patterns of R-134a at the dividing header entrance of the channel.

(3) The result of air-water flow distribution test confirmed that the test condition of equal superficial velocities of gas and liquid phase of R-134a has the most identical two phase flow distribution behavior in the simulated downward test channel.

(4) Test result using inlet pipe with swaging treatment of inner diameter of 1.5mm shows that even at different or higher velocity, the inlet condition of air-water that best to simulate the flow distribution behavior in downward channel is the one that equal to superficial velocities of gas and liquid phase of R-134a.

(5) Also, it was found that when the inlet condition to be swaged to a smaller diameter, the flow distribution uniformity of liquid phase of R-134a is become better and the flow pattern of R-134a flow from the inlet pipe that swaged to inner diameter of 1.5mm is at annular flow pattern on the Baker' flow pattern map.

However, when simulating a flow distribution of real refrigerant inside compact evaporator that has upward and downward channel that run simultaneously, the result of visual observation and air-water flow distribution test confirmed that the inlet condition of equal to kinetic energies is favorable, wiser and safer to use.

References

- Ahmad M., Berthoud G. and Mercier P., “General Characteristics of Two-phase Flow Distribution in a Compact Heat Exchanger”, Int. J. Heat Mass Transfer, 52 (2009), pp 442-450
- Arai A., Senshu T. and Hosoe Y., “Development of High Efficiency Air Conditioners”, Hitachi Review, Vol. 30 (1981), No. 1, pp 6–10
- Barnea D. and Taitel Y., "Flow Pattern Transition in Two-Phase Gas-Liquid Flows", The Encyclopedia of Fluid Mechanics, 3, (1986) Chapter 16, pp 403-474
- Bernoux P., Mercier P. and Lebouche M., “Two-phase Flow Distribution in a Compact Heat Exchanger”, Proc. 3rd Int. Conf. Compact Heat Exchanger, (2001), pp 347-352
- Brookes C.J., Betteley I.G., Loxston S.M., “Fundamentals of Mathematics and Statistics for Students of Chemistry and Allied Subjects”, (1979), John Wiley & Sons, New York, chapter 18, pp 398-425
- Hansen J., Johnson D., Lacis A., Lebedeff S., Lee P., Rind D. and Russell G., “Climate Impact of Increasing Atmospheric Carbon Dioxide”, Science, Vol. 213 (1981), No. 4511, pp 957-966
- Hansen J., Ruedy R., Sato M. and Lo K., “Global Surface Temperature Change”, Reviews of Geophysics, Vol. 48 (2010), No. RG4004, Paper no. 2010RG000345

- Horiki, S. and Osakabe, M., "Water Flow Distribution in Horizontal Protruding-type Header Contaminated with Bubbles", Proceedings of the ASME Heat Transfer Division, HDT-Vol. 364-2 (1999), 2, pp 69-76
- Hwang S. T., Soliman H. M., and Lahey R. T. Jr., "Phase Separation in Dividing Two-phase Flows", International Journal of Multiphase Flow, 14(4), (1988), pp 439-458
- Ito M., Kimura H. and Senshu T., "Development of High Efficiency Air-Cooled Heat Exchangers", Hitachi Review, Vol. 26 (1977), No. 10, pp 323-326
- Kashiwazaki S., Akatsuka M. and Tatsukawa O., "Home Appliances Using Inverter Technology", Hitachi Review Vol. 38 (1989), No. 6, pp 303–306
- Katsuta M., Watanabe M., Nomura D., Tanaka S. and Sueyosi C., "Distribution Characteristics of Two-phase Gas-liquid Flow in Multipass Tube - Discussion on T-junction and Multipass Tube Concerning on the Phase Separation Characteristics-", Proc. 2008 Japan Soc. Refrigerating Air Conditioning Engineers Annual Conf., (2008), pp 405-408 (in Japanese)
- Katsuta M., Yamagata K. and Fukai K., "Distribution Characteristics of Two-phase Gas-liquid Flow in Horizontal Multipass Tube - The Effect of Branch's Local Geometry", Proc. 2009 Japan Soc. Refrigerating Air Conditioning Engineers Annual Conf., (2009), pp 551-554 (in Japanese).
- Kim N-H. and Han S-P., "Distribution of Air-water Annular Flow in a Header of a Parallel Flow Heat Exchanger", Int. J. Heat Mass Transfer, 51 (2008), pp 977-992
- Koyama S., Kuwahara K., Miyazaki H., Wijayanta A. T., Kanzaki M. and Ikuta S., "Experimental Study on Refrigerant Flow Distribution Inside Branch Headers of Evaporators", Proc. of the 43rd National Heat Transfer Symposium of Japan (HTSJ), 2006-5 (2006), paper no. A122
- Lee J. K. and Lee S. Y., "Distribution of Two Phase Annular Flow at Header-channel Junctions", Experimental Thermal Fluid Science, 28 (2004), pp 217-222.
- Lee J. K., "Two-phase Flow Behavior inside a Header Connected to Multiple Parallel Channels", Experimental Thermal Fluid Science, 33 (2009), pp 195-202
- Lee S. Y., "Flow Distribution Behavior in Condensers and Evaporators", Proc. 13th

Int. Heat Transfer Conf., KN-08 (2006), in CD-ROM.

- Marchitto A., Devia F., Fossa M., Guglielmini G. and Schenone C., "Experiments on Two-phase Flow Distribution inside Parallel Channels of Compact Heat Exchangers", Int. J. Multiphase Flow, 34 (2008), pp 128-144
- Nakamura H., Yokoyama H. and Morimoto M., "An Energy Saving and Comfortable Dehumidification Method for Air Conditioners", Proceeding of Asia-Pacific Conference on the Built Environment, Singapore, 1995
- Nakamura T., Kuroyanagi I., Kamiya S. and Ohara T., "Ultra-Thin and Light-Weight RS Evaporator", SAE paper 2003-01-0527 (2003)
- Osakabe M., Hamada T. and Horiki S., "Water Flow Distribution in Horizontal Header Contaminated with Bubbles", Int. J. Multiphase Flow, 25 (1999), 827-840.
- Tatsumi A., Oizumi K., Hayashi M. and Ito M., "Application of Inner Groove Tubes to Air Conditioners", Hitachi Cable Review, No. 1 (1982), pp 55–60
- Vist S. and Pettersen J., "Two-phase Flow Distribution in Compact Heat Exchanger Manifolds", Experimental Thermal Fluid Science, 28 (2004), pp 209-215
- Watanabe M., Katsuta M. and Nagata K., "Prediction of Two-phase Flow Distribution in Multipass Tube by Utilizing Annular Flow Division Model", Proc. 11th Int. Heat Transfer Conf., 2 (1998), pp 151-156
- Watanabe M., Katsuta M. and Nagata K., "Two-phase Flow Distribution in Multi-pass Tube Modeling Serpentine Type Evaporator", Proc. ASME/JSME Thermal Engineering Conf., 2 (1995), pp 35-42
- Watanabe M., Katsuta M., Nagata K., Sakakura S. and Iijima H., "Two-phase Refrigerant Flow Distribution in a Multipass Evaporator with Vertical Upward Main Tube (1st report: Equal Heating Load on Each Pass)", Trans. Japanese Assoc. Refrigeration, 13-3 (1996), pp 277-284 (in Japanese)
- Watanabe M., Katsuta M., Nagata K., Sakakura S. and Iijima H., "Two-phase Refrigerant Flow Distribution in a Multipass Evaporator with Vertical Upward Main Tube (2nd report: Unequal Heating Load on Each Pass)", Trans. Japanese Assoc. Refrigeration, 13-3 (1996), pp 285-291 (in Japanese)
- Webb R. and Chung K., "Two-Phase Flow Distribution to Tubes of Parallel Flow Air-Cooled Heat Exchangers", Heat Transfer Engineering, 26-4 (2005), pp 3-18

List of Publications
Related to Doctoral Dissertation

Refereed Journal Publications

1. Mohamad-Razlan ZURADZMAN, Ryota ISOBE, Hiroaki GOSHIMA, Masafumi HIROTA, Yasuhiro MIZUNO, Naoki MARUYAMA, Akira NISHIMURA, "Experimental Study on Gas-Liquid Flow Distributions in Upward Multi-pass Channels", Journal of the Japanese Society for Experimental Mechanics, Vol. 11, pp ss79-ss85, Special issue, August, 2011.

2. Zuradzman bin Mohamad Razlan, Hiroaki Goshima, Masafumi Hirota, Ryota Isobe, Yasuhiro Mizuno, Naoki Maruyama, Akira Nishimura, "Gas-Liquid Flow Distributions in Multipass Channels with Vertical Upward Branches", The Open Transport Phenomena Journal, Bentham Open, Vol. 3, pp. 17-30, June, 2011.

3. ZURADZMAN M.R., GOSHIMA Hiroaki, HIROTA Masafumi, MIZUNO Yasuhiro, MARUYAMA Naoki, NISHIMURA Akira, ISOBE Ryota, "Gas-Liquid Flow Distribution in Multi-Pass Upward Channels", Japanese Journal of Multiphase Flow (JJMF), Vol. 24 (2010), No. 5, pp. 577-585, June, 2011.

International / National Conference Proceedings

1. Mohamad-Razlan Zuradzman, Hiroaki Goshima, Kohji Takiguchi, Toshiaki Tsuchiya, Motohide Okamoto, Masaaki Ajima, Yujiro Kitade, Masafumi Hirota, Naoki Maruyama, Akira Nishimura, "Experimental Study on Gas-liquid Flow Distributions in Upward Multi-pass Channel Comparison of R-134a Flow and Air-water Flow", Proceeding of the 6th International Symposium on Advanced Science and Technology in Experimental Mechanics, Osaka, Japan, paper no. 074, Nov., 2011

2. Yamato Nakagawa, Razlan Zuradzman, Koji Takiguchi, Toshiaki Tsuchiya, Motohide Okamoto, Masaaki Ajima, Yujiro Kitade, Masafumi Hirota, Naoki Maruyama, Akira Nishimura, "Experimental Study on Gas-liquid Flow Distributions in Multi-pass Channels", Proceedings of JSME Thermal Engineering Conference 2011, Hamamatsu, Japan, Paper no.11-36, Oct., 2011.

3. Razlan Mohamad Zuradzman, Hiroaki Goshima, Koji Takiguchi, Toshiaki Tsuchiya, Motohide Okamoto, Masaaki Ajima, Yujiro Kitade, Masafumi Hirota, Naoki Maruyama, Akira Nishimura, "Experimental Study on Gas-liquid Flow Distributions in Upward Multi-pass Channel (Comparison of R-134a Flow and Air-water Flow)", Proceedings of ASME-JSME-KSME Joint Fluids Engineering Conference 2011 (AJK2011-FED), Hamamatsu, Japan, Paper no. AJK2011-32008, July, 2011

4. Razlan ZURADZMAN, Hiroaki GOSHIMA, Koji TAKIGUCHI, Toshiaki TSUCHIYA, Masaaki AJIMA, Masafumi HIROTA, Motohide OKAMOTO, Yujiro KITAIDE, Naoki MARUYAMA and Akira NISHIMURA, "Experimental Study on Gas-Liquid Distributions in Multi-pass Channels", 48th National Heat Transfer Symposium of Japan (HTSJ), paper no. 2011-6, Okayama, Japan, 1st-3rd June 2011

5. Hiroaki Goshima, Zuradzman M.R, Masafumi Hirota, Koji Takiguchi, Toshiaki Tsuchiya, Yujiro Kitade, "Gas-Liquid Flow Distributions in Multi-pass Upward Channels", 60th Tokai Regional Annual Meeting of Japan Society of Mechanical Engineers (JSME), paper no. 865, Toyohashi, Japan, 14-15 Mar. 2011

6. Mohamad-Razlan ZURADZMAN, Ryota ISOBE, Hiroaki GOSHIMA, Masafumi HIROTA, Yasuhiro MIZUNO, Naoki MARUYAMA, Akira NISHIMURA, "Experimental Study on Gas-Liquid Flow Distributions in Upward Multi-pass Channels", 5th International Symposium on Advanced Science and Technology in Experimental Mechanics (5th ISEM), paper no. 28, Ryukoku University, Kyoto, Japan, 4-7 Nov. 2010

7. Zuradzman Razlan, Hiroaki Goshima, Kohji Takiguchi, Toshiaki Tsuchiya, Motohide Okamoto, Yujiro Kitade, Masafumi Hirota, Naoki Maruyama, Akira Nishimura, "Two-phase Flow Distributions in Multi-pass Channels Comparison of Refrigerant Flow and Air-water Flow", 2010 Annual Conference of Japan Society of Refrigerating and Air-Conditioning Engineers (JSRAE), paper no. B223-1, Kanazawa, Japan, 15-17 Sept. 2010

8. Zuradzman Mohamad Razlan, Ryota Isobe, Yasuhiro Mizuno, Hiroaki Goshima, Masafumi Hirota, Naoki Maruyama, "Gas-liquid Distributions in Upward Multi-pass Channels of Compact Evaporator", 14th International Heat Transfer Conference (IHTC14), paper no. IHTC14-22588, Washington D.C., USA, 8-13 Aug. 2010

9. ZURADZMAN M.R, GOSHIMA Hiroaki, HIROTA Masafumi, MIZUNO Yasuhiro, MARUYAMA Naoki, ISOBE Ryota, NISHIMURA Akira, "Gas-liquid Flow Distribution on Multi-pass Upward Channel", 2010 Annual Meeting of The Japan Society for Multiphase Flow (JSMF), paper no. A-142, Hamamatsu, Japan, 17-19 Jul. 2010

10. Zuradzman M.R, Hiroaki Goshima, Masafumi Hirota, Naoki Maruyama, Akira Nishimura, Ryota Isobe, "Two-phase Flow Distribution in Multi-pass Channel", 59th Tokai Regional Annual Meeting of Japan Society of Mechanical Engineers (JSME), paper no. 304, pp. 149-150, Meijou University, Nagoya, Japan, 9-10 Mar. 2010

Appendix

Testing Data

These are the testing data upon conducting the visual observation of R-134a refrigerant. Mainly, monitoring the thermodynamic properties at each point on Mollier diagram especially at point no. ③, i.e., at test channel header entrance, and the cooling cycle mass flow rate, by adjusting the parameters to archive the quality x and mass flow rate M as in Table 3.4.

Folder: 1 evp vis/5 flow recogition

Channel orientation	Upward	Intrusion height h	0mm
Inlet pipe diameter	4.7mm	Branch quantity	22

1atm = 0.101325 mPa
1mPa = 10.197162 kgf/cm2

	Test date		38(2010/01/14)	40	41	42	43(2010/01/15)	44	45	47	48	49(2010/01/16)	50	52(2010/01/18)
Parameter	evp out flow direction		reverse	←	←	←	←	←	←	←	←	←	←	←
	R134a amount	g	435	←	←	←	←	←	←	←	←	←	←	←
	comp Rev	rpm	1500	←	2700	2000	3400	3000	2800	←	2100	4500	3200	4500
	Exp Valve opening value	pulse	44	64	78	69	114	95	66	55	47	79	60	77
	water flow	ml/min	40	450	310	300	420	165	135	105	110	50	40	95
	outdoor fan speed	V	4.27	5.2	5	←	5.13	4.15	4.14	←	←	←	4.12	4.23
	remark		in4, out2 layer	←	←	←	←	←	←	←	←	←	←	←
Testing data	flow rate	ml/min	61.73	55.91	87.7	71.773	114.75	123.16	90.53	73.6	58.44	97.74	77.26	124.55
	P entering Exp valve	mPaG	1.193	0.468	0.599	0.562	0.540	0.948	0.945	0.939	0.903	1.301	1.264	1.304
	P absolute	mPa	1.294	0.569	0.700	0.663	0.641	1.049	1.046	1.040	1.004	1.402	1.365	1.405
	P leaving exp valve	mPaG	0.083	0.085	0.086	0.097	0.099	0.138	0.092	0.08	0.064	0.097	0.082	0.102
	P absolute	mPa	0.184	0.186	0.187	0.198	0.200	0.239	0.193	0.181	0.165	0.198	0.183	0.203
	T entering Exp valve	°C	45.122	19.459	19.478	20.826	20.139	38.048	34.124	33.706	31.691	49.143	47.579	44.715
	T leaving exp valve	°C	-11.269	-10.870	-10.898	-9.382	-9.368	-4.808	-10.151	-11.640	-13.875	-9.573	-11.291	-8.711
	Ps	mPaG	0.08	0.09	0.09	0.09	0.08	0.12	0.08	0.07	0.07	0.07	0.07	0.08
		mPa	0.181	0.191	0.191	0.191	0.181	0.221	0.181	0.171	0.171	0.171	0.171	0.181
	Pd	mPaG	1.29	0.55	0.68	0.65	0.65	1.05	1.05	1.02	0.98	1.38	1.35	1.40
		mPa	1.391	0.651	0.781	0.751	0.751	1.151	1.151	1.121	1.081	1.481	1.451	1.501
	T at flow meter	°C	46.9	18.5	19.100	20.200	20.200	38.300	34.800	34.600	31.400	48.900	48.400	45.100
	Cs	°C	15.30	14.30	14.30	14.90	14.30	15.80	14.40	13.70	13.10	12.60	12.10	13.00
	Cd	°C	na	na	na	na	na	na	na	na	na	na	na	na
Calculation value	saturated point temp	°C	49.27	19.84	26.71	24.87	23.74	41.17	41.06	40.85	39.53	52.48	51.40	52.57
	subcool amount	°C	4.15	0.38	7.23	4.04	3.60	3.12	6.94	7.14	7.84	3.34	3.82	7.86
	Enthalpy at entering exp valve (h)	kJ/kg	264.09	226.71	226.75	228.64	227.67	253.49	247.71	247.1	244.16	270.25	267.84	263.44
	T leaving exp valve (calculation value)	°C	-12.19	-11.92	-11.78	-10.35	-10.09	-5.49	-10.99	-12.59	-14.86	-10.35	-12.32	-9.72
	Quality (x)	**kg/kg**	**0.3868**	**0.2052**	**0.2046**	**0.2056**	**0.1995**	**0.3001**	**0.3015**	**0.3071**	**0.3049**	**0.4074**	**0.4055**	**0.3712**
	Density	kg/m^3	1125.75	1227.35	1228	1222.73	1225.19	1155.63	1172.38	1174.08	1182.15	1107.48	1114.74	1128.69
	Mass flow	**kg/h**	**4.17**	**4.12**	**6.46**	**5.27**	**8.44**	**8.54**	**6.37**	**5.18**	**4.15**	**6.49**	**5.17**	**8.43**
	Gas Specific Volume (header)	m^3/kg	1.081E-01	1.070E-01	1.065E-01	1.008E-01	9.987E-02	8.424E-02	1.033E-01	1.098E-01	1.199E-01	1.008E-01	1.087E-01	9.846E-02
	Gas Density (header)	kg/m^3	9.2490	9.3440	9.3923	9.9177	10.0132	11.8715	9.6787	9.1050	8.3389	9.9177	9.2013	10.1564
	Gas superficial velocity (header)	m/s	0.12	0.06	0.10	0.08	0.12	0.15	0.14	0.12	0.11	0.19	0.16	0.21
	Liquid Specific Volume (header)	m^3/kg	7.496E-04	7.501E-04	7.503E-04	7.529E-04	7.533E-04	7.618E-04	7.517E-04	7.489E-04	7.449E-04	7.529E-04	7.494E-04	7.540E-04
	Liquid Density (header)	kg/m^3	1334.03	1333.17	1332.76	1328.23	1327.42	1312.71	1330.26	1335.31	1342.41	1328.23	1334.45	1326.22
	Liquid superficial velocity (header)	m/s	0.0013	0.0017	0.0027	0.0022	0.0035	0.0032	0.0023	0.0019	0.0015	0.0020	0.0016	0.0028
	Pressure drop (Pleaving -Ps)	mPa	0.00	(0.00)	(0.00)	0.01	0.02	0.02	0.01	0.01	(0.01)	0.03	0.01	0.02

Folder: 2 evp vis/6 flow recogition

Channel orientation	Downward	Intrusion height h	0mm
Inlet pipe diameter	4.7mm	Branch quantity	22

1atm = 0.101325 mPa
1mPa = 10.197162 kgf/cm2

	Test date		60(2010/03/10)	61	62(2010/03/11)	63	64	65	66	67	68(2010/03/12)	69	70	71
Parameter	evp out flow direction		reverse	←	←	←	←	←	←	←	←	←	←	←
	R134a amount	g	380	←	420	←	←	←	←	←	←	←	420-α	421-α+β
	comp Rev	rpm	1650	2650	4200	1950	3350	3700	3000	2350	2000	3700	3100	1850
	Exp Valve opening value	pulse	60	84	74	67	89	84	66	59	50	72	65	48
	water flow	ml/min	300	365	20	250	255	70	50	40	25	15	55	10
	outdoor fan speed	V	5.24	5.2	4.17	4.99	5.13	4.82	4.31	4.28	4.19	4.19	4.13	4.12
		A	0.08	0.07	0.04	0.08	0.08	0.07	0.06	0.06	0.04	0.05	0.04	0.04
	remark		in4, out2 layer	←	←	←	←	←	←	←	←	←	←	←
Testing data	flow rate	ml/min	56	87.63	127.16	71.01	114.91	121.28	91.07	73.79	59.65	98.17	77.28	63.94
	P entering Exp valve	mPaG	0.480	0.509	1.307	0.607	0.716	1.012	0.994	0.939	0.927	1.342	1.205	1.250
	P absolute	mPa	0.581	0.610	1.408	0.708	0.817	1.113	1.095	1.040	1.028	1.443	1.306	1.351
	P leaving exp valve	mPaG	0.078	0.083	0.107	0.093	0.106	0.113	0.086	0.081	0.062	0.112	0.087	0.067
	P absolute	mPa	0.179	0.184	0.208	0.194	0.207	0.214	0.187	0.182	0.163	0.213	0.188	0.168
	T entering Exp valve	°C	18.444	20.511	46.608	20.283	21.066	36.075	33.700	33.735	31.360	49.719	47.602	47.782
	T leaving exp valve	°C	-12.209	-11.416	-8.337	-10.030	-8.366	-7.392	-10.898	-11.532	-14.194	-7.649	-10.692	-13.517
	Ps	mPaG	0.08	0.08	0.08	0.09	0.09	0.08	0.08	0.08	0.06	0.08	0.08	0.06
		mPa	0.181	0.181	0.181	0.191	0.191	0.181	0.181	0.181	0.161	0.181	0.181	0.161
	Pd	mPaG	0.55	0.60	1.42	0.70	0.82	1.10	1.10	1.05	1.05	1.45	1.28	1.35
		mPa	0.651	0.701	1.521	0.801	0.921	1.201	1.201	1.151	1.151	1.551	1.381	1.451
	T at flow meter	°C	18.400	20.7	48.5	19.6	20.6	35.9	34.3	34.600	33.800	50.300	47.100	48.400
	Cs	°C	10.60	10.90	11.30	12.40	14.60	14.20	13.10	13.00	9.20	13.10	12.00	11.50
	Cd	°C	na	na	na	na	na	na	na	na	na	na	na	na
Calculation value	saturated point temp	°C	20.51	22.10	52.66	27.09	32.06	43.42	42.79	40.85	40.41	53.65	49.64	50.99
	subcool amount	°C	2.07	1.59	6.05	6.81	10.99	7.35	9.09	7.12	9.05	3.93	2.04	3.21
	Enthalpy at entering exp valve (h	kJ/kg	225.29	228.19	266.33	227.88	228.99	250.56	247.08	247.14	243.68	271.13	267.9	268.16
	T leaving exp valve (calculation value)	°C		-12.19	-9.22	-10.86	-9.22	-8.37	-11.78	-12.46	-15.16	-8.49	-11.65	-14.42
	Quality (x)	**kg/kg**	**0.2037**	**0.2138**	**0.3827**	**0.2049**	**0.2009**	**0.3013**	**0.3027**	**0.3066**	**0.3042**	**0.4024**	**0.4025**	**0.4174**
	Density	kg/m^3	1231.21	1223.62	1119.82	1225.02	1222.68	1164.63	1174.5	1173.96	1183.67	1105.06	1117.03	1113.61
	Mass flow	**kg/h**	**4.14**	**6.43**	**8.54**	**5.22**	**8.43**	**8.47**	**6.42**	**5.20**	**4.24**	**6.51**	**5.18**	**4.27**
	Gas Specific Volume (header)	m^3/kg	1.110E-01	1.081E-01	9.664E-02	1.028E-01	9.664E-02	9.362E-02	1.065E-01	1.093E-01	1.213E-01	9.404E-02	1.059E-01	1.179E-01
	Gas Density (header)	kg/m^3	9.0098	9.2490	10.3473	9.7267	10.3473	10.6810	9.3923	9.1533	8.2427	10.6333	9.4402	8.4825
	Gas superficial velocity (header)	m/s	0.06	0.10	0.22	0.08	0.11	0.17	0.14	0.12	0.11	0.17	0.15	0.15
	Liquid Specific Volume (header)	m^3/kg	7.484E-04	7.496E-04	7.549E-04	7.520E-04	7.549E-04	7.565E-04	7.503E-04	7.091E-04	7.444E-04	7.563E-04	7.506E-04	7.457E-04
	Liquid Density (header)	kg/m^3	1336.17	1334.03	1324.64	1329.86	1324.64	1321.93	1332.76	1410.18	1343.33	1322.31	1332.34	1341.04
	Liquid superficial velocity (header)	m/s	0.0017	0.0026	0.0028	0.0022	0.0035	0.0031	0.0023	0.0018	0.0015	0.0020	0.0016	0.0013
	Pressure drop (Pleaving -Ps)	mPa	(0.00)	0.00	0.03	0.00	0.02	0.03	0.01	0.00	0.00	0.03	0.01	0.01

Folder: 3 evp vis/7 flow recogition

Channel orientation		Horizontal Branch, Top paralel		Intrusion height h		0mm					1atm = 0.101325 mPa		
Inlet pipe diameter		4.7mm		Branch quantity		22					1mPa = 10.197162 kgf/cm2		
Test date		80(2010/03/30)	81	82(2010/03/31)	83	84	85	86(2010/04/01)	87	88(2010/04/02)	89	90(2010/04/03)	91
Parameter evp out flow direction		Parallel	←	←	←	←	←	←	←	←	←	←	←
R134a amount	g	365	←	←	←	←	←	←	←	←	365-α	←	←
comp Rev	rpm	1650	2650	1950	3350	4000	3000	2300	1950	4200	3800	2950	1850
Exp Valve opening value	pulse	60	79	64	93	77	63	55	45	74	57	53	45
water flow	ml/min	420	430	320	220	70	50	45	20	20	60	50	35
outdoor fan speed	V	8.67	6.88	8.71	8.14	4.28	4.26	4.22	4.19	4.2	4.22	4.11	4.1
	A	0.14	0.1	0.13	0.12	0.06	0.05	0.05	0.04	0.05	0.05	0.04	0.03
remark		in4, out2 layer	←	←	←	←	←	←	←	←	←	←	←
Testing data flow rate	ml/min	56.64	87.21	70.71	116.01	119.66	91.8	74.98	58.74	127.35	93.94	76.01	62.94
P entering Exp valve	mPaG	0.526	0.551	0.570	0.670	1.081	1.004	0.943	0.992	1.353	1.335	1.197	1.307
P absolute	mPa	0.627	0.652	0.671	0.771	1.182	1.105	1.044	1.093	1.454	1.436	1.298	1.408
P leaving exp valve	mPaG	0.079	0.081	0.086	0.102	0.1	0.083	0.08	0.068	0.101	0.069	0.061	0.076
P absolute	mPa	0.180	0.182	0.187	0.203	0.201	0.184	0.181	0.169	0.202	0.170	0.162	0.177
T entering Exp valve	°C	19.202	18.019	19.185	20.645	34.343	33.081	33.894	32.359	46.227	44.858	44.425	46.903
T leaving exp valve	°C	-11.499	-11.347	-11.425	-8.667	-8.865	-11.304	-11.552	-13.249	-9.117	-13.290	-14.171	-12.076
Ps	mPaG	0.08	0.08	0.08	0.08	0.08	0.08	0.08	0.07	0.08	0.06	0.05	0.08
	mPa	0.181	0.181	0.181	0.181	0.181	0.181	0.181	0.171	0.181	0.161	0.151	0.181
Pd	mPaG	0.60	0.62	0.65	0.75	1.18	1.10	1.08	1.10	1.45	1.45	1.30	1.40
	mPa	0.701	0.721	0.751	0.851	1.281	1.201	1.181	1.201	1.551	1.551	1.401	1.501
T at flow meter	°C	18.300	17.4	19.4	20.5	34.4	34.3	35.8	34.000	47.300	47.100	44.425	49.800
Cs	°C	12.90	13.20	12.50	14.90	14.20	13.80	9.60	8.00	11.10	8.60	12.00	11.30
Cd	°C	na	na	na	na	na	na	na	na	na	na	na	na
Calculation value saturated point temp	°C	23.01	24.31	25.27	30.03	45.73	43.14	40.99	42.73	53.96	53.45	49.40	52.66
subcool amount	°C	3.81	6.29	6.09	9.39	11.39	10.06	7.10	10.37	7.73	8.59	4.98	5.76
Enthalpy at entering exp valve (h	kJ/kg	226.35	224.7	226.33	228.39	248.02	246.18	247.37	245.13	265.73	263.65	263.03	266.78
T leaving exp valve (calculation value)	°C	-12.73	-12.46	-11.78	-9.72	-9.97	-12.19	-12.59	-14.28	-9.84	-14.14	-15.31	-13.15
Quality (x)	**kg/kg**	**0.2080**	**0.1985**	**0.2026**	**0.2008**	**0.2976**	**0.3005**	**0.3084**	**0.3065**	**0.3829**	**0.3944**	**0.3972**	**0.4045**
Density	kg/m^3	1228.63	1233.16	1228.93	1224.01	1172.45	1177.14	1173.32	1180.03	1122.07	1128.31	1129.05	1118.41
Mass flow	**kg/h**	**4.18**	**6.45**	**5.21**	**8.52**	**8.42**	**6.48**	**5.28**	**4.16**	**8.57**	**6.36**	**5.15**	**4.22**
Gas Specific Volume (header)	m^3/kg	1.104E-01	1.093E-01	1.065E-01	9.846E-02	9.939E-02	1.081E-01	1.098E-01	1.172E-01	9.893E-02	1.166E-01	1.220E-01	1.122E-01
Gas Density (header)	kg/m^3	9.0572	9.1533	9.3923	10.1564	10.0610	9.2490	9.1050	8.5302	10.1087	8.5785	8.1947	8.9135
Gas superficial velocity (header)	m/s	0.07	0.10	0.08	0.12	0.17	0.15	0.12	0.10	0.23	0.20	0.17	0.13
Liquid Specific Volume (header)	m^3/kg	7.487E-04	7.491E-04	7.503E-04	7.540E-04	7.536E-04	7.496E-04	7.489E-04	7.459E-04	7.538E-04	7.462E-04	7.442E-04	7.479E-04
Liquid Density (header)	kg/m^3	1335.74	1334.88	1332.76	1326.22	1327.02	1334.03	1335.31	1340.59	1326.63	1340.14	1343.80	1337.04
Liquid superficial velocity (header)	m/s	0.0017	0.0027	0.0022	0.0036	0.0031	0.0024	0.0019	0.0015	0.0028	0.0020	0.0016	0.0013
Pressure drop (Pleaving -Ps)	mPa	(0.00)	0.00	0.01	0.02	0.02	0.00	0.00	(0.00)	0.02	0.01	0.01	(0.00)

Folder: 4 evp vis/8 flow recogition

Channel orientation	Horizontal Branch, Top reverse	Intrusion height h	0mm
Inlet pipe diameter	4.7mm	Branch quantity	22

1atm = 0.101325 mPa
1mPa = 10.197162 kgf/cm2

	Test date		100(2010/05/12)	101	102(2010/05/13)	103	104	105(2010/05/14)						
Parameter	evp out flow direction		Reverse	←	←	←	←	←						
	R134a amount	g	370-α+110-β+50+80	←	←	←	←	←+(40-δ)						
	comp Rev	rpm	1950	4000	2900	2300	1800	2750						
	Exp Valve opening value	pulse	73	92	69	54	44	57						
	water flow	ml/min	435	130	80	70	65	35						
	outdoor fan speed	V	8.31	4.3	4.19	4.16	4.14	4.13						
		A	0.13	0.06	0.04	0.04	0.04	0.04						
	remark		in4, out2 layer	←	←	←	←	←						
Testing data	flow rate	ml/min	71.45	121.79	90.3	73.75	58.47	77.38						
	P entering Exp valve	mPaG	0.541	0.924	0.909	0.936	0.955	1.210						
	P absolute	mPa	0.642	1.025	1.010	1.037	1.056	1.311						
	P leaving exp valve	mPaG	0.094	0.094	0.075	0.076	0.078	0.08						
	P absolute	mPa	0.195	0.195	0.176	0.177	0.179	0.181						
	T entering Exp valve	°C	21.934	33.875	32.236	32.413	33.248	46.168						
	T leaving exp valve	°C	-9.927	-9.927	-12.746	-12.511	-12.243	-11.903						
	Ps	mPaG	0.10	0.08	0.07	0.07	0.08	0.07						
		mPa	0.201	0.181	0.171	0.171	0.181	0.171						
	Pd	mPaG	0.62	1.02	1.00	1.02	1.05	1.28						
		mPa	0.721	1.121	1.101	1.121	1.151	1.381						
	T at flow meter	°C	21.800	34.1	33.6	34.2	35.4	46.7						
	Cs	°C	12.00	13.10	6.50	7.80	9.10	9.30						
	Cd	°C	na	na	na	na	na	na						
Calculation value	saturated point temp	°C	23.80	40.30	39.75	40.74	41.42	49.79						
	subcool amount	°C	1.87	6.43	7.51	8.33	8.17	3.62						
	Enthalpy at entering exp valve (h)	kJ/kg	230.2	247.34	244.95	245.21	246.43	265.69						
	T leaving exp valve (calculation value)	°C	-10.73	-10.73	-13.29	-13.15	-12.87	-12.59						
	Quality (x)	**kg/kg**	**0.2154**	**0.2984**	**0.3004**	**0.3009**	**0.3053**	**0.3965**						
	Density	kg/m^3	1218.4	1173.27	1179.96	1179.42	1176.12	1120.97						
	Mass flow	**kg/h**	**5.22**	**8.57**	**6.39**	**5.22**	**4.13**	**5.20**						
	Gas Specific Volume (header)	m^3/kg	1.023E-01	1.023E-01	1.128E-01	1.122E-01	1.110E-01	1.098E-01						
	Gas Density (header)	kg/m^3	9.7742	9.7742	8.8660	8.9135	9.0098	9.1050						
	Gas superficial velocity (header)	m/s	0.08	0.18	0.15	0.12	0.10	0.16						
	Liquid Specific Volume (header)	m^3/kg	7.522E-04	7.522E-04	7.477E-04	7.479E-04	7.484E-04	7.489E-04						
	Liquid Density (header)	kg/m^3	1329.45	1329.45	1337.47	1337.04	1336.17	1335.31						
	Liquid superficial velocity (header)	m/s	0.0021	0.0031	0.0023	0.0019	0.0015	0.0016						
	Pressure drop (Pleaving -Ps)	mPa	(0.01)	0.01	0.01	0.01	(0.00)	0.01						

Folder: 5 evp vis/9 flow recogition

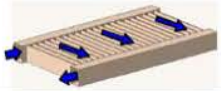

1atm = 0.101325 mPa

1mPa = 10.197162 kgf/cm2

	Channel orientation		Flat channel, reverse		Intrusion height h	0mm								
	Inlet pipe diameter		4.7mm		Branch quantity	22								
	Test date		110(2010/05/25)	111	112(2010/05/26)	113	114	115(2010/05/28)	116	117	118(2010/05/30)	119(2010/05/31)	120(2010/06/03)	121(2010/06/04)
Parameter	evp out flow direction		Reverse	←	←	←	←	←	←	←	←	←	←	double
	R134a amount	g	425-α+165	←-β	←-γ	←	←-δ	←	←	←	←-σ	←±τ	355	←
	comp Rev	rpm	1650	1950	2350	3350	4000	3000	2300	1950	4200	2950	4300	1650
	Exp Valve opening value	pulse	48	60	73	90	80	67	54	44	84	64	74	45
	water flow	ml/min	310	450	490	←	105	95	95	90	68	65	20	10
	outdoor fan speed	V	9.68	←	←	←	4.2	4.19	4.18	4.15	4.12	4.12	4.18	4.15
		A	0.16	←	←	←	0.05	0.04	0.04	0.04	0.04	0.04	0.05	0.04
	remark		in4, out2 layer	←	←	←	←	←	←	←	←	←	←	←
Testing data	flow rate	ml/min	56.87	71.07	87.92	116.37	119.32	90.29	73.71	58.06	95.98	76.27	126.6	63.08
	P entering Exp valve	mPaG	0.711	0.675	0.710	0.803	1.121	0.926	0.909	0.988	1.323	1.175	1.312	1.108
	P absolute	mPa	0.812	0.776	0.811	0.904	1.222	1.027	1.010	1.089	1.424	1.276	1.413	1.209
	P leaving exp valve	mPaG	0.082	0.095	0.105	0.106	0.104	0.077	0.077	0.067	0.111	0.085	0.091	0.074
	P absolute	mPa	0.183	0.196	0.206	0.207	0.205	0.178	0.178	0.168	0.212	0.186	0.192	0.175
	T entering Exp valve	℃	21.634	21.221	21.724	21.713	35.639	32.680	32.199	31.915	50.204	46.485	45.889	45.992
	T leaving exp valve	℃	-11.623	-9.957	-9.021	-8.873	-8.849	-12.451	-12.369	-13.576	-8.153	-11.427	-10.067	-12.468
	Ps	mPaG	0.08	0.09	0.10	0.10	0.09	0.07	0.08	0.07	0.09	0.08	0.08	0.08
		mPa	0.181	0.191	0.201	0.196	0.191	0.171	0.181	0.171	0.191	0.181	0.181	0.181
	Pd	mPaG	0.80	0.75	0.80	0.90	1.20	1.02	1.00	1.10	1.42	1.25	1.42	1.30
		mPa	0.901	0.851	0.901	1.001	1.301	1.121	1.101	1.201	1.521	1.351	1.521	1.401
	T at flow meter	℃	21.600	21.2	21.8	21.9	36.1	34.1	33.9	33.600	50.000	46.500	47.400	46.000
	Cs	℃	9.10	9.30	11.30	12.60	12.20	9.70	11.30	11.70	14.60	13.60	10.20	13.70
	Cd	℃	na	na	na	na	na	na	na	na	na	na	na	na
Calculation value	saturated point temp	℃	31.85	30.25	31.80	35.68	47.02	40.38	39.75	42.59	53.11	48.72	52.80	46.61
	subcool amount	℃	10.22	9.03	10.08	13.97	11.38	7.70	7.55	10.68	2.91	2.24	6.91	0.62
	Enthalpy at entering exp valve (h)	kJ/kg	229.78	229.2	229.91	229.9	249.91	245.6	244.9	244.48	271.9	266.18	265.23	265.45
	T leaving exp valve (calculation value)	℃	-12.32	-10.6	-9.34	-9.22	-9.47	-13.01	-13.01	-14.42	-8.61	-11.92	-11.12	-13.43
	Quality (x)	**kg/kg**	**0.2222**	**0.2098**	**0.2061**	**0.2053**	**0.3041**	**0.3021**	**0.2987**	**0.3041**	**0.4067**	**0.3955**	**0.3870**	**0.3995**
	Density	kg/m^3	1220.51	1221.87	1220.16	1223.73	1167.3	1178.25	1180.11	1181.82	1102.44	1119.11	1123.28	1120.82
	Mass flow	**kg/h**	**4.16**	**5.21**	**6.44**	**8.54**	**8.36**	**6.38**	**5.22**	**4.12**	**6.35**	**5.12**	**8.53**	**4.24**
	Gas Specific Volume (header)	m^3/kg	1.087E-01	1.018E-01	9.709E-02	9.664E-02	9.754E-02	1.116E-01	1.116E-01	1.179E-01	9.450E-02	1.070E-01	1.038E-01	1.134E-01
	Gas Density (header)	kg/m^3	9.2013	9.8222	10.2996	10.3473	10.2519	8.9614	8.9614	8.4825	10.5823	9.3440	9.6311	8.8183
	Gas superficial velocity (header)	m/s	0.07	0.08	0.09	0.12	0.17	0.15	0.12	0.10	0.17	0.15	0.24	0.13
	Liquid Specific Volume (header)	m^3/kg	7.494E-04	7.524E-04	7.547E-04	7.549E-04	7.545E-04	7.482E-04	7.482E-04	7.457E-04	7.560E-04	7.501E-04	7.515E-04	7.474E-04
	Liquid Density (header)	kg/m^3	1334.45	1329.04	1325.05	1324.64	1325.43	1336.61	1336.61	1341.04	1322.70	1333.17	1330.67	1337.92
	Liquid superficial velocity (header)	m/s	0.0017	0.0022	0.0027	0.0036	0.0030	0.0023	0.0019	0.0015	0.0020	0.0016	0.0027	0.0013
	Pressure drop (Pleaving -Ps)	mPa	0.00	0.01	0.00	0.01	0.01	0.01	(0.00)	(0.00)	0.02	0.01	0.01	(0.01)

Folder: 6 evp vis/10 flow recogition

Channel orientation	Downward	Intrusion height h	0mm
Inlet pipe diameter	2.0mm	Branch quantity	22

1atm = 0.101325 mPa
1mPa = 10.197162 kgf/cm2

	Test date		131(2010/08/20)	132(2010/08/23)	133(2010/08/25)	134	135	136(2010/08/26)	137	138(2010/09/01)	139	140(2010/09/03)	141	142
Parameter	evp out flow direction		←	←	←	←	←	←	←	←	←	←	←	←
	R134a amount	g	400	←	405(Recharge)	←	←	←	460	460-α	460-β	510-α	←	←
	comp Rev	rpm	4000	3000	2300	2000	3800	2850	1650	4300	1850	2650	1650	3350
	Exp Valve opening value	pulse	91	71	59	52	74	54	65	78	47	74	59	89
	water flow	ml/min	150	100	130	←	75	50	550	15	5	300	300	300
	outdoor fan speed	V	4.4	4.44	4.18	←	4.19	4.11	7.57	4.23	4.21	8.23	9.09	←
		A	0.06	0.07	0.04	←	0.05	0.04	0.12	0.06	0.04	0.13	0.14	←
	remark		in4, out2 layer	←	←	←	←	←	←	←	←	←	←	←
Testing data	flow rate	ml/min	122.18	89.85	74.73	58.13	94.78	76.45	72.27	128.22	62.15	86.63	56.87	116.75
	P entering Exp valve	mPaG	0.980	0.886	0.959	0.897	1.159	1.280	0.686	1.316	1.335	0.654	0.623	0.745
	P absolute	mPa	1.081	0.987	1.060	0.998	1.260	1.381	0.787	1.417	1.436	0.755	0.724	0.846
	P leaving exp valve	mPaG	0.105	0.093	0.087	0.067	0.09	0.069	0.12	0.109	0.084	0.087	0.085	0.107
	P absolute	mPa	0.206	0.194	0.188	0.168	0.191	0.170	0.221	0.210	0.185	0.188	0.186	0.208
	T entering Exp valve	°C	36.247	34.314	35.230	32.737	45.648	42.613	26.464	48.143	49.357	21.200	23.710	23.137
	T leaving exp valve	°C	-8.600	-10.236	-11.076	-11.982	-10.442	-13.812	-6.651	-8.048	-10.390	-11.218	-9.276	-8.438
	Ps	mPaG	0.08	0.08	0.08	0.07	0.07	0.06	0.12	0.09	0.08	0.08	0.09	0.10
		mPa	0.181	0.181	0.181	0.171	0.171	0.161	0.221	0.191	0.181	0.181	0.191	0.201
	Pd	mPaG	1.08	1.00	1.05	1.00	1.25	1.38	0.78	1.42	1.40	0.72	0.70	0.85
		mPa	1.181	1.101	1.151	1.101	1.351	1.481	0.881	1.521	1.501	0.821	0.801	0.951
	T at flow meter	°C	36.4	35.1	36.6	33.7	45.8	44.8	27.000	49.000	50.600	20.900	23.000	22.900
	Cs	°C	15.20	14.90	14.50	13.20	14.00	11.30	9.70	16.70	13.10	14.40	11.60	15.20
	Cd	°C	77.70	69.00	63.50	60.20	79.40	70.80	48.80	86.20	60.70	55.40	50.20	67.60
Calculation value	saturated point temp	°C	42.31	38.90	41.57	39.31	48.22	51.87	30.75	52.91	53.45	29.30	27.86	33.30
	subcool amount	°C	6.06	4.59	6.34	6.57	2.57	9.26	4.29	4.77	4.09	8.10	4.15	10.16
	Enthalpy at entering exp valve (h)	kJ/kg	250.82	247.99	249.33	245.68	264.9	260.26	236.64	268.69	270.57	229.17	232.71	231.91
	T leaving exp valve (calculation value)	°C	-9.34	-10.86	-11.65	-14.42	-11.25	-14.14	-7.54	-8.85	-12.05	-11.65	-11.92	-9.1
	Quality (x)	**kg/kg**	**0.3078**	**0.3022**	**0.3129**	**0.3099**	**0.3860**	**0.3782**	**0.2287**	**0.3923**	**0.4174**	**0.2155**	**0.2341**	**0.2144**
	Density	kg/m^3	1163.66	1171.15	1167.82	1177.81	1122.95	1138.11	1201.72	1112.53	1106.78	1221.83	1212.07	1214.99
	Mass flow	**kg/h**	**8.53**	**6.31**	**5.24**	**4.11**	**6.39**	**5.22**	**5.21**	**8.56**	**4.13**	**6.35**	**4.14**	**8.51**
	Gas Specific Volume (header)	m^3/kg	9.709E-02	1.028E-01	1.059E-01	1.179E-01	1.044E-01	1.166E-01	9.079E-02	9.533E-02	1.076E-01	1.059E-01	1.070E-01	9.620E-02
	Gas Density (header)	kg/m^3	10.2996	9.7238	9.4402	8.4825	9.5831	8.5785	11.0147	10.4903	9.2963	9.4402	9.3440	10.3950
	Gas superficial velocity (header)	m/s	0.18	0.14	0.12	0.10	0.18	0.16	0.08	0.22	0.13	0.10	0.07	0.12
	(Inlet pipe Ø2mm)	m/s	22.54	17.35	15.35	13.27	22.74	20.35	9.57	28.30	16.38	12.82	9.16	15.52
	Liquid Specific Volume (header)	m^3/kg	7.547E-04	7.520E-04	7.506E-04	7.457E-04	7.513E-04	7.462E-04	7.580E-04	7.556E-04	7.499E-04	7.506E-04	7.501E-04	7.551E-04
	Liquid Density (header)	kg/m^3	1325.05	1329.86	1332.34	1341.04	1331.10	1340.14	1319.28	1323.49	1333.60	1332.34	1333.17	1324.26
	Liquid superficial velocity (header)	m/s	0.0031	0.0023	0.0019	0.0015	0.0020	0.0017	0.0021	0.0027	0.0013	0.0026	0.0017	0.0035
	(Inlet pipe Ø2mm)	m/s	0.3940	0.2929	0.2388	0.1869	0.2605	0.2142	0.2694	0.3475	0.1594	0.3306	0.2101	0.4464
	Pressure drop (Pleaving -Ps)	mPa	0.03	0.01	0.01	(0.00)	0.02	0.01	0.00	0.02	0.00	0.01	(0.00)	0.01

Folder: 7 evp vis/11 flow recogition

1atm = 0.101325 mPa
1mPa = 10.197162 kgf/cm2

	Channel orientation		Downward		Intrusion height h	0mm								
	Inlet pipe diameter		1.0mm		Branch quantity	22								
	Test date		150(2010/09/14)	151	152(2010/09/15)	153(2010/09/17)	154(2010/09/24)	155	156(2010/09/27)	157	158(2010/09/28)	159		
Parameter	evp out flow direction		Reverse	←	←	←	←	←	←	←	←	←		
	R134a amount	g	380	←	400	400-α	**350**(recharge)	←	←	←	←	←		
	comp Rev	rpm	3000	2300	3400	3450	2300	2800	3400	4400	4400	4200		
	Exp Valve opening value	pulse	64	55	69	95	45	51	66	80	70	48		
	water flow	ml/min	230	←	65	140	60	←	75	100	35	15		
	water bath temperature	°C	13	14.2	13	13	26	←	←	←	30	←		
	outdoor fan speed	V	5.08	4.72	4.79	6.58	4.14	←	4.15	4.13	4.13	4.11		
		A	0.08	0.07	0.07	0.1	0.04	←	0.04	0.04	0.04	0.04		
	remark		in4, out2 layer	←	←	←	←	←	←	←	←	←		
Testing data	flow rate	ml/min	70.16	57.07	87.41	116.4	59.9	73.44	90.33	125.86	77.49	65.21		
	P entering Exp valve	mPaG	0.594	0.583	0.802	0.712	1.036	1.096	1.129	1.223	1.320	1.334		
	P absolute	mPa	0.695	0.684	0.903	0.813	1.137	1.197	1.230	1.324	1.421	1.435		
	P leaving exp valve	mPaG	0.097	0.084	0.134	0.199	0.104	0.132	0.169	0.25	0.218	0.157		
	P absolute	mPa	0.198	0.185	0.235	0.300	0.205	0.233	0.270	0.351	0.319	0.258		
	T entering Exp valve	°C	19.079	20.718	22.936	29.776	34.422	38.586	39.608	43.406	50.490	46.696		
	T leaving exp valve	°C	-9.532	-11.216	-5.267	1.264	-8.847	-5.068	-1.314	5.963	3.031	-2.614		
	Ps	mPaG	0.05	0.05	0.05	0.08	0.05	0.05	0.05	0.08	0.05	0.01		
		mPa	0.151	0.151	0.151	0.181	0.151	0.151	0.151	0.181	0.151	0.111		
	Pd	mPaG	0.68	0.65	0.85	0.80	1.10	1.18	1.20	1.32	1.40	1.40		
		mPa	0.781	0.751	0.951	0.901	1.201	1.281	1.301	1.421	1.501	1.501		
	T at flow meter	°C	18.500	19.8	23.0	30.2	36.8	40.0	40.9	44.600	49.200	49.600		
	Cs	°C	11.60	14.20	10.20	13.20	12.80	13.10	11.30	13.00	8.10	6.20		
	Cd	°C	60.10	54.80	65.40	66.60	59.90	65.80	67.70	82.10	80.20	71.80		
Calculation value	saturated point temp	°C	26.46	25.92	35.64	31.89	44.23	46.22	47.28	50.19	53.03	53.43		
	subcool amount	°C	7.38	5.20	12.70	2.11	9.81	7.63	7.67	6.78	2.54	6.73		
	Enthalpy at entering exp valve (h)	kJ/kg	226.19	228.49	231.63	241.4	248.14	254.27	255.78	261.47	272.35	266.46		
	T leaving exp valve (calculation value)	°C	-10.35	-12.05	-5.94	0.66	-9.47	-6.16	-2.23	5.1	2.37	-3.46		
	Quality (x)	**kg/kg**	**0.1937**	**0.2145**	**0.1948**	**0.2045**	**0.2955**	**0.3076**	**0.2935**	**0.2804**	**0.3514**	**0.3533**		
	Density	kg/m^3	1229.46	1223.25	1216.08	1188.66	1171.79	1154.46	1150.25	1133.99	1100.97	1119.67		
	Mass flow	**kg/h**	**5.18**	**4.19**	**6.38**	**8.30**	**4.21**	**5.09**	**6.23**	**8.56**	**5.12**	**4.38**		
	Gas Specific Volume (header)	m^3/kg	1.008E-01	1.076E-01	8.561E-02	6.770E-02	9.754E-02	8.631E-02	7.493E-02	5.815E-02	6.380E-02	7.828E-02		
	Gas Density (header)	kg/m^3	9.9177	9.2963	11.6813	14.7715	10.2519	11.5860	13.3458	17.1960	15.6742	12.7753		
	Gas superficial velocity (header)	m/s	0.07	0.07	0.07	0.08	0.08	0.09	0.10	0.10	0.08	0.08		
	(Inlet pipe Ø1mm)	m/s	35.75	34.18	37.62	40.65	42.93	47.77	48.49	49.39	40.59	42.85		
	Liquid Specific Volume (header)	m^3/kg	7.529E-04	7.499E-04	7.610E-04	7.736E-04	7.545E-04	7.605E-04	7.680E-04	7.826E-04	7.771E-04	7.656E-04		
	Liquid Density (header)	kg/m^3	1328.23	1333.60	1314.15	1292.61	1325.43	1314.86	1302.12	1277.74	1286.90	1306.11		
	Liquid superficial velocity (header)	m/s	0.0022	0.0017	0.0027	0.0035	0.0016	0.0019	0.0023	0.0033	0.0018	0.0015		
	(Inlet pipe Ø1mm)	m/s	1.1112	0.8726	1.3821	1.8069	0.7917	0.9474	1.1963	1.7057	0.9125	0.7672		
	Pressure drop (Pleaving -Ps)	mPa	0.05	0.03	0.08	0.12	0.05	0.08	0.12	0.17	0.17	0.15		

Folder: 9 evp vis/12 flow recogition

1atm = 0.101325 mPa
1mPa = 10.197162 kgf/cm2

	Channel orientation		Downward		Intrusion height h	0mm								
	Inlet pipe diameter		3.0mm		Branch quantity	22								
	Test date		170 (2010/11/12)	171	172 (restart	173	174 (2010/11/15)	175	176	177	178 (2010/11/17)	179	180	181
Parameter	evp out flow direction		Reverse	←	←	←	←	←	←	←	←	←	←	←
	R134a amount	g	370	←	←	←	←	←	←	←	←	←	←	←
	comp Rev	rpm	2400	3400	2100	1700	4000	3000	2200	1800	2600	2550	3500	3300
	Exp Valve opening value	pulse	83	95	69	56	82	63	54	47	50	44	74	60
	water flow	ml/min	510	315	250	150	110	75	70	60	40	20	75	55
	water bath temperature	°C	14	←	←	←	27	←	←	←	41.8	41.9	40.3	39.3
	outdoor fan speed	V	5.48	4.92	4.98	4.35	4.27	4.2	4.15	←	4.11	4.1	4.15	4.13
		A	0.08	0.07	0.08	0.06	0.06	0.05	0.04	←	0.04	0.04	0.05	0.04
	remark		in4, out2 layer	←	←	←	←	←	←	←	←	←	←	←
Testing data	flow rate	ml/min	87.21	116.26	69.56	55.63	120.13	89.3	73.48	60.02	74.77	57.41	126.88	94.24
	P entering Exp valve	mPaG	0.547	0.673	0.563	0.615	1.031	1.045	1.080	1.025	1.294	1.350	1.337	1.321
	P absolute	mPa	0.648	0.774	0.664	0.716	1.132	1.146	1.181	1.126	1.395	1.451	1.438	1.422
	P leaving exp valve	mPaG	0.093	0.1	0.075	0.077	0.095	0.079	0.09	0.087	0.07	0.041	0.109	0.08
	P absolute	mPa	0.194	0.201	0.176	0.178	0.196	0.180	0.191	0.188	0.171	0.142	0.210	0.181
	T entering Exp valve	°C	18.441	19.851	18.017	19.750	35.472	34.873	34.880	33.366	42.013	38.229	46.470	42.886
	T leaving exp valve	°C	-10.191	-9.086	-12.811	-11.994	-9.840	-11.847	-10.403	-10.798	-13.149	-17.462	-7.982	-11.655
	Ps	mPaG	0.10	0.09	0.08	0.08	0.08	0.07	0.09	0.09	0.07	0.04	0.10	0.07
		mPa	0.201	0.191	0.181	0.181	0.181	0.171	0.191	0.191	0.171	0.141	0.201	0.171
	Pd	mPaG	0.62	0.78	0.63	0.68	1.24	1.15	1.18	1.11	1.38	1.44	1.42	1.40
		mPa	0.721	0.881	0.731	0.781	1.341	1.251	1.281	1.211	1.481	1.541	1.521	1.501
	T at flow meter	°C	18.700	19.6	18.4	19.6	35.8	36.0	36.3	35.100	44.200	41.600	47.600	39.300
	Cs	°C	14.30	15.60	9.30	9.90	12.50	12.20	13.20	13.10	11.40	10.90	14.00	12.40
	Cd	°C	51.70	65.70	45.50	47.60	75.50	69.10	63.20	58.30	68.50	63.40	78.40	76.50
Calculation value	saturated point temp	°C	24.11	30.16	24.92	27.48	44.06	44.53	45.70	43.86	52.28	53.88	53.51	53.06
	subcool amount	°C	5.67	10.31	6.90	7.73	8.59	9.66	10.82	10.49	10.27	15.65	7.04	10.17
	Enthalpy at entering exp valve (h	kJ/kg	225.29	227.28	224.7	227.13	249.68	248.76	248.8	246.59	259.35	253.7	266.11	260.66
	T leaving exp valve (calculation value)	°C	-10.86	-9.97	-13.29	-13.01	-10.6	-12.73	-11.25	-11.65	-13.99	-18.45	-8.85	-12.59
	Quality (x)	**kg/kg**	**0.1923**	**0.1969**	**0.2032**	**0.2133**	**0.3090**	**0.3158**	**0.3082**	**0.2996**	**0.3731**	**0.3684**	**0.3797**	**0.3723**
	Density	kg/m^3	1231.58	1227	1233.23	1227.07	1167.34	1170.07	1170.19	1176.11	1140.94	1158.02	1120.77	1137.24
	Mass flow	**kg/h**	**6.44**	**8.56**	**5.15**	**4.10**	**8.41**	**6.27**	**5.16**	**4.24**	**5.12**	**3.99**	**8.53**	**6.43**
	Gas Specific Volume (header)	m^3/kg	1.028E-01	9.939E-02	1.128E-01	1.116E-01	1.018E-01	1.104E-01	1.044E-01	1.059E-01	1.159E-01	1.383E-01	9.533E-02	1.098E-01
	Gas Density (header)	kg/m^3	9.7267	10.0610	8.8660	8.9614	9.8222	9.0572	9.5831	9.4402	8.6266	7.2322	10.4903	9.1050
	Gas superficial velocity (header)	m/s	0.09	0.12	0.08	0.07	0.18	0.15	0.12	0.09	0.15	0.14	0.21	0.18
	(Inlet pipe Ø3mm)	m/s	5.01	6.58	4.64	3.83	10.40	8.59	6.52	5.28	8.70	7.98	12.14	10.33
	Liquid Specific Volume (header)	m^3/kg	7.520E-04	7.536E-04	7.477E-04	7.482E-04	7.524E-04	7.487E-04	7.513E-04	7.506E-04	7.464E-04	7.388E-04	7.556E-04	7.489E-04
	Liquid Density (header)	kg/m^3	1329.86	1327.02	1337.47	1336.61	1329.04	1335.74	1331.10	1332.34	1339.69	1353.49	1323.49	1335.31
	Liquid superficial velocity (header)	m/s	0.0027	0.0036	0.0021	0.0017	0.0030	0.0022	0.0019	0.0015	0.0017	0.0013	0.0028	0.0021
	(Inlet pipe Ø3mm)	m/s	0.1538	0.2036	0.1205	0.0947	0.1719	0.1262	0.1054	0.0875	0.0941	0.0731	0.1571	0.1188
	Pressure drop (Pleaving -Ps)	mPa	(0.01)	0.01	(0.01)	(0.00)	0.02	0.01	0.00	(0.00)	0.00	0.00	0.01	0.01

Folder: 11 evp vis/14 flow recogition

1atm = 0.101325 mPa
1mPa = 10.197162 kgf/cm2

	Channel orientation		Upward		Intrusion height h	0mm								
	Inlet pipe diameter		2.0mm		Branch quantity	22								
	Test date		210(2010/11/29)	211	212	213	214(2010/11/30)	215	216	217	218(2010/11/30)	219	220	221
Parameter	evp out flow direction		Reverse	←	←	←	←	←	←	←	←	←	←	←
	R134a amount	g	450	←	←	←	←	←	←	←	←	480	←	480-α
	comp Rev	rpm	3700	2800	2200	1800	4200	3400	2800	2200	4000	3600	3050	2800
	Exp Valve opening value	pulse	111	81	74	64	94	71	59	50	100	60	52	46
	water flow	ml/min	590	470	390	380	280	200	130	110	200	20	0	0
	water bath temperature	°C	14	←	←	←	25.9	27.4	29.1	30	40.3	45	45	45
	outdoor fan speed	V	4.21	4.21	←	←	4.24	4.17	←	4.16	4.15	4.14	4.11	4.1
		A	0.04	0.04	0.03	←	0.04	0.04	←	0.03	0.04	0.04	0.04	0.04
	remark		in4, out2 layer	←	←	←	←	←	←	←	←	←	←	←
Testing data	flow rate	ml/min	116.68	84.79	70.57	55.64	121.45	91.44	73.1	58.44	130.42	91.22	75.72	58.35
	P entering Exp valve	mPaG	0.551	0.529	0.525	0.497	0.815	0.886	0.903	0.889	1.260	1.306	1.335	1.344
	P absolute	mPa	0.652	0.630	0.626	0.598	0.916	0.987	1.004	0.990	1.361	1.407	1.436	1.445
	P leaving exp valve	mPaG	0.087	0.074	0.078	0.072	0.087	0.068	0.055	0.051	0.149	0.071	0.06	0.039
	P absolute	mPa	0.188	0.175	0.179	0.173	0.188	0.169	0.156	0.152	0.250	0.172	0.161	0.140
	T entering Exp valve	°C	17.327	17.165	17.822	17.790	30.826	31.141	32.432	31.873	48.251	41.883	39.492	39.703
	T leaving exp valve	°C	-11.059	-12.822	-12.170	-12.110	-11.196	-13.658	-15.576	-15.720	-3.900	-13.007	-14.587	-17.622
	Ps	mPaG	0.08	0.07	0.08	0.08	0.08	0.06	0.05	0.05	0.12	0.06	0.05	0.04
		mPa	0.181	0.171	0.181	0.181	0.181	0.161	0.151	0.151	0.221	0.161	0.151	0.141
	Pd	mPaG	0.65	0.62	0.60	0.58	0.92	0.98	1.00	0.98	1.33	1.40	1.42	1.44
		mPa	0.751	0.721	0.701	0.681	1.021	1.081	1.101	1.081	1.431	1.501	1.521	1.541
	T at flow meter	°C	18.000	17.4	17.9	17.6	31.8	32.3	34.4	34.900	40.300	43.800	42.100	44.400
	Cs	°C	9.90	10.00	11.00	11.00	9.70	8.70	8.80	9.20	11.70	10.30	10.00	10.00
	Cd	°C	58.90	54.20	50.30	46.80	69.90	66.80	61.80	55.10	74.70	75.00	70.00	64.10
Calculation value	saturated point temp	°C	24.31	23.17	22.96	21.45	36.16	38.90	39.53	39.01	51.29	52.63	53.45	53.71
	subcool amount	°C	6.98	6.01	5.14	3.66	5.33	7.76	7.10	7.14	3.04	10.75	13.96	14.01
	Enthalpy at entering exp valve (h)	kJ/kg	223.74	223.51	224.42	224.38	242.91	243.37	245.24	244.43	268.88	259.16	255.58	255.89
	T leaving exp valve (calculation value)	°C	-11.65	-13.43	-12.87	-13.71	-11.65	-14.28	-16.22	-16.84	-4.3	-13.85	-15.46	-18.78
	Quality (x)	**kg/kg**	**0.1893**	**0.1983**	**0.1995**	**0.2040**	**0.2819**	**0.2981**	**0.3171**	**0.3164**	**0.3698**	**0.3715**	**0.3624**	**0.3804**
	Density	kg/m^3	1235.72	1236.2	1233.75	1233.72	1185.09	1184.29	1179.11	1181.31	1111.43	1141.63	1152.44	1151.59
	Mass flow	**kg/h**	**8.65**	**6.29**	**5.22**	**4.12**	**8.64**	**6.50**	**5.17**	**4.14**	**8.70**	**6.25**	**5.24**	**4.03**
	Gas Specific Volume (header)	m^3/kg	1.059E-01	1.134E-01	1.110E-01	1.147E-01	1.059E-01	1.172E-01	1.265E-01	1.296E-01	8.068E-02	1.153E-01	1.228E-01	1.401E-01
	Gas Density (header)	kg/m^3	9.4402	8.8183	9.0098	8.7222	9.4402	8.5302	7.9064	7.7143	12.3948	8.6745	8.1466	7.1362
	Gas superficial velocity (header)	m/s	0.12	0.10	0.08	0.07	0.18	0.16	0.14	0.12	0.18	0.19	0.16	0.15
	(Inlet pipe Ø2mm)	m/s	15.34	12.50	10.23	8.52	22.80	20.08	18.34	15.02	22.94	23.66	20.59	19.00
	Liquid Specific Volume (header)	m^3/kg	7.506E-04	7.474E-04	7.484E-04	7.469E-04	7.506E-04	7.459E-04	7.426E-04	7.416E-04	7.640E-04	7.467E-04	7.439E-04	7.383E-04
	Liquid Density (header)	kg/m^3	1332.34	1337.92	1336.17	1338.80	1332.34	1340.59	1346.60	1348.53	1308.85	1339.24	1344.25	1354.52
	Liquid superficial velocity (header)	m/s	0.0037	0.0026	0.0022	0.0017	0.0032	0.0024	0.0018	0.0015	0.0029	0.0020	0.0017	0.0013
	(Inlet pipe Ø2mm)	m/s	0.4654	0.3332	0.2767	0.2165	0.4115	0.3008	0.2319	0.1857	0.3703	0.2593	0.2196	0.1631
	Pressure drop (Pleaving -Ps)	mPa	0.01	0.00	(0.00)	(0.01)	0.01	0.01	0.01	0.00	0.03	0.01	0.01	(0.00)

Folder: 16 evp vis/19 flow recogition

Channel orientation	Downward	Intrusion height h	0mm
Inlet pipe diameter	1.5mm	Branch quantity	22

1atm = 0.101325 mPa
1mPa = 10.197162 kgf/cm2

	Test date		310(2011/05/20)	311	312	313	314(2011/05/23)	315	316(2011/05/24)	317	318	319(2011/05/25)	320	321(2011/05/26)
Parameter	evp out flow direction		Reverse	←	←	←	←	←	←	←	←	←	←	←
	R134a amount	g	330	←	←	←	355	355-α	←	←	←	←	←	360
	comp Rev	rpm	3400	2700	2400	1850	3800	3000	2400	2000	4200	3900	3100	2600
	Exp Valve opening value	pulse	104	80	68	55	92	70	65	52	74	60	49	44
	water flow	ml/min	395	295	285	←	220	175	180	160	125	145	190	65
	water bath temperature act/set	°C	13.6/6.7	13.3/6.7	12.7/6.7	12.4/6.7	32.4/35.0	33.8/35	34.8/35	34.8/35	47/47	47/47	47/47	47/47
	outdoor fan speed	V	5.13	4.24	4.22	4.21	4.3	4.17	4.17	←	4.11	4.16	4.16	4.13
		A	0.07	0.04	0.04	0.04	0.06	0.04	0.04	←	0.04	0.04	0.04	0.04
	remark		in4, out2 layer	←	←	←	←	←	←	←	←	←	←	←
Testing data	flow rate	ml/min	115.07	87.2	69.42	54.95	119.98	89.08	74.48	57.09	127.05	91.49	74.63	59.44
	P entering Exp valve	mPaG	0.585	0.616	0.575	0.527	0.948	1.007	0.972	0.884	1.368	1.441	1.256	1.154
	P absolute	mPa	0.686	0.717	0.676	0.628	1.049	1.108	1.073	0.985	1.469	1.542	1.357	1.255
	P leaving exp valve	mPaG	0.106	0.085	0.065	0.063	0.114	0.087	0.078	0.059	0.101	0.081	0.055	0.039
	P absolute	mPa	0.207	0.186	0.166	0.164	0.215	0.188	0.179	0.160	0.202	0.182	0.156	0.140
	T entering Exp valve	°C	23.447	20.501	19.151	19.018	34.920	34.018	31.424	30.803	45.899	45.393	40.763	38.364
	T leaving exp valve	°C	-8.584	-11.184	-13.855	-14.228	-7.622	-11.044	-12.830	-14.952	-9.124	-11.745	-15.380	-18.019
	Ps	mPaG	0.09	0.08	0.07	0.07	0.08	0.08	0.07	0.06	0.07	0.05	0.04	0.03
		mPa	0.191	0.181	0.171	0.171	0.181	0.181	0.171	0.161	0.171	0.151	0.141	0.131
	Pd	mPaG	0.59	0.70	0.65	0.60	1.06	1.10	1.08	0.98	1.46	1.52	1.35	1.20
		mPa	0.691	0.801	0.751	0.701	1.161	1.201	1.181	1.081	1.561	1.621	1.451	1.301
	T at flow meter	°C	23.600	20.8	18.8	18.3	35.5	35.1	33.1	32.9	47.2	47.1	44.3	(36.6)
	Cs	°C	13.00	11.70	10.60	10.80	13.50	11.80	8.90	9.00	11.40	7.10	6.00	(9.5)
	Cd	°C	62.90	58.60	54.60	50.10	73.20	68.00	50.40	53.50	81.00	74.70	67.00	(56)
Calculation value	saturated point temp	°C	26.02	27.52	25.52	23.06	41.17	43.24	42.03	38.82	54.38	56.38	51.17	48.07
	subcool amount	°C	2.57	7.02	6.37	4.04	6.25	9.22	10.61	8.02	8.48	10.99	10.41	9.71
	Enthalpy at entering exp valve (h	kJ/kg	232.34	228.18	226.29	226.1	248.87	247.55	243.77	242.88	265.23	264.43	257.49	253.93
	T leaving exp valve (calculation value)	°C	-9.22	-11.92	-14.72	-15.01	-8.25	-11.65	-12.87	-15.61	-9.84	-12.46	-16.22	-18.78
	Quality (x)	**kg/kg**	**0.2172**	**0.2122**	**0.2187**	**0.2195**	**0.2924**	**0.3043**	**0.2925**	**0.3027**	**0.3831**	**0.3898**	**0.3753**	**0.3711**
	Density	kg/m^3	1212.86	1224.25	1229.09	1229.32	1169.05	1173.27	1183.72	1185.65	1123.76	1126.81	1146.2	1155.89
	Mass flow	**kg/h**	**8.37**	**6.41**	**5.12**	**4.05**	**8.42**	**6.27**	**5.29**	**4.06**	**8.57**	**6.19**	**5.13**	**4.12**
	Gas Specific Volume (header)	m^3/kg	9.664E-02	1.070E-01	1.192E-01	1.206E-01	9.321E-02	1.059E-01	1.110E-01	1.235E-01	9.893E-02	1.093E-01	1.265E-01	1.401E-01
	Gas Density (header)	kg/m^3	10.3473	9.3440	8.3864	8.2905	10.7287	9.4402	9.0098	8.0985	10.1087	9.1533	7.9064	7.1362
	Gas superficial velocity (header)	m/s	0.12	0.10	0.09	0.07	0.16	0.14	0.12	0.11	0.23	0.18	0.17	0.15
	(Inlet pipe Ø1.5mm)	m/s	27.63	22.87	20.99	16.87	36.05	31.77	26.99	23.86	51.03	41.41	38.30	33.70
	Liquid Specific Volume (header)	m^3/kg	7.549E-04	7.501E-04	7.452E-04	7.447E-04	7.567E-04	7.506E-04	7.484E-04	7.437E-04	7.538E-04	7.491E-04	7.426E-04	7.383E-04
	Liquid Density (header)	kg/m^3	1324.64	1333.17	1341.94	1342.86	1321.55	1332.34	1336.17	1344.72	1326.63	1334.88	1346.60	1354.52
	Liquid superficial velocity (header)	m/s	0.0034	0.0026	0.0021	0.0016	0.0031	0.0023	0.0019	0.0015	0.0028	0.0020	0.0017	0.0013
	(Inlet pipe Ø1.5mm)	m/s	0.7779	0.5950	0.4685	0.3703	0.7083	0.5147	0.4403	0.3310	0.6262	0.4445	0.3743	0.3009
	Pressure drop (Pleaving -Ps)	mPa	0.02	0.01	(0.01)	(0.01)	0.03	0.01	0.01	(0.00)	0.03	0.03	0.02	0.01

Folder: 17 evp vis/20 flow recogition

Channel orientation	Downward	Intrusion height h	3mm
Inlet pipe diameter	1.5mm	Branch quantity	22

1atm = 0.101325 mPa
1mPa = 10.197162 kgf/cm2

	Test date		330(2011/06/08)	331	332	333	334(2011/06/09)	335	336	337	338	339	340(2011/06/10)	341
Parameter	evp out flow direction		Reverse	←	←	←	←	←	←	←	←	←	←	←
	R134a amount	g	325	←	←	←	345	←	←	←	←	←	345-α	←
	comp Rev	rpm	3400	2700	2400	1850	4000	3100	2400	2000	4200	3800	3100	2600
	Exp Valve opening value	pulse	116	86	74	64	92	75	64	52	75	67	53	46
	water flow	ml/min	420	290	285	←	275	←	200	←	120	110	70	90
	water bath temperature act/set	°C	6.6/6.0	9.2/6.0	11.2/6.0	11.7/6.0	33.6/35.0	32.9/35.0	32.5/35.0	33.5/35.0	47.0/47.0	←	←	←
	outdoor fan speed	V	4.77	4.24	4.2	4.18	4.23	4.19	4.17	←	4.12	4.09	4.13	4.16
		A	0.07	0.04	0.04	0.04	0.05	0.04	0.04	←	0.04	0.04	0.04	0.04
	remark		in4, out2 layer	←	←	←	←	←	←	←	←	←	←	←
Testing data	flow rate	ml/min	113.66	89.33	69.71	54.58	126.84	91.07	73.57	57.82	121.98	95.12	74.01	60.97
	P entering Exp valve	mPaG	0.474	0.540	0.525	0.493	0.953	0.910	0.894	0.854	1.302	1.370	1.421	1.214
	P absolute	mPa	0.575	0.641	0.626	0.594	1.054	1.011	0.995	0.955	1.403	1.471	1.522	1.315
	P leaving exp valve	mPaG	0.098	0.087	0.065	0.061	0.109	0.085	0.078	0.06	0.103	0.091	0.069	0.041
	P absolute	mPa	0.199	0.188	0.166	0.162	0.210	0.186	0.179	0.161	0.204	0.192	0.170	0.142
	T entering Exp valve	°C	18.912	22.044	20.927	20.874	36.360	32.751	31.469	30.122	46.201	43.343	43.811	40.710
	T leaving exp valve	°C	-9.617	-11.162	-14.112	-14.636	-8.599	-11.517	-12.369	-14.766	-8.811	-10.570	-13.656	-17.588
	Ps	mPaG	0.08	0.08	0.06	0.06	0.08	0.07	0.08	0.06	0.06	0.06	0.05	0.04
		mPa	0.181	0.181	0.161	0.161	0.181	0.171	0.181	0.161	0.161	0.161	0.151	0.141
	Pd	mPaG	0.58	0.62	0.60	0.58	1.05	1.00	0.98	0.98	1.38	1.45	1.52	1.28
		mPa	0.681	0.721	0.701	0.681	1.151	1.101	1.081	1.081	1.481	1.551	1.621	1.381
	T at flow meter	°C	20.100	22.3	21.6	21.0	37.4	34.0	32.7	32.0	47.5	45.1	48.2	45.4
	Cs	°C	12.60	12.50	11.60	11.70	11.50	10.50	10.40	9.70	11.00	12.20	6.80	13.50
	Cd	°C	57.40	55.70	53.20	49.40	69.70	67.10	61.20	54.80	77.70	76.40	64.10	55.30
Calculation value	saturated point temp	°C	20.18	23.74	22.96	21.23	41.35	39.79	39.20	37.68	52.51	54.44	55.84	49.91
	subcool amount	°C	1.27	1.70	2.03	0.36	4.99	7.04	7.73	7.56	6.31	11.10	12.03	9.20
	Enthalpy at entering exp valve (h	kJ/kg	225.94	230.35	228.78	228.7	250.99	245.7	243.84	241.89	265.71	261.34	262.04	257.42
	T leaving exp valve (calculation value)	°C	-10.22	-11.65	-14.72	-15.31	-8.85	-11.92	-12.87	-15.46	-9.59	-11.12	-14.14	-18.45
	Quality (x)	**kg/kg**	**0.1918**	**0.2212**	**0.2306**	**0.2335**	**0.3030**	**0.2968**	**0.2929**	**0.2972**	**0.3816**	**0.3682**	**0.3867**	**0.3860**
	Density	kg/m^3	1229.43	1217.98	1222.14	1222.16	1162.96	1177.84	1183	1188.21	1121.71	1135.59	1133.92	1146.08
	Mass flow	**kg/h**	**8.38**	**6.53**	**5.11**	**4.00**	**8.85**	**6.44**	**5.22**	**4.12**	**8.21**	**6.48**	**5.04**	**4.19**
	Gas Specific Volume (header)	m^3/kg	1.004E-01	1.059E-01	1.192E-01	1.220E-01	9.533E-02	1.070E-01	1.110E-01	1.228E-01	9.800E-02	1.038E-01	1.166E-01	1.383E-01
	Gas Density (header)	kg/m^3	9.9651	9.4402	8.3864	8.1947	10.4903	9.3440	9.0098	8.1466	10.2042	9.6311	8.5785	7.2322
	Gas superficial velocity (header)	m/s	0.11	0.11	0.10	0.08	0.18	0.14	0.12	0.10	0.21	0.17	0.16	0.16
	(Inlet pipe Ø1.5mm)	m/s	25.37	24.04	22.09	17.93	40.18	32.13	26.68	23.64	48.26	38.95	35.68	35.17
	Liquid Specific Volume (header)	m^3/kg	7.531E-04	7.506E-04	7.452E-04	7.442E-04	7.556E-04	7.501E-04	7.484E-04	7.439E-04	7.542E-04	7.515E-04	7.462E-04	7.388E-04
	Liquid Density (header)	kg/m^3	1327.83	1332.34	1341.94	1343.80	1323.49	1333.17	1336.17	1344.25	1325.84	1330.67	1340.14	1353.49
	Liquid superficial velocity (header)	m/s	0.0035	0.0026	0.0020	0.0016	0.0032	0.0024	0.0019	0.0015	0.0027	0.0021	0.0016	0.0013
	(Inlet pipe Ø1.5mm)	m/s	0.8022	0.5998	0.4607	0.3589	0.7327	0.5336	0.4344	0.3388	0.6019	0.4837	0.3622	0.2990
	Pressure drop (Pleaving -Ps)	mPa	0.02	0.01	0.01	0.00	0.03	0.02	(0.00)	0.00	0.04	0.03	0.02	0.00

Folder: 18 evp vis/21 flow recogition

Channel orientation	Downward	Intrusion height h	3mm
Inlet pipe diameter	2.0mm	Branch quantity	22

1atm = 0.101325 mPa
1mPa = 10.197162 kgf/cm2

	Test date		350(2011/06/20)	351	352(2011/06/210)	353	354	355	356	357	358	359	360	361
Parameter	evp out flow direction		Reverse	←	←	←	←	←	←	←	←	←	←	←
	R134a amount	g	330	←	←	←	345	←	←	←	←	←	←	345-α
	comp Rev	rpm	3500	2700	2000	1850	3900	3100	2400	2000	4200	←	3400	2800
	Exp Valve opening value	pulse	116	86	81	68	92	73	61	50	79	67	56	44
	water flow	ml/min	395	430	210	210	300	←	215	←	125	105	105	50
	water bath temperature act/set	°C	11.0/6.0	13.5/6.0	6.7/6.0	7.1/6.0	33.7/35.0	32.7/35.0	33.2/35.0	33.7/35.0	47.0/47.0	←	←	←
	outdoor fan speed	V	4.34	4.25	4.22	4.22	4.27	4.22	4.19	←	4.11	4.1	←	4.09
		A	0.06	0.05	0.04	0.04	0.05	0.04	0.04	←	0.04	0.04	←	0.04
	remark		in4, out2 laye	←	←	←	←	←	←	←	←	←	←	←
Testing data	flow rate	ml/min	112.59	85.85	69.71	55.01	119.33	88.49	70.77	58	131.28	92.12	75.31	57.14
	P entering Exp valve	mPaG	0.528	0.518	0.534	0.496	1.038	0.973	0.985	0.948	1.392	1.331	1.254	1.333
	P absolute	mPa	0.629	0.619	0.635	0.597	1.139	1.074	1.086	1.049	1.493	1.432	1.355	1.434
	P leaving exp valve	mPaG	0.089	0.075	0.08	0.058	0.098	0.074	0.071	0.066	0.124	0.084	0.061	0.035
	P absolute	mPa	0.190	0.176	0.181	0.159	0.199	0.175	0.172	0.167	0.225	0.185	0.162	0.136
	T entering Exp valve	°C	22.774	22.363	21.988	17.889	35.327	31.223	30.428	30.220	47.995	43.961	41.840	39.783
	T leaving exp valve	°C	-10.735	-12.666	-11.855	-15.049	-9.730	-12.994	-13.298	-13.996	-6.468	-11.461	-14.823	-18.366
	Ps	mPaG	0.08	0.08	0.08	0.07	0.08	0.07	0.08	0.07	0.08	0.05	0.04	0.02
		mPa	0.181	0.181	0.181	0.171	0.181	0.171	0.181	0.171	0.181	0.151	0.141	0.121
	Pd	mPaG	0.65	0.62	0.61	0.58	1.15	1.05	1.08	1.02	1.45	1.42	1.35	1.36
		mPa	0.751	0.721	0.711	0.681	1.251	1.151	1.181	1.121	1.551	1.521	1.451	1.461
	T at flow meter	°C	23.000	22.4	22.4	17.3	36.3	31.4	31.3	30.6	49.6	45.3	41.2	44.3
	Cs	°C	13.00	12.20	10.40	9.60	10.40	9.80	9.70	9.70	14.40	10.70	8.60	11.50
	Cd	°C	61.60	56.00	47.40	46.00	65.90	66.80	60.40	56.60	79.70	77.30	71.90	61.80
Calculation value	saturated point temp	°C	23.12	22.59	23.43	21.40	44.30	42.06	42.48	41.14	55.04	53.34	51.11	53.40
	subcool amount	°C	0.35	0.23	1.44	3.51	8.97	10.84	12.05	10.92	7.05	9.38	9.27	13.62
	Enthalpy at entering exp valve (I	kJ/kg	231.38	230.8	230.27	224.51	249.46	243.48	242.33	242.03	268.44	262.29	259.1	256.01
	T leaving exp valve (calculation value)	°C	-11.39	-13.29	-12.59	-15.76	-10.22	-13.43	-13.85	-14.57	-7.07	-12.05	-15.31	-19.46
	Quality (x)	**kg/kg**	**0.2247**	**0.2325**	**0.2261**	**0.2160**	**0.3059**	**0.2941**	**0.2908**	**0.2932**	**0.3820**	**0.3775**	**0.3785**	**0.3842**
	Density	kg/m^3	1215.11	1216.63	1218.16	1233.35	1168	1184.54	1187.85	1188.44	1114.02	1132.42	1141.37	1151.15
	Mass flow	**kg/h**	**8.21**	**6.27**	**5.10**	**4.07**	**8.36**	**6.29**	**5.04**	**4.14**	**8.77**	**6.26**	**5.16**	**3.95**
	Gas Specific Volume (header)	m^3/kg	1.049E-01	1.128E-01	1.098E-01	1.242E-01	1.004E-01	1.134E-01	1.153E-01	1.186E-01	8.925E-02	1.076E-01	1.220E-01	1.440E-01
	Gas Density (header)	kg/m^3	9.5356	8.8660	9.1075	8.0509	9.9651	8.8183	8.6745	8.4345	11.2051	9.2963	8.1947	6.9430
	Gas superficial velocity (header)	m/s	0.13	0.11	0.09	0.08	0.18	0.15	0.12	0.10	0.21	0.18	0.17	0.15
	(Inlet pipe Ø2mm)	m/s	17.10	14.53	11.18	9.66	22.70	18.55	14.95	12.71	26.45	22.47	21.06	19.31
	Liquid Specific Volume (header)	m^3/kg	7.510E-04	7.477E-04	7.489E-04	7.434E-04	7.531E-04	7.474E-04	7.467E-04	7.454E-04	7.589E-04	7.499E-04	7.442E-04	7.371E-04
	Liquid Density (header)	kg/m^3	1331.50	1337.47	1335.29	1345.19	1327.83	1337.92	1339.24	1341.49	1317.78	1333.60	1343.80	1356.59
	Liquid superficial velocity (header)	m/s	0.0033	0.0025	0.0021	0.0016	0.0030	0.0023	0.0019	0.0015	0.0029	0.0020	0.0017	0.0012
	(Inlet pipe Ø2mm)	m/s	0.4226	0.3180	0.2611	0.2098	0.3865	0.2934	0.2362	0.1927	0.3639	0.2583	0.2109	0.1584
	Pressure drop (Pleaving -Ps)	mPa	0.01	(0.01)	0.00	(0.01)	0.02	0.00	(0.01)	(0.00)	0.04	0.03	0.02	0.02

Folder: 19 evp vis/22 flow recogition

1atm = 0.101325 mPa
1mPa = 10.197162 kgf/cm2

	Channel orientation		Downward	Intrusion height h		1mm								
	Inlet pipe diameter		2.0mm	Branch quantity		22								
	Test date		370(2011/06/23)	371	372	373	374(2011/06/24)	375	376	377	378	379	380	381
Parameter	evp out flow direction		Reverse	←	←	←	←	←	←	←	←	←	←	←
	R134a amount	g	345	←	←	←	←	←	←	←	370	←	←	←
	comp Rev	rpm	3400	2700	2400	1850	3800	3100	2400	2000	4200	3800	3100	2800
	Exp Valve opening value	pulse	116	88	80	70	96	84	73	65	90	80	64	55
	water flow	ml/min	415	305	310	←	285	240	←	←	100	←	60	40
	water bath temperature act/set	°C	9.0/6.0	8.8/6.0	9.1/6.0	9.8/6.0	25.0/25.0	←	←	25.6/27.0	40.0/40.0	←	44.0/44.0	←
	outdoor fan speed	V	4.77	4.24	4.21	←	4.22	4.19	←	←	4.12	4.11	4.1	←
		A	0.07	0.04	0.04	←	0.04	0.04	←	←	0.04	0.04	0.04	←
	remark		in4, out2 layer	←	←	←	←	←	←	←	←	←	←	←
Testing data	flow rate	ml/min	113.45	85.21	72.62	55.19	123.18	91.12	71.88	58.8	117.42	94.88	78.31	59.81
	P entering Exp valve	mPaG	0.531	0.549	0.525	0.486	0.929	0.914	0.837	0.815	1.328	1.312	1.331	1.272
	P absolute	mPa	0.632	0.650	0.626	0.587	1.030	1.015	0.938	0.916	1.429	1.413	1.432	1.373
	P leaving exp valve	mPaG	0.092	0.076	0.067	0.06	0.098	0.087	0.08	0.074	0.082	0.079	0.061	0.044
	P absolute	mPa	0.193	0.177	0.168	0.161	0.199	0.188	0.181	0.175	0.183	0.180	0.162	0.145
	T entering Exp valve	°C	19.711	19.725	18.487	19.190	36.884	34.691	32.404	31.735	47.309	44.304	43.546	40.542
	T leaving exp valve	°C	-10.230	-12.574	-13.847	-14.916	-9.583	-11.059	-11.895	-12.612	-11.614	-12.114	-14.551	-17.125
	Ps	mPaG	0.08	0.08	0.07	0.07	0.08	0.08	0.08	0.08	0.07	0.06	0.06	0.04
		mPa	0.181	0.181	0.171	0.171	0.181	0.181	0.181	0.181	0.171	0.161	0.161	0.141
	Pd	mPaG	0.65	0.65	0.61	0.58	1.02	1.02	0.92	0.88	1.42	1.40	1.45	1.32
		mPa	0.751	0.751	0.711	0.681	1.121	1.121	1.021	0.981	1.521	1.501	1.551	1.421
	T at flow meter	°C	20.800	19.1	18.1	17.6	37.1	35.3	33.3	31.5	48.2	45.4	46.1	44.3
	Cs	°C	16.00	14.60	14.10	14.00	14.80	14.40	14.10	13.90	10.10	9.80	8.90	8.60
	Cd	°C	60.90	58.80	54.30	51.40	75.70	70.80	65.80	61.40	78.30	77.20	71.20	63.10
Calculation value	saturated point temp	°C	23.27	24.21	22.96	20.85	40.49	39.94	37.03	36.16	53.26	52.80	53.34	51.64
	subcool amount	°C	3.56	4.49	4.47	1.66	3.61	5.25	4.63	4.43	5.95	8.50	9.79	11.10
	Enthalpy at entering exp valve (I	kJ/kg	227.07	227.09	225.35	226.33	251.77	251.77	245.2	244.23	267.4	262.81	261.66	257.15
	T leaving exp valve (calculation value)	°C	-10.99	-13.15	-14.42	-15.46	-10.22	-11.65	-12.59	-13.43	-12.32	-12.73	-15.61	-17.95
	Quality (x)	**kg/kg**	**0.2017**	**0.2139**	**0.2126**	**0.2230**	**0.3171**	**0.3246**	**0.2979**	**0.2977**	**0.4034**	**0.3834**	**0.3907**	**0.3823**
	Density	kg/m^3	1226.75	1226.8	1231.29	1228.46	1160.53	1160.41	1178.76	1181.36	1116.68	1130.67	1132	1147.31
	Mass flow	**kg/h**	**8.35**	**6.27**	**5.36**	**4.07**	**8.58**	**6.34**	**5.08**	**4.17**	**7.87**	**6.44**	**5.32**	**4.12**
	Gas Specific Volume (header)	m^3/kg	1.033E-01	1.122E-01	1.179E-01	1.228E-01	1.004E-01	1.059E-01	1.098E-01	1.134E-01	1.087E-01	1.104E-01	1.220E-01	1.356E-01
	Gas Density (header)	kg/m^3	9.6787	8.9135	8.4825	8.1466	9.9651	9.4402	9.1050	8.8183	9.2013	9.0572	8.1947	7.3774
	Gas superficial velocity (header)	m/s	0.12	0.10	0.09	0.08	0.19	0.15	0.12	0.10	0.24	0.19	0.18	0.15
	(Inlet pipe Ø2mm)	m/s	15.39	13.31	11.89	9.85	24.13	19.29	14.71	12.44	30.50	24.09	22.42	18.87
	Liquid Specific Volume (header)	m^3/kg	7.517E-04	7.479E-04	7.457E-04	7.439E-04	7.531E-04	7.506E-04	7.489E-04	7.474E-04	7.494E-04	7.487E-04	7.442E-04	7.397E-04
	Liquid Density (header)	kg/m^3	1330.26	1337.04	1341.04	1344.25	1327.83	1332.34	1335.31	1337.92	1334.45	1335.74	1343.80	1351.99
	Liquid superficial velocity (header)	m/s	0.0035	0.0026	0.0022	0.0016	0.0031	0.0022	0.0019	0.0015	0.0024	0.0021	0.0017	0.0013
	(Inlet pipe Ø2mm)	m/s	0.4431	0.3261	0.2785	0.2079	0.3900	0.2844	0.2363	0.1934	0.3110	0.2627	0.2132	0.1663
	Pressure drop (Pleaving -Ps)	mPa	0.01	(0.00)	(0.00)	(0.01)	0.02	0.01	0.00	(0.01)	0.01	0.02	0.00	0.00

Folder: 20 evp vis/23 flow recogition

Channel orientation	Downward	Intrusion height h	1mm
Inlet pipe diameter	1.5mm	Branch quantity	22

1atm = 0.101325 mPa
1mPa = 10.197162 kgf/cm2

	Test date		390(2011/06/27)	391	392	393	394	395	396	397	398	399	400	401
Parameter	evp out flow direction		Reverse	←	←	←	←	←	←	←	←	←	←	←
	R134a amount	g	345	←	←	←	←	←	←	←	←	←	←	←
	comp Rev	rpm	3400	2700	2400	1850	4200	3100	2500	2100	4000	3700	3100	2800
	Exp Valve opening value	pulse	119	91	84	73	108	91	80	71	110	69	57	48
	water flow	ml/min	390	300	←	←	250	←	240	←	120	120	←	100
	water bath temperature act/set	°C	8.0/6.0	11.3/6.0	10.4/6.0	9.9/6.0	25.0/25.0	←	←	25.9/27.0	39.7/40.0	39.8/40.0	←	44.0/44.0
	outdoor fan speed	V	4.77	4.26	←	←	4.23	4.16	←	←	4.11	4.11	←	←
		A	0.07	0.05	←	←	0.04	0.04	←	←	0.04	0.04	←	←
	remark		in4, out2 layer	←	←	←	←	←	←	←	←	←	←	←
Testing data	flow rate	ml/min	114.96	84.69	69.44	55.63	122.17	89.61	72.13	59.35	127.97	95.99	74.44	58.76
	P entering Exp valve	mPaG	0.556	0.621	0.553	0.505	0.871	0.865	0.811	0.773	1.343	1.409	1.233	1.231
	P absolute	mPa	0.657	0.722	0.654	0.606	0.972	0.966	0.912	0.874	1.444	1.510	1.334	1.332
	P leaving exp valve	mPaG	0.112	0.09	0.076	0.078	0.104	0.092	0.082	0.073	0.116	0.101	0.074	0.05
	P absolute	mPa	0.213	0.191	0.177	0.179	0.205	0.193	0.183	0.174	0.217	0.202	0.175	0.151
	T entering Exp valve	°C	20.067	21.781	19.491	19.569	35.402	33.056	32.090	30.198	47.825	45.850	44.413	40.887
	T leaving exp valve	°C	-7.500	-10.515	-12.454	-12.170	-8.694	-10.310	-11.591	-12.875	-7.503	-9.251	-12.819	-16.267
	Ps	mPaG	0.09	0.09	0.08	0.08	0.07	0.08	0.07	0.08	0.08	0.08	0.06	0.04
		mPa	0.191	0.191	0.181	0.181	0.171	0.181	0.171	0.181	0.181	0.181	0.161	0.141
	Pd	mPaG	0.65	0.71	0.65	0.59	0.98	0.98	0.90	0.85	1.43	1.50	1.33	1.32
		mPa	0.751	0.811	0.751	0.691	1.081	1.081	1.001	0.951	1.531	1.601	1.431	1.421
	T at flow meter	°C	21.000	21.6	19.2	18.4	35.4	33.8	32.6	31.1	48.4	47.0	46.3	43.4
	Cs	°C	16.00	15.00	14.10	14.00	13.50	13.30	13.20	13.00	13.10	13.50	13.60	12.60
	Cd	°C	58.70	59.60	57.40	53.80	68.90	68.60	62.80	59.80	79.20	74.80	75.60	68.10
Calculation value	saturated point temp	°C	24.57	27.76	24.41	21.89	38.33	38.11	36.00	34.46	53.68	55.51	50.49	50.43
	subcool amount	°C	4.50	5.98	4.92	2.32	2.93	5.05	3.91	4.26	5.86	9.66	6.08	9.54
	Enthalpy at entering exp valve (I	kJ/kg	227.57	229.99	226.76	226.87	249.59	246.15	244.75	242.01	268.19	265.14	263	257.68
	T leaving exp valve (calculation value)	°C	-8.49	-11.25	-13.15	-12.87	-9.47	-10.99	-12.32	-13.57	-8.01	-9.84	-13.43	-16.99
	Quality (x)	**kg/kg**	**0.1898**	**0.2173**	**0.2123**	**0.2113**	**0.3025**	**0.2940**	**0.2943**	**0.2878**	**0.3856**	**0.3801**	**0.3878**	**0.3801**
	Density	kg/m^3	1225.55	1219.44	1227.7	1227.14	1166.43	1176.26	1179.87	1187.36	1114.34	1124.38	1129.44	1145.44
	Mass flow	**kg/h**	**8.45**	**6.20**	**5.12**	**4.10**	**8.55**	**6.32**	**5.11**	**4.23**	**8.56**	**6.48**	**5.04**	**4.04**
	Gas Specific Volume (header)	m^3/kg	9.404E-02	1.044E-01	1.122E-01	1.110E-01	9.754E-02	1.033E-01	1.087E-01	1.140E-01	9.239E-02	9.893E-02	1.134E-01	1.305E-01
	Gas Density (header)	kg/m^3	10.6333	9.5831	8.9135	9.0098	10.2519	9.6787	9.2013	8.7704	10.8240	10.1087	8.8183	7.6658
	Gas superficial velocity (header)	m/s	0.10	0.10	0.08	0.07	0.18	0.13	0.11	0.10	0.21	0.17	0.15	0.14
	(Inlet pipe Ø1.5mm)	m/s	23.72	22.09	19.15	15.10	39.66	30.20	25.67	21.81	47.91	38.28	34.87	31.48
	Liquid Specific Volume (header)	m^3/kg	7.563E-04	7.513E-04	7.479E-04	7.484E-04	7.545E-04	7.517E-04	7.494E-04	7.475E-04	7.571E-04	7.538E-04	7.474E-04	7.413E-04
	Liquid Density (header)	kg/m^3	1322.31	1331.10	1337.04	1336.17	1325.43	1330.26	1334.45	1337.83	1320.79	1326.63	1337.92	1349.02
	Liquid superficial velocity (header)	m/s	0.0036	0.0025	0.0021	0.0017	0.0031	0.0023	0.0019	0.0016	0.0028	0.0021	0.0016	0.0013
	(Inlet pipe Ø1.5mm)	m/s	0.8142	0.5727	0.4737	0.3800	0.7073	0.5276	0.4245	0.3538	0.6256	0.4757	0.3628	0.2917
	Pressure drop (Pleaving -Ps)	mPa	0.02	0.00	(0.00)	(0.00)	0.03	0.01	0.01	(0.01)	0.04	0.02	0.01	0.01

Folder: 21 evp vis/24 flow recogition

Channel orientation	Downward	Intrusion height h	3mm
Inlet pipe diameter	1.5mm	Branch quantity	11

1atm = 0.101325 mPa
1mPa = 10.197162 kgf/cm2

	Test date		410(2011/06/30)	411	412	413	414	415	416	417	418	419	420	421
Parameter	evp out flow direction		Reverse	←	←	←	←	←	←	←	←	←	←	←
	R134a amount	g	345	←	←	←	←	←	←	←	←	←	←	←
	comp Rev	rpm	3500	2700	2400	1850	4100	3100	2400	2100	4200	3800	3400	2600
	Exp Valve opening value	pulse	130	93	79	68	99	81	69	56	78	70	57	45
	water flow	ml/min	360	←	←	350	250	←	240	215	140	←	100	95
	water bath temperature act/set	°C	8.3/6.0	9.9/6.0	10.2/6.0	10.7/6.0	25.0/25.0	←	←	26.9/27.0	40.0/40.0	←	44.0/44.0	←
	outdoor fan speed	V	4.77	4.24	←	4.21	4.21	4.18	4.16	4.15	4.21	4.19	4.13	←
		A	0.07	0.04	←	0.04	0.04	0.04	0.04	0.04	0.04	0.04	0.04	←
	remark		in4, out2 layer	←	←	←	←	←	←	←	←	←	←	←
Testing data	flow rate	ml/min	114.6	88.08	70.97	55.73	122.85	90.82	73.41	58.36	123.87	95.35	77.34	59.27
	P entering Exp valve	mPaG	0.561	0.555	0.516	0.490	0.868	0.841	0.809	0.861	1.311	1.327	1.421	1.299
	P absolute	mPa	0.662	0.656	0.617	0.591	0.969	0.942	0.910	0.962	1.412	1.428	1.522	1.400
	P leaving exp valve	mPaG	0.109	0.096	0.077	0.078	0.1	0.092	0.086	0.074	0.104	0.093	0.071	0.056
	P absolute	mPa	0.210	0.197	0.178	0.179	0.201	0.193	0.187	0.175	0.205	0.194	0.172	0.157
	T entering Exp valve	°C	23.300	21.587	18.925	19.418	34.736	32.703	32.343	31.415	46.727	44.697	43.767	41.809
	T leaving exp valve	°C	-8.782	-9.864	-12.282	-11.940	-9.257	-10.698	-10.999	-12.840	-8.921	-10.357	-13.426	-15.587
	Ps	mPaG	0.09	0.09	0.08	0.08	0.06	0.08	0.08	0.08	0.07	0.07	0.06	0.04
		mPa	0.191	0.191	0.181	0.181	0.161	0.181	0.181	0.181	0.171	0.171	0.161	0.141
	Pd	mPaG	0.66	0.64	0.62	0.58	0.96	0.94	0.90	0.95	1.40	1.40	1.50	1.38
		mPa	0.761	0.741	0.721	0.681	1.061	1.041	1.001	1.051	1.501	1.501	1.601	1.481
	T at flow meter	°C	23.500	21.6	18.6	18.5	35.1	33.8	33.0	31.9	48.2	45.8	46.5	45.0
	Cs	°C	15.30	14.50	13.80	13.30	11.50	11.80	11.60	12.10	10.10	10.10	8.10	9.10
	Cd	°C	56.20	58.40	56.00	50.20	70.00	68.80	62.30	57.10	72.50	74.30	63.70	63.40
Calculation value	saturated point temp	°C	24.82	24.52	22.48	21.07	38.22	37.18	35.92	37.95	52.77	53.23	55.84	52.42
	subcool amount	°C	1.52	2.93	3.56	1.65	3.48	4.48	3.58	6.54	6.04	8.53	12.07	10.61
	Enthalpy at entering exp valve (h	kJ/kg	232.13	229.71	225.96	226.65	248.61	245.64	245.12	243.76	266.51	263.4	261.97	259.05
	T leaving exp valve (calculation value)	°C	-8.85	-10.48	-13.01	-12.87	-9.97	-10.99	-11.78	-13.43	-9.47	-10.86	-13.85	-16.06
	Quality (x)	**kg/kg**	**0.2141**	**0.2115**	**0.2077**	**0.2102**	**0.3004**	**0.2915**	**0.2932**	**0.2954**	**0.3848**	**0.3768**	**0.3849**	**0.3820**
	Density	kg/m^3	1213.28	1215.87	1229.61	1227.62	1169.23	1177.55	1178.81	1183	1119.29	1128.99	1134.12	1141.9
	Mass flow	**kg/h**	**8.34**	**6.43**	**5.24**	**4.10**	**8.62**	**6.42**	**5.19**	**4.14**	**8.32**	**6.46**	**5.26**	**4.06**
	Gas Specific Volume (header)	m^3/kg	9.533E-02	1.013E-01	1.116E-01	1.110E-01	9.939E-02	1.033E-01	1.065E-01	1.134E-01	9.754E-02	1.028E-01	1.153E-01	1.257E-01
	Gas Density (header)	kg/m^3	10.4903	9.8697	8.9614	9.0098	10.0610	9.6787	9.3923	8.8183	10.2519	9.7267	8.6745	7.9548
	Gas superficial velocity (header)	m/s	0.12	0.10	0.08	0.07	0.18	0.13	0.11	0.10	0.22	0.17	0.16	0.14
	(Inlet pipe Ø1.5mm)	m/s	26.76	21.64	19.08	15.05	40.45	30.38	25.48	21.81	49.08	39.33	36.71	30.65
	Liquid Specific Volume (header)	m^3/kg	7.556E-04	7.527E-04	7.482E-04	7.481E-04	7.536E-04	7.517E-04	7.503E-04	7.474E-04	7.545E-04	7.520E-04	7.467E-04	7.429E-04
	Liquid Density (header)	kg/m^3	1323.49	1328.64	1336.61	1336.72	1327.02	1330.26	1332.76	1337.92	1325.43	1329.86	1339.24	1346.13
	Liquid superficial velocity (header)	m/s	0.0034	0.0026	0.0022	0.0017	0.0032	0.0024	0.0019	0.0015	0.0027	0.0021	0.0017	0.0013
	(Inlet pipe Ø1.5mm)	m/s	0.7787	0.5994	0.4879	0.3812	0.7142	0.5372	0.4328	0.3429	0.6069	0.4758	0.3799	0.2930
	Pressure drop (Pleaving -Ps)	mPa	0.02	0.01	(0.00)	(0.00)	0.04	0.01	0.01	(0.01)	0.03	0.02	0.01	0.02

Folder: 22 evp vis/25 flow recogition

Channel orientation	Downward	Intrusion height h	3mm
Inlet pipe diameter	3.0mm	Branch quantity	11

1atm = 0.101325 mPa
1mPa = 10.197162 kgf/cm2

	Test date		430(2011/07/05)	431	432	433	434	435	436	437	438(2011/07/07)	439	440	441
Parameter	evp out flow direction		Reverse	←	←	←	←	←	←	←	←	←	←	←
	R134a amount	g	345	←	←	←	←	←	←	←	355	←	←	←
	comp Rev	rpm	3300	2700	2400	1850	3800	3200	2400	2000	4200	3800	3100	2600
	Exp Valve opening value	pulse	130	101	86	68	96	77	66	56	83	70	60	54
	water flow	ml/min	630	←	410	350	240	230	170	150	140	100	70	50
	water bath temperature act/set	°C	9.8/6.0	13.0/6.0	6.1/6.0	10.2/6.0	25.0/25.0	←	←	←	40.0/40.0	←	41.5/42.0	42.0/42.0
	outdoor fan speed	V	4.18	4.14	4.21	4.19	4.14	4.12	4.13	←	4.11	←	4.1	←
		A	0.04	0.04	0.04	0.04	0.04	0.04	0.04	←	0.04	←	0.04	←
	remark		in4, out2 layer	←	←	←	←	←	←	←	←	←	←	←
Testing data	flow rate	ml/min	116.02	88.13	69.68	55.25	119.75	92.08	74.75	58.15	116.93	93.72	75.36	59.56
	P entering Exp valve	mPaG	0.511	0.520	0.493	0.510	0.967	0.933	0.927	0.885	1.350	1.278	1.254	1.224
	P absolute	mPa	0.612	0.621	0.594	0.611	1.068	1.034	1.028	0.986	1.451	1.379	1.355	1.325
	P leaving exp valve	mPaG	0.103	0.088	0.067	0.074	0.1	0.082	0.085	0.07	0.1	0.072	0.06	0.047
	P absolute	mPa	0.204	0.189	0.168	0.175	0.201	0.183	0.186	0.171	0.201	0.173	0.161	0.148
	T entering Exp valve	°C	20.692	20.453	16.746	17.991	35.901	31.637	32.649	30.974	45.603	42.595	41.906	39.521
	T leaving exp valve	°C	-9.219	-11.146	-13.854	-12.954	-9.447	-11.799	-11.346	-13.398	-9.507	-13.276	-14.834	-17.003
	Ps	mPaG	0.09	0.09	0.07	0.08	0.08	0.08	0.09	0.08	0.09	0.06	0.06	0.05
		mPa	0.191	0.191	0.171	0.181	0.181	0.181	0.191	0.181	0.191	0.161	0.161	0.151
	Pd	mPaG	0.62	0.62	0.58	0.59	1.05	1.05	1.02	0.98	1.46	1.36	1.34	1.31
		mPa	0.721	0.721	0.681	0.691	1.151	1.151	1.121	1.081	1.561	1.461	1.441	1.411
	T at flow meter	°C	21.200	20.4	15.9	16.6	36.1	32.4	33.5	31.2	46.6	44.4	44.1	43.0
	Cs	°C	14.60	14.20	12.50	12.90	11.40	11.10	11.20	10.80	11.10	10.00	9.40	8.90
	Cd	°C	62.80	58.60	46.90	48.20	68.30	67.30	62.00	58.20	77.90	76.90	71.50	63.90
Calculation value	saturated point temp	°C	22.21	22.69	21.23	22.16	41.85	40.63	40.41	38.86	53.88	51.82	51.11	50.22
	subcool amount	°C	1.52	2.24	4.48	4.17	5.95	8.99	7.76	7.89	8.28	9.23	9.20	10.70
	Enthalpy at entering exp valve (I	kJ/kg	228.44	228.11	222.92	224.66	250.31	244.08	245.55	243.12	264.78	260.23	259.2	255.64
	T leaving exp valve (calculation value)	°C	-9.59	-11.52	-14.42	-13.43	-9.97	-12.32	-11.92	-13.99	-9.97	-13.71	-15.46	-17.47
	Quality (x)	**kg/kg**	**0.2003**	**0.2097**	**0.2010**	**0.2038**	**0.3087**	**0.2911**	**0.2960**	**0.2954**	**0.3789**	**0.3759**	**0.3797**	**0.3727**
	Density	kg/m^3	1222.95	1223.9	1237.55	1233.05	1165.03	1182.58	1178.38	1184.96	1124.98	1138.18	1141.08	1151.41
	Mass flow	**kg/h**	**8.51**	**6.47**	**5.17**	**4.09**	**8.37**	**6.53**	**5.29**	**4.13**	**7.89**	**6.40**	**5.16**	**4.11**
	Gas Specific Volume (header)	m^3/kg	9.800E-02	1.054E-01	1.179E-01	1.134E-01	9.939E-02	1.087E-01	1.070E-01	1.159E-01	9.939E-02	1.147E-01	1.228E-01	1.330E-01
	Gas Density (header)	kg/m^3	10.2042	9.4877	8.4825	8.8183	10.0610	9.2013	9.3440	8.6266	10.0610	8.7222	8.1466	7.5216
	Gas superficial velocity (header)	m/s	0.12	0.10	0.09	0.07	0.18	0.14	0.12	0.10	0.21	0.19	0.17	0.14
	(Inlet pipe Ø3mm)	m/s	6.57	5.62	4.82	3.71	10.09	8.12	6.58	5.56	11.68	10.84	9.45	8.01
	Liquid Specific Volume (header)	m^3/kg	7.542E-04	7.508E-04	7.457E-04	7.474E-04	7.536E-04	7.494E-04	7.501E-04	7.464E-04	7.536E-04	7.469E-04	7.439E-04	7.405E-04
	Liquid Density (header)	kg/m^3	1325.84	1331.93	1341.04	1337.92	1327.02	1334.45	1333.17	1339.69	1327.02	1338.80	1344.25	1350.49
	Liquid superficial velocity (header)	m/s	0.0036	0.0027	0.0021	0.0017	0.0030	0.0024	0.0019	0.0015	0.0026	0.0021	0.0017	0.0013
	(Inlet pipe Ø3mm)	m/s	0.2018	0.1509	0.1211	0.0956	0.1714	0.1364	0.1097	0.0854	0.1452	0.1172	0.0936	0.0751
	Pressure drop (Pleaving -Ps)	mPa	0.01	(0.00)	(0.00)	(0.01)	0.02	0.00	(0.00)	(0.01)	0.01	0.01	0.00	(0.00)

Folder: 24 evp vis/26 flow recogition

Channel orientation	Upward	Intrusion height h	3mm
Inlet pipe diameter	2mm	Branch quantity	11

1atm = 0.101325 mPa
1mPa = 10.197162 kgf/cm2

	Test date		450(2011/11/28)	451	452	453	454	455	456	457	458	459	460	461
Parameter	evp out flow direction				Reverse		←	←	←	←			←	
	R134a amount	g			410		←	←	←	←			←	
	comp Rev	rpm			2200		4200	3400	2800	2200			3600	
	Exp Valve opening value	pulse			83		105	86	67	58			64	
	water flow	ml/min			270		210	190	145	120			80	
	water bath temperature act/set	°C			14.0/14.0		29.7/30.0	29.6/30.0	30.0/30.0	←			45.0/45.0	
	outdoor fan speed	V			4.26		4.32	←	4.24	4.21			4.2	
		A			0.04		0.04	0.05	0.04	0.04			0.04	
	remark				in4, out2 layer		←	←	←	←			←	
Testing data	flow rate	ml/min			69.82		121.37	90.93	71.29	58.45			76.34	
	P entering Exp valve	mPaG			0.553		1.005	0.906	0.980	0.971			1.309	
	P absolute	mPa			0.654		1.106	1.007	1.081	1.072			1.410	
	P leaving exp valve	mPaG			0.083		0.106	0.076	0.065	0.067			0.072	
	P absolute	mPa			0.184		0.207	0.177	0.166	0.168			0.173	
	T entering Exp valve	°C			17.491		35.133	31.280	29.342	29.736			42.132	
	T leaving exp valve	°C			-11.623		-8.564	-12.525	-14.138	-13.827			-12.945	
	Ps	mPaG			0.08		0.09	0.06	0.07	0.07			0.04	
		mPa			0.181		0.191	0.161	0.171	0.171			0.141	
	Pd	mPaG			0.63		1.10	1.00	1.06	1.06			1.40	
		mPa			0.731		1.201	1.101	1.161	1.161			1.501	
	T at flow meter	°C			18.2		35.8	32.8	30.9	32.1			43.8	
	Cs	°C			9.10		10.20	9.20	9.40	9.80			8.80	
	Cd	°C			47.30		70.60	67.00	62.40	57.90			65.60	
Calculation value	saturated point temp	°C			24.41		43.17	39.64	42.31	41.99			52.71	
	subcool amount	°C			6.92		8.04	8.36	12.97	12.25			10.58	
	Enthalpy at entering exp valve (h)	kJ/kg			223.96		249.18	243.57	240.77	241.33			259.53	
	T leaving exp valve (calculation value)	°C			-12.19		-9.22	-13.15	-14.72	-14.42			-13.71	
	Quality (x)	**kg/kg**			**0.1934**		**0.2992**	**0.2930**	**0.2879**	**0.2843**			**0.3725**	
	Density	**kg/m^3**			1235.12		1168.57	1183.86	1192.18	1190.54			1140.54	
	Mass flow	**kg/h**			**5.17**		**8.51**	**6.46**	**5.10**	**4.18**			**5.22**	
	Gas Specific Volume (header)	m^3/kg			1.081E-01		9.664E-02	1.122E-01	1.192E-01	1.179E-01			1.147E-01	
	Gas Density (header)	kg/m^3			9.2490		10.3473	8.9135	8.3864	8.4825			8.7222	
	Gas superficial velocity (header)	m/s			0.08		0.17	0.15	0.12	0.10			0.15	
	(Inlet pipe Ø2mm)	m/s			9.57		21.76	18.77	15.48	12.37			19.73	
	Liquid Specific Volume (header)	m^3/kg			7.496E-04		7.549E-04	7.479E-04	7.452E-04	7.457E-04			7.469E-04	
	Liquid Density (header)	kg/m^3			1334.03		1324.64	1337.04	1341.94	1341.04			1338.80	
	Liquid superficial velocity (header)	m/s			0.0022		0.0031	0.0024	0.0019	0.0015			0.0017	
	(Inlet pipe Ø2mm)	m/s			0.2766		0.3981	0.3020	0.2393	0.1970			0.2165	
	Pressure drop (Pleaving -Ps)	mPa			0.00		0.02	0.02	(0.01)	(0.00)			0.03	

Folder: 25 evp vis/27 flow recogition

Channel orientation	Upward	Intrusion height h	3mm
Inlet pipe diameter	2mm	Branch quantity	22

1atm = 0.101325 mPa
1mPa = 10.197162 kgf/cm2

	Test date		470(2012/01/11)	471	472	473	474	475	476(2012/01/12)	477	478	479	480	481
Parameter	evp out flow direction				Reverse		←	←	←	←			←	
	R134a amount	g			410		←	←	←	←			←	
	comp Rev	rpm			2200		4200	3400	2800	2200			3800	
	Exp Valve opening value	pulse			90		84	70	64	50			56	
	water flow	ml/min			200		220	200	170	150			25	
	water bath temperature act/set	°C			14.0/14.0		32.0/32.2	34.0/34.4	36.0/35.6	36.0/36.0			48.0/48.5	
	outdoor fan speed	V			4.25		4.19	4.18	4.19	4.16			4.11	
		A			0.04		0.04	0.04	0.04	0.04			0.04	
	remark				in4, out2 layer		←	←	←	←			←	
Testing data	flow rate	ml/min			70.07		120.28	89.24	70.98	58.66			73.49	
	P entering Exp valve	mPaG			0.625		1.004	0.979	0.859	0.915			1.263	
	P absolute	mPa			0.726		1.105	1.080	0.960	1.016			1.364	
	P leaving exp valve	mPaG			0.074		0.095	0.068	0.047	0.053			0.041	
	P absolute	mPa			0.175		0.196	0.169	0.148	0.154			0.142	
	T entering Exp valve	°C			19.420		32.442	30.338	29.550	30.161			39.814	
	T leaving exp valve	°C			-13.039		-9.953	-13.671	-17.309	-16.199			-17.686	
	Ps	mPaG			0.08		0.08	0.06	0.04	0.05			0.03	
		mPa			0.181		0.181	0.161	0.141	0.151			0.131	
	Pd	mPaG			0.70		1.10	1.06	0.94	1.00			1.35	
		mPa			0.801		1.201	1.161	1.041	1.101			1.451	
	T at flow meter	°C			19.4		34.4	31.0	31.2	30.8			42.9	
	Cs	°C			11.60		12.70	11.20	5.80	7.10			8.30	
	Cd	°C			49.20		75.60	70.50	49.40	49.30			68.90	
Calculation value	saturated point temp	°C			27.95		43.14	42.27	37.88	39.98			51.38	
	subcool amount	°C			8.53		10.70	11.93	8.33	9.82			11.57	
	Enthalpy at entering exp valve (I	kJ/kg			226.67		245.25	242.2	241.07	241.95			256.07	
	T leaving exp valve (calculation value)	°C			-13.43		-10.6	-14.28	-17.47	-16.52			-18.45	
	Quality (x)	**kg/kg**			**0.2134**		**0.2876**	**0.2925**	**0.3038**	**0.3030**			**0.3796**	
	Density	kg/m^3			1228.35		1179.77	1188.17	1190.55	1188.46			1150.44	
	Mass flow	**kg/h**			**5.16**		**8.51**	**6.36**	**5.07**	**4.18**			**5.07**	
	Gas Specific Volume (header)	m^3/kg			1.134E-01		1.018E-01	1.172E-01	1.330E-01	1.280E-01			1.383E-01	
	Gas Density (header)	kg/m^3			8.8183		9.8222	8.5302	7.5216	7.8101			7.2322	
	Gas superficial velocity (header)	m/s			0.09		0.17	0.15	0.14	0.11			0.18	
	(Inlet pipe Ø2mm)	m/s			11.05		22.04	19.29	18.11	14.35			23.54	
	Liquid Specific Volume (header)	m^3/kg			7.474E-04		7.524E-04	7.459E-04	7.405E-04	7.421E-04			7.388E-04	
	Liquid Density (header)	kg/m^3			1337.92		1329.04	1340.59	1350.49	1347.56			1353.49	
	Liquid superficial velocity (head	m/s			0.0021		0.0032	0.0023	0.0018	0.0015			0.0016	
	(Inlet pipe Ø2mm)	m/s			0.2685		0.4035	0.2969	0.2311	0.1913			0.2056	
	Pressure drop (Pleaving -Ps)	mPa			(0.01)		0.02	0.01	0.01	0.00			0.01	

Folder: 25 evp vis/27 flow recogition

Channel orientation	Upward	Intrusion height h	0mm
Inlet pipe diameter	2.0mm	Branch quantity	11

1atm = 0.101325 mPa
1mPa = 10.197162 kgf/cm2

	Test date		490(2012/01/19)	491	492	493	494(2012/01/27)	495	496	497	498	499	500	501(repeat)
Parameter	evp out flow direction				Reverse		←	←	←	←			←	
	R134a amount	g			410		←	←	←	←			←	
	comp Rev	rpm			2200		4200	3400	2800	2200			3800	4200
	Exp Valve opening value	pulse			72		98	70	58	49			53	97
	water flow	ml/min			230		215	200	160	130			25	232
	water bath temperature act/set	°C			14.0/14.0		30.0/30.1	32.0/32.4	34.0/34.0	34.0/33.8			46.0/45.8	30.0/29.8
	outdoor fan speed	V			4.22		4.17	4.18	4.14	4.14			4.11	4.12
		A			0.04		0.04	0.04	0.04	0.04			0.04	0.04
	remark				in4, out2 layer		←	←	←	←			←	←
Testing data	flow rate	ml/min			70.24		119	91.43	72.82	57.55			77.54	120.25
	P entering Exp valve	mPaG			0.595		0.984	0.951	0.993	0.943			1.392	1.046
	P absolute	mPa			0.696		1.085	1.052	1.094	1.044			1.493	1.147
	P leaving exp valve	mPaG			0.071		0.101	0.078	0.068	0.063			0.056	0.106
	P absolute	mPa			0.172		0.202	0.179	0.169	0.164			0.157	0.207
	T entering Exp valve	°C			18.326		34.836	32.987	31.823	31.996			42.077	37.343
	T leaving exp valve	°C			-13.439		-9.458	-12.151	-13.556	-14.244			-15.363	-8.816
	Ps	mPaG			0.08		0.08	0.07	0.06	0.06			0.04	0.08
		mPa			0.181		0.181	0.171	0.161	0.161			0.141	0.181
	Pd	mPaG			0.68		1.10	1.05	1.08	1.04			1.48	1.12
		mPa			0.781		1.201	1.151	1.181	1.141			1.581	1.221
	T at flow meter	°C			18.7		35.6	33.6	33.1	34.5			44.3	38.2
	Cs	°C			10.20		11.90	10.80	10.70	10.50			9.80	13.70
	Cd	°C			44.60		72.50	61.90	61.30	56.30			69.30	77.60
Calculation value	saturated point temp	°C			26.51		42.00	41.28	42.76	40.99			55.04	44.57
	subcool amount	°C			8.18		7.16	8.29	10.94	8.99			12.96	7.23
	Enthalpy at entering exp valve (I	kJ/kg			225.13		248.75	246.05	244.35	244.6			259.43	252.43
	T leaving exp valve (calculation value)	°C			-13.85		-9.84	-12.87	-14.28	-15.01			-16.06	-9.22
	Quality (x)	**kg/kg**			**0.2084**		**0.3004**	**0.3035**	**0.3028**	**0.3078**			**0.3838**	**0.3150**
	Density	kg/m^3			1232.26		1169.67	1177.15	1182.23	1181.18			1141.5	1159.4
	Mass flow	**kg/h**			**5.19**		**8.35**	**6.46**	**5.17**	**4.08**			**5.31**	**8.37**
	Gas Specific Volume (header)	m^3/kg			1.153E-01		9.893E-02	1.110E-01	1.172E-01	1.206E-01			1.257E-01	9.664E-02
	Gas Density (header)	kg/m^3			8.6745		10.1087	9.0098	8.5302	8.2905			7.9548	10.3473
	Gas superficial velocity (header)	m/s			0.09		0.17	0.15	0.13	0.11			0.18	0.18
	(Inlet pipe Ø2mm)	m/s			11.03		21.94	19.23	16.21	13.39			22.66	22.52
	Liquid Specific Volume (header)	m^3/kg			7.467E-04		7.538E-04	7.484E-04	7.459E-04	7.447E-04			7.429E-04	7.549E-04
	Liquid Density (header)	kg/m^3			1339.24		1326.63	1336.17	1340.59	1342.86			1346.13	1324.64
	Liquid superficial velocity (header)	m/s			0.0021		0.0031	0.0023	0.0019	0.0015			0.0017	0.0030
	(Inlet pipe Ø2mm)	m/s			0.2714		0.3894	0.2976	0.2375	0.1859			0.2149	0.3825
	Pressure drop (Pleaving -Ps)	mPa			(0.01)		0.02	0.01	0.01	0.00			0.02	0.03